Imaging Investigations of the Ruthenium(III) Anti-Cancer Drugs, NAMI-A and KP1019, and Novel Analogues

Sumy Antony
(*M.Sc. Chemistry*)

Supervised by Associate Professor Hugh H. Harris

School of Chemistry and Physics
The University of Adelaide
March 2014

A thesis submitted in total fulfilment of the requirements for the degree of Doctor of Philosophy

General Declaration

I, Sumy Antony, certify that this work contains no material which has been accepted for the award of any other degree or diploma in my name, in any university or other tertiary institution and, to the best of my knowledge and belief, contains no material previously published or written by another person, except where due reference has been made in the text. In addition, I certify that no part of this work will, in the future, be used in a submission in my name, for any other degree or diploma in any university or other tertiary institution without the prior approval of the University of Adelaide and where applicable, any partner institution responsible for the joint-award of this degree.

I give consent to this copy of my thesis when deposited in the University Library, being made available for loan and photocopying, subject to the provisions of the Copyright Act 1968.

The author acknowledges that copyright of published works contained within this thesis resides with the copyright holder(s) of those works.

I also give permission for the digital version of my thesis to be made available on the web, via the University's digital research repository, the Library Search and also through web search engines, unless permission has been granted by the University to restrict access for a period of time.

………………………………………………..
Sumy Antony

……….28/03/2014…………………………
Date

Acknowledgements

First and foremost, I would like to thank Assoc. Prof. Hugh H. Harris, The University of Adelaide for giving me an opportunity to do PhD under his guidance. I acknowledge his motivation, patience, constant support and optimistic outlook whilst my PhD and I could not imagine a better advisor and mentor to pursue my PhD. I sincerely appreciate his guidance and willingness to show faith and drive me back on right track when needed.

I have been fortunate enough to work under the guidance of Prof. Leone Spiccia, Monash University and I am indebted to him for giving me an opportunity to continue my research in his group. I would like to thank him wholeheartedly as he was excessively kind with his time and profound feedback.

I would like to thank Dr. Ian Musgrave, The University of Adelaide and Assoc. Prof. Tracey Brown, Monash University, for their time, tremendous support and for authorising access to their cell culture laboratory as well as for their willingness to discuss research. I am extremely grateful to Dr. Jade Aitken for her valuable teachings in synchrotron-related work. I would like to express my sincere thanks to Dr. Aviva Levina and Assoc. Prof. Paul Witting, University of Sydney, for the constant guidance and support with cell culture studies.

My PhD journey could not have been completed without the support from the staff of School of Chemistry and Physics, University of Adelaide and School of Chemistry, Monash University. I am thankful to Dr. Chris Sumby, The University of Adelaide and Prof. Jonathan C. Morris, The University of New South Wales, for their prerequisite help to endure my research. I would like to thank all the staff of Monash University especially, Dr Peter Nicholas for the help with NMR measurements, Ms Sally Duck for mass spectrometry and Dr. Craig Forsyth for X-ray crystallography. I also would like to thank all the staff of Adelaide Microscopy and Monash Micro Imaging for their enormous support and guidance whilst fluorescent microscopy experiments.

A big thank you to all my friends in The University of Adelaide, members of the Harris group especially Claire M. Weekly – I have been lucky enough to work in her company and friendship. I am also thankful to Dr. Ashok Pehere for his generous help and suggestions with synthetic techniques, Dr. Marcus and all other members of Prof. Abell's group for sharing their lab facilities in the beginning of my PhD. Members of the past and present Spiccia group – Jenny, Dominique, Michelle, Yan, D'Souza, Leena, Archana, Tanmaya, Monica, Bopha, Solmas and all others – thank you all for your company while working in the lab, office and making this PhD journey a great learning experience. I would like to express my sincere gratitude towards Vera and Andrian, for their help and support in cell culture studies.

Last but not least, I am indebted to my whole family for their constant support and encouragement. My great motivation was my mom and dad, I am thankful for their blessings and love which uphold me when obstacles came to my passage throughout my education. I may not be achieving this higher degree without their prayer support, sacrifices and dedication. I do not have enough words to express my gratitude towards Vino and Angie for their unwavering support – emotional and moral – during PhD and this thesis would certainly not have existed without them. My deepest gratitude to my siblings – Smitha, Julie, Anto, Anoop – for their unconditional love and support, which gave me enough inspiration to complete my studies. I would like to dedicate this thesis to my beloved Parents, Vino and Angie.

Thank you all once again, for making this PhD a great success.

Abbreviations

aq	aqueous
BSA	bovine serum albumin
br	broad (spectroscopic)
calcd	calculated
conc	concentrated
°C	degrees Celsius
DMF	dimethyl formamide
DMSO	dimethyl sulfoxide
d	doublet
ESI	electrospray ionisation
eV	electron volt
FTIR	Fourier transform infrared
g	gram(s)
h	hour(s)
HPLC	high-performance liquid chromatography
Hz	Hertz
IR	infrared
J	coupling constant
MS	mass spectrometry
m/z	mass-to-charge ratio
MP	melting point
mg	milligram(s)
min	minute(s)
mL	millilitre(s)
mmol	millimole(s)
M	molarity
m	multiplet
NMR	nuclear magnetic resonance
q	quintet

Rf	retention factor
RT	room temperature
s	singlet
SAR	structure activity relationship
SRIXE	synchrotron radiation induced X-ray emission
t	triplet
TLC	thin layer chromatography
TMS	tetramethyl silane
UV	ultraviolet
XRF	X-ray fluorescence
NMR	nuclear magnetic resonance
δ	chemical shift (in ppm)
μM	micromolar

Abstract

The success of platinum-based anti-cancer agents, such as cisplatin, has led to further investigation of the utilisation of other non-platinum metal compounds in cancer therapy. The research has generated particular interest in ruthenium-based chemotherapeutics, as ruthenium species display numerous characteristics which make them appropriate for drug design. Numerous small-molecule ruthenium complexes e.g., NAMI-A (new anti-metastatic inhibitor; 'A' stands for first compound in the series; [ImH][*trans*-$RuCl_4$(DMSO)(Im)]; Im = imidazole) and KP1019 (Keppler compound 1019; [IndH][*trans*-$RuCl_4Ind_2$]; Ind = indazole), have been discovered and found to exhibit promising anti-cancer properties without complete knowledge about the mechanism of their activity.

To develop more targeted drugs with reduced toxicity, it is important to have an accurate knowledge about the mechanism of anti-metastatic activity of these drugs in a complete biological system. Our specific interest in this research has been concerned with the investigation of anti-metastatic activity of analogues of NAMI-A and KP1019 by advanced techniques such as synchrotron-based X-ray fluorescence imaging (XRF) and fluorescent microscopy imaging.

A series of ruthenium(III) complexes, which are analogous to either NAMI-A or KP1019, have been synthesised and structurally characterised and their pharmacological activities have been investigated *in vitro*. The intracellular uptake and distribution of these complexes in human lung cancer cell line (A549) was explored by synchrotron-based X-ray fluorescence microscopy and optical fluorescent microscopy. The intracellular distribution of ruthenium in individual A549 cells treated with KP1019 was revealed by XRF and the results demonstrate an accumulation of ruthenium inside the cytosol and the nucleus. On the contrary, NAMI-A treated cells are devoid of any alteration in intracellular distribution of elements, indicating a membrane-binding mechanism for the cytotoxic activity of NAMI-A. The results in turn demonstrate a different cellular destiny for the complexes, NAMI-A and KP1019.

The selective aggregation or intracellular speciation of ruthenium inside the cancer cells, treated with iodine substituted KP1019 analogues, was investigated by synchrotron-based μ-XRF studies. The addition of an iodinated ligand to the parent complex significantly altered the overall distribution of ruthenium across the cell from that observed for the parent complex. The 'double-tag' approach, tagging the N-heterocyclic ligand on KP1019 analogues with iodine and then tracking the cellular distribution of both ruthenium and iodine, demonstrated that the Ru-N bond in the treatment compound remained intact inside the cells. A significant increase in the concentration of both ruthenium and iodine inside the nucleus compared to that of control cells proved that the complexes selectively targeted and aggregated inside the nucleus of the treated cells.

The distinct cellular pathways of the ruthenium(III) complexes have been investigated by the functionalisation of the imidazole ligand of NAMI-A with other optically fluorescent functionalities. With the aim of eliminating the fluorescence arising from the counter cations, tetramethylammonium analogues were synthesised and characterised. The observed optical properties thus reflected the contribution from the metal complex anion only. The *in vitro* investigation of the synthesised complexes in lung cancer cells (A549) demonstrated that the functionalisation of NAMI-A does not significantly change the cytotoxic properties of the synthesised analogues. Numerous analogues of NAMI-A with enhanced imaging and targeting functionalities could be synthesised to investigate the biotransformation of ruthenium containing metabolites inside the cancer cell.

In general, a number of new biologically active ruthenium(III) complexes, which are analogous to the model complexes NAMI-A and KP1019, have been synthesised and characterised. Their intracellular speciation, aggregation and the optical fluorescent properties have been investigated. The acquired knowledge on the cytotoxicity, intracellular distribution and speciation of treated NAMI-A and KP1019 analogues can contribute to the investigation of the mechanism of anti-metastatic activity of these drugs inside the cancer cells. It may lead to the further development of new ruthenium chemotherapeutics having wide spectrum of activity when compared to platinum-based drugs.

Table of Contents

Chapter 1. Introduction

(journal page numbers are displayed for published articles)

(journal page numbers are displayed for published articles)

Chapter 1

Introduction

1. Cancer – A general overview

1.1. Cancer

Cancer is a term that represents a broad group of diseases. In cancer, the genetic material (DNA) of a cell is altered by mutations[1, 2] (caused by infections, radiation, environmental pollutants and tobacco consumption), that have an impact on traditional cell development and reproduction. The alterations may result in errors in the replication of DNA or chemical instability of certain DNA bases[3, 4]. The process of apoptosis (programmed cell death) is often disrupted in cancer and new cells develop where the body does not require them. This prompts the establishment of an anomalous mass of tissue forming benign (does not spread, or metastasize) or alternatively, a malignant tumour[5] (able to invade other tissues, or metastasize; neoplastic or cancerous) (Figure 1).

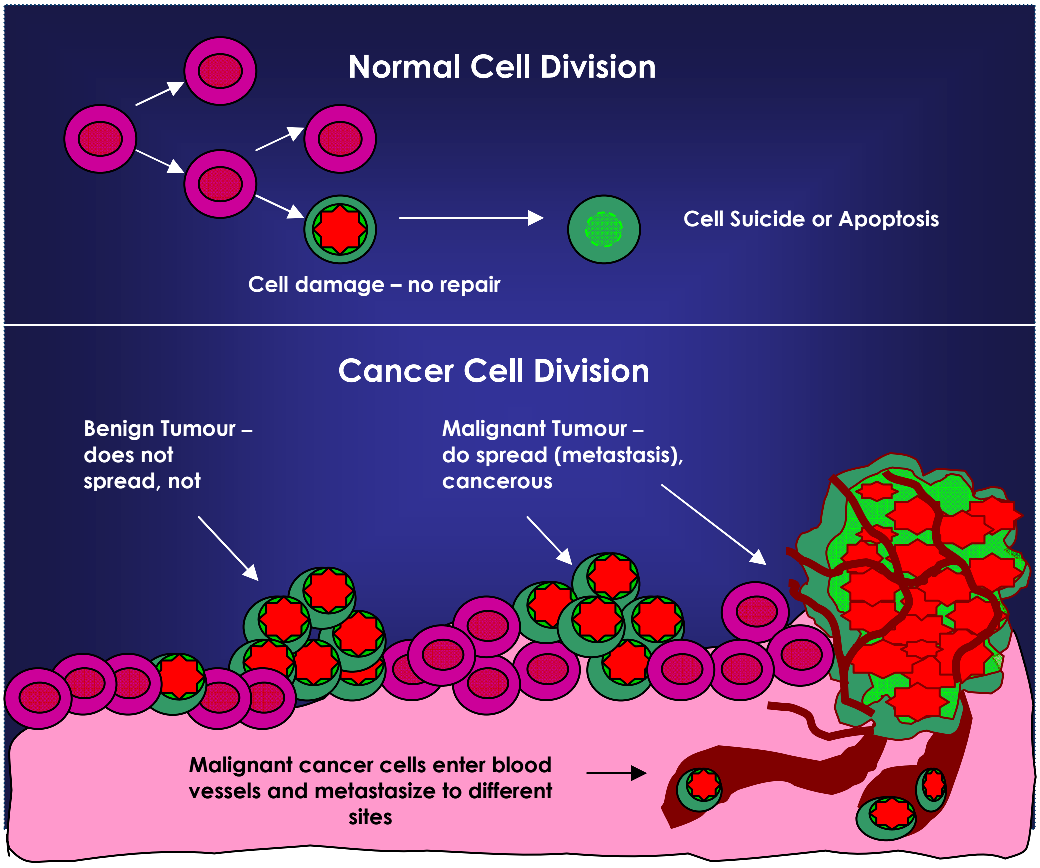

Figure 1: Comparison of normal cell division and cancer cell division[6] (Adapted from http://www.cancer.gov/cancertopics/understandingcancer/cancer/).

Malignant tumours may be gathered into broader classifications[5, 6]. The main categories include[6, 7]:

- Carcinoma - abnormal tissue growth that originates within the skin or in the tissues that line or cover internal organs; e.g., adenocarcinoma, basal cell carcinoma, squamous cell carcinoma, and transitional cell carcinoma.
- Sarcoma - anomalous development within the bone, cartilage, fat, muscle, blood vessels, or supportive tissue; e.g., osteosarcoma (bone cancer), chondrosarcoma (cartilage cancer), liposarcoma (fat cancer), breast cancer (tissue cancer), and lung cancer (tissue cancer).
- Leukaemia - tumour that originates in myeloid and lymphoid tissue (blood-structuring tissue) which stimulates the production of large number of aberrant blood cells that penetrate through the blood stream; e.g., lymphocytic leukaemia, chronic lymphocytic leukaemia, acute myelogenous leukaemia, and chronic myelogenous leukaemia.
- Lymphoma and myeloma - malignancies that originate within the cells of the immune system; e.g., plasma cell myeloma and Hodgkin’s lymphoma.
- Central nervous system (CNS) cancers - abnormal development inside the tissues of the brain and spinal cord; e.g., CNS embryonal cancer and neoplastic meningitis.

Cancer is the major cause of death in the developing world[8] with 13% of all deaths that occur worldwide resulting from cancer[8]. Consistent with reports by the American Cancer Society[8], the National Health Interview Survey[9] and the International Agency for Research on Cancer (IARC)[10], approximately 12 million people worldwide died from cancer in 2008. The most common malignancies reported in 2008 are; lung cancer (1.6 million deaths), stomach cancer (738,000 deaths), liver cancer (695,900 deaths), colorectal cancer (608,700), and breast cancer (458,400 deaths)[11]. Current trends suggest that mortality associated with cancer is predicted to rise to 21 million by 2030, and new diagnoses of cancer are anticipated to increase from 11 million to 16 million per annum[12]. In Australia, 121,500 new instances of cancer will be diagnosed in 2014, and the number will rise to 150,000 by 2020[13].

1.2. Treatment of cancer

Cancer may be effectively treated by early detection and surgical removal of the tumour before metastasis. If metastasis occurs before the detection of a tumour, then surgery alone is not sufficient; secondary treatments such as radio- or chemotherapy are required. Three prevailing methods utilised in cancer treatment, either independently or in combination, are; surgery, radiotherapy and chemotherapy[14, 15]. Surgery is usually employed in conjunction with radiotherapy and chemotherapy. Radiotherapy is utilised as a therapeutic medicine, in association with alternate methodologies, in that radiation is employed to eradicate and prevent the development of cancer cells[10, 16, 17]. Significantly, side effects such as hair loss and fatigue are common in radiotherapy. Chemotherapy or drug therapy is designed to kill, or to delay the growth of cancer cells. In chemotherapy, the drugs interfere with mechanisms of cell division which leads to the side effects, such as nausea and vomiting (caused by damage to the gut lining and brain), hair loss (damage to hair follicles), anemia and risk of infection (by damage to the production of white blood cells)[18, 19]. Targeted drug therapy is an advanced type of cancer treatment, which can be defined as drugs developed against a specific target based on its important biological function in the treatment of cancer[20]. It appears to be a promising area for the treatment of cancer as it uses drugs or alternate substances to selectively recognise and eradicate cancer cells, while doing minimal damage to the healthy cells[21, 22].

1.3. Targeted therapy

Targeted cancer therapies use drugs which aim to specifically inhibit biochemical pathways in tumour growth and progression[20], rather than inhibiting all promptly dividing cells (as in traditional chemotherapy). The fundamental classification of targeted therapy incorporates drugs that may interfere with angiogenesis (development of blood vessels inside the tumour), inhibit metastasis, stimulate the precise death of cancer cells or elevate the immune system to specifically kill cancer cells[20, 22].

A classical example of targeted therapy is that of the drug imatinib mesylate (also known as Gleevec or STI-571)[23]. Imatinib is administered in cases of gastrointestinal stromal tumours (a rare cancer of the gastrointestinal tract), leukaemia, dermatofibrosarcoma protuberans, myelodysplastic or myeloproliferative disorders, and systemic mastocytosis[23]. The drug focuses on distinct members of category of proteins known as tyrosine kinase enzymes that take part in signal transduction. The mechanism of action of imatinib mesylate is given below (Figure 2).

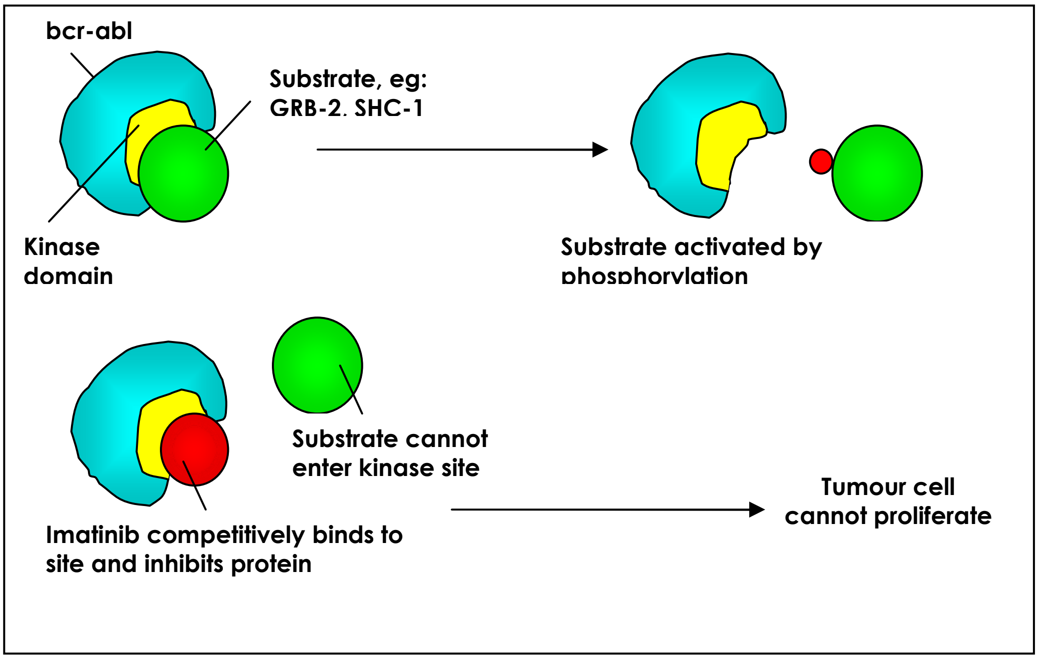

Figure 2: Mode of action of Imatinib[23]; Tyrosine Kinase = Enzyme that can transfer a phosphate group from ATP to a protein in a cell; BCR-ABL = tyrosine kinase inhibitor gene; GRB-2 = Growth factor receptor-bound protein 2 (an adaptor protein involved in cell communication); SHC-1 = Src homology 2 domain containing protein 1 (regulates apoptosis and drug resistance in mammalian cells).

The fundamental challenge of targeted therapy is to overcome the ability of the cancer cell to develop resistance to the drug[20, 22]. For instance, a mutation in the BCR-ABL gene may result in acquired resistance to Imatinib[20] and prevent it from being inhibited by the drug. Hence, targeted therapies may work advantageously together, either with alternate targeted therapies or with various conventional therapies[20, 23], an approach known as co-administration or cocktail therapy.

1.4. Challenges of drug discovery and current cancer therapies

Current cancer drugs generally suffer from the problem that they are only slightly less toxic to healthy cells than towards the cancer cells[24], in other words they have a narrow therapeutic window. Common symptoms and side-effects may result from both radiotherapy and chemotherapy as the treatments affect rapidly developing and normally multiplying cells in addition to rapidly proliferating malignant cells. Nausea, vomiting, hair loss, fatigue, low white blood cell count and low platelet count are generally observed symptoms in cancer patients receiving these therapies[17]. Research in drug design for the treatment of cancer is hence guided towards designing medications that are more toxic towards cancerous cells than healthy cells[25, 26].

The main challenge of drug discovery is the management of drug toxicity and comprehension of the species which are responsible for tumour malignancy. Research to date has demonstrated important progress in the application of metal complexes as drugs to treat numerous human diseases[27-30]. For instance, the gold anti-rheumatic drug auranofin (2,3,4,5-tetra-O-acetyl-1-1-β-D-thioglucose(triethylphosphine)gold(I)) is employed to treat rheumatic arthritic patients who are intolerant of other medicines[31, 32]. It was the first orally administered gold anti-rheumatic drug, however, its precise pharmaceutical mode of action is unknown[33, 34]. To analyse the mechanism of biological action of the drug, we must independently consider the roles played by either the metal or its ligands or the whole metal complex itself. For example, the anti-cancer pharmaceutical agent bleomycin apparently interacts with metal ions which have important functions in the body[35]. The biological efficiency of bleomycin is believed to be conferred by its ability to induce single- and double-strand DNA duplex cleavage and this DNA cleavage activity has been shown to be both Fe^{2+} and O_2 dependent[36]. In bleomycin, the metal binding domain is joined through a linker peptide to a positively charged bithiazole "tail" (C-terminal) that alters the drug-DNA binding affinity[37]. The metal binding domain is also bound to a disaccharide moiety that improves the efficiency of DNA cleavage[38]. The discovery of metal-based drugs has led to increased application of metal complexes in the treatment of cancer.

2. Metal-based drugs

Transition metal complexes have made a tremendous contribution to medicine, particularly in cancer therapy[39]. Many compounds have been synthesised, screened, investigated and then modified in an attempt to increase their efficacy. From a chemical standpoint, the main advantage of metal-based drugs, in comparison with other cancer drugs, is their ability to change coordination number, geometry, and redox state[39-41]. In addition, metals can alter the biological characteristics of organic-based drugs by making coordination complexes with them[42]. According to Hambley, T. W. (2007)[43], metal-based pharmaceuticals can be organised into seven classes relying upon the properties of the metal and ligand components;

1) metal complexes that are active in their inert form,
2) metal complexes that are active in their reactive form,
3) metal complexes in which the metal can act as a radiation enhancer,
4) compounds which can hold a radioactive metal,
5) complexes in which the metal or its bio-transformation product is unstable,
6) ligands that are biologically active (targeting strategy), and
7) complexes in which only one component is active (prodrug strategy).

The outcomes of the research based on the above classification[43] illustrates the importance of metals in the pharmaceutical research, as complexes in each category displayed different biological activity and had varied challenges in the preclinical trials[43]. Hence, the current biomedical or pharmaceutical research should focus more on the role of the metals in the treatment of metastasis, and more metal complexes should be explored for inhibiting metastasis either by molecular targeting or chemical targeting[43].

2.1. Platinum-based anti-cancer agents

Cisplatin, *cis*-$[PtCl_2(NH_3)_2]$ was the first metal-based anti-cancer drug[44] to undergo a clinical trial for cancer and is widely used for the treatment of testicular and ovarian cancers. It is employed against different types of solid tumours (head or neck, lung, cervical, and bladder), and offers more than 90% cure rate in the case of testicular cancer[45, 46]. It was first synthesised by Peyrone in 1845 (known as Peyrone's salt)[47], and its structure was elucidated by Alfred Werner in 1893[44, 48]. The anti-cancerous activity of cisplatin was first ascertained serendipitously by the bio-physicist Barnett Rosenberg[44, 49], during experiments on the role of electric currents in cellular division. In the solutions of NH_4Cl, platinum electrodes and sunlight, *E.coli* cells grew up to three hundred times their normal length; however the cells failed to divide. Rosenberg came to the conclusion that the inhibition of cellular division was not due to the electric current, instead because of the formation of hydrolysis products close to the platinum electrodes[49]. It was also eventually noted by Rosenberg and his co-workers that the *cis*-form of the hydrolysis product as resposible for the inhibition of cellular division and the *trans*-form was discovered to be inactive against cancer cells[44].

Based on these outcomes, the platinum(II) complex, *cis*-$[PtCl_2(NH_3)_2]$, and the platinum(IV) complex, *cis*-$[PtCl_4(NH_3)_2]$, were tested against sarcoma tumours in Swiss white mice. The complexes exhibited anti-cancerous activity and improved survival of the mice was reported[44]. Subsequently, cisplatin entered clinical trial and is currently administered as one of the most efficacious anti-cancer drugs in the clinic[44].

The mechanism of action of cisplatin is attributed to the formation of stable bi-functional adducts with DNA, which then prevent replication, or inhibit transcription, of DNA[44, 50]. Cisplatin is transported into tumour cells by passive diffusion and activated because of the low intracellular concentration of chloride ions (as the chloride ions in cisplatin are displaced by water molecules)[51, 52]. About 98% of the absorbed cisplatin binds to the DNA of the tumour cell and creates bent structures which then inhibit DNA replication, resulting in apoptosis[53].

Cisplatin treatment shows severe side effects including blood clotting, thinned or bristled hair, loss of appetite or weight, diarrhoea, nausea and vomiting[53]. Other disadvantages of cisplatin include; resistance towards colon and non-small lung cancer cells, decreased drug accumulation (as increased drug resistance of cancer cells), and poor target selectivity[53]. In an attempt to reduce these side effects and disadvantages, cisplatin analogues have been developed and tested for anti-cancer activity[54]. Several of these analogues were found to have equivalent activity to that of cisplatin. Some of the most important platinum complexes are given in Scheme 1.

Carboplatin is a Pt(II) cisplatin derivative in which two chlorido ligands of cisplatin are replaced by a cyclobutane dicarboxylate group and is active against ovarian carcinoma, lung, head and neck cancer[51]. Carboplatin exhibits a considerably lower nephrotoxicity when compared to cisplatin since it can act as an alkylating agent which can trigger the formation of cross links between DNA strands[51]. The intracellular reaction replacing the chlorido ligands by water molecules is then slowed, leading to the inhibition of protein synthesis and a decreased reactivity of the compound towards DNA and other molecules in the cell[55].

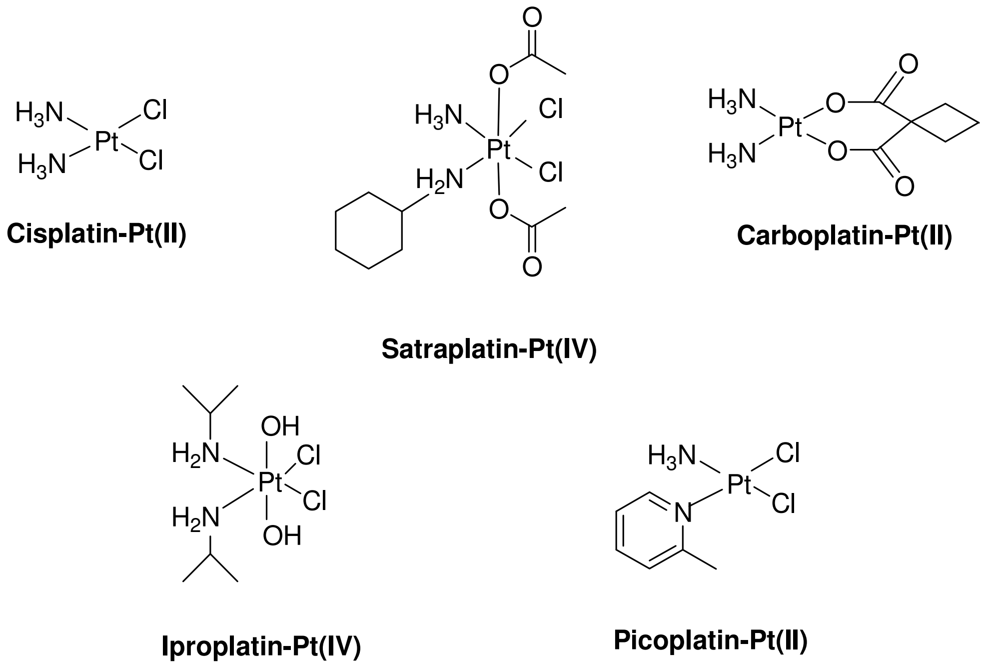

Cisplatin-Pt(II)

Satraplatin-Pt(IV)

Carboplatin-Pt(II)

Iproplatin-Pt(IV)

Picoplatin-Pt(II)

Scheme 1: Reported platinum-based anti-cancer agents[45].

Iproplatin was the first platinum(IV) complex in clinical trials having an octahedral configuration, rather than the square-planar Pt(II) configuration of cisplatin and carboplatin[56]. Iproplatin is also less toxic than cisplatin, however it is more toxic and less active than carboplatin[57].

The Pt(IV) complex, satraplatin, possesses increased water solubility and is the primary orally available derivative of cisplatin. The increased solubility was accomplished by the addition of a lipophilic acetate leaving group[51]. It is active against some cisplatin-resistant cell lines, suggesting substantial changes in the mechanism of action or in the cellular responses to the DNA damage caused by cisplatin and satraplatin[56].

Picoplatin (a Pt(II) complex) is a cisplatin derivative in which the platinum center is less susceptible to ligand replacement by thiol-containing molecules[51] which render the compound inactive. It is orally available and is efficacious against cisplatin resistant cancers, where the resistance arises from the elevated intracellular levels of glutathione[56] to which picoplatin is less reactive.

In spite of the fact that cisplatin and its analogues are effective in the treatment of testicular and ovarian cancer[45], they have restricted activity against bladder and lung cancer[21]. The main disadvantages of these drugs are that they display a limited spectrum of activity, extensive side effects and a narrow therapeutic window[56]. The success of cisplatin and its analogues as anti-cancer agents have created interest in the use of other coordination metal compounds which may display a broader spectrum of activity and a wider therapeutic window.

2.2. Ruthenium-based anti-cancer agents

2.2.1. Platinum to ruthenium

Despite the success of platinum-based anti-cancer compounds in the clinic, anti-cancer research requires the development of enhanced anti-cancer drugs having wide therapeutic windows. Platinum drugs bind DNA, causing damage that affects protein synthesis and replication, and stimulate apoptosis[58]. Ruthenium drugs were initially intended to mimic platinum drugs, especially in targeting DNA. Ruthenium complexes were generally found to have reduced toxicity and a limited side effect profile when compared with platinum drugs[21]. They additionally have the capacity to overcome the resistance elicited by platinum drugs in cancer cells due to their distinctive physiochemical properties[59] which are discussed below.

Ruthenium can access different oxidation states under biologically relevant conditions[21, 60, 61] viz; Ru(II) (d^6, diamagnetic) and Ru(III) (d^5, paramagnetic)[60]. The energy required for the conversion between these oxidation states inside the cell is small when compared to that in physiological solution; apparently prompt interconversion occurs inside the cell[62]. Ruthenium ions can adhere to intracellular bio-molecules, and may remain attached for the remainder of that cell’s lifetime[45] (Figure 3). Ruthenium forms strong chemical bonds in both its oxidation states with chemical compounds of varied chemical properties, such as hardness and electronegativity and thus may bind to different bio-molecules in addition to DNA[21, 63].

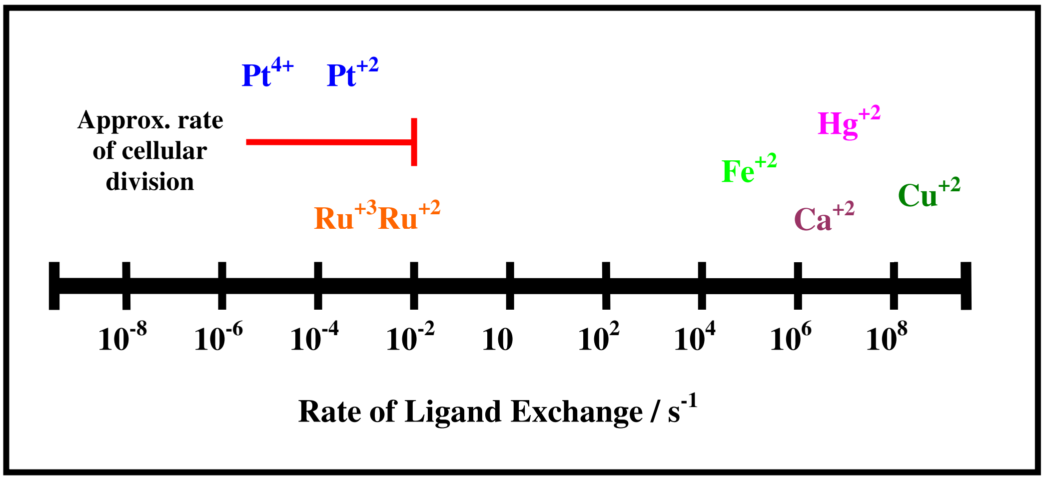

Figure 3: A selection of ligand exchange rates of platinum group metals with those of other metals[45, 64]. The approximate rate of cellular division (10^{-2} / s^{-1}) is closer to ligand exchange rates of platinum group metals (Pt and Ru). (Adapted from Page, 2012[64]).

2.2.2. Ruthenium(III) complexes

Ruthenium red (**1**, Scheme 2) was the first ruthenium complex investigated for its anti-cancer properties[65, 66]. The anti-tumour properties of ruthenium complexes were further examined with the compounds *fac*-$[RuCl_3(NH_3)_3]$ (**2**, Scheme2) and *cis*-$[RuCl_2(NH_3)_4]Cl$ (**3**, Scheme 2)[67]. The main disadvantage of these complexes (**1**, **2**, and **3**; Scheme 2) was their low solubility in physiological media and, as a result, a broader range of ruthenium(III) complexes were investigated for biological activity. The synthetic efforts led to the development of exceptionally water soluble *cis*- and *trans*-$Ru(DMSO)_4Cl_2$ complexes (**4** and **5**, Scheme 2) and the *trans* derivative was discovered to have enhanced anti-metastatic activity compared to the *cis* form[60, 68-71]. Two classes of Ru(III) complexes, based on these prototypes, were synthesised and thoroughly investigated, as both were demonstrated to have *in vivo* activities distinct from those of the platinum drugs[21, 59].

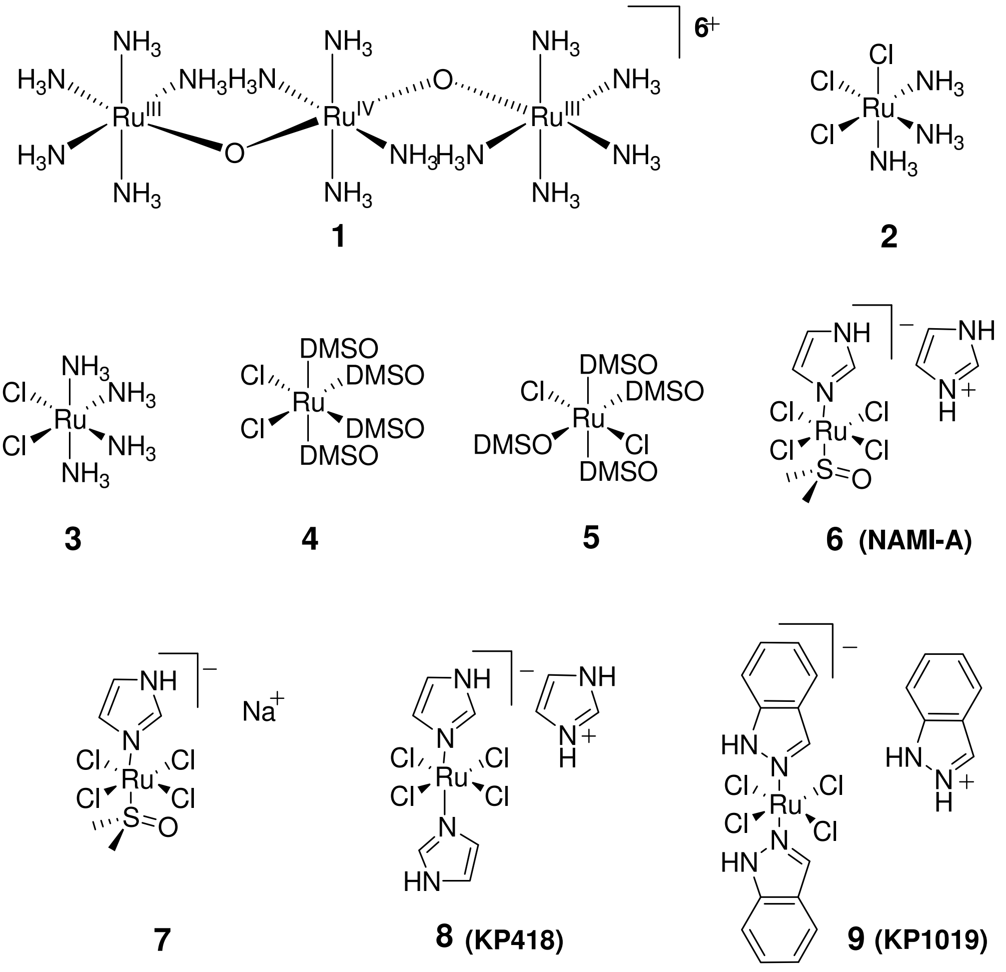

Scheme 2: Representative examples of Ru(III) complexes explored as anti-cancer agents.

Mestroni *et al.* (1998) introduced the Ru(III) complex, NAMI-A[72] ([ImH][*trans*-$RuCl_4$(DMSO)(Im)], **6**, Scheme 2; Im = Imidazole) as the imidazolium salt of the previously discovered compound NAMI (**7**, Scheme 2; [Na][*trans*-$RuCl_4$(DMSO)(Im)]). The acronym, NAMI stands for new anti-metastatic inhibitor and 'A' means the first reported analogue in the series. Both **6** and **7** exhibit specific activity against solid metastasizing tumours in mice[68]. NAMI-A was the first ruthenium anti-tumour complex to enter clinical testing[68] and has successfully completed a Phase I clinical trial at the Netherlands Cancer Institute of Amsterdam[67].

Keppler and co-workers subsequently introduced a second class of Ru(III) complexes; KP418 or ICR (**8**, Scheme 2)[73] and KP1019 (**9**, Scheme 2)[74]. Keppler-type complexes [HL][*trans*-$RuCl_4L_2$] (**8**; L=imidazole and **9**; L=indazole), displayed promising results in preclinical studies against colorectal autochthonous tumours (which are resistant to platinum based drugs),[75, 76] and a variety of primary ex-planted human tumours[77].

NAMI-A and KP1019 are quite similar in structure (**6** and **9**, Scheme 2), however they show remarkably diverse malignant neoplasm activities. KP1019 is effective against primary neoplasm[21, 78] (i.e., the principle tumour mass formed first in a patient), while NAMI-A is effective against secondary neoplasm[21] (i.e., the metastases formed when cancer cells from the primary neoplasm have displaced to a distant organ, through the bloodstream).

NAMI-A undergoes aquation reactions immediately when dissolved in plasma, whereas KP1019 is more resistant when compared to NAMI-A, and undergoes ligand exchange reactions (loss of chlorine ligand) within minutes under physiologically relevant conditions to yield a mono-aqua complex[62, 79]. These compounds have been demonstrated to target both bio-molecules (such as DNA) and proteins[62]. KP1019 adheres to transferrin (an iron transporting protein), and is released as a Ru(II) species once reduced by ascorbate or glutathione[80, 81]. The disruption of iron metabolism can be considered as a potential mechanism for the anti-tumour activity of Ru(III) complexes[62], although the precise mechanism of action is not yet fully understood.

2.2.3. Ruthenium(II) arene complexes

Several ruthenium(II) based organometallic compounds are well known for their increased water- and air-stability and exceptional anti-cancer activity[61, 64, 82-84]. The Ru(II) complexes are stabilised by a π-bonded arene ring and hence, do not undergo facile oxidation to Ru(III). The synthesised compounds are ionic and have an exceptional solubility in water[61, 64] (Scheme 3).

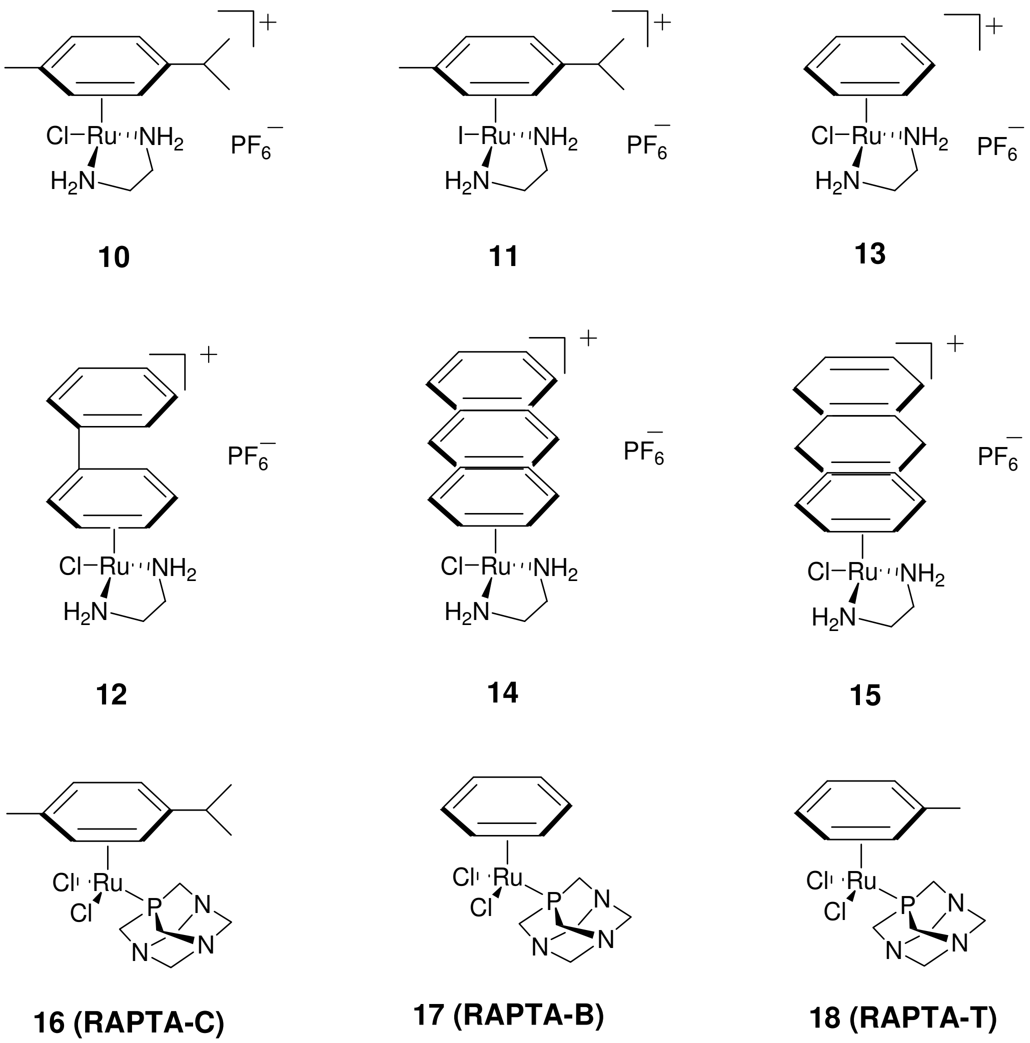

Scheme 3: Representative examples Ru(II) complexes and RAPTA compounds that have been evaluated *in vitro* and/or *in vivo*[85].

The anti-cancer activity of ruthenium(II) arene complexes, [(η^6-p-cymene)RuCl(en)]PF_6 (**10**, Scheme 3), [(η^6-p-cymene)RuI(en)]PF_6 (**11**, Scheme 3), and [(η^6-$C_6H_5C_6H_5$)RuCl(en)]PF_6 (**12**, Scheme 3), (p-cymene = 1-isopropyl-4-methylbenzene) were examined in a human ovarian cancer cell line (A2780) and the results indicated that the IC_{50} values were in the same range as that of the anti-tumour drug carboplatin (6-9 μM) [86, 87]. The IC_{50} values were found to increase when arene group present in the complex was modified. The increasing order of IC_{50}: benzene (**13**) < p-cymene (**10**) < biphenyl (**12**) < dihydroanthracene (**14**) < tetrahydroanthracene (**15**).

Anti-tumour activity was discovered in a second subclass of highly water soluble organometallic ruthenium(II) compounds [(η^6-p-cymene)RuX$_2$(pta)] (X = Cl, Br, I, SCN; pta = 1,3,5-triaza-7-phosphatricyclo [3.3.1.1]decane)[88, 89] generally known as RAPTA complexes (**16**, **17**, **18**; Scheme 3). Investigations in SK-N-SH neuroblastoma cells have reported that these compounds induce apoptosis at low micro-molar concentrations through an unidentified mechanism[88, 89]. RAPTA complexes are constituted by a facially coordinated aromatic ring (which is moderately hydrophobic) and a PTA (1,3,5-triaza-7-phosphaadamantane) ligand (which confers the high water solubility)[88, 89]. Surprisingly, the RAPTA complexes display a spectrum of activity which is comparable to that of the coordination complex NAMI-A, despite their apparent differences in oxidation state, ligands, charge and geometry[88, 89] The *in vivo* anti-cancer activity of both classes of complexes may be due to the hydrolysis of chlorido ligands and the extent of activity is believed to depend on the number of such ligands present in the complex and the pH of the solution[88, 89].

2.2.4. Ruthenium multinuclear complexes

The application of ruthenium complexes in pharmaceutical chemistry has recently been investigated due to their ability to form multinuclear and supramolecular compounds with anti-cancer properties. These investigations produced several novel concepts that include ruthenium platinum mixed-metal compounds[90], ruthenium cluster complexes[91, 92], ruthenium DNA intercalators[93-96] and supramolecular 'Trojan Horses', that can produce a poisoning effect once delivered to the cancer cell[97].

Amongst these categories, ruthenium DNA intercalators have received a lot of recent attention. It has been suggested[95, 96] that ruthenium(II) octahedral complexes can be developed as anti-cancer DNA intercalators (**19**, **20**, and **21**; Scheme 4).

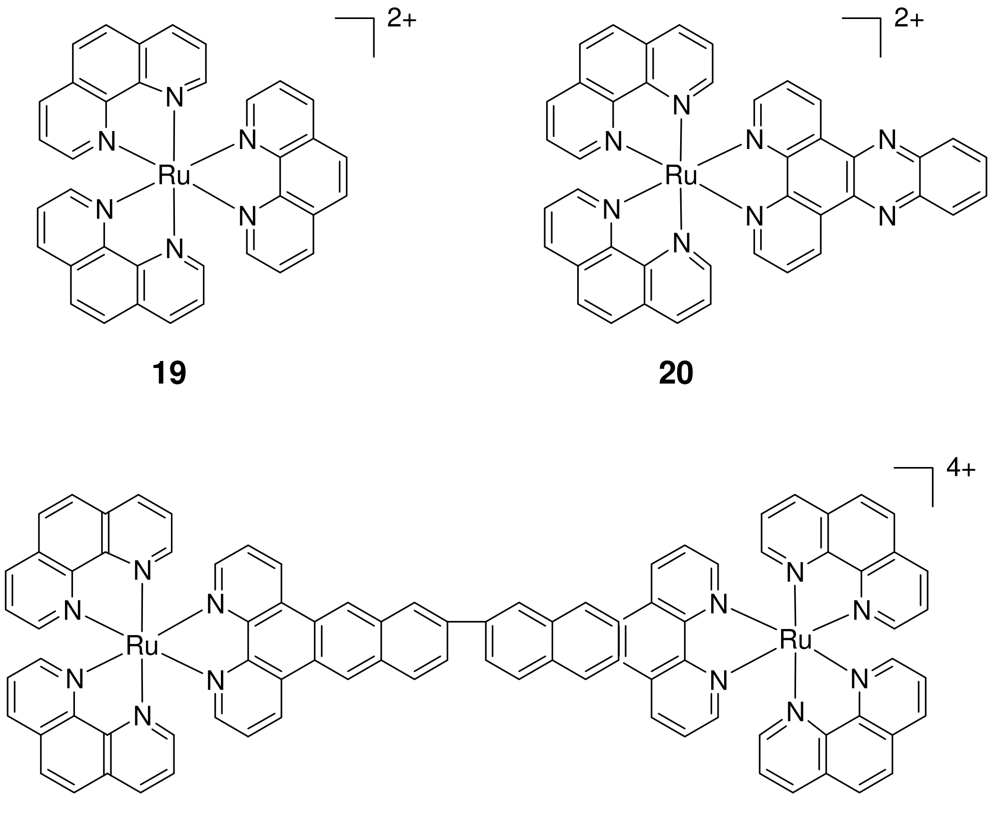

19 **20**

21

Scheme 4: Representative examples of ruthenium(II) octahedral metallointercalators[95]. Anions have been omitted for clarity.

The biological activity of **19** was first shown by Dwyer *et al.* (1952)[98]. The studies conducted in mice demonstrated a difference in the biological activity of Λ- (left-handed; lambda isomer) and Δ- (right-handed; delta isomer) enantiomers of **19** ($[Ru(phen)_3]^{2+}$, phen = 1,10-phenanthroline; Scheme 4)[95, 98]. Subsequent investigations on the binding properties of this complex demonstrated two modes of interaction with DNA, either through intercalation or through surface interaction[95]. The DNA binding properties of **20** ($[Ru(phen)_2dppz]^{2+}$, dppz = dipyrido [3,2-a:2`,3`-c]phenazine, phen = 1,10-phenanthroline; Scheme 4) were investigated and it was reported that the complex bound to DNA by intercalation[95]. The binding constant for this intercalation was found to be greater than 10^6 M^{-1} which is a characteristic of a metal complex containing the dppz ligand[95].

Compound **21** ($[\{Ru(phen)_2\}_2\mu\text{-}(didppz)_2]^4$+; Scheme 4) is an example for bis-intercalator which has greater cytotoxicity than **19** or **20**, due to its increased DNA binding affinity (ability to bind more than one DNA base pair)[95]. Bis-intercalators can specifically target cancer cells due to their DNA specificity and selectivity towards specific gene sequences[95]. When the DNA binding affinity increases, an increased number of DNA-drug adducts will be formed and the complex will be more cytotoxic due to the non-repairable conformational changes to DNA[95].

2.3. Challenges of ruthenium-based drugs

Current chemotherapies regularly fail to attain cancer cell selectivity as apparent from the regularity of the side-effect symptoms that are observed[17]. This is due to the fact that the therapeutic agent will affect both normally proliferating cells and rapidly developing malignant cells[17, 99].

Research in drug design for the treatment of cancer is still largely focussed on creating drugs which are more toxic towards cancerous cells than they are against normal tissues[99, 100]. The research mainly focuses on the interaction of the active drug with critical biomolecules (e.g., cisplatin, which interacts with DNA[44]) that are needed in excessive amounts for the rapidly dividing tumour cell, such as amino acids and nucleotides[100]. Cisplatin and its derivatives are toxic to cancer cells as well as to normal healthy cells[100]. Ruthenium-based drugs, however, are toxic towards cancer cells, but display significantly lower toxicity towards normal cells, in comparison with cisplatin analogues[45, 85, 101]. Henceforth, new ruthenium complexes with fewer side effects could replace the platinum-based drug which is the ultimate challenge for the development of ruthenium-based chemotherapeutics.

2.4. Importance of this study

In order to overcome the main drawbacks of metal-based drugs such as drug resistance and cytotoxicity, it is necessary to have an accurate knowledge about the actual mechanism of action of these drugs in a complete biological system.

This project is mainly based on the study of the mechanism of action of NAMI-A and KP1019, using advanced techniques such as synchrotron-based X-ray absorption spectroscopy (XAS) and X-ray fluorescence (XRF) imaging. Knowledge about the reduced toxicity of ruthenium-based anti-cancer drugs towards normal healthy cells can lead to the discovery of some new drugs which have a wider therapeutic window than platinum-based drugs.

3. Mechanism of action of ruthenium-based drugs

Various pathways have been proposed to explain the anti-cancer activity of ruthenium-based drugs. These are summarised in the general mechanism of intercellular transport of ruthenium anti-cancer agents indicated in Figure 4. It has been suggested that NAMI-A selectively inhibits tumour metastasis *in vivo* because of its greater interaction with either collagen or actin-type proteins on the cell surface[102-104]. This may influence the interaction of the cancer cells with the extracellular matrix, resulting in diminished cell invasiveness and relocation of tumour cells[105-108]. A recent study by Levina *et al.* (2013) demonstrated that the cellular uptake of KP1019 is nearly twenty-fold more than that of NAMI-A under identical experimental conditions[109]. Both compounds (NAMI-A and KP1019) may undergo changes in the coordination environment of ruthenium under biological relevant conditions to form polynuclear $Ru^{IV/III}$ clusters. On contrary, rate of ligand exchange for KP1019 was found to be lower than that of NAMI-A as evidenced by the results from XAS analysis[109]. The uptake of KP1019 decreases rapidly following dissolution of KP1019 in the cell-culture media, which demonstrates that the complex is taken up by cells via passive diffusion due to the higher lipophilicity of the ligands present in KP1019 than in NAMI-A[109].

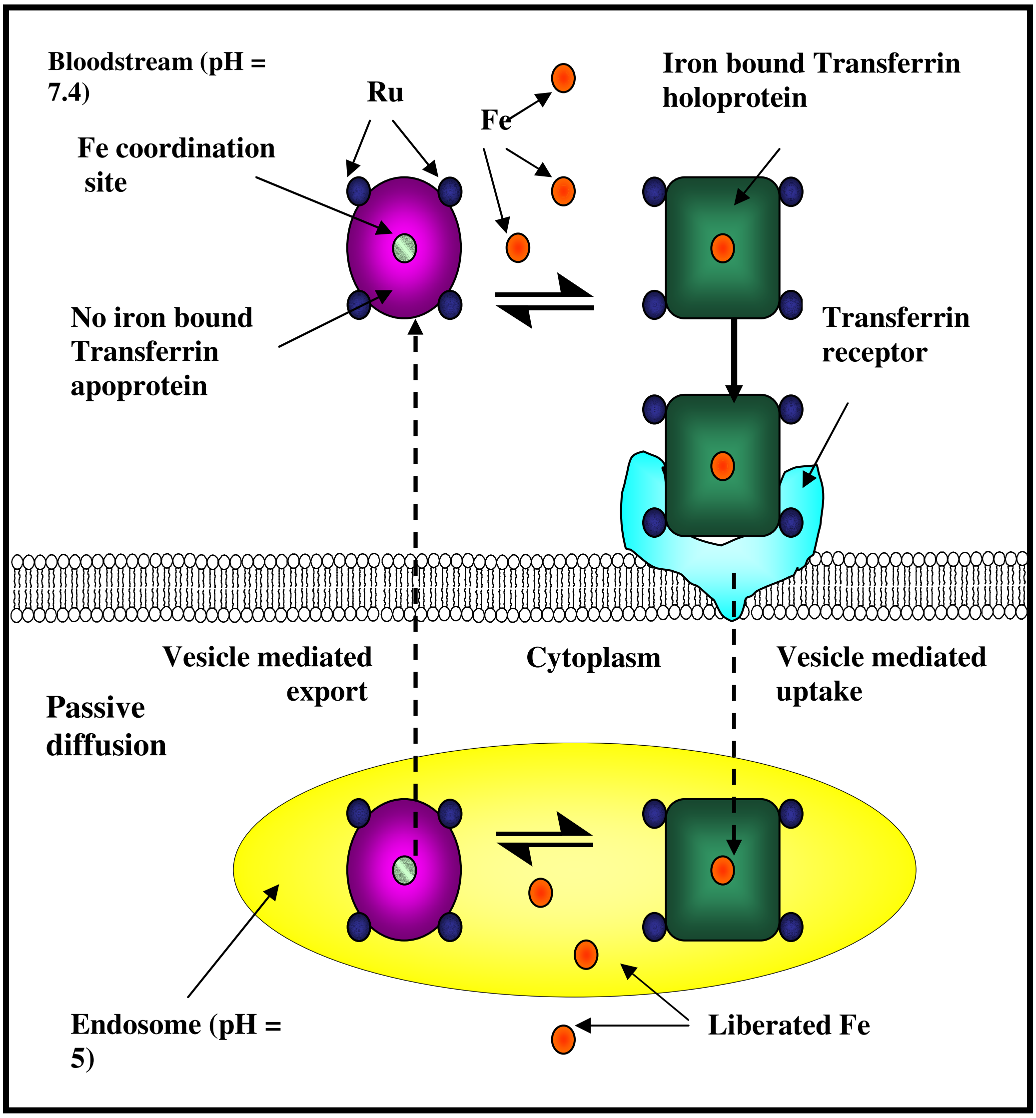

Figure 4: Proposed mechanism of intercellular transport of ruthenium based anti-cancer agents[64]. (Adapted from Page, 2012[64])

3.1. Activation by reduction

One theory proposed for the low toxicity of ruthenium compounds towards healthy cells when compared with platinum drugs is the so-called 'Activation by Reduction'[21, 110] proposal. Numerous *in vitro* experiments have indicated that ruthenium-based complexes are activated by reduction[21, 110]. This theory is dependent on the perception that ruthenium(III) complexes are kinetically inert when coordinated by a number of $\pi-$ donating ligands such as chlorido[21, 111]. When ruthenium drugs are administered to a cancer patient, the complexes maintain their +III oxidation state until they reaches at the tumour site. The Ru(III) species will then be reduced to more active Ru(II) species once entering the tumour cells, as they have a low molecular oxygen concentration and greater reducing environment, when compared to healthy cells[111]. This hypothesis has recently undergone extensive scrutiny and the fate of the ruthenium complexes in the tumour cells has been the topic of extensive literature discussion[58, 59, 64, 112, 113] (*explained in detail* **6.1**).

3.2. Iron mimicking

Iron and ruthenium belong to the same group in the periodic table. This has resulted in the proposal that Ru is capable of substituting for Fe in some proteins, e.g., in the chaperone and uptake protein transferrin[114, 115]. Ru(III) complexes have been shown to bind with serum proteins, such as albumin and transferrin, soon after entering the blood stream[116-119]. Evidently, serum transferrin (an iron-binding protein) has been recognised as a potential target for ruthenium-based drugs[63].

Because ruthenium can potentially simulate iron in biological systems, investigations have assessed whether or not ruthenium-based drugs bind to the transferrin at iron sites[120]. The results suggested that the transferrin–ruthenium complexes may be carried into tumour cells, as they have high transferrin-receptor densities[120]. The complex may then liberate Ru(III) inside the cancer cell which could be reduced to Ru(II) as a consequence of the diminished oxygen content and pH compared to healthy cells[120]. Nevertheless, the healthy cells generally have iron binding sites with great affinity towards iron; for instance, human serum transferrin has two iron binding sites in two structurally similar lobes (N- and C- lobes) connected together by a short peptide[121, 122]. In the iron binding site, iron is octahedrally coordinated to four amino acid residues such as two tyrosine (oxygen, O-), one histidine (nitrogen, N-) and one aspartic acid (oxygen, O-) and two ligands (oxygen, O-) of a bidentate carbonate anion or synergistic anion with a binding affinity of 10^5 to 10^{10} M^{-1} [64, 121, 123]. The presence of a synergistic anion facilitates high affinity iron binding in transferrin[122]. The synergistic bidentate carbonate anion has an enhanced iron binding affinity greater than the sum of the binding effects exerted by two individual carbonate ions[121, 122].

During the uptake of the iron, transferrin undergoes structure reorganization or conformation changes to distorted octahedral geometry to form diferric-transferrin molecule (Fe_2-Tf)[121, 122]. The healthy cells uptake iron from Fe_2-Tf adduct via a transmembrane transport known as endocytosis[121]. The process is initiated when the diferric-transferrin molecule was bound to a specific transferrin receptor (TfR) on the outer face of the cell membrane[121, 122]. The resulting complex was then internalized into endosome through endocytosis[121]. At pH ~ 5.5, the acidified endosome releases the iron which was then transported to the cytoplasm by the divalent metal transporter (DMT1)[121]. The released iron was utilized for metabolic activities or stored in Ferritin. The transferrin (Tf) and the transferrin receptor (TfR) were returned to the cell surface or plasma membrane and undergo further cycles of intracellular iron uptake[121].

It has been questioned whether ruthenium can challenge iron in those conditions and has an inclination towards 'softer' ligands[124] (*explained in detail* **6.2**).

3.3. Hydrolytic pathway to activity

According to Bacbac *et al.* (2004), the biological activity of ruthenium(III)-based drugs can be attributed to their hydrolysis products[125]. NAMI-A and its analogues undergo pH-dependent hydrolysis in aqueous solution, which can influence their biological properties[126, 127]. In aqueous medium, chlorido ligands were displaced by water resulting in the formation of mono- and di- aqua complexes (Figure 5). NMR evaluation of the hydrolysis of NAMI-A[125] in a diverse range of chloride ion concentrations (0 – 1 M) and pH (3.0 – 7.4) has demonstrated that NAMI-A experiences hydrolysis of both chloride and DMSO ligands at pH ~ 7.4. The hydrolysis resulted in a mixture of species which accounts for the disappearance of the parent compound from the solution within 15 minutes. When the pH was less than 6.0, the complex was more reluctant to hydrolysis, leading to a controlled chloride hydrolysis and a moderate DMSO hydrolysis. It has been proposed that NAMI-A may undergo degradation in aqueous media in two different ways[125]. The first type of degradation may occur immediately after hydrolysis, i.e., substitution of the ligands based on the pH of the buffer solution[125] (e.g., chloride ions are replaced by water molecules). The second degradation may be induced by more substitution of ligands, polymerization, or reduction of the Ru(III) to Ru(II) (e.g., formation of mono- and di- aqua complexes)[125, 128].

The formation of mono- and di- aqua complexes were further investigated by a reported density functional study of model complex NAMI-A[128]. The coordinated DMSO ligand in NAMI-A may undergo dissociation in aqueous media at slightly acidic pH[128]. The rate of this dissociation was found to be inversely related to the basicity of the coordinated heterocyclic nitrogen ligand[21, 128]. It was also demonstrated that the presence of weakly basic ligands, such as pyrazine, pyrazole and thiazole, *trans* to DMSO increase the aqueous stability of the complexes compared to the model compound NAMI-A[126, 129, 130] (*explained in detail* **6.3**).

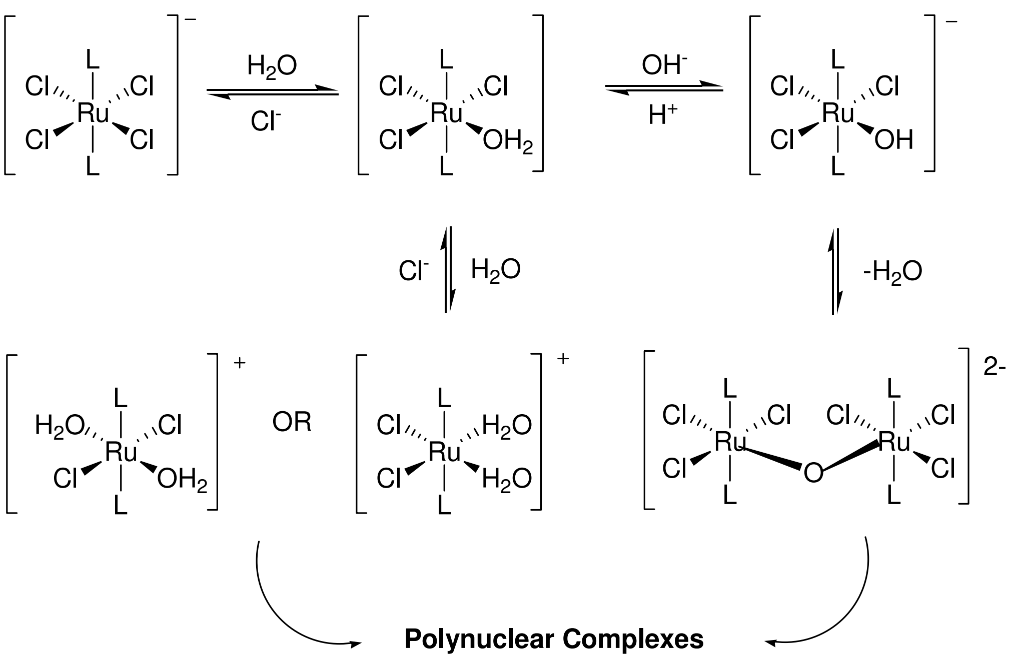

Figure 5: Possible hydrolysis pathways and decomposition species of the complex anion *trans*-$[RuCl_4L_2]^-$ in NAMI-A analogues[21], L = DMSO or imidazole or indazole.

3.4. Need for further studies

To date, a large amount of research has been directed toward the investigation of different modes of action of ruthenium-based drugs and their biomolecular targets. Presently, the two principle theories are that ruthenium compounds may target either DNA or proteins. Frausin *et al.* (2005), investigated the uptake and release of NAMI-A in KB-cells (KERATIN-forming tumour cell line HeLa; mouth epidermal carcinoma cells)[105]. KB cells were treated with NAMI-A for an hour at a concentration of 0.1 mM. The study suggested that the rapid release of ruthenium into the extracellular medium could be related to the pro-adhesive effect of NAMI-A at very low concentrations[105]. However, the mechanism of anti-metastatic activity of ruthenium-based drugs is still not fully understood. The model ruthenium compounds (NAMI-A and KP1019) were tested across a biological target in accordance with current progression in structure-based drug discovery[61, 84, 131, 132] (i.e., drug design is based on particular structural data of a biological target). However, a major restriction in the field is the absence of a proven biological target.

4. Ruthenium complexes as anti-cancer agents

4.1. Ru-based drugs act as prodrugs

A prodrug is defined as a medication which is given to a patient in the form of an inert complex that may consequently be converted to an active pharmacological drug when inside the body through various metabolic activities[40, 81]. Prodrug activation can be triggered by factors such as pH, light, and the redox environment[40]. Some ruthenium complexes are hypothesised to act as prodrugs[40] and to understand this prodrug mechanism, the redox chemistry of Ru(II)/Ru(III) has been studied[81, 133] (Figure 6).

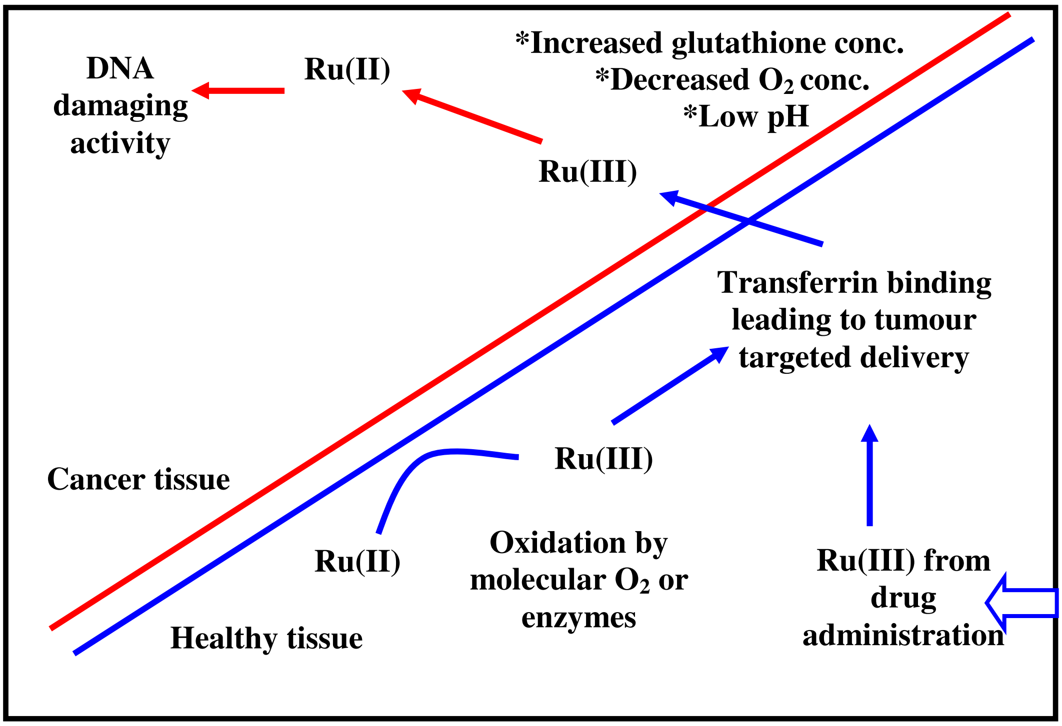

Figure 6: Change in oxidation state of ruthenium in cancer and healthy cells[112]. (Adapted from Dyson *et al*., 2001[112]).

Liu *et al.* (2010)[133] have investigated the biological properties of a Ru(III)-BSA (bovine serum albumin) adduct and the mode of Ru(III) binding in BSA, in comparison with NAMI-A by Ru K-edge XAS spectroscopy. The XAS studies showed that the coordination environment in Ru(III)-BSA adduct was considerably different from that of NAMI-A and 90% of the injected NAMI-A was intravenously delivered to blood where it binds with blood albumin[133]. These findings supported the idea that the pharmacological activity of NAMI-A could be attributed to its reactions in the biological environment and hence the conclusion that NAMI-A acts as a prodrug[133] (*discussed in detail* **6.2**).

To investigate whether a tumour hypoxic environment is necessary for the biological reduction of these Ru(III) complexes, a homologous series of Ru(III) complexes with a general formula $[RuCl_{(6-n)}(ind)_n]^{(3-n)-}$ (where n = 0–4; ind = indazole; counterions = Hind+ or Cl-) were synthesised and characterised electrochemically[134]. Cyclic voltametry investigations of these complexes showed that the reduction potential was increased with an increase in the ratio of indazole to chloride ligands[134]. A similar trend was observed for the cellular uptake of these complexes in colon cancer cells (SW480) and ovarian cancer cells (CH1)[134]. The complex *trans*-$[Ru^{III}Cl_2(ind)_4]Cl$, was reported to have a higher reduction potential than other complexes and reduced to *trans*-$[Ru^{II}Cl_2(ind)_4]$ by medium constituents[134]. The study[134] thus proposed that the reduction of Ru(III) to Ru(II) was catalysed by biological reductants and the hypoxic environment inside the tumour.

4.2. Anti-metastatic activity of NAMI-A analogues

One of the most significant challenges in cancer treatment is the prevention of metastases. The anti-metastatic effect is recognised to be a consolidated effect of anti-angiogenetic and anti-invasive properties of ruthenium complexes[85] (Figure 7).

NAMI-A is vigorously active across tumour metastases[135] and it specifically decreases the structuring and development of lung metastases (Figure 7) of malignant tumours such as MC a mammary carcinoma, lewis lung carcinoma (LLC) and adenocarcinoma[67]. *In vitro* studies[136] reported an impact on cell multiplication by the temporary interruption at G2-M phase (pre-mitotic stage) of the cell cycle. Studies also revealed that NAMI-A tends to bind with either proteins or RNA and thus alters protein expression, resulting in the thickening of the protein layer surrounding metastases[112, 137, 138]. Apparently, the tumour becomes secluded which prevents angiogenesis (formation of new blood vessels) and the escape of metastasizing cells[64, 113].

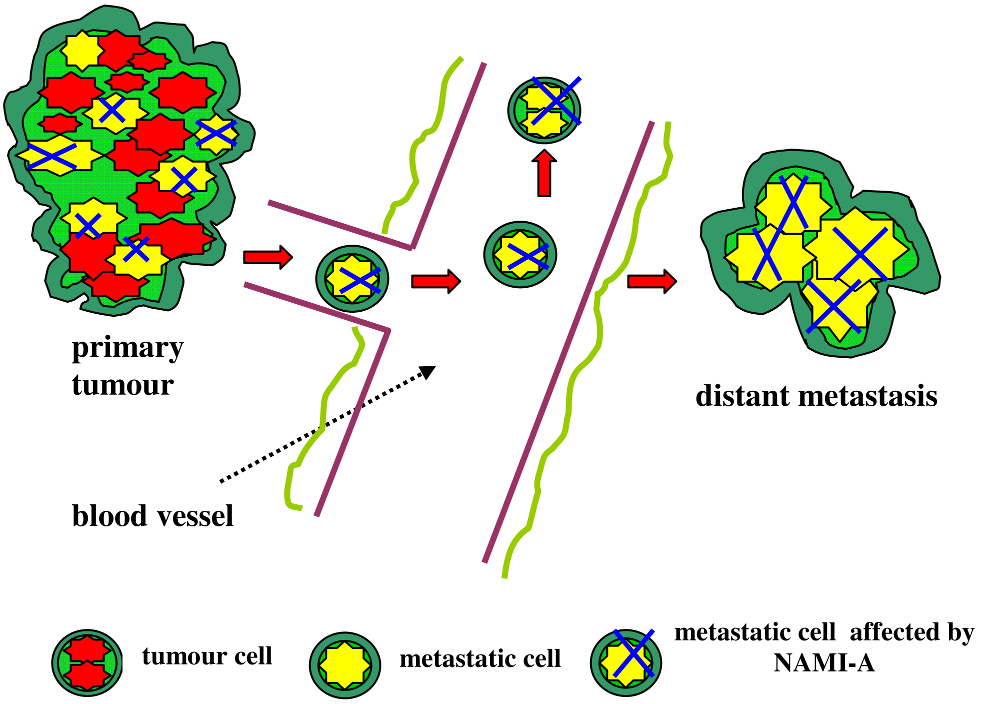

Figure 7: Selective treatment of metastasis by NAMI-A[135]. (Adapted from Bergamo *et al*., 2007)[135].

NAMI-A showed significant *in vitro* and *in vivo* anti-angiogenetic effect under VEGF (Vascular Endothelial Growth Factor) stimulus in a rabbit cornea model[139] and under FGF (Fibroblast Growth Factor) stimulus in a CAM (Chick embryo chorioallantoic membrane) model[107]. A recent *in vivo* study[140] indicated that triruthenium-carbonyl clusters demonstrated significant inhibition of angiogenesis in the CAM model and that these compounds may play an important role in cancer drug design.

Other *in vitro* and *in vivo* pharmacological examinations have demonstrated that NAMI-A - type compounds display limited cytotoxicity, and their cytotoxic effect may vary from that of platinum drugs and may be independent of interactions with DNA[141, 142]. A current *in vivo* study revealed that the possible cytotoxicity of NAMI-A against propagated tumours is that it intercedes with NO metabolism *in vivo*[103]. Nitric oxide is known to play a significant part in numerous biological functions, and act as a mediator in the angiogenic process, inhibition of which could subsequently prevent the development of metastases[104]. NO has been found to combine with iron proteins (e.g., PKC - Protein Kinase C - involved in the regulation of proliferation, MMP - Matrix Metallo Proteinases, zinc-dependent endopeptidases - involved in tissue remodelling) and oncogenes (e.g., c-myc, c-jun, and c-fos are protein encoding genes involved in cell cycling) *in vivo* and hence the cytotoxic activity of ruthenium may alternatively be exerted through an iron-mimicking mechanism.[85, 141, 142]

5. Aim

This project aims to provide more knowledge about the mechanism of action of reduced toxicity and selective inhibitory anti-metastatic activity of NAMI-A and KP1019 analogues in complete biological systems.

This will be achieved by:

- synthesizing structural analogues of NAMI-A and KP1019 tagged with either a heavy element that could be traced with XRF, or with an optically fluorescent moeity;
- assessing cytotoxicity of the newly synthesised complexes by cell culture studies to ensure that they are not dramatically modified with respect to the parent complexes

- studying the distribution of ruthenium in individual cells (chemical mapping), treated with the drugs, by a synchrotron-based XRF method; and
- identifying the biological targets of ruthenium in treated cells by fluorescent microscopy.

6. Significance of the project

6.1. Anti-neoplastic properties

A compound having anti-neoplastic properties is believed to prevent, repress or stop the formation of a neoplasm (a tumour)[143]. The anti-neoplastic properties of NAMI-A analogues were investigated by Groessl *et al.* (2007)[143].

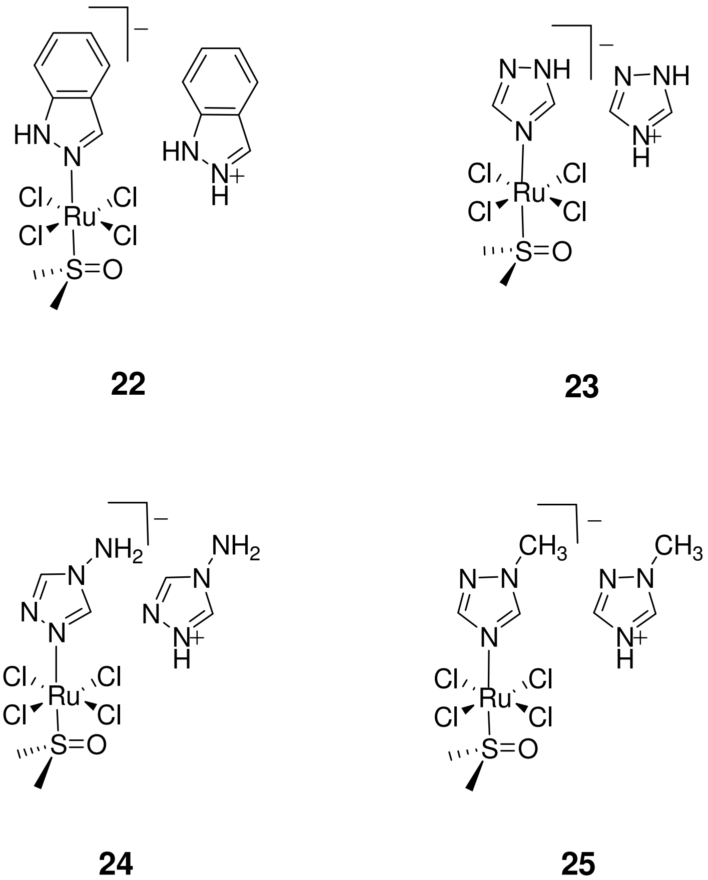

22 **23**

24 **25**

Scheme 5: Schematic representation of NAMI-A analogues with anti-neoplastic properties.

They determined the bio-transformation of the complex inside the human body by various *in vivo* and *in vitro* analyses. In that study[143], the imidazole ligand of NAMI-A was substituted by indazole (**22**, Scheme 5), 1,2,4-triazole (**23**, Scheme 5), 4-amino-1,2,4-triazole (**24**, Scheme 5), and 1-methyl-1,2,4-triazole (**25**, Scheme 5).

Investigations were performed to determine the stability of these complexes in aqueous solution, the interaction of plasma proteins with the complexes, their redox potentials, and anti-proliferative activity. It was demonstrated that in phosphate buffer (pH 7.4) at 37 °C, all compounds exhibited hydrolytic stabilities with less than 30 min half-lives[143]. The kinetic binding constants for albumin and transferrin were in the order of 0.02 - 0.34 min^{-1} and 0.01 - 0.26 min^{-1} respectively, and the indazole-bearing compound (**22**) displayed more *in vitro* anti-proliferative activity when compared to other compounds[143]. Their mode of action is shown in figure 8.

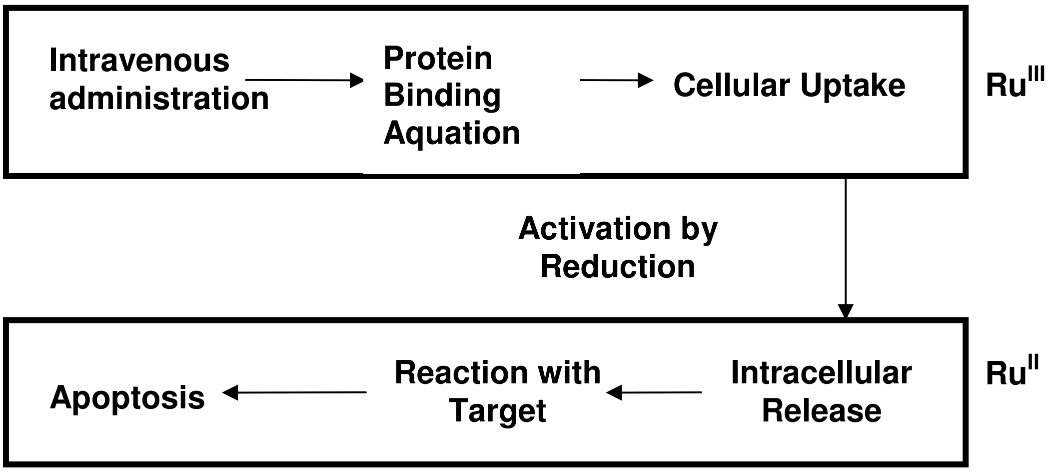

Figure 8: Mode of action of Ru-Based anti-cancer agents[143] (Adapted from Groessl *et al.*, 2007)[143].

Among the investigated ruthenium complexes (Scheme 5), **22** binds with proteins more quickly despite a slow rate of aquation compared to NAMI-A, which illustrates the significant impact of the indazole group on the drug protein interaction[143]. The vicinity of the primary amine group in **24** increases the protein-complex binding rate, whereas the methyl group **25** has an inverse hindering effect[143]. The substituted triazole complex **23** was found to have the least hydrogen bonding interactions compared to others[143].

6.2. Protein binding ability

The anti-neoplastic properties and reduced toxicity of ruthenium drugs when compared to platinum compounds, have been attributed to the ability of the ruthenium species to imitate iron when bound to numerous bio-molecules (e.g., serum transferrin and albumin)[112]. Cancer cells require more iron for metabolism than healthy cells and hence they have more transferrin receptors on their cell surfaces compared to healthy cells[112]. When treated with a ruthenium complex, more drug molecules will be targeted to cancer cells as they have more iron or transferrin receptors and the healthy cells will hence be less affected.

Opposing the above perception, an animal model study by Sava and co-workers[137] inferred that the binding of NAMI-A to serum proteins (albumin or transferrin) decreased its bio-availability and anti-metastatic action. Meanwhile, other studies[26, 61, 79, 143-145] have reported that the protein binding ability of cancer cells will make the drug inactive as it will remain bound to the transferrin sites rather than be taken up by the cells.

In a recent study by Liu *et al.* (2010)[133] (*discussed briefly in* **4.1**), the rate of protein binding of Ru(III) complexes and the rate of Ru(III)-protein adduct formation were investigated and reported. In this study, samples of Ru(III)–BSA adducts were prepared by the reactions of bovine serum albumin (BSA – used as a protein concentration standard) with NAMI-A in buffered saline (pH = 7.4)[133]. Three independent assays; substrate adhesion assays, cell motility assays and collagen invasion assays, of the purified Ru(III)–BSA (1:1) adduct were done by adding the adduct to cell culture medium. The results displayed the ability of Ru(III) species to interact with collagen in human lung cancer cells (A549)[133]. Ru(III)–BSA adduct formation enhanced the cell adhesion to the substrate, reduced the cell motility and thus decreased the ability of the cells to infiltrate into collagen gels[133]. Significantly, the experiment demonstrated that a purified Ru(III)–BSA adduct has a comparable activity in all the three independent assays to that of NAMI-A freshly added to the cell medium, which was anticipated to form a Ru(III)–BSA adduct within minutes[146].

Other studies on protein binding ability[143] of NAMI-A type complexes demonstrated that the rate of protein binding is directly proportional to the rate of aquation or hydrolysis, i.e., as the rate of aquation increases, protein binding ability increases and this eventually expedites the inactivation of the drug. It is hence apparent that a better understanding of the ligand exchange kinetics in NAMI-A type complexes may be required to explain the anti-metastatic effect of NAMI-A.

6.3. Rate of ligand exchange

Ruthenium complexes can act as pro-drugs (**4.1**) and can alter their coordination environment upon reaction with the bio-molecules which may lead to their therapeutic action[147]. The pro-drug, in an inert form, may be converted to an active compound by ligand exchange or hydrolytic reactions[147]. The time taken for the inert form of pro-drug to convert to an active drug is significant in cancer drug research, as the drug must act quickly upon treatment to prevent the growth of rapidly multiplying cancer cells[147].

The fact that the drug has to reach its biological target without modification is a very important determinant of classical pharmacological activity[147]. This can be problematic for Ru(III) complexes as they can interact with macromolecules, such as proteins, through ligand exchange reactions or hydrolytic reactions[21] and may not reach the target without modification. This may lead to drug inactivation as discussed in **6.2**. A better understanding of the characteristics of ligand exchange kinetics of Ru(III) complexes to assertion whether any unwanted ligand exchange reactions occur before the intended biological target is reached.

Alessio *et al.* (1996) reported[148] the pH dependence of ligand exchange reactions in Ru complexes. They investigated the interaction of two anti-tumour ruthenium(III) complexes, with human serum apotransferrin (apoTf) through various spectroscopic methods such as UV-Vis spectrophotometry, CD and ^{1}H NMR spectroscopy[148]. They demonstrated that the protein binding occurs in the first step of the hydrolytic process[148]. The adducts formed were stable for an indefinite period under the same biological conditions and the addition of excess citrate at low pH induced the loss of the bound ruthenium(III)[148]. The development of binuclear or polynuclear oxo or hydroxo bridged complexes was shown to be accelerated at higher pH and, thus, it was demonstrated that the extent of ligand exchange in the ruthenium complex was strongly pH dependent[148].

Messori L *et. al.* (2000) demonstrated[146] that the ligand exchange reactions in NAMI-A involve the sequential replacement of the two ruthenium-coordinated chloride ligands. The investigation monitored the hydrolysis of NAMI-A spectrophotometrically in the presence of bovine serum albumin at 25°C in phosphate buffer[146]. It was found that the process of hydrolysis occurred via two distinct steps; first, diminution of the characteristic band around 400 nm and the consequent increase in the band of comparable intensity around 346 nm; second, the successive diminution of the latter band (at 346 nm) after several minutes. These changes were related to the progressive displacements of the two ruthenium-coordinated chloride ligands by hydrolysis[146].

Mura *et al.* (2004) investigated and reported[149] the rate of ligand exchange reactions in NAMI-A type complexes. When the imidazole in NAMI-A was replaced by a less basic ligand, thiazole, a significant reduction in the ligand exchange rate was observed resulting in a further decrease in the chloride ion release[149]. The secondary ligand stabilized the ruthenium(III) species so that the metal ion was not released to the tissues, thus preventing the hydrolysis or redox processes until it reached the final target[149].

Ligand exchange reactions may likewise be viewed as a process of hydrolysis (**3.3**). Besker *et al.* (2008) carried out the first and second hydrolytic pathways of NAMI-A analogues by density functional studies (Scheme 6)[128] and the third aquation of NAMI-A analogues has been investigated by Vargiu *et al.* (2008) using DFT-PCM calculations[150].

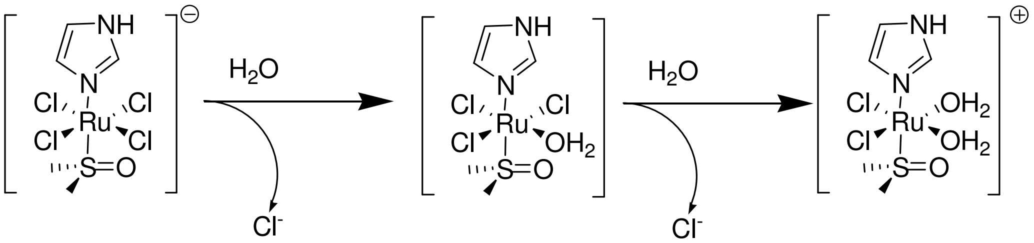

Scheme 6: Proposed first and second aquation processes for NAMI-A[128].

It was reported that the rate of ligand exchange or rate of aquation is subject to the concentration of the exchanging ligands in the reaction media[112, 128, 150]. Understanding the factors influencing ligand exchange reactions (e.g., pH and concentration) is significant as the information yields knowledge on the stability of NAMI-A type complexes and, thus, enables a better understanding of their clinical activity[21].

6.4. Contribution to the discipline

Studies up to this point show the interactions between the drug molecule and DNA, drug molecule and protein or between drug molecule and a single bio-molecular target via activation by reduction, protein binding or aquation. Numerous endeavours have brought about either positive or critical findings[26, 113, 116, 135, 151], however, several studies have inadequate conclusions[152, 153]. The research todate could not illustrate the biological target of the model complexes, NAMI-A and KP1019, and hence could not explain the mechanism of the pharmacological action of these drugs or its analogues when uptake by cancer cells.

The significance of this project is that it investigates the mechanism of action of NAMI-A and KP1019 analogues in a complete biological system. In this thesis, cell culture studies have been used to track the bio-distribution of ruthenium from these drugs. Synchrotron-based XRF techniques can provide data concerning time-dependent uptake, distribution and bio-transformation of ruthenium in individual and bulk human cells[154]. Knowledge of the distribution of ruthenium in cells may provide useful information to elucidate the mechanism of anti-metastatic activity of the NAMI-A analogues and the chemical species responsible for reduced cytotoxicity. In turn this might prompt the discovery of new anti-cancer agents which have a wider therapeutic window.

7. Methodology

7.1. Cell culture studies

The growth of cells derived from an organism or an animal in a pharmacological medium under favourable conditions is termed as cell culture[155]. A localised group of cells grown in a defined pattern derived from an organism is referred as a tissue[156]. Cells can be isolated from tissues and the first culture after this isolation is known as a primary cell culture[155]. The continuous division of cells in a fresh growth medium, after transferring to a new vessel from primary cell culture vessel is termed to be subculture or 'passaging'[155]. An established cell culture which can undergo indefinite multiplication under favourable conditions is known as a cell line[156].

7.1.1. Finite cell lines

After continuous multiplications and divisions, some cell lines may die or lose their ability to proliferate. These type of cell lines can be referred as a finite cell line and the genetically determined event which causes the formation of a finite cell line is known as ‘senescence’[155]. A finite cell line is usually derived from a primary cell culture and will have a short life span[155].

7.1.2. Continuous cell lines

Some cell lines will have the greatest growth capacity after passaging, these are known as continuous cell lines. The process by which a cell line becomes ‘immortal’ and become a continuous cell line is referred as cell alteration or ‘transformation’[155]. A finite cell line can become a continuous cell line by acquiring the ability to divide spontaneously through the process called transformation[155, 157].

The advantages of continuous cell lines are[158]:

a) easily segregated;
b) high development rate and yield with a high nucleus-cytoplasm ratio;
c) low serum prerequisite;
d) less adherence and ease of maintenance in simple media; and
e) ability to develop and multiply in suspension with a high cell density.

7.1.3. Cell culture conditions

The conditions in which cells grow may be varying with the cell line or cell type. The cell culture conditions may also dependent on pH, light, temperature, growth factors in the nutrient media and gases[155, 157]. Adherent cells or anchorage-dependent cells (e.g., A549 cells, Human Lung Carcinoma cells) can be cultured as monolayers while non-anchorage dependent cells (floating cells, e.g., blood cells) can be grown in the culture medium as a suspension culture[155].

7.1.4. Advantages of cell culture as an *in vivo* model

Cell culture techniques are widely used for studying basic cell biology, as model systems for investigating metabolic activities and ageing, toxic effect of drugs on cells, nutritional studies, as an *in vivo* model in cancer research (Figure 9), in drug screening and development, and in virology and genetic engineering[155, 157].

The other major advantages of cell cultures in drug design and development are[155, 157, 158];

a) Propagation and expansion: Cell culture techniques are independent of any structural organization. As such they can be easily utilised for the synthesis of biological compounds on a large scale (e.g., vaccines).

b) Consistency and reproducibility: The results of cell culture studies are consistent and exhibit good reproducibility[155] as the cells can form indistinguishable replicates in each culture.

c) Selection, purification and preservation: Since identical cells can be formed by cloning, cells can be chosen uniformly, purified and preserved after treating with appropriate protective agent (e.g., DMSO or glycerol); the process is referred as cryopreservation[155].

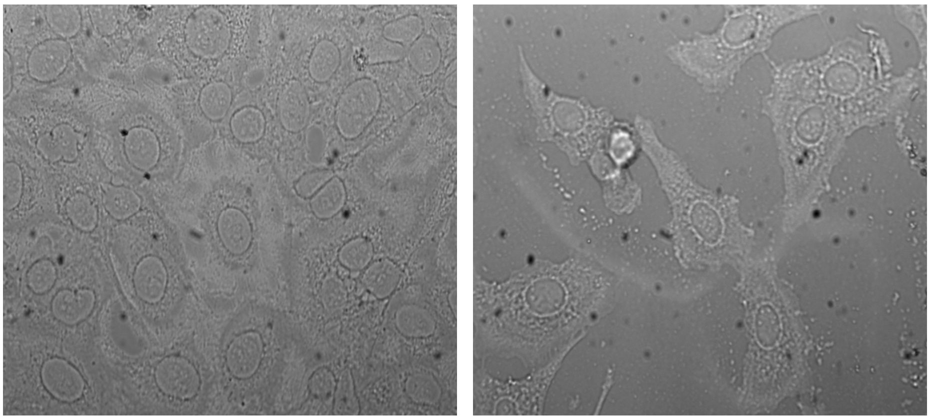

(a) (b)

Figure 9: Microscopic view of fixed A549 cells on silicon nitride windows; (a) A549 cells treated with NAMI-A for 24 hours and (b) A549 cells treated with control (PBS – phosphate Buffer saline) for 24 hours.

In this project, the cell lines of A549 (human lung cancer cells) and S5-SH5Y (human neuroblastoma cells), are used as *in vivo* models of cancer cells.

7.2. X-ray fluorescence spectroscopy (XRF)

7.2.1. Theory behind XRF

When an X-ray is incident on an atom, it may be absorbed and its energy transferred to a core electron. The resulting ionisation or electronic excitation leaves a hole in the core orbital. This process is known as the photoelectric effect[159]. To attain stability, the electrons of an atom will relax to the inner shells from the outer shells by discharging a characteristic amount of energy[159]. This X-ray emission is called X-ray fluorescence (XRF) and the energy released is the characteristic property of a particular element[159]. To ionise an electron of an atom, the incident X-rays must have a higher energy than the binding energy of the excited or ionised electron[159]. This excitation energy must be higher than the energy of fluorescent X-rays, which is the difference between two binding energies of the corresponding shells involved in the relaxation process. If the excitation energy is far greater than the ionisation energy, numerous photons will pass the atom and only relatively few electrons will be ionised, generating only negligible fluorescence[159].

The innermost K- and L-shells of an atom (equivalent to the $n = 1$ and $n = 2$; principal quantum number shells) are most commonly used in XRF detection[160]. The corresponding X-rays are labelled as K, L, M or N to represent the shells they are produced from. To distinguish the X-rays that are generated from the transition of electrons from higher shells, additional designations such as α, β, γ are utilised (Siegbahn notation)[160]. Hence, K_α denotes the X-ray originated from a transition of an electron from L- to K-shell; K_β is that from M- to K-shell, and so on. Usually, the fluorescence produced from K-shell is more intense than that from L-shell, which in turn is more intense than those from the M-shell. An outline of the most important lines with their transitions in Siegbahn notation is given below (Figure 10)[160].

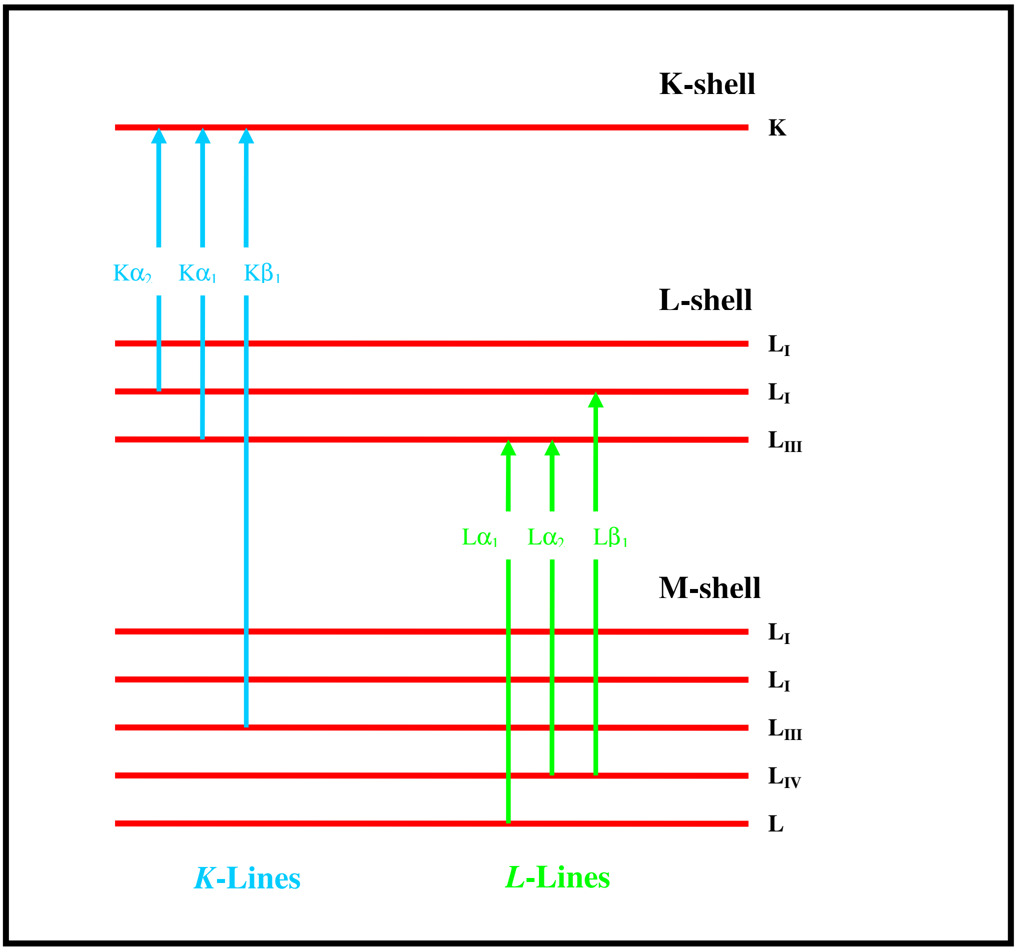

Figure 10: Major lines and their transitions; $K\alpha_1$, $K\alpha_2$, and $K\beta_1$ are *K*-lines (blue) and $L\alpha_1$, $L\alpha_2$, and $L\beta_1$ are *L*-lines (green)[159, 161] (Adapted from http://webh01.ua.ac.be/mitac4/micro_xrf.pdf[161]).

7.2.2. Synchrotron-based XRF technique

X-rays generated by synchrotron sources are approximately 100 million times brighter than those generated by an X-ray rotating anode tube source in the laboratory[162]. Synchrotron X-ray fluorescence (XRF) imaging is capable of providing sub-micron scale 2D/3D maps of elements in ppm (parts per million) concentrations at rapid scanning rates (~30 sec/cm^2 at 100 micron resolution)[163, 164]. Microscopic or nanoscopic digital images of the samples are produced through pixel-by-pixel scanning of the sample across the beam. The X-ray fluorescence spectrum obtained is characteristic of the chemical elements present at that pixel[162, 165]. Numerical data obtained from the XRF spectrum discloses the basic structure and elemental composition, from which micro elemental images of the sample are generated. Through this methodology, we can unravel distinct biological structures and advantageous bio-chemical data[162, 164].

Synchrotron-based XRF imaging has a wide range of applications; imaging and detection of elements in micro-molar concentration[166, 167], structural characterisation of biological entities[168], microanalysis in cell physiology[169], and structure determination in bio-inorganic chemistry[62, 109, 169, 170].

7.3. Silicon Nitride (Si_3N_4) membranes as growth substrates for imaging

Si_3N_4 membranes are extremely thin (500 nm) and inert membranes (Figure 11) which are convenient substrates for imaging individual microscopic cells using synchrotron-based methodologies[171].

The main advantage of Si_3N_4 membranes are their ability for direct culturing and fixing of the adherent cells (**7.1.3**) in comparison to formerly used substrates (e.g., Al-coated quartz slides) which require cells to be grown first and then deposited on the slides for investigation[171]. By utilising this technique, the bio-chemical characteristics of the nuclei and other sub-cellular organelles can be investigated by obtaining SR-FTIR and XRF spectral information of cells grown on Si_3N_4 membranes (e.g., combinatorial analysis - Figure 12). The image of a nucleus acquired by ordinary microscopic techniques are blurred or darkened and we may have to use stains to obtain a clear image. By using Si_3N_4 membranes, the nucleus can be visualised without staining and images of exceptional clarity can be obtained [171]. A detailed chemical or elemental distribution of the sample could be obtained without any obstruction of infrared or X-ray radiation, is an added advantage of thin Si_3N_4 membranes.

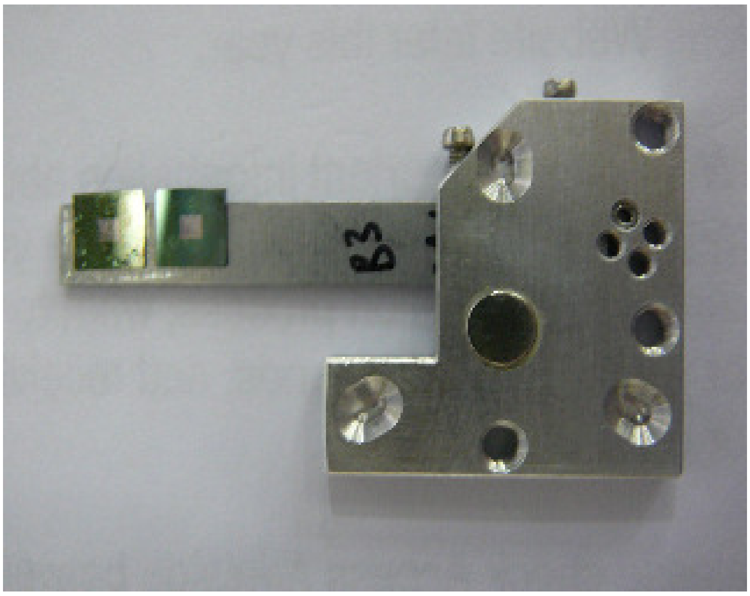

Figure 11: Si_3N_4 membranes attached to kinematic mount prepared for XRF imaging (window dimensions = 500 x 500 microns).

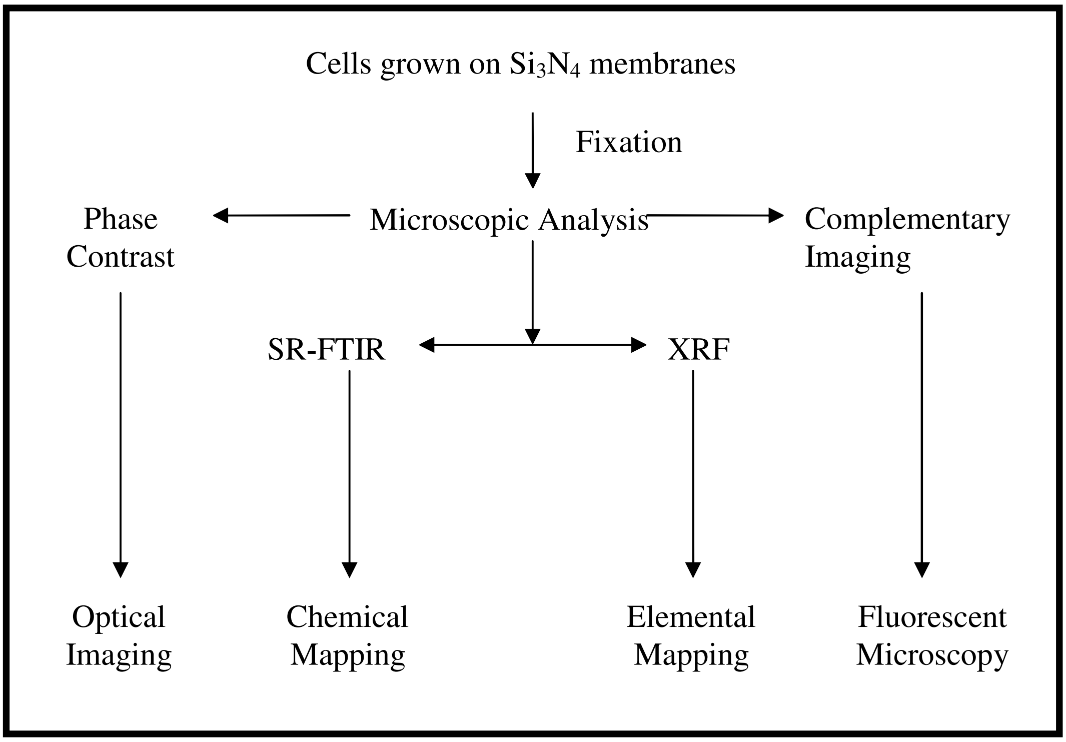

Figure 12: A schematic representation of the analytical techniques used in the combinatorial analysis[171]. (Adapted from Carter *et al*. 2010)[171].

7.4. Fluorescent microscopy - live cell imaging techniques

The discharge of photons from electronically excited states of an atom or molecule to ground states without any variation in the spin orientation is regarded as fluorescence[172]. It is a characteristic property of an atom to absorb light at a specific wavelength and emit light at an extended wavelength after a certain time interval[172].

Fluorescent microscopy is an important methodology for investigating cell structure and function by cell imaging, interactions of molecules in biological frameworks, and identification and speciation of nucleic acids and proteins in gel electrophoresis[173, 174]. A fluorescent microscope is a basic light microscope (utilises visible light to illuminate and construct a magnified image of the sample) with added characteristics such as high intensity light and components with more enhanced capabilities that can include xenon or mercury light source, light filters, the dichroic mirror and shutter to illuminate the sample[174, 175] (*Applications discussed in detail **8.4***).

Continuous monitoring of living cells under culture conditions using a confocal microscope is referred as "live cell imaging"[176]. Current research reports an increasing number of studies using live cell imaging techniques to gather significant information about the underlying features of cells, tissues and other cellular components[177]. This methodology is used for applications such as chemotaxis, angiogenesis, migration and wound healing[176]. Live-cell imaging has been proven to be a significant analytical methodology by numerous laboratories and a routine practice in many fields of bio-medical research such as neurobiology, developmental biology and pharmacology[176, 177]. The primary challenge of live cell imaging is to maintain cells in a healthy and functioning state whilst illuminated under a microscope[176]. Different parameters that can affect live cell imaging are temperature, atmospheric conditions (gas mixture and humidity), nutritional supplements, growth medium buffering (pH), and osmolarity of the culture medium[176].

Most Ru(III) complexes, including the NAMI-A and KP1019 analogues investigated here, absorb light in the visible region of the electromagnetic spectrum. In recent research, their photophysical characteristics have been explored in detail and have been provided information about Stokes shifts, metal to ligand charge transfer (MLCT) states, ligand to metal charge transfer (LMCT) states or as well as their absorption (in the visible region) and emission properties (long lived excited states at far emission region or at longer wavelength ~ 500 nm or above)[178-180]. Live cell imaging by fluorescent microscopy is utilised in the current research, for the identification of the biological target of ruthenium in NAMI-A, or NAMI-A analogue treated cells.

8. Capabilities of the techniques

8.1. Elemental distribution in single cells by XRF techniques

The analysis of intracellular elemental concentration and chemical speciation is vital in comprehending the activity of bio-metals across cellular metabolism[163]. XRF techniques can be effectively applied for the determination of intracellular and cellular elemental distribution levels in human tissues[180]. The interpretation of XRF elemental maps provides an insight on the cellular metabolism and hence these methods possess unique capability in bio-medical research[180]. The low detection limit and high spatial resolution are recognised advantages of XRF technique[180] compared to other available elemental imaging methods, such as electron microscopy/EDAX[181, 182].

Several studies have demonstrated the advantages of synchrotron radiation induced XRF microprobe imaging (SR-XRF). One example is the imaging of cisplatin treated cancer cells[183, 184] using an XRF microprobe. The XRF imaging was performed at a lower platinum dosage of 10 µM compared to 30 µM which was used in a similar proton microprobe experiment, and this lower concentration was similar to the clinically relevant concentration[183, 184]. The results indicated a nuclear accumulation of platinum in treated cancer cells which was also confirmed by proton microprobe analysis[183]. The same methodology was subsequently employed to correlate the intracellular distribution of model platinum complex (cisplatin, Pt(II) complex), and newly synthesised platinum Pt(IV) complexes[185, 186]. A comparable intracellular accumulation of platinum was found in the two cases[185, 186].

Microprobe XRF mapping was shown to be an efficient tool for analysing the intracellular metabolism of heavy metals or bio-metals in human body. Munro *et al.* (2008)[187] employed the high sensitivity and accuracy of SR-XRF to investigate the intracellular targets of arsenic, delivered in the form of arsenite. This study demonstrated a clear aggregation of arsenic in the euchromatin regions of the nucleus suggesting that the toxicity was due to binding of arsenic with DNA or with DNA transcription proteins[187].

Studies were conducted to investigate the metabolism of several selenium species in human lung cancer cells employing a combination of XRF and XAS techniques[166, 188]. The speciation of selenium in A549 cells was studied between 24 hr and 48 hr after treatment with selenite. The time dependent XAS investigation have shown that selenite was metabolised to elemental selenium and GSSeSG species within the first 4 hr of treatment[166]. A diselenide species was formed and its presence was used as evidence for intracellular oxidation between 24 hr and 48 hr after treatment. The mapping of distribution of selenium by XRF microscopy revealed that the elemental selenium was accumulated in specific regions of cytoplasm of the treated cells where it was found to be co-localised with copper[166]. The results revealed the combination of XRF and XAS microscopy is a powerful combination to study the metabolism of selenium compounds in biological systems.

In other reported work[189], XRF imaging and mapping were used to investigate the intracellular distribution of the metals Mo and Nb in cancer cells treated with anti-tumour metallocene complexes. The interpretation of the data obtained from elemental distribution maps revealed that Mo was distributed across the cells while Nb was specifically accumulated in some areas inside the cell. Thus, XRF imaging is capable of investigating cellular targets of Mo and Nb in the treated cells.

Similar studies were conducted in order to investigate the selective aggregation of platinum-gadolinium complex within a tumour-cell nucleus[190]. The XRF elemental distribution maps revealed that the complex selectively targets the nucleus which was evidenced by a significant increase in the intracellular concentration of both platinum and gadolinium in comparison with that of control cells. It was concluded that the DNA-metallointercalator complex had the ability to deliver gadolinium in a targeted manner into tumour cell nuclei[190] which was a crucial requirement for this prototype drug. This 'double-tag' approach, where two heavy exogenous elements in the same molecule are followed, is utilised in this project to investigate the accumulation of ruthenium inside the cells treated with KP1019 analogues in which N-heterocycle is modified by incorporating elements such as iodine (*see* **Chapter 3**).

The studies described above demonstrate the capabilities of XRF in investigating the cellular fates and cellular targeting characteristics of the metallo-drug species which can be linked to the biological activities of the studied complexes. Using similar methods in this project, attempts are made to draw conclusions about the time-dependent uptake, distribution and bio-transformation of ruthenium in NAMI-A and KP1019 analogue-treated cells.

8.2. Linking results with bio-chemical assays

The outcomes of XRF experiments can be correlated with those from traditional bio-chemical assays. Clonogenic survival assays were used to illustrate and interpret the outcomes of Cr uptake in Cr(VI)-treated A549 cells by Harris *et al.* (2005)[154]. The cellular uptake of chromium was measured at specific time intervals. After each time period (0, 5, 20, 60, 120 and 240 minute), chromium was removed from the system and the cells were allowed to replicate for 24 hours and the number of new colonies formed (clonogenic survival) were found to decrease; 100 colonies after 20 minute, 80 colonies after 25 minute, 82 colonies after 60 minutes, and the number of colonies were suddenly dropped to 20 after 125 minutes. It was noted from the clonogenic survival assay that no colonies were formed after 250 minutes. It was concluded from this study that the cells stop proliferation after certain time intervals because of genetic alteration in chromium-treated cells[154]. The absence of morphological progressions additionally confirmed that the cells were not in a progressive phase of apoptosis and the Cr(VI) species was diminished as indicated by the absence of colony formation after 250 minutes. The XRF studies confirmed the predominance of Cr(III) species as evidenced from the intracellular Cr hotspots, which appeared in the micro-XANES spectrum. The results of clonogenic assays hence can be related to XRF and micro–XANES results, and a similar technique could be applied to investigate the intracellular uptake of ruthenium and the elemental form of ruthenium (Ru(III) to Ru(II)) inside the cancer cells treated with NAMI-A or its analogues.

8.3. Average X-ray absorption spectra of bulk cells

XAS of bulk cell pellets is a very useful tool to reinforce the results mentioned above (**8.1 – 8.2**). Levina *et al.* (2007)[169] used the correlation of XANES spectra and difference XANES spectra to identify the chemical forms of Cr in pellets of mammalian cells treated with Cr(VI) compounds. A549 cells were treated with Cr(VI) compounds and XANES spectra were recorded for whole and lysed cells after 4 hrs of treatment. The results of the XANES spectra and the difference XANES spectra were compared with published data for the Cr(III) compound, chromodulin. They showed that Cr(III) formed in Cr(VI) treated cells was bound to ligands with high molecular mass such as proteins and the chemical environment of chromium was altered by the cell lysis strategy[169]. The Cr(III) species was redistributed during the cell lysis procedure which led to the formation of a fraction with low molecular mass and the spectroscopic properties of this fraction was closely related to that of chromodulin[169]. From this result, it was concluded that chromodulin was an artefact of the lysis procedure and that the dietary essentiality of chromium was hence called into question. Thus, it can be postulated that the comparison of XANES spectra and difference XANES spectra could be an effective tool in research investigating changes in the chemical speciation of ruthenium ions in NAMI-A treated cancer cells.

8.4. Identifying biological targets of the drugs by fluorescent microscopy

A fluorescence microscopic investigation facilitates the visualisation of treated fluorescent compounds inside living cells (**7.4**). Hence, fluorescence microscopy has been generally utilised to examine cellular distribution and biological destination of different organic drugs[191, 192] and has been adapted for platinum complexes[193-196]. The platinum compounds shown below (**26** and **27**; Scheme 7) were investigated[195] for their activity *in vitro* after modification with fluorogenic reporters, namely, CFDA (carboxyfluorescein diacetate) and DNP (dinitrophenyl).

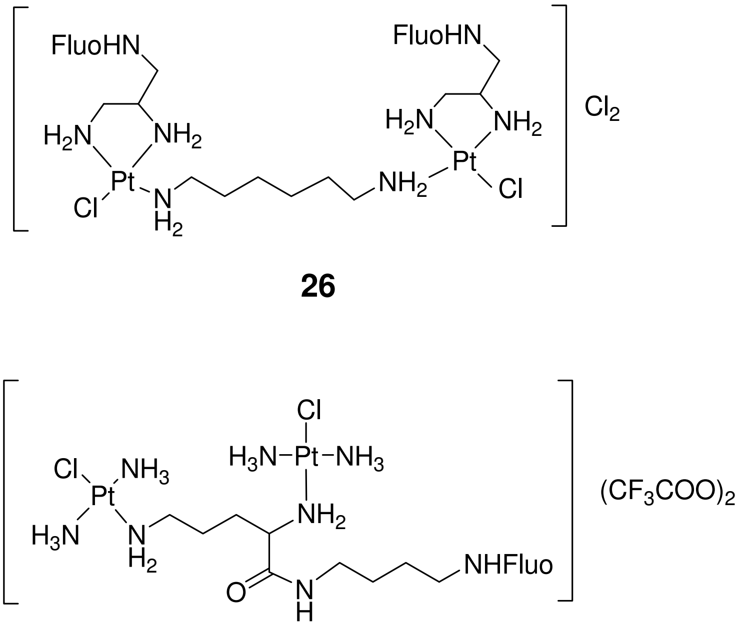

26

27 **Fluo = CFDA or DNP**

Scheme 7: Fluorescent probe-tagged platinum compounds investigated for their *in vitro* activity.

Compounds **26** ($[\{cis\text{-}Pt(NH_3)_2Cl\}_2(\mu\text{-}H_2N(CH_2)_6NH_2)](NO_3)_2$ (1,1/c,c)) and **27** ($[\{trans\text{-}Pt(NH_3)_2Cl\}_2(\mu\text{-}H_2N(CH_2)_4NH_2)](NO_3)_2$ (1,1/t,t)) are dinuclear platinum complexes containing aliphatic diamines, which are found to be active against different cancer cell lines *in vitro*[195]. Uptake studies of the modified complexes and the corresponding unlabelled complexes were carried out in U2-OS (human osteosarcoma cell line) and U2-OS/Pt (cis-platin resistant derivative cell line)[195]. The uptake of the labelled complexes was found to be influenced by the fluorescent moiety as indicated by the high cellular accumulation of the labelled compounds in comparison with the respective parent compounds[195]. Both the labelled and parent compounds interacted with a guanine base indicating that the structural modification by a fluorogenic reporter did not influence the binding properties of the platinum complexes to nucleobases[195].

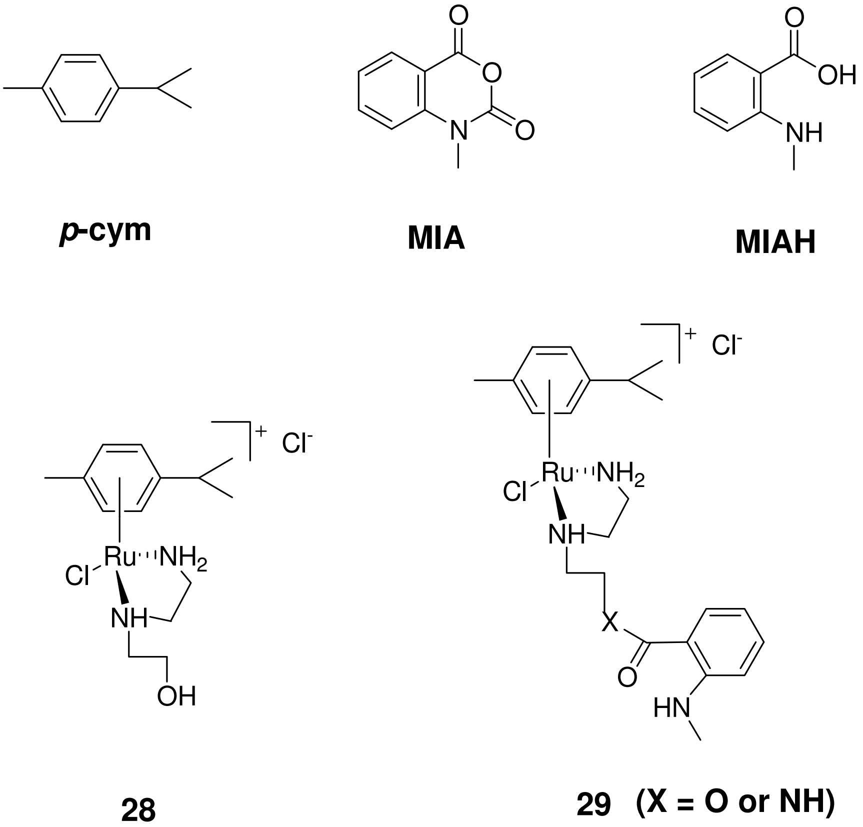

***p*-cym** **MIA** **MIAH**

28 **29 (X = O or NH)**

Scheme 8: The investigated ruthenium complexes (**28** and **29**) and their fluorescent moieties; p-Cymene (*p*-cym), methylisatoic anhydride (MIA), and methylisatoic acid (MIAH).

The capability of fluorescence microscopy to research the biological distribution, cellular transportation and mechanism of biological action was further demonstrated[82] by tagging of newly synthesised (arene)ruthenium(II) complexes with a fluorescent reporter. The study was conducted using complexes **28** and **29** and the fluorogenic reporters were shown in Scheme 8[82]. The fluorescent emission properties of the chelating ligands were discovered to be quenched after coordination with the ruthenium metal centre and the results shows that the coordination occurs through an ester or amide linkage[82].

If the coordination occurred through an ester bond, the complex would act as a substrate for ester hydrolysis and the apparent variation in the fluorescent profile would provide significant insight about the cellular distribution and ruthenium based prodrug delivery mechanism initiated by ester hydrolysis[82]. However, if the fluorescent ligand is attached to the (arene)ruthenium(II) complex through an amide linkage, then a stable penta-chelate complex was formed by the prompt de-protonation of amide nitrogen atom in physiologically relevant conditions[82].

A similar approach is employed in this research in an attempt to elucidate the mechanism of biological action of NAMI-A analogues, by tagging with suitable fluorescent probes and using fluorescent microscopy to image treated cells (***Chapter 5*, *Appendix I and Appendix II***).

9. Summary of the present work

The research outlined in this thesis is directed towards investigating the mechanism of anti-metastatic activity of ruthenium-based anti-cancer drugs, NAMI-A and KP1019. The individual chapters depict distinctive perspectives of the investigated complexes which are analogues of NAMI-A and KP1019. The work illustrated in each chapter is briefly described in the ensuing paragraphs. To conclude, the synthetic methodologies, physiochemical, photochemical and electronic properties of some synthesised analogues of NAMI-A and KP1019 complexes have been investigated thoroughly and the information collected was utilised to explore the pharmacological activity of these complexes.

Chapter 2 comprises a published paper[132] which describes the distinct cellular fates for KP1019 and NAMI-A, determined by X-ray fluorescence imaging of single treated cells. The uptake and distribution of NAMI-A and KP1019 in A549 human lung cancer cells was investigated using synchrotron based X-ray fluorescence spectroscopy.

Chapter 3 is an another published paper[197] which describes the synthesis of iodinated analogues of NAMI-A and KP1019, their characterisation, cytotoxicity and investigation of intracellular distribution of ruthenium and iodine in human lung cancer cells (A549 cell line) by synchrotron-based XRF methods,.

Chapter 4 contains a submitted manuscript[198] which explores the design, synthesis, and characterisation of fluorescent analogues of NAMI-A and their tetramethylammonium salts. Complexes were designed for the investigation of cellular pathways of tetramethylammonium analogues of NAMI-A labelled with a fluorescent reporter. The biological activities of these complexes and their fluorescent properties are investigated and reported.

Chapter 5 describes the exploration of cellular distribution of NAMI-A type complexes. This was achieved by synthesising a series of new Ru(III) complexes, which are analogues of model complex NAMI-A, namely, 4-bromoimidazolium [*trans*-tetrachlorido(4-bromo-1H-imidazole)(S-dimethylsulfoxide)ruthen(III)ate] (**M1**), 2-iodoimidazolium [*trans*-tetrachlorido(2-iodo-1H-imidazole)(S-dimethylsulfoxide)ruthen(III)ate] (**M2**), and quinolium [*trans*-tetrachlorido(quinoline)(S-dimethylsulfoxide)ruthen(III)ate] (**M3**). The complexes were then investigated for their electronic and cytotoxic properties and those properties were compared with that of the model compound, NAMI-A.

Chapter 6 summarizes the overall research carried out on the investigation of the mechanism of biological action of novel anti-cancer compounds NAMI-A and KP1019 and emphasises the relevant research areas with potential for future developments.

References:

1. Van Cruchten, S.; Van Den Broeck, W., *Anat. Histol. Embryol.* **2002,** 31, 214-223.
2. Mardis, E. R.; Wilson, R. K., *Hum. Mol. Genet.* **2009,** 18, R163-R168.
3. Bertram, J. S., *Mol. Aspects Med.* **2000,** 21, 167-223.
4. Scharer, O. D., *Angew. Chem. Int. Ed.* **2003,** 42, 2946-2974.
5. Engers, R.; Gabbert, H. E., *J. Cancer Res. Clin. Oncol.* **2000,** 126, 682-692.
6. http://www.cancer.gov/cancertopics/understandingcancer/cancer/ (August 2013),
7. http://www.cancer.gov/cancertopics/types/alphalist (April 2013),
8. Jemal, A.; Center, M. M.; DeSantis, C.; Ward, E. M., *Cancer Epidemiol. Biomarkers Prev.* **2010,** 19, 1893-1907.
9. Parkin, D. M.; Bray, F.; Ferlay, J.; Pisani, P., *Int. J. Cancer* **2001,** 94, 153-156.
10. Baskar, R.; Lee, K. A.; Yeo, R.; Yeoh, K. W., *Int. J. Med. Sci.* **2012,** 9, 193-199.
11. Jemal, A.; Bray, F.; Center, M. M.; Ferlay, J.; Ward, E. M.; Forman, D., *CA-Cancer J. Clin.* 61, 69-90.
12. http://www.wcrf.org/cancer_statistics/cancer_facts/index.php (November 2012),
13. http://www.cutyourcancerrisk.org.au/cancer-stats#.UwLPcmKSxIE (February 2014),
14. Mittal, B. B.; Pauloski, B. R.; Haraf, D. J.; Pelzer, H. J.; Argiris, A.; Vokes, E. E.; Rademaker, A.; Logemann, J. A., *Int. J. Radiat. Oncol. Biol. Phys.* **2003,** 57, 1219-1230.
15. Green, J. A.; Kirwan, J. M.; Tierney, J. F.; Symonds, P.; Fresco, L.; Collingwood, M.; Williams, C. J., *Lancet* **2001,** 358, 781-786.
16. Symonds, R. P., *Br. Med. J.* **2001,** 323, 1107-1110.
17. Nettina, S. M., *Lippincott's Prim. Care Pract.* **2000,** 4, 452-454.
18. Love, R. R.; Leventhal, H.; Easterling, D. V.; Nerenz, D. R., *Cancer* **1989,** 63, 604-612.
19. Johnstone, R. W.; Ruefli, A. A.; Lowe, S. W., *Cell* **2002,** 108, 153-164.
20. Hait, W. N.; Hambley, T. W., *Cancer Res.* **2009,** 69, 1263-1267.
21. Kostova, I., *Curr. Med. Chem.* **2006,** 13, 1085-1107.
22. Fisher, R.; Pusztai, L.; Swanton, C., *Br. J. Cancer* **2013,** 108, 479-485.
23. Verweij, J.; van Oosterom, A.; Blay, J. Y.; Judson, I. R.; Rodenhuis, S.; van der Graaf, W.; Radford, J.; Le Cesne, A.; Hogendoorn, P. C.; di Paola, E. D.; Brown, M.; Nielsen, O. S., *Eur. J. Cancer* **2003,** 39, 2006-2011.
24. Malinowsky, K.; Wolff, C.; Gundisch, S.; Berg, D.; Becker, K. F., *J. Cancer* **2010,** 2, 26-35.
25. Hartinger, C. G.; Dyson, P. J., *Chem. Soc. Rev.* **2009,** 38, 391-401.
26. Bruijnincx, P. C. A.; Sadler, P. J., *Curr. Opin. Chem. Biol.* **2008,** 12, 197-206.
27. Zhang, C. X.; Lippard, S. J., *Curr. Opin. Chem. Biol.* **2003,** 7, 481-489.
28. Warra, A. A., *J. Chem. Pharm. Res.* **2011,** 3, 951-958.

29. Sadler, P. J.; Guo, Z., *Pure Appl. Chem.* **1998,** 70, 863-872.
30. Stochel, G.; Wanat, A.; Kulis, E.; Stasicka, Z., *Coord. Chem. Rev.* **1998,** 171, 203-220.
31. Glennas, A.; Kvien, T. K.; Andrup, O.; Clarke-Jenssen, O.; Karstensen, B.; Brodin, U., *Br. J. Rheumatol.* **1997,** 36, 870-877.
32. Vint, I. A.; Foreman, J. C.; Chain, B. M., *Eur. J. Immunol.* **1994,** 24, 1961-1965.
33. Madeira, J. M.; Gibson, D. L.; Kean, W. F.; Klegeris, A., *Inflammopharmacology* **2012,** 20, 297-306.
34. Chaffman, M.; Brogden, R. N.; Heel, R. C.; Speight, T. M.; Avery, G. S., *Drugs* **1984,** 27, 378-424.
35. Bishun, N. P.; Smith, N. S.; Williams, D. C., *Oncology* **1978,** 35, 228-234.
36. Sausville, E. A.; Peisach, J.; Horwitz, S. B., *Biochem. Biophys. Res. Commun.* **1976,** 73, 814-822.
37. Boger, D. L.; Cai, H., *Angew. Chem. Int. Ed.* **1999,** 38, 448-476.
38. Chen, J.; Stubbe, J., *Nat. Rev. Cancer* **2005,** 5, 102-112.
39. Garbutcheon-Singh, K. B.; Grant, M. P.; Harper, B. W.; Krause-Heuer, A. M.; Manohar, M.; Orkey, N.; Aldrich-Wright, J. R., *Curr. Top. Med. Chem.* **2011,** 11, 521-542.
40. Graf, N.; Lippard, S. J., *Adv. Drug Deliv. Rev.* **2012,** 64, 993-1004.
41. van Rijt, S. H.; Sadler, P. J., *Drug Discov. Today* **2009,** 14, 1089-1097.
42. Hambley, T. W., *Science* **2007,** 318, 1392-1393.
43. Hambley, T. W., *Dalton Trans.* **2007**, 4929-4937.
44. Alderden, R. A.; Hall, M. D.; Hambley, T. W., *J. Chem. Educ.* **2006,** 83, 728-734.
45. Fricker, S. P., *Dalton Trans.* **2007**, 4903-4917.
46. Kelland, L., *Nat. Rev. Cancer* **2007,** 7, 573-584.
47. Kauffman, G. B.; Pentimalli, R.; Doldi, S.; Hall, M. D., *Platinum Met. Rev.* **2010,** 54, 250-256.
48. Werner, A., *Z. Anorg. Allg. Chem.* **1893,** 3, 267-330.
49. Rosenberg, B., *Platinum Met. Rev.* **1971,** 15, 42-51

50. Zamble, D. B.; Lippard, S. J., *Trends Biochem. Sci.* **1995,** 20, 435-439.
51. Kostova, I., *Recent Pat. Anticancer Drug Discov.* **2006,** 1, 1-22.
52. Pasini, A.; Zunino, F., *Angew. Chem. Int. Ed.* **1987,** 26, 615-624.
53. Ivanove, A. I.; Christodoulou, J.; Parkinson, J. A.; Barnham, K. J.; Tucker, A.; Woodrow, J.; Sadler, P. J., *J. Biol. Chem.* **1998,** 273, 14721-14730.
54. Bergamo, A.; Gaiddon, C.; Schellens, J. H. M.; Beijnen, J. H.; Sava, G., *J. Inorg. Biochem.* **2012,** 106, 90-99.
55. Tornaghi, E.; Andreoni, W.; Carloni, P.; Hutter, J.; Parrinello, M., *Chem. Phys. Lett.* **1995,** 246, 469-474.
56. Kelland, L. R.; Sharp, S. Y.; O'Neill, C. F.; Raynaud, F. I.; Beale, P. J.; Judson, I. R., *J. Inorg. Biochem.* **1999,** 77, 111-115.
57. Paolozzi, F. P.; Gaver, R.; Poiesz, B. J.; Louie, A.; DiFino, S.; Comis, R. L.; Newman, N.; Ginsberg, S., *Invest. New Drugs* **1988,** 6, 199-206.
58. Clarke, M. J., *Coord. Chem. Rev.* **2003,** 236, 209-233.
59. Bergamo, A.; Sava, G., *Dalton Trans.* **2011,** 40, 7817-7823.

60. Bratsos, I.; Bergamo, A.; Sava, G.; Gianferrara, t.; Zangrando, E.; Alessio, E., *J. Inorg. Biochem.* **2008,** 102, 606-617.
61. Sava, G.; Bergamo, A.; Dyson, P. J., *Dalton Trans.* **2011,** 40, 9069-9075.
62. Levina, A.; Mitra, A.; Lay, P. A., *Metallomics* **2009,** 1, 458-470.
63. Li, H. Y.; Qian, Z. M., *Med. Res. Rev.* **2002,** 22, 225-250.
64. Page, S., *Educ. Chem.* **2012,** 49, 26-29.
65. Anghileri, L. J.; Krebsforsch, Z., *Klin. Onkol. Cancer Res. Clin. Oncol.* **1975,** 83, 213-217.
66. Michael, J. C., *Coord. Chem. Rev.* **2002,** 232, 69-93.
67. Alessio, E.; Mestroni, G.; Bergamo, A.; Sava, G., *Curr. Top. Med. Chem.* **2004,** 4, 1525-1535.
68. Mestroni, G.; Alessio, E.; Sava, G.; Pacor, S.; Coluccia, M.; Boccarelli, A., *Met. Based Drugs* **1994,** 1, 41-63.
69. Alessio, E.; Mestroni, G.; Nardin, G.; Attia, W. M.; Calligaris, M.; Sava, G.; Zorzet, S., *Inorg. Chem.* **1988,** 27, 4099-4106.
70. Coluccia, M.; Sava, G.; Loseto, F.; Nassi, A.; Boccarelli, A.; Giordano, D.; Alessio, E.; Mestroni, G., *Eur. J. Cancer* **1993,** 29A, 1873-1879.
71. Sava, G.; Pacor, S.; Zorzet, S.; Alessio, E.; Mestroni, G., *Pharmacol. Res.* **1989,** 21, 617-628.
72. Mestroni, G.; Alessio, E.; Sava, G., **1998,** WO 98/00431.
73. Keppler, B. K.; Rupp, W.; Juhl, U. M.; Endres, H.; Niebl, R.; Balzer, W., *Inorg. Chem.* **1987,** 26, 4366-4370.
74. Lipponer, K.; Vogel, E.; Keppler, B. K., *Met. Based Drugs* **1996,** 3, 243-260.
75. Antonarakis, E. S.; Emadi, A., *Cancer Chemother. Pharmacol.* **2010,** 66, 1-9.
76. Berger, M. R.; Garzon, F. T.; Keppler, B. K.; Schmahl, D., *Anticancer Res.* **1989,** 9, 761-765.
77. Pieper, T.; Borsky, K.; Keppler, B. K., *Top. Biol. Inorg. Chem.* **1999,** 1, 171-199.
78. Seelig, M. H.; Berger, M. R.; Keppler, B. K., *J. Cancer Res. Clin. Oncol.* **1992,** 118, 195-200.
79. Webb, M. I.; Walsby, C. I., *Dalton Trans.* **2011,** 40, 1322-1331.
80. Pongratz, M.; Schluga, P.; Jakupec, M. A.; Arion, V. B.; Hartinger, C. G.; Allmaier, G.; Keppler, B. K., *J. Anal. At. Spectrom.* **2004,** 19, 46-51.
81. Reisner, E.; Arion, V. B.; Keppler, B. K.; Pombeiro, A. J. L., *Inorg. Chim. Acta* **2008,** 361, 1569-1583.
82. Zobi, F.; Mood, B. B.; Wood, P. A.; Fabbiani, F. P. A.; Parsons, S.; Sadler, P. J., *Eur. J. Inorg. Chem.* **2007,** 18, 2783-2796.
83. Gasser, G.; Ott, I.; Metzler-Nolte, N., *J. Med. Chem.* **2010,** 54, 3-25.
84. Nazarov, A. A.; Hartinger, C. G.; Dyson, P. J., *J. Organomet. Chem.* **2014,** 751, 251-260.
85. Dyson, P. J.; Sava, G., *Dalton Trans.* **2006**, 1929-1933.
86. Morris, R. E.; Aird, R. E.; Murdoch, D. S.; Chen, H.; Cummings, J.; Hughes, N. D., *J. Med. Chem* . **2001,** 44, 3616-3621.
87. Aird, R. E.; Cummings, J.; Ritchie, A. A.; Muir, M.; Morris, R. E.; Chen, H.; Sadler, P. J.; Jodrell, D. I., *Br. J. Cancer* **2002,** 86, 1652-1657.

88. Allardyce, C. S.; Dyson, P. J.; Ellis, D. J.; Heath, S. L., *Chem. Commun.* **2001**, 1396-1397.

89. Allardyce, C. S.; Dyson, P. J.; Ellis, D. J.; Salter, P. A.; Scopelliti, R., *J. Organomet. Chem.* **2003,** 668, 35-42.

90. Herman, A.; Tanski, J. M.; Tibbetts, M. F.; Anderson, C. M., *Inorg. Chem.* **2008,** 47, 274-280.

91. Therrien, B.; Ang, W. H.; Cherioux, F.; Vieille-Petit, L.; Juillerat-Jeanneret, L.; Suss-Fink, G.; Dyson, P. J., *J. Cluster Sci.* **2007,** 18, 741-752.

92. Ito, T.; Hamaguchi, T.; Nagino, H.; Yamaguchi, T.; Kido, H.; Zavarine, I. S.; Richmond, T.; Washington, J.; Kubiak, C. P., *J. Am. Chem. Soc.* **1999,** 121, 4625-4632.

93. Hotze, A. C. G.; van der Geer, E. P. L.; Kooijman, H.; Spek, A. L.; Haasnoot, J. G.; Reedijk, J., *Eur. J. Inorg. Chem.* **2005,** 2005, 2648-2657.

94. Wang, K.; Gao, E., *Anticancer Agents Med. Chem.* **2014,** 14, 147-169.

95. Wheate, N. J.; Brodie, C. R.; Collins, J. G.; Kemp, S.; Aldrich-Wright, J. R., *Mini-Rev. Med. Chem.* **2007,** 7, 627-648.

96. Keene, R. F.; Smith, J. A.; Collins, J. G., *Coord. Chem. Rev.* **2009,** 253, 2021-2035.

97. Therrien, B.; Suss-Fink, G.; Govindaswamy, P.; Renfrew, A. K.; Dyson, P. J., *Angew. Chem. Int. Ed.* **2008,** 47, 3773-3776.

98. Dwyer, F. P.; Gyarfas, E. C.; Rogers, W. P.; Koch, J. H., *Nature* **1952,** 170, 190-191.

99. Cho, K.; Wang, X.; Nie, S.; Chen, Z.-G.; Shin, D. M., *Clin. Cancer Res.* **2008,** 14, 1310-1316.

100. Van Zutphen, S.; Reedijk, J., *Coord. Chem. Rev.* **2005,** 249, 2845-2853.

101. Vock, C. A.; Ang, W. H.; Scolaro, C.; Phillips, A. D.; Lagopoulos, L.; Juillerat-Jeanneret, L.; Sava, G.; Scopelliti, R.; Dyson, P. J., *J. Med. Chem.* **2007,** 50, 2166-2175.

102. Zorzet, S.; Bergamo, A.; Cocchietto, M.; Sorc, A.; Gava, B.; Alessio, E.; Iengo, E.; Sava, G., *J. Pharmacol. Exp. Ther.* **2000,** 295, 927-933.

103. Sava, G.; Zorzet, S.; Turrin, C.; Vita, F.; Soranzo, M.; Zabucchi, G.; Cocchietto, M.; Bergamo, A.; DiGiovine, S.; Pezzoni, G.; Sartor, L.; Garbisa, S., *Clin. Cancer Res.* **2003,** 9, 1898-1905.

104. Sava, G.; Frausin, F.; Cocchietto, M.; Vita, F.; Podda, E.; Spessotto, P.; Furlani, A.; Scarcia, V.; Zabucchi, G., *Eur. J. Cancer* **2004,** 40, 1383-1396.

105. Frausin, F.; Scarcia, V.; Cocchietto, M.; Furlani, A.; Serli, B.; Alessio, E.; Sava, G., *J. Pharmacol. Exp. Ther.* **2005,** 313, 227-233.

106. Pacor, S.; Zorzet, S.; Cocchietto, M.; Bacac, M.; Vadori, M.; Turrin, C.; Gava, B.; Castellarin, A.; Sava, G., *J. Pharmacol. Exp. Ther.* **2004,** 310, 737-744.

107. Vacca, A.; Bruno, M.; Boccarelli, A.; Coluccia, M.; Ribatti, D.; Bergamo, A.; Garbisa, S.; Sartor, L.; Sava, G., *Br. J. Cancer* **2002,** 86, 993-998.

108. Pluim, D.; van Waardenburg, R. C.; Beijnen, J. H.; Schellens, J. H., *Cancer Chemother. Pharmacol.* **2004,** 54, 71-78.

109. Levina, A.; Aitken, J. B.; Gwee, Y. Y.; Lim, Z. J.; Liu, M.; Singharay, A. M.; Wong, P. F.; Lay, P. A., *Chem. Eur. J.* **2013,** 19, 3609-3619.

110. Reisner, E.; Arion, V. B.; Fatima, M.; da Silva, C. G.; Lichtenecker, R.; Eichinger, A.; Keppler, B. K.; Kukushkin, V. Y.; Pombeiro, A. J. L., *Inorg. Chem.* **2004,** 43, 7083-7093.

111. Schluga, P.; Hartinger, C. G.; Egger, A.; Reisner, E.; Galanski, M.; Jakupec, M. A.; Keppler, B. K., *Dalton Trans.* **2006**, 1796-1802.
112. Claire, S.; Dyson, P. J., *Platinum Met. Rev.* **2001,** 45, 62-69.
113. Bratsos, l.; Jedner, S.; Gianferrara, T.; Alessio, E., *Chimia* **2007,** 61, 692-697.
114. Vincent, J.; Love, S., *Biochim. Biophys. Acta.* **2011,** [in press].
115. Bartnikas, T. B., *Biometals* **2012,** 25, 677-686.
116. Hartinger, C. G.; Zorbas-Seifried, S.; Jakupec, M. A.; Kynast, B.; Zorbas, H.; Keppler, B. K., *J. Inorg. Biochem.* **2006,** 100, 891-904.
117. Trynda-Lemiesz, L.; Karaczyn, A.; Keppler, B. K.; Kozlowski, H., *J. Inorg. Biochem.* **2000,** 78, 341-346.
118. Kratz, F.; Hartmann, M.; Keppler, B. K.; Messori, L., *J. Biol. Chem.* **1994,** 269, 2581-2588.
119. Messori, L.; Vilchez, F. G.; Vilaplana, R.; Piccioli, F.; Alessio, E.; Keppler, B. K., *Met. Based Drugs* **2000,** 7, 335-342.
120. Rademaker-Lakhai, J. M.; van den Bongard, D.; Pluim, D.; Beijnen, J. H.; Schellens, J. H. M., *Clin. Cancer Res.* **2004,** 10, 3717-3727.
121. Qian, Z. M.; Li, H. Y.; Sun, H.; Ho, K., *Pharmacol. Rev.* **2002,** 54, 561-587.
122. Sun, H.; Li, H.; Sadler, P. J., *Chem. Rev.* **1999,** 99, 2817-2842.
123. Taetle, R., *Exp. Hematol.* **1990,** 18, 360-365.
124. Page, S. M.; Boss, S. R.; Barker, P. D., *Future Med. Chem.* **2009,** 1, 541-559.
125. Bacac, M.; Hotze, A. C. G.; van der Schilden, K.; Haasnoot, J. G.; Pacor, S.; Alessio, E.; Sava, G.; Reedijk, J., *J. Inorg. Biochem.* **2004,** 98, 402-412.
126. Sava, G.; Bergamo, A.; Zorzet, S.; Gava, B.; Casarsa, C.; Cocchietto, M.; Furlani, A.; Scarcia, V.; Serli, B.; Iengo, E.; Alessio, E.; Mestroni, G., *Eur. J. Cancer* **2002,** 38, 427-435.
127. Chen, L. M.; Chen, J. C.; Luo, H.; Liao, S. Y.; Zheng, K. C., *J. Theor. Comput. Chem.* **2011,** 10, 581-604.
128. Besker, N.; Coletti, C.; Marrone, A.; Re, N., *J. Phys. Chem. B* **2008,** 112, 3871-3875.
129. Iengo, E.; Mestroni, G.; Geremia, S.; Calligaris, M.; Alessio, E., *J. Chem. Soc. Dalton Trans.* **1999**, 3361-3371.
130. Alessio, E.; Balducci, G.; Lutman, G.; Mestroni, G.; Calligaris, M.; Attia, W. M., *Inorg. Chim. Acta* **1993,** 203, 205-217.
131. Stevens, R., *Nat. Struct. Mol. Biol.* **2004,** 11, 293-295.
132. Aitken, J. B.; Antony, S.; Weekley, C. M.; Lai, B.; Spiccia, L.; Harris, H. H., *Metallomics* **2012,** 4, 1051-1056.
133. Liu, M.; Lim, Z. J.; Gwee, Y. Y.; Levina, A.; Lay, P. A., *Angew. Chem. Int. Ed.* **2010,** 49, 1661-1664.
134. Jakupec, M. A.; Reisner, E.; Eichinger, A.; Pongratz, M.; Arion, V. B.; Galanski, M.; Hartinger, C. G.; Keppler, B. K., *J. Med. Chem.* **2005,** 48, 2831-2837.
135. Bergamo, A.; Sava, G., *Dalton Trans.* **2007**, 1267-1272.
136. Bergamo, A.; Gagliardi, R.; Scarcia, V.; Furlani, A.; Alessio, E.; Mestroni, G.; Sava, G., *J. Pharmacol. Exp. Ther.* **1999,** 289, 559-564.

137. Bergamo, A.; Messori, L.; Piccioli, F.; Cocchietto, M.; Sava, G., *Invest. New Drugs* **2003,** 21, 401-411.
138. Sanna, B.; Debidda, M.; Pintus, G.; Tadolini, B.; Posadino, A. M.; Bennardini, F.; Sava, G.; Ventura, C., *Arch. Biochem. Biophys.* **2002,** 403, 209-218.
139. Morbidelli, L.; Donnini, S.; Filippi, S.; Messori, L.; Piccioli, F.; Orioli, P.; Sava, G.; Ziche, M., *Br. J. Cancer* **2003,** 88, 1484-1491.
140. Nazarov, A. A.; Baquie, M.; Nowak-Sliwinska, P.; Zava, O.; van Beijnum, J. R.; Groessl, M.; Chisholm, D. M.; Ahmadi, Z.; McIndoe, J. S.; Griffioen, A. W.; van den Bergh, H.; Dyson, P. J., *Sci. Rep.* **2013,** 3, 1485.
141. Serli, B.; Zangrando, E.; Iengo, E.; Alessio, E., *Inorg. Chim. Acta* **2002,** 339, 265-272.
142. Serli, B.; Zangrando, E.; Iengo, E.; Mestroni, G.; Yellowlees, L.; Alessio, E., *Inorg. Chem.* **2002,** 41, 4033-4043.
143. Groessl, M.; Reisner, E.; Hartinger, C. G.; Eichinger, R.; Semenova, O.; Timerbaev, A. R.; Jakupec, M. A.; Arion, V. B.; Keppler, B. K., *J. Med. Chem.* **2007,** 50, 2185-2193.
144. Khalaila, I.; Bergamo, A.; Bussy, F.; Sava, G.; Dyson, P. J., *Int. J. Oncol.* **2006,** 29, 261-268.
145. Bruijnincx, P. C. A.; Sadler, P. J., *Adv. Inorg. Chem.* **2009,** 61, 1-62.
146. Messori, L.; Orioli, P.; Vullo, D.; Alessio, E.; Iengo, E., *Eur. J. Biochem.* **2000,** 267, 1206-1213.
147. Chatlas, J.; Eldik, R. V.; Keppler, B. K., *Inorg. Chim. Acta* **1995,** 233, 59-63.
148. Messori, L.; Kratz, F.; Alessio, E., *Met. Based Drugs* **1996,** 3, 1-9.
149. Mura, P.; Camalli, M.; Messori, L.; Piccioli, F.; Zanello, P.; Corsini, M., *Inorg. Chem.* **2004,** 43, 3863-3870.
150. Vargiu, A. V.; Robertazzi, A.; Magistrato, A.; Ruggerone, P.; Carloni, P., *J. Phys. Chem. B* **2008,** 112, 4401-4409.
151. Messori, L.; Merlino, A., *Dalton Trans.* **2014,** [In press].
152. Gava, B.; Zorzet, S.; Spessotto, P.; Cocchietto, M.; Sava, G., *J. Pharmacol. Exp. Ther.* **2006,** 317, 284-291.
153. Galanski, M.; Arion, V. B.; Jakupec, M. A.; Keppler, B. K., *Curr. Pharm. Des.* **2003,** 9, 2078-2089.
154. Harris, H. H.; Levina, A.; Dillon, C. T.; Mulyani, I.; Lai, B.; Cai, Z.; Lay, P. A., *J. Biol. Inorg. Chem.* **2005,** 10, 105-118.
155. http://www.lifetechnologies.com/us/en/home/references/gibco-cell-culture-basics/introduction-to-cell-culture.html (September 2013),
156. John, P., 5th ed.; Churchill livingstone, Edinburgh: 1975.
157. Philippeos, C.; Hughes, R. D.; Dhawan, A.; Mitry, R. R., *Methods Mol. Biol.* **2012,** 806, 1-13.
158. Freshney, R. I., 2nd ed.; Oxford University Press, Oxford: 1992.
159. Hook, G. R.; Hosseini, J. M.; Elin, R. J., *J. Am. Coll. Nutr.* **1985,** 4, 599-612.
160. www.amptek.com/pdf/xrf.pdf (September 2013),
161. http://webh01.ua.ac.be/mitac4/micro_xrf.pdf (September 2013),
162. Jones, K. W.; Gordon, B. M.; Hanson, A. L.; Kwiatek, W. M.; Pounds, J. G., *Ultramicroscopy* **1988,** 24, 313-328.

163. Ortega, R.; Deves, G.; Carmona, A., *J. R. Soc. Interface* **2009,** 6, S649-S658.
164. Fahrni, C. J., *Curr. Opin. Chem. Biol.* **2007,** 11, 121-127.
165. Snigireva, I.; Snigirev, A., *J. Environ. Monit.* **2006,** 8, 33-42.
166. Weekley, C. M.; Aitken, J. B.; Vogt, S.; Finney, L. A.; Paterson, D. J.; de Jonge, M. D.; Howard, D. L.; Witting, P. K.; Musgrave, I. F.; Harris, H. H., *J. Am. Chem. Soc.* **2011,** 133, 18272-18279.
167. Kono, K.; Yoshida, Y., *Bull. Osaka Med. Coll.* **1989,** 35, 1-9.
168. Bazin, D.; Daudon, M.; Chevallier, P.; Rouzie're, S.; Elkaim, E.; Thiaudiere, D.; Fayard, B.; Foy, E.; Albouy, P. A.; Andre, G.; Matzen, G.; Veron, E., *Ann. Biol. Clin.* **2006,** 64, 125-139.
169. Levina, A.; Harris, H. H.; Lay, P. A., *J. Am. Chem. Soc.* **2007,** 129, 1065-1075.
170. Harris, T. V.; Szilagyi, R. K.; McFarlane Holman, K. L., *J. Biol. Inorg. Chem.* **2009,** 14, 891-898.
171. Carter, E. A.; Rayner, B. S.; McLeod, A. I.; Wu, L. E.; Marshall, C. P.; Levina, A.; Aitken, J. B.; Witting, P. K.; Lai, B.; Cai, Z.; Vogt, S.; Lee, Y.-C.; Chen, C.-I.; Tobin, M. J.; Harris, H. H.; Lay, P. A., *Mol. BioSyst.* **2010,** 6, 1316-1322.
172. Lakowicz, J. R., 3rd ed.; Springer, New York: 2006.
173. Matsumoto, B., Academic Press: 2003.
174. Shotton, D. M., *J. Cell Sci.* **1989,** 94, 175-206.
175. Ghiran, I. C., *Methods Mol. Biol.* **2011,** 689, 93-136.
176. Zimmermann, T.; Rietdorf, J.; Pepperkoka, R., *FEBS Lett.* **2003,** 546, 87-92.
177. Stephens, D. J.; Allan, V. J., *Science* **2003,** 300, 82-86.
178. Vos, J. G.; Kelly, J. M., *Dalton Trans.* **2006**, 4869-4883.
179. Spiccia, L.; Deacon, G. B.; Kepert, C. M., *Coord. Chem. Rev.* **2004,** 248, 1329-1341

180. Carvalho, M. L.; Magalhaes, T.; Becker, M.; von Bohlen, A., *Spectroc. Acta Pt. B-Atom. Spectr.* **2007,** 62, 1004-1011.
181. Elrefaie, F. A.; Smeltzer, W. W., *Oxid. Met.* **1982,** 17, 407-413.
182. Bullock, G. R., *J. Microsc.* **1984,** 133, 1-15.
183. Ortega, R.; Moretto, P.; Fajac, A.; Benard, J.; Llabador, Y.; Simonoff, M., *Cell Mol. Biol.* **1996,** 42, 77-88.
184. Ilinski, P.; Lai, B.; Cai, Z.; Yun, W.; Legnini, D.; Talarico, T.; Cholewa, M.; Webster, L. K.; Deacon, G. B.; Rainone, S.; Phillips, D. R.; Stampfl, A. P., *Cancer Res.* **2003,** 63, 1776-1179.
185. Hall, M. D.; Dillon, C. T.; Zhang, M.; Beale, P.; Cai, Z.; Lai, B.; Stampfl, A. P.; Hambley, T. W., *J. Biol. Inorg. Chem.* **2003,** 8, 726-732.
186. Hall, M. D.; Alderden, R. A.; Zhang, M.; Beale, P. J.; Cai, Z.; Lai, B.; Stampfl, A. P.; Hambley, T. W., *J. Struct. Biol.* **2006,** 155, 38-44

187. Munro, K. L.; Mariana, A.; Klavins, A. I.; Foster, A. J.; Lai, B.; Vogt, S.; Cai, Z.; Harris, H. H.; Dillon, C. T., *Chem. Res. Toxicol* . **2008,** 21, 1760-1769.

188. Weekley, C. M.; Aitken, J. B.; Vogt, S.; Finney, L. A.; Paterson, D. J.; de Jonge, M. D.; Howard, D. L.; Musgrave, I. F.; Harris, H. H., *Biochem.* **2011,** 50, 1641-1650.
189. Waern, J. B.; Harris, H. H.; Lai, B.; Cai, Z.; Harding, M. M.; Dillon, C. T., *J. Biol. Inorg. Chem.* **2005,** 10, 443-452.
190. Crossley, E. L.; Aitken, J. B.; Vogt, S.; Harris, H. H.; Rendina, L. M., *Angew. Chem. Int. Ed.* **2010,** 49, 1231-1233.
191. Arancia, G.; Calcabrini, A.; Meschini, S.; Molinari, A., *Cytotechnology* **1998,** 27, 95-111.
192. Larsen, A. K.; Escargueil, A. E.; Skladanowski, A., *Pharmacol. Ther.* **2000,** 85, 217-229.
193. Kalayda, G.; Jansen, B. A. J.; Wielaard, P.; Tanke, H. J.; Reedijk, J., *J. Biol. Inorg. Chem.* **2005,** 10, 305-315.
194. Kalayda, G. V.; Jansen, B. A. J.; Molenaar, C.; Wielaard, P.; Tanke, H. J.; Reedijk, J., *J. Biol. Inorg. Chem.* **2004,** 9, 414-422.
195. Kalayda, G. V.; Zhang, G.; Abraham, T.; Tanke, H. J.; Reedijk, J., *J. Med. Chem.* **2005,** 48, 5191-5202.
196. Jansen, B. A. J.; Wielaard, P.; Kalayda, G. V.; Ferrari, M.; Molenaar, C.; Tanke, H. J.; Brouwer, J.; Reedijk, J., *J. Biol. Inorg. Chem.* **2004,** 9 403-413.
197. Antony, S.; Aitken, J. B.; Vogt, S.; Lai, B.; Brown, T.; Spiccia, L.; Harris, H. H., *J. Biol. Inorg. Chem.* **2013,** 18, 845-853.
198. Antony, S.; Morris, J. C.; Bell, T.; Brown, T.; Spiccia, L.; Harris, H. H., *Aust. J. Chem.* **2014,** Accepted.

Chapter 2

Distinct cellular fates for KP1019 and NAMI-A determined by X-ray fluorescence imaging of single cells[†]

Jade B. Aitken, [1, 2, 3] Sumy Antony, [4, 5] Claire M. Weekley, [5] Barry Lai, [6] Leone Spiccia [4] and Hugh H. Harris [5]

[1] School of Chemistry, The University of Sydney, New South Wales, 2006, Australia
[2] Australian Synchrotron, Clayton, Victoria, 3168, Australia
[3] Institute of Materials Structure Science, KEK, Tsukuba, Ibaraki 305-0801, Japan
[4] School of Chemistry, Monash University, Clayton, Victoria 3800, Australia
[5] School of Chemistry and Physics, The University of Adelaide, SA 5005, Australia.
[6] X-ray Science Division, Argonne National Laboratory, Argonne IL 60439, USA.

[†] Aitken, J.; Antony, S.; Weekley, C.; Lai, B.; Spiccia, L.; Harris, H., *Metallomics* 2012, 4, 1051-1056.

Chapter 2

Aitken, J. B., **Antony, S**., Weekley, C., Lai, B., Spiccia, L., & Harris, H. H. (2012), Distinct cellular fates for KP1019 and NAMI-A determined by X-ray fluorescence imaging of single cells. *Metallomics*, 4, 1051-1056.

Antony, S. (Candidate)

Shared responsibility for the design and development of the work. Performed syntheses and cytotoxicity assays, developed treatment and sample preparation protocols through a series of pilot experiments, contributed to analysis and interpretation of final results, contributed to the manuscript preparation and revision.

I hereby certify that the statement of contribution is accurate.

Signed: Date: 03/10/2013

Aitken, J. B. (Principal Author)

Performed final XRF data collection and analysis; interpreted results and contributed to manuscript preparation and revision.

I hereby certify that the statement of contribution is accurate and I give permission for the inclusion of the paper in the thesis.

Signed: Date: 1/10/2013

Weekley, C.

Prepared final samples for XRF experiments and assisted with manuscript revision.

I hereby certify that the statement of contribution is accurate and I give permission for the inclusion of the paper in the thesis.

Signed: Date: 3/10/13

Lai, B.

Assisted with XRF experiments and revision of the manuscript.

I hereby certify that the statement of contribution is accurate and I give permission for the inclusion of the paper in the thesis.

Signed: Date: Oct. 1, 2013

Spiccia, L.

Supervised experimental work, assisted with interpretation of results, and in the revision of the manuscript.

I hereby certify that the statement of contribution is accurate and I give permission for the inclusion of the paper in the thesis.

Signed: Date: 3\10\13

Harris, H. H.

Supervised the development of the work, assisted with experimental design, XRF experiments, interpretation of the data, and in the conception and revision of the manuscript and acted as corresponding author.

I hereby certify that the statement of contribution is accurate and I give permission for the inclusion of the paper in the thesis.

Signed: Date: 3/10/13

Aitken, J.B., Antony, S., Weekley, C.M., LaI, B., Spiccia, L. & Harris, H.H. (2012) Distinct cellular fates for KP1019 and NAMI-A determined by X-ray fluorescence imaging of single cells.

Metallomics, v. 4 (10), pp. 1051-1056 + Supplementary information PDF

Chapter 3

X-ray fluorescence imaging of single human cancer cells reveals that the N-heterocyclic ligands of iodinated analogues of ruthenium anticancer drugs remain coordinated after cellular uptake†

Sumy Antony, [1, 5] Jade B. Aitken, [2] Stefan Vogt, [3] Barry Lai, [3] Tracey Brown, [4] Leone Spiccia [5] and Hugh H. Harris [1]

[1] School of Chemistry and Physics, The University of Adelaide, SA 5005, Australia.

[2] School of Chemistry, The University of Sydney, New South Wales, 2006, Australia [3] X-ray Science Division, Argonne National Laboratory, Argonne IL 60439, USA.

[4] School of Biochemistry and Molecular Biology, Monash University, Clayton, VIC 3800, Australia

[5] School of Chemistry, Monash University, Clayton, VIC 3800, Australia

---

† Antony, S.; Aitken, J. B.; Vogt, S.; Lai, B.; Brown, T.; Spiccia, L.; Harris, H. H., *J. Biol. Inorg. Chem.* 2013, 18, 845-853.

Chapter 3

Antony, S., Aitken, J. B., Vogt, S., Lai, B., Brown, T., Spiccia, L., & Harris, H. H. (2013), X-ray fluorescence imaging of single human cancer cells reveals that the N-heterocyclic ligands of iodinated analogues of ruthenium anticancer drugs remain coordinated after cellular uptake. *J. Biol. Inorg. Chem.* 18, 845-853.

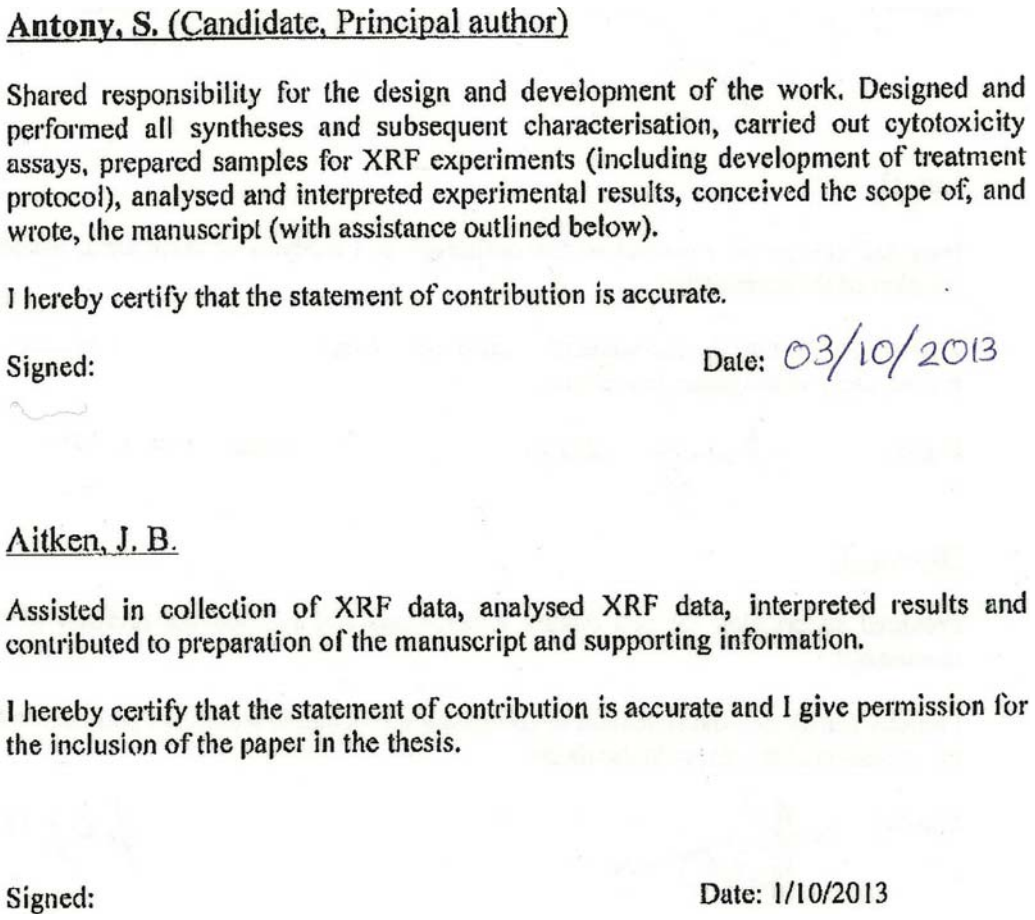

Antony, S. (Candidate, Principal author)

Shared responsibility for the design and development of the work. Designed and performed all syntheses and subsequent characterisation, carried out cytotoxicity assays, prepared samples for XRF experiments (including development of treatment protocol), analysed and interpreted experimental results, conceived the scope of, and wrote, the manuscript (with assistance outlined below).

I hereby certify that the statement of contribution is accurate.

Signed: Date: 03/10/2013

Aitken, J. B.

Assisted in collection of XRF data, analysed XRF data, interpreted results and contributed to preparation of the manuscript and supporting information.

I hereby certify that the statement of contribution is accurate and I give permission for the inclusion of the paper in the thesis.

Signed: Date: 1/10/2013

Vogt, S.

Provided advice with respect to the collection and analysis of XRF data, assisted revision of the manuscript.

I hereby certify that the statement of contribution is accurate and I give permission for the inclusion of the paper in the thesis.

Signed: Date: 10/1/2013

Lai, B.

Provided advice with respect to the collection and analysis of XRF data, assisted revision of the manuscript.

I hereby certify that the statement of contribution is accurate and I give permission for the inclusion of the paper in the thesis.

Signed: Date: Oct. 1, 2013

Brown, T.

Provided supervision for cell culture experiments and assisted the revision of the manuscript.

I hereby certify that the statement of contribution is accurate and I give permission for the inclusion of the paper in the thesis.

Signed: Date: 3/10/2013

Spiccia, L.

Supervised synthetic work, assisted with interpretation of results, and in the revision of the manuscript.

I hereby certify that the statement of contribution is accurate and I give permission for the inclusion of the paper in the thesis.

Signed: Date: 3/10/13

Harris, H. H.

Supervised the design and development of the work, assisted with experimental design, XRF experiments, interpretation of the data, and in the conception and revision of the manuscript and acted as corresponding author.

I hereby certify that the statement of contribution is accurate and I give permission for the inclusion of the paper in the thesis.

Signed: Date: 3/10/13

Antony, S., Aitken, J.B., Vogt, S., Lai, B., Brown, T., Spiccia, L. & Harris, H.H. (2013) X-ray fluorescence imaging of single human cancer cells reveals that the N-heterocyclic ligands of iodinated analogues of ruthenium anticancer drugs remain coordinated after cellular uptake.
Journal of Biological Inorganic Chemistry, v. 18 (7), pp. 845-853 + Supplementary information PDF

Chapter 4

Fluorescent analogues of NAMI-A: Synthesis, characterization, fluorescent properties and preliminary biological studies in human lung cancer cells (A549) †

Sumy Antony, [1, 2] Jonathan C. Morris, [3] Toby Bell, [2] Tracey Brown, [4] Leone Spiccia, [2] and Hugh H. Harris [1]

[1] School of Chemistry and Physics, The University of Adelaide, SA 5005, Australia

[2] School of Chemistry, Monash University, Clayton, VIC 3800, Australia

[3] School of Chemistry, The University of New South Wales, Sydney, NSW 2052, Australia

[4] School of Biochemistry and Molecular Biology, Monash University, Clayton, VIC 3800, Australia

---

† Antony, S.; Morris, J. C.; Bell, T.; Brown, T.; Spiccia, L.; Harris, H. H., *Aust. J. Chem.* 2014, *accepted.*

Chapter 4

Antony, S., Morris, J. C., Bell, T., Brown, T., Spiccia, L., & Harris, H. H. (2013), Fluorescent analogues of NAMI-A: Synthesis, characterization, fluorescent properties and preliminary biological studies in human lung cancer cells. *Aust. J. Chem., Manuscript accepted.*

Antony, S. (Candidate, Principal Author)

Shared responsibility for the design and development of the work. Designed and performed all synthetic experimental work, fluorescent imaging and cytotoxicity assays, analysed and interpreted results, conceived the scope of, and wrote the manuscript (with assistance outlined below).

I hereby certify that the statement of contribution is accurate.

Signed: Date: 03/10/2013

Morris, J. C.

Provided guidance for the design and development of the synthetic work, and assisted with revision of the manuscript.

I hereby certify that the statement of contribution is accurate and I give permission for the inclusion of the paper in the thesis.

Signed: Date: 3/10/13

Bell, T.

Supervised fluorescent quantum yield experiments and assisted with the revision of the manuscript.

I hereby certify that the statement of contribution is accurate and I give permission for the inclusion of the paper in the thesis.

Signed: Date: 7/10/13.

Brown, T.

Supervised cell culture experiments and assisted the revision of the manuscript.

I hereby certify that the statement of contribution is accurate and I give permission for the inclusion of the paper in the thesis.

Signed: Date: 7/10/2013

Spiccia, L.

Supervised all experimental work, assisted with interpretation of results, and assisted the revision of the manuscript.

I hereby certify that the statement of contribution is accurate and I give permission for the inclusion of the paper in the thesis.

Signed: Date: 3/10/13

Harris, H. H.

Supervised in the design and development of the work, assisted with experimental design, interpretation of the data, and in the conception and revision of the manuscript and acted as corresponding author.

I hereby certify that the statement of contribution is accurate and I give permission for the inclusion of the paper in the thesis.

Signed: Date: 3/10/13

Abstract:

Two new fluorescent ruthenium(III) complexes namely, 7-azaindolium *trans*-tetrachloridobis(7-azaindole)(dimethyl sulfoxide)ruthen(III)ate (**F1**) and N-[histaminedihydrolium]-1,8-naphthalenecarboximidic *trans*-tetracholorobis(dimethyl sulfoxide)(N-[histaminedihydro]-1,8-naphthalenecarboximide)ruthen(III)ate (**F2**) and their respective tetramethylammonium analogues (**F3** and **F4**) are reported herein. The compounds were characterised by elemental analysis, mass spectrometry, UV-Vis spectrophotometry and fluorescence spectroscopy. Molar extinction coefficients (ε_{max}) and fluorescence emission spectra were compared to evaluate the electronic properties of the synthesized fluorescent analogues, and hence their value as intracellular fluorescence probes. **F3** and **F4** were synthesized and characterised in order to eliminate fluorescence arising from the counter cations in **F1** and **F2** and thus to obtain a fluorescence quantum yield which reflects only a contribution from the metal complex anion. Half inhibitory concentrations (IC$_{50}$) were determined (reported as mean, [μM] ± S.E.M.; $n = 3$) for A549 cells exposed to the Ru complexes for 24 h: **F3** (203 ± 26) and **F4** (185 ± 20).

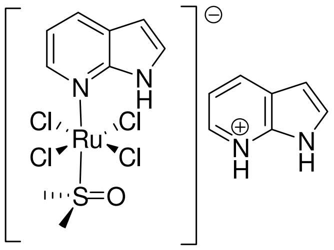

F1

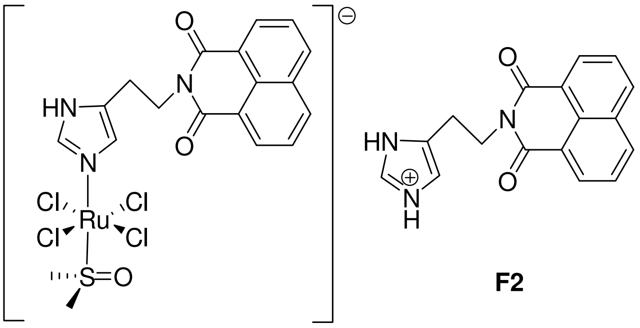

F2

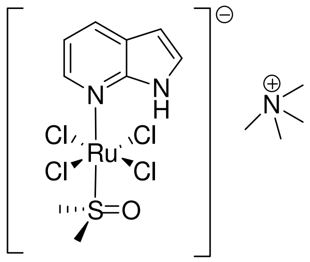

F3

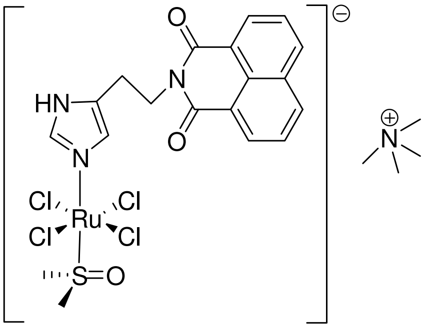

F4

Introduction

Ruthenium based drugs are promising anti-metastatic agents amongst metal based anticancer drugs. They exhibit activity against various types of tumours,[1, 2] and thus have been shown to be valid potential alternatives to *cis*-platin. There are several classes of ruthenium-based drugs (Scheme I), including RAPTA complexes (**A**, **B**), Ru-ethylenediamine complexes (**C**), Ru-azypy complexes (**D**), Keppler-type complexes (**E** = **KP1019**, **F** = **ICR**) and NAMI- type complexes (**G** = **NAMI**, **H** = **NAMI-A**).[3, 4] The development of these classes of ruthenium-based drugs has been recently reviewed,[4] and a wider range of species and their activities is discussed therein.

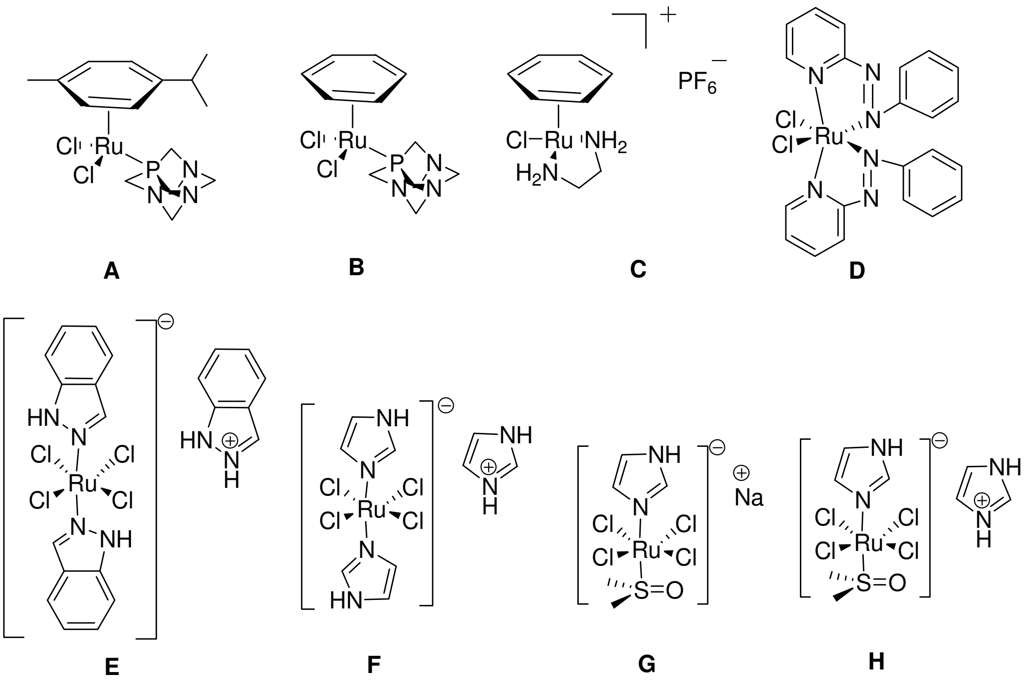

Scheme 1: A selection of the most widely studied ruthenium anticancer complexes.

Among these, the imidazole/sulfoxide complexes, NAMI (**G**) and NAMI-A (**H**), have been the focus for many researchers in recent years. These compounds display specific anti-metastatic activity which is not associated with direct cytotoxicity inside tumour cells,[5] indicating an opportunity for cancer treatment outside the existing predominant approach of selective toxicity. NAMI-A ([ImH]$^{+}$*trans*-[Ru(III)(DMSO)(Im)Cl$_4$]$^{-}$; Im = imidazole, DMSO =

dimethylsulfoxide) was the first ruthenium(III) complex to enter Phase I clinical trials.[6, 7] The complex is relatively non-toxic to normal human healthy cells and has shown marked efficacy against metastases (lung metastases, colorectal tumour).[1, 8] This has been suggested to be due to the ability of ruthenium to mimic iron when bound to bio-molecules such as serum transferrin and albumin which are known to be responsible for solubilization, transport, and detoxification of iron in mammals.[2, 7] NAMI-A also displayed significant anti-angiogenic activity in a number of *in vitro* and *in vivo* models.[3]

The anti-metastatic activity of NAMI-A type complexes can be explained on the basis of inhibition of a number of different steps in metastasis, including: tumour cell de-adhesion; motility (directed cell movement); and invasion (entry of foreign particle).[5] Many mechanisms for the underlying chemistry at the ruthenium centre have been proposed to explain these phenomena, including most commonly: (i) the activation by reduction mechanism,[9] and (ii) hydrolysis and ligand exchange of the complex.[1] In the first of these the Ru(III) complex is reduced to a Ru(II) species which then interacts with bio-molecules inside hypoxic tumours.[10] The activation by reduction concept is not yet supported by solid evidence, however, it cannot yet be discounted[4]. We note that EPR (Electron Paramagnetic Resonance) of reaction mixtures containing NAMI-A and physiologically relevant concentrations of serum albumin,[11] and XAS of cells,[12] or tissues from animals,[13] treated with NAMI-A all suggest that the majority of the ruthenium remains in the +III oxidation state.

Ligand exchange in the biological media was found to be a characteristic of these Ru(III) complexes,[1] and the stepwise hydrolysis of chloride ions has been proposed to be related with their biological activity. Indeed a Ru-BSA adduct, formed from NAMI-A, but stripped of all original ligands except perhaps the imidazole, shows significant anti-metastatic activity.[14] The same group suggest that, for a particular species, the relative importance of cytotoxicity (exerted through intracellular mechanism/s following uptake) versus anti-metastatic activity (most likely exerted predominantly through multiple extracellular mechanisms) depends on the interplay between the kinetics of ligand exchange, plasma protein binding and cell uptake. Despite the many efforts dedicated to unravelling the mechanism(s) of action of NAMI-A-type complexes, the origin of the anti-metastatic activities of these drugs is not yet completely comprehended.

We recently demonstrated distinct cellular fates for NAMI-A and KP1019 by using μ-X-ray fluorescence imaging (XRF) to compare the cellular distribution of ruthenium in cells treated with the complexes.[15] Co-localisation of Ru with P was connected to KP1019 uptake into the nucleus, whereas there was no significant change in the cellular elemental distribution when the cells were treated with NAMI-A.[15] To date, the question of whether imidazole remains attached to ruthenium *in vivo* remains unanswered, although our recent work has sought to address this question.[16] We envisage several approaches to attempt to address this question and report, herein, the development of synthetic chemistry to support one of these, along with biological experiments as preliminary validation.

In this study, we compare the cellular distribution of ruthenium (by XRF imaging, as previously demonstrated for the parent drug[11]) with that of the imidazole moiety (or proxy) by incorporating a fluorescent tag onto the N-heterocyclic ligand. The two main requirements for this to be successful are that the fluorophore is not quenched by coordination to the metal centre, and that the biological characteristics of the modified species remain close enough to the parent drug to be relevant.

The initial target complexes **F1** and **F2**, which were generated by replacing the imidazole group in NAMI-A with the fluorescent ligands 7-azaindole (**F5**) and N-[histaminedihydro]-1,8-naphthalenecarboximide (**F6**), are shown in scheme 2. In addition, the cation exchanged complexes (**F3** and **F4**, scheme 2) were designed to limit any fluorescence emission to the metal complex.

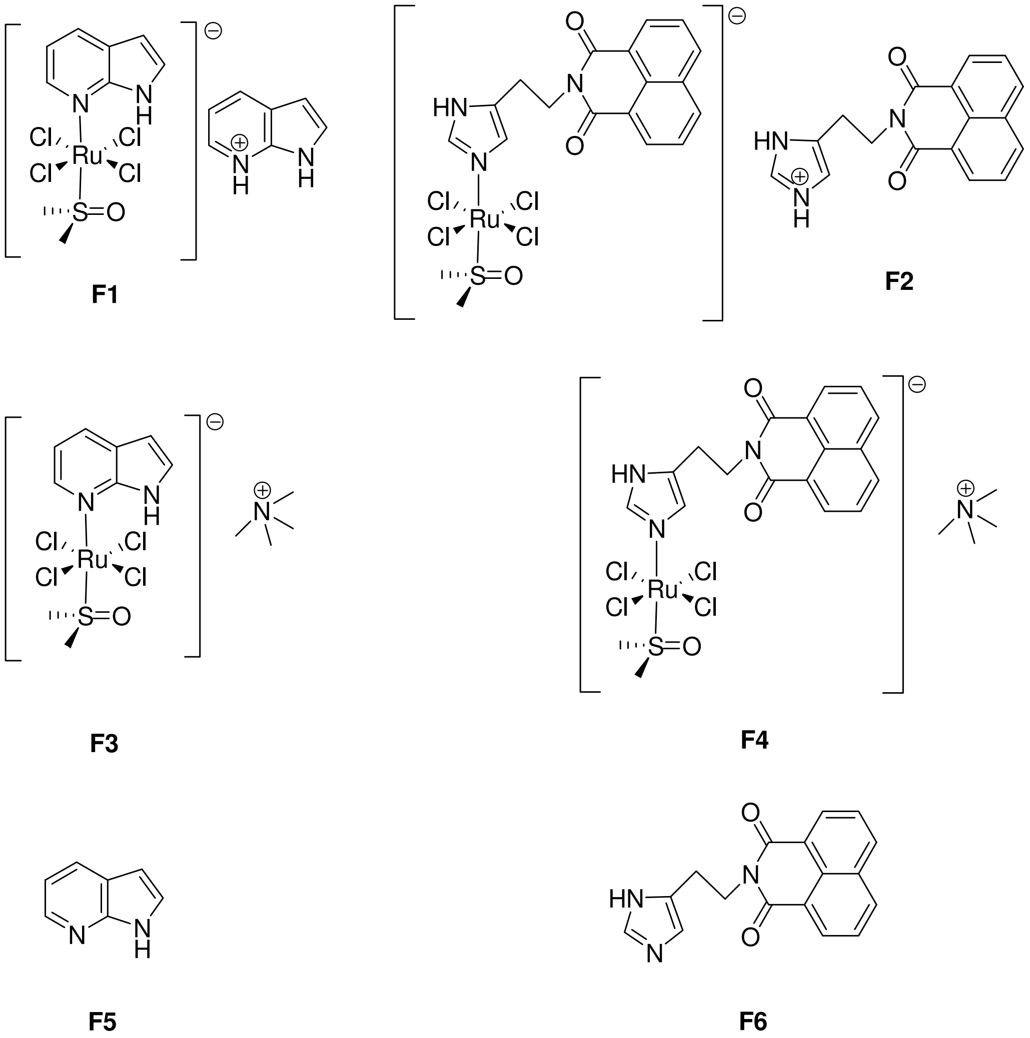

Scheme 2: Structures of the Ru(III) compounds studied (**F1**, **F2**, **F3**, and **F4**) with those of the free ligands, 7-azaindole (**F5**), and N-[histaminedihydro]-1,8-naphthalenecarboximide (**F6**).

Results and discussion

Syntheses and characterisation

The biological activities and applications of several NAMI-A derivatives bearing monodentate heterocyclic nitrogen ligands have already been reported.[17]. Our aim here was to assess the binding of NAMI-A analogues to biological targets and the stability of the Ru-N bond in *in vitro* cell culture as a means to provide further information to understand the mechanism of anti-metastatic activity of NAMI-A type complexes. Towards this end, fluorescent analogues of NAMI-A (**F1**-**F2**) were prepared by mixing a suspension of the ruthenium precursor, $[RuCl_4(DMSO)_2]^-$, in acetone, adding an equi molar amount of the ligand (**F5**-**F6**) and stirring overnight (Scheme 3).

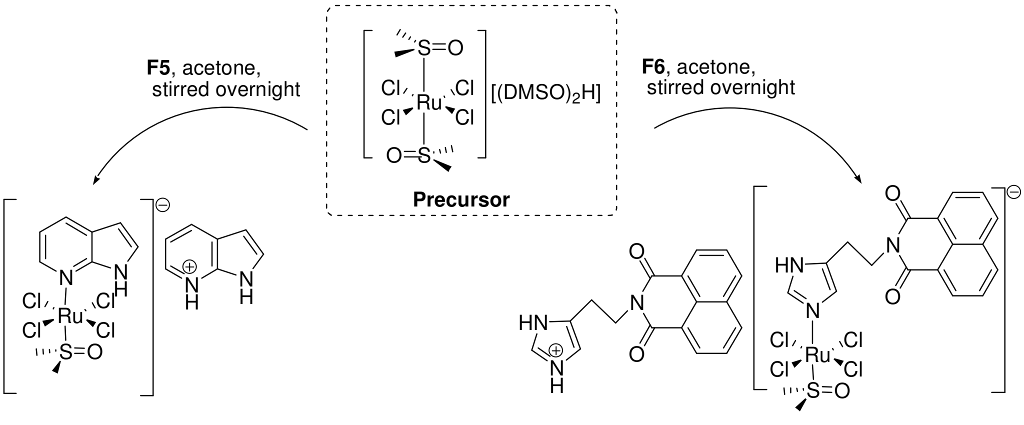

F1 **F2**

Scheme 3: Schematic representation of the synthetic route used for the preparation of ruthenium complexes **F1** and **F2**.

The tetramethylammonium analogues of **F1** and **F2** (**F3** and **F4**, respectively) were obtained by stirring the complexes with an excess of tetramethylammonium chloride in a suitable solvent (acetone for **F1** and methanol for **F2**). **F3** and **F4** were synthesized in order to increase the solubility of the parent complexes in physiological media and to probe the photophysical properties of the complexes more accurately by avoiding fluorescence from the N-heterocyclic cation present in the parent complex. The identity of the compounds was confirmed by elemental analysis, ^{1}H NMR spectroscopy (for **F6**), ATR-IR and ESI-MS (an X-ray crystal structure for a solvent-substituted version of **F1**, presented in the Supporting Information, supports the identity of the parent compound but highlights the lability of the chlorido ligands).

Parent ions (*m*/*z* –ve ion: 439.8 and 612.8 respectively for **F1** and **F2**) were observed in the ESI-MS spectra along with the expected daughter fragmentation products (*m*/*z* –ve ion: 361.8, 321.8 and 243.8 for **F1** and *m*/*z* –ve ion: 321.8 and

243.8 for **F2**, *see Table SI, supporting information*). Minimal contaminants were observed confirming the purity of the samples.

UV-Vis absorption spectroscopy

A summary of UV-Vis spectral data obtained for the complexes and the free ligands is shown in Table I. The UV-Vis spectra of **F1**, **F2, F3,** and **F4** displayed intense bands for ligand-centred (LC) $\pi-\pi^*$ transitions (~300-330 nm) and less intense ligand-to-metal charge-transfer (MC) transitions (390-430 nm) as shown in Figure 1 (A1, B1 and C1) and Figure 2 (X1, Y1 and Z1).

Table I: UV-Vis spectral data obtained for F1-F6 in methanol

Complex	**λ_{max} (nm) [LC]**	**Molar extinction coefficient* (M^{-1} cm^{-1}) ; ε_{max}**	**λ_{max} (nm) [MC]**	**Molar extinction coefficient* (M^{-1} cm^{-1}) ; ε_{max}**	**Emission Maxima E1 (nm) with λ_{exc} in brackets**	**Quantum yield (ϕ_f)**
F1; complex	291	18900	400	4200	366 (290)	0.010[a]
F3; tma-complex	302	7100	402	3000	365 (290)	0.008[a]
F5; ligand	290	8000	----	----	368 (290)	0.012[a]
F2; complex	333	46300	390	5300	384 (333)	0.0023[b]
F4; tma-complex	334	23300	375	4500	382 & 405 (333)	0.0013[b]
F6; ligand	332	27800	----	----	383 (333)	0.0036[b]
H; NAMI-A	239 294	8800 1200	397 ----	3800 ----	340 (230)[#]	----

* Stock solutions of compounds F2 and F4 were prepared in DMF and then diluted with methanol. To measure the molar extinction coefficient standards of known concentration were prepared and their absorbance was recorded. Graphs (*see graphs S15 – S20; supporting information*) were plotted with concentration versus absorbance and the gradient of these graphs (each graph contained a minimum of four data points) correspond to the molar extinction coefficient of the respective compounds. [#]Fluorescent emission spectrum of NAMI-A closely

matches with that reported in literature[18]. Quantum yield with respect to: [a)] 7-azaindole (0.012),[19] and [b)] anthracene (0.27)[20].

The UV-Vis spectral data showing two main absorption bands are consistent with those reported previously for NAMI-A and related complexes.[21] The MC transitions were more intense, relative to the LC bands, in the tetramethylammonium analogues **F3** and **F4** when compared to their parent complexes **F1** and **F2**, as a result of replacing the counter cation which would contribute to the intensity of the LC band. A red shift in the LC peak position was observed for the tetramethylammonium complex **F3** when compared to parent complex **F1**, or the bare ligand **F5**. This suggests the possibility of a cation-ligand stacking interaction for **F1**, which is infeasible for **F3**. However, a similar red shift was not observed for **F4** compared to **F2**. The added complication of the fluorophore being directly connected to ruthenium in **F1** and **F3**, but not in **F2** and **F4**, hinders the understanding of the source of the red shift impossible with the available data.

Emission spectra and quantum yield

The absorption and emission spectra obtained for **F1** and **F3,** in comparison with their free ligand **F5,** are shown in Figure 1 and those measured for **F2** and **F4,** in comparison with their free ligand **F6,** in Figure 2. Based on the absorption at excitation wavelength, and the area under the emission curve, quantum yields for the compounds **F1**-**F6** have been calculated using equation 1 given below.

$$\frac{\phi_1}{\phi_{ref}} = \frac{A_1}{A_{ref}} \times \frac{n_1^2}{n_{ref}^2} \times \frac{1-10^{-abs_{ref}}}{1-10^{-abs_1}} \text{ ---------------- Equation 1,}^{[19,\,22]}$$

Where, ϕ_1 = Quantum yield of the unknown compound, ϕ_{ref} = Quantum yield of the reference compound, A = area under the emission curve, n = refractive index of the solvent; and *abs* = absorbance at the excitation wavelength. The quantum yields are listed in Table I. **F5** (ϕ_f = 0.012,[19] in methanol at RT) was used as a reference compound for **F1** and **F3**; anthracene (ϕ_f = 0.27,[20] in ethanol at 20°C) was used a reference compound for **F2**, **F4**, and **F6**.

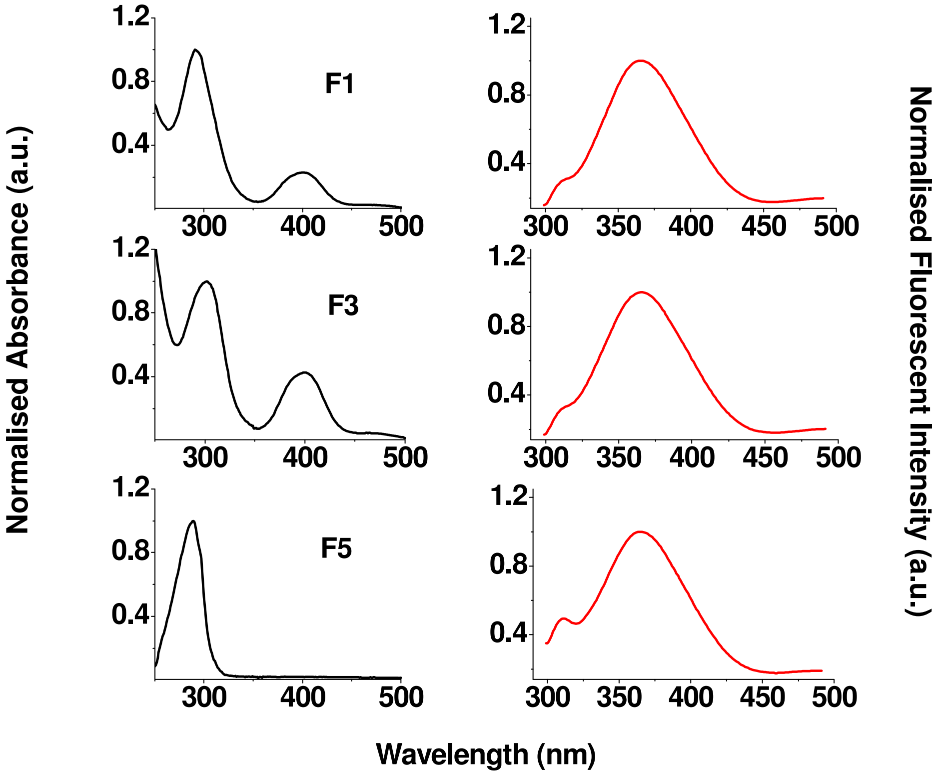

Figure 1: UV-Visible absorption (left column panels) and emission spectra (right column panels) for **F1**, **F3** and **F5.**

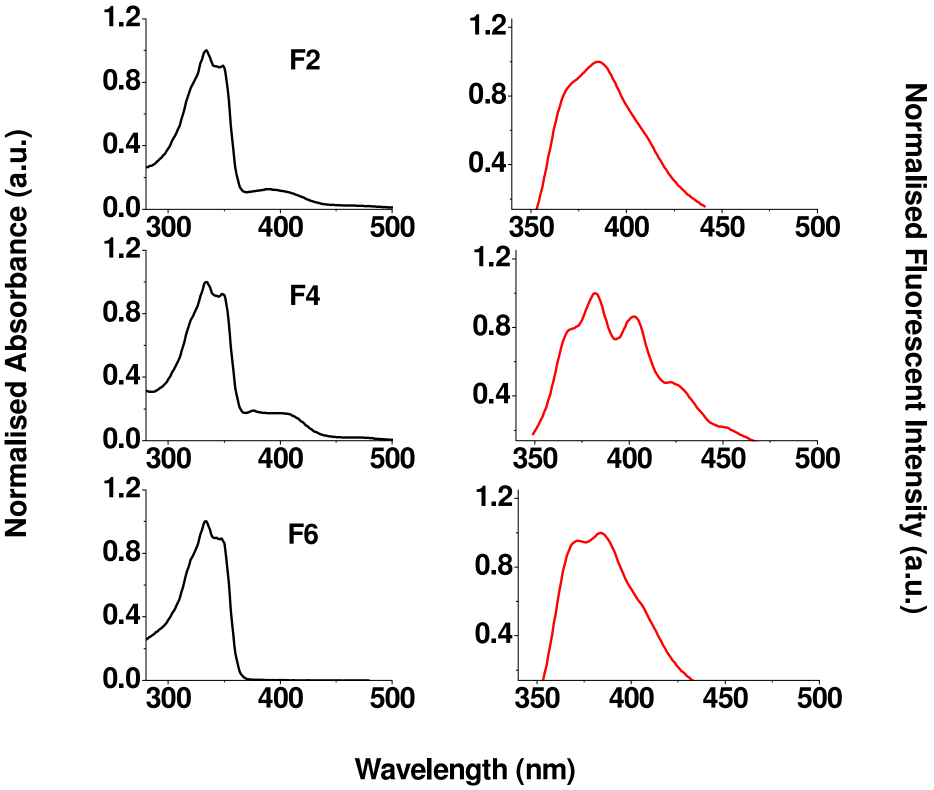

Figure 2: UV-Visible absorption (left column panels) and emission spectra (right column panels) for **F2, F4** and **F6**.

The fluorescent emissions of a complex and its tetramethylammonium analogue were closely related to that of the free ligand, i.e. complexes **F1** and **F3** exhibited emission maxima at 368 and 367 nm respectively, similar to the **F5** (free ligand) emission wavelength 368 nm; complexes **F2** and **F4** exhibit emission maxima at 383 and 380 nm respectively, similar to **F6** (free ligand) emission wavelength 383 nm. The emission spectrum of **F4** is significantly more structured than that of the parent complex or the bare ligand. The presumably reflects a greater vibrational contribution to the emission, potentially as a result of ligand-metal coupled process, which we intend to pursue in future studies. Emission quantum yields (ϕ_f) for **F1**-**F6** were determined using equation 1 and were found to be < 1% (Table 1).

Cytotoxicity (IC_{50}) by cell adhesion impedance assay

F3 and **F4** were tested on the human lung carcinoma cell line, A549, with 10,000 cells/well densities, in order to evaluate their cytotoxicity. The IC_{50} values determined after 24 h exposure to **F3** and **F4** were 203 ± 26 and 185 ± 20 μM, respectively. The IC_{50} value for the model compound NAMI-A determined by the same method was 305 ± 18 μM, which was in good agreement with literature reports (IC_{50} = 300).[23]

Potential of synthetic approach demonstrated through proof of concept

We have recently reported[16] XRF imaging of single cells treated with KP1019 and NAMI-A analogues in which the N-heterocyclic ligands were tagged with iodine which demonstrated that these ligands likely remain attached to ruthenium after uptake and processing in cells. By extension, this indicates that functionalisation of the same heterocyclic ligands with more complex moieties that provide either optically fluorescent or potentially organelle or tissue targeting functionalities would connect those properties to those inherent to the biotransformed ruthenium-containing metabolites of the parent complexes. This may lead to better understanding of the mode of action of the parent complexes and possibly improved activities, respectively. The research reported in this article demonstrates a facile synthetic route to functionalising the imidazole ligand of NAMI-A in a manner that does not dramatically alter the cytotoxicity of the parent complex and provides an important proof of concept for inclusion of more advanced imaging and targeting functionalities into this class of complexes.

Conclusion

A number of analogues of NAMI-A tagged with fluorescent ligands (**F1**-**F4**) were synthesised and characterised, demonstrating that extension of the synthetic route to NAMI-A to a wider set of N-heterocyclic ligands was feasible. The cytotoxic and fluorescent properties of the synthesised complexes were investigated. Further investigation based on fluorescent imaging can be done with the development of related compounds containing chromophores which have strong absorption in the longer wavelength region. This would represent a powerful tool for the investigation of distribution of the compounds in live cells and thus improve understanding of the mechanism of action of NAMI-A type complexes.

Experimental

Instrumentation

A Micromass Platform II Quadrupole Mass Spectrometer was used for obtaining low-resolution electrospray mass spectra (ESI-MS). The instrument was fitted with a capillary source and the capillary potential was maintained at 3.5 V, and the cone potential was 15 V. The identity of pure and dry samples was confirmed by *microanalytical* (C, H, and N) analyses performed by Campbell Microanalytical service, Otago, New Zealand. ^{1}H NMR spectra were measured on Bruker DRX 400 spectrometer. The chemical shifts are reported in parts per million (ppm) relative to signals from the residual protons of the deuterated solvent. The coupling constant, J, is given in Hertz (Hz) and the peak multiplicities are abbreviated as follows: s (singlet), d (doublet), t (triplet), and m (multiplet). IR spectra were measured using a Bruker Equinox 55 FT-IR spectrometer, fitted with Specac 'Golden Gate' diamond ATR and MCT detectors. *UV-Vis* spectra were recorded in quartz cuvettes using a Cary 300 Bio UV-Vis spectrophotometer. Absolute quantum yields and corrected fluorescence spectra were recorded on solutions at low concentration, which gave an absorbance less than 0.1, in quartz cuvettes using a Cary Eclipse fluorescence spectrophotometer. This instrument measures both emission and absorption and corrects for both monochromator and phototube response. It is programmed to correct for inner filter effects for solutions with optical densities up to 1.0.

Analytical HPLC was performed on an Agilent 1260 Infinity HPLC using a Supelco Discovery C5 column. Eluent A, 0.1% (v/v) TFA in water; eluent B, 0.1% (v/v) TFA in CH_3CN; gradient elution, 5% to 75% of eluent B in 25 min, 1.5 mL/min. An xCELLigence cell adhesion impedance system (Roche Applied

Science and ACEA Biosciences) was used to carry out cytotoxicity measurements.

Materials and methods

Ruthenium(III) chloride hydrate, 7-azaindole (**F5**), 1,8-naphthalic anhydride, histamine dihydrochloride and the solvents were purchased from Sigma-Aldrich and used without further purification. High purity water was used for cell culture, obtained from a Millipore Synergy 185 UV Ultra pure water system. Dulbecco's Minimum Essential Medium (DMEM), phosphate-buffered saline (PBS), L-glutamine (2mM), trypsin-EDTA solution (0.25%), pencillin-streptomycin, foetal bovine serum (2% v/v) and non-essential amino acids, used for culturing human lung carcinoma cells (A549), were obtained from Sigma-Aldrich.

Syntheses of complexes

Crystallization of the complexes was difficult due to facile hydrolysis of ligands in most of the suitable solvents. NAMI-A was synthesized as according to the reported procedure.[24]

7-azaindolium *trans*-tetrachlorido(7-azaindole)(dimethylsulfoxide)ruthen(III)ate (F1)

The precursor, $[(DMSO)_2H][trans\text{-}RuCl_4(DMSO)_2]$ was synthesized according to the previously reported procedure.[25]A sample was suspended (0.50 g, 0.89 mmol) in acetone (10 mL) at room temperature and stirred for 2 h. After addition of the ligand, 7-azaindole (0.2 g, 1.69 mmol), stirring was continued overnight. During this time the colour of the precipitate gradually changed from bright orange to yellow. The precipitate was collected on a sintered filter, washed with acetone (10 mL) followed by diethyl ether (10 mL), and dried under vacuum at room temperature (yield: 0.45 g, 91%). Crystals for XRD analysis were grown by layering acetone over a DMF solution of complex **F1**. Crystals appeared in the solution after two weeks (*see Supporting Information for X-ray crystallographic data*).

ν_{max} (ATR-IR/cm^{-1}, selected frequencies) 3158m (NH), 3062vs (C- H$_{aromatic}$), 1146s (SO), 1067vs, 1018m, 793vs, 726vs, 613s. λ_{max}/nm (ε/M^{-1} cm^{-1}) 290 (18,900), 400 (4,200). *m/z* (ESI) 439.8 ($M^{-\cdot}$, 100%). HPLC retention time = 5.15 min. Anal. Calc. for $C_{16}H_{19}N_4Cl_4ORuS$ (558.3): C 34.42, H 3.43, N 10.04, S 5.74. Found: C 34.59, H 3.69, N 9.94, S 5.44 %.

N-[histaminedihydrolium]-1,8-naphthalenecarboximidic *trans*-tetrachlorido(dimethylsulfoxide)(N-[histaminedihydro]-1,8-naphthalenecarboximide) ruthen(III)ate (F2)

a) Synthesis of N-[histaminedihydro]-1,8-naphthalenecarboximide (F6)

1,8-Naphthalic anhydride (0.5 g, 2.5 mmol) was added to a stirred solution of histamine dihydrochloride (1.15 g, 6.25 mmol) and triethylamine (2.6 mL) in dry ethanol (8 mL) under nitrogen, and then mixture was refluxed for 30 minutes (T = 85^0C). TLC analysis (silica gel, MeOH/ CH_2Cl_2 (1:10), $KMnO_4$ as developer) after 4 h showed the completion of the reaction; so water (2 x 25 mL) was added to the yellow suspension and the mixture was transferred to a separating funnel. Concentrated hydrochloric acid was added dropwise to pH = 2 and the resulting aqueous solution was washed with ethyl acetate (2 x 20 mL). The aqueous layer was then separated, concentrated under vacuum and cooled in an ice bath. Fine light cream crystals were collected by filtration and washed with diethyl ether (yield: 0.58 g, 80%).

ν_{max} (ATR-IR/cm^{-1}, selected frequencies) 3151vs (NH), 2976s, 2810m, 2773br, 1653vs, 1587s, 1082m, 1031m, 782vs, 740m, 622s. λ_{max}/nm (ε/M^{-1} cm^{-1}) 330 (27,700). δ_H (400 MHz, D_2O) 8.46 (d, J = 1.2 Hz, 1H), 8.03-8.05 (m, 8H, ArH), 7.50-7.54 (t, J = 8 Hz, 4H, ArH), 7.06 (d, J = 0.8 Hz, 1H), 4.10 - 4.13 (t, J = 6.8 Hz, 4H, N$CH_2$$CH_2$), 2.96 - 2.99 (t, J = 6.8 Hz, 4H, $NCH_2$$CH_2$) (*see Supporting Information Figure 10*). *m/z* (ESI) 292.2 ($M^{+\cdot}$, 100%).

b) Synthesis of F2

[$(DMSO)_2H$][*trans*-$RuCl_4(DMSO)_2$] (0.26 g, 0.46 mmol) was stirred in acetone (10 mL) under nitrogen at room temperature for 2 h. N-[histaminedihydro]-1,8-naphthalenecarboximide (**F6**, 0.80 g, 2.76 mmol) was added and the mixture was stirred overnight. A dark yellow precipitate was obtained which was collected by filtration and washed with acetone (10 mL), diethyl ether (10 mL), and dried under vacuum at room temperature (yield: 0.37 g, 89%).

$\nu_{\max}$ (ATR-IR/cm^{-1}, selected frequencies) 3152vs (NH), 3010s, 2813m, 2777br, 1656vs, 1589s, 1082m, 1017m, 776vs, 785m, 739m, 623s. $\lambda_{\max}$/nm (ε/M^{-1} cm^{-1}) 333 (46,300), 390 (530). *m/z* (ESI) 612.8 (M$^{-\cdot}$, 100%). HPLC system: Retention time = 7.0 min and 8.3 min. Anal. Calc. for $C_{36}H_{33}N_6Cl_4O_5RuS.2H_2O$ (940.66): C 45.97, H 3.96, N 8.93, S 3.41, Cl 15.08. Found: C 45.96, H 3.65, N 8.91, S 3.28, Cl 18.74 %.

Tetramethylammonium *trans*-tetrachlorido(7-azaindole)(dimethyl sulfoxide)ruthen(III)ate (F3)

F1 was synthesized according to the procedure given above. **F1** (0.037 gm, 0.06 mmol) was sonicated and stirred in acetone for 15 min to obtain a dark red solution. To this, tetramethylammonium chloride (0.0286 g, 0.26 mmol) was added (in excess) and stirring was maintained until a red microcrystalline precipitate formed. The precipitate was filtered, washed with cold acetone and diethyl ether (yield: 0.023 g (23 mg), 75%) and recrystallised from methanol/acetone by isothermal evaporation of the solvent in air.

$\nu_{\max}$ (ATR-IR/cm^{-1}, selected frequencies) 3381br (NH), 3023vs (C-H$_{\text{aromatic}}$), 1485vs, 1111vs, 1012vs, 949vs, 785vs, 719vs, 680m, 625s. $\lambda_{\max}$/nm (ε/M^{-1} cm^{-1}) 302 (7,060), 402 (2,980). *m/z* (ESI) 439.7 (M$^{-\cdot}$, 100%). HPLC system: Retention time = 5.3 min. Anal. Calc. for $C_{13}H_{24}N_3Cl_4ORuS$ (513.3): C 30.42, H 4.71, N 8.19, S 6.25, Cl 27.63. Found: C 30.30, H 5.89, N 8.61, S 5.13, Cl 27.28%.

Tetramethylammonium *trans*-tetrachlorido(dimethylsulfoxide)(N-[histaminedihydro]-1,8-naphthalenecarboximide)ruthen(III)ate (F4)

Compound **F2** (0.05 gm, 0.055 mmol) was sonicated in methanol until a fine yellow precipitate was obtained. To this, an excess of tetramethylammonium chloride (0.02 g, 0.18 mmol) was added to give a clear yellow-orange solution and then refluxed for one hour (T = 85^{0}C). A fine yellow microcrystalline precipitate was obtained after isothermal evaporation of the solvent in air. The precipitate was filtered and washed with diethyl ether (yield: 0.03 g, 80%).

ν_{max} (ATR-IR/cm^{-1}, selected frequencies) 3168br (NH), 3016s, 1701vs, 1660vs, 1591s, 1104br, 1019m, 778vs, 682s. λ_{max}/nm (ε/M^{-1} cm^{-1}) 334 (23,300), 375 (4,420). *m*/*z* (ESI) 612.8 ($M^{-\cdot}$, 100%). HPLC retention time = 7 min (minor) and 8.25 min. Anal. Calc. for $C_{23}H_{31}N_4Cl_4O_3RuS$ (686.46): C 40.24, H 4.55, N 8.16, S 4.67, Cl 20.66. Found: C 39.17, H 4.54, N 8.03, S 3.40, Cl 19.48%.

Fluorescent quantum yield (ϕ_f) :

Fluorescent quantum yields were determined by the direct comparison with another compound of a known quantum yield, according to equation 1. To measure the quantum yield, solutions of the reference compounds and the unknown compounds were prepared at a concentration for which the absorption is less than 0.1 in order to reduce inner filter effects. Since oxygen is a fluorescence quencher, both absorption and emission measurements were carried out in de-aerated solvent (30 minutes of nitrogen bubbling) in a quartz cell with a 1 cm optical path. The areas under the fluorescence emission curve were calculated and the data used in equation 1 and a mean of three experimental data were taken in to consideration in order to determine the quantum yield of the unknown compound.

Cell culture and *in vitro* cytotoxicity testing

A549 cells, originally purchased from American Tissue Culture Collection, were a gift from Dr Aviva Levina (University of Sydney). The A549 cells were cultured as monolayers in Dulbecco's modified Eagle's medium (DMEM) supplemented with foetal bovine serum (2% v/v), antibiotic-antimicotic mixture (100 mg mL^{-1} pencillin and 100 U mL^{-1} streptomycin), L-glutamine (2mM), and non-essential amino acids (100 U mL^{-1}) at 310 K in a 5% CO_2-humidified incubator and were subcultured in every 4-6 days.

The tetramethylammonium salts, **F3** and **F4,** were tested for *in vitro* cytotoxicity by an electronic cell sensor technology ACEA RT-CES system (xCELLigence; Roche Diagnostics, Germany). The complexes were dissolved in 5% DMF in PBS immediately prior to the experiment to avoid premature hydrolysis. A proliferation or growth curve for A549 cells was established by plating cells at the cell densities of 3000 to 60,000 cells per well of an xCELLigence E-plate or sensor plate.[26] xCELLigence cell index (CI) impedances measurements were performed according to the instructions of the supplier. The optimal seeding concentration for proliferation experiments was found to be 10,000 cells per well. After seeding 100 µL of the cell suspensions into the wells of the E-plate 96 (10,000 cells per well), cells were monitored every 15 minutes for a period up to 18 h by xCELLigence system. After 18 h, when the cells were in the log growth phase, they were exposed to 20 µL of test solutions of either **F3** or **F4** in 5% DMF in PBS for a concentration range 30 µM to 3000 µM. Controls were exposed to 20 µL of 5% DMF only in PBS (final DMF concentration was limited to 0.5%). The adhesion of the cells was monitored by impedance measurements every 15 min for a period up to 24 h by the xCELLigence system.

All calculations were performed using the RTCA-integrated software of the xCELLigence system. The RTCA software performs a curve fitting of a sigmoidal dose-response equation to the experimental data points and calculates IC_{50} values from 50% reduction of CI (cell index) value relative to solvent control CI value (100%). Inhibiting concentrations (IC) were determined by curve-fitting plots of cell viability against the log of compound concentration. Data are represented as mean [µM] ± S.E.M. ($n = 3$).

Acknowledgements

We thank Australian Research Council for funding (DP0985807 to HHH, DP130100816 and DORA to LS) and Craig Forsyth for X-ray crystallography. A549 cells were a gift from Aviva Levina, University of Sydney.

References:

[1] I. Kostova. *Curr. Med. Chem.* **2006**, *13*, 1085.

[2] C. G. Hartinger, S. Zorbas-Seifried, M. A. Jakupec, B. Kynast, H. Zorbas, B. K. Keppler. *J. Inorg. Biochem.* **2006**, *100*, 891.

[3] E. Alessio, G. Mestroni, A. Bergamo, G. Sava. *Curr. Top. Med. Chem.* **2004**, *4*, 1525.

[4] A. Levina, A. Mitra, P. A. Lay. *Metallomics*. **2009**, *1*, 458.

[5] A. Bergamo, G. Sava. *Dalton Trans.* **2007**, 1267.

[6] M. Galanski, V. B. Arion, M. A. Jakupec, B. K. Keppler. *Curr. Pharm. Des.* **2003**, *9*, 2078.

[7] A. Bergamo, G. Sava. *Dalton Trans.* **2011**, *40*, 7817.

[8] A. Bergamo, C. Gaiddon, J. H. M. Schellens, J. H. Beijnen, G. Sava. *J. Inorg. Biochem.* **2012**, *106*, 90.

[9] E. Reisner, V. B. Arion, M. Fatima, C. G. da Silva, R. Lichtenecker, A. Eichinger, B. K. Keppler, V. Y. Kukushkin, A. J. L. Pombeiro. *Inorg. Chem.* **2004**, *43*, 7083.

[10] N. Graf, S. J. Lippard. *Adv. Drug Deliv. Rev.* **2012**, *64*, 993.

[11] M. I. Webb, C. I. Walsby. *Dalton Trans.* **2011**, *40*, 1322.

[12] A. Levina, J. B. Aitken, Y. Y. Gwee, Z. J. Lim, M. Liu, A. M. Singharay, P. F. Wong, P. A. Lay. *Chem. Eur. J.* **2013**, *19*, 3609.

[13] A. A. Hummer, P. Heffeter, W. Berger, M. Filipits, D. Batchelor, G. E. Buchel, M. A. Jakupec, B. K. Keppler, A. Rompel. *J. Med. Chem.* **2013**, *56*, 1182.

[14] M. Liu, Z. J. Lim, Y. Y. Gwee, A. Levina, P. A. Lay. *Angew. Chem. Int. Ed.* **2010**, *49*, 1661.

[15] J. B. Aitken, S. Antony, C. M. Weekley, B. Lai, L. Spiccia, H. H. Harris. *Metallomics*. **2012**, *4*, 1051.

[16] S. Antony, J. B. Aitken, S. Vogt, B. Lai, T. Brown, L. Spiccia, H. H. Harris. *J. Biol. Inorg. Chem.* **2013**, *18*, 845.

[17] F. Zobi, B. B. Mood, P. A. Wood, F. P. A. Fabbiani, S. Parsons, P. J. Sadler. *Eur. J. Inorg. Chem.* **2007**, *18*, 2783; J. J. Fiol, A. García-Raso, F. M. Albertí, A. Tasada, M. Barceló-Oliver, A. Terrón, M. J. Prieto, V. Moreno, E. Molins. *Polyhedron*. **2008**, *27*, 2851; S. P. Fricker. *Dalton Trans.* **2007**, 4903; M. Groessl, E. Reisner, C. G. Hartinger, R. Eichinger, O. Semenova, A. R. Timerbaev, M. A. Jakupec, V. B. Arion, B. K. Keppler. *J. Med. Chem.* **2007**, *50*, 2185.

[18] O. Mazuryk, K. Kurpiewska, K. Lewinski, G. Stochel, M. Brindell. *J. Inorg. Biochem.* **2012**, *116*, 11.

[19] F. Gai, R. L. Rich, J. W. Petrich. *J. Am. Chem. Soc.* **1994**, *116*, 735.

[20] W. R. Dawson, M. W. Windsor. *J. Phys. Chem.* **1968**, *72*, 3251.

[21] K. Kalyanasundaram, S. M. Zakeeruddin, M. K. Nazeeruddin. *Coord. Chem. Rev.* **1994**, *132*, 259; F. Kratz, M. Hartmann, B. K. Keppler, L. Messori. *J. Biol. Chem.* **1994**, *269*, 2581; L. Messori, P. Orioli, D. Vullo, E. Alessio, E. Iengo. *Eur. J. Biochem.* **2000**, *267*, 1206; E. M. Nagy, C. Nardon, L. Giovagnini, L. Marchio, A. Trevisan, D. Fregona. *Dalton Trans.* **2011**, *40*, 11885; M. Delferro, L. Marchio, M. Tegoni, S. Tardito, R. Franchi-Gazzola, M. Lanfranchi. *Dalton Trans.* **2009**, 3766.

[22] M. Zhou, G. P. Robertson, J. Roovers. *Inorg. Chem.* **2005**, *44*, 8317.

[23] A. Egger, B. C. Losantos, I. N. Stephaneko, B. K. Keppler. *Chem. Biodivers.* **2008**, *5*, 1588; A. Herman, J. M. Tanski, M. F. Tibbetts, C. M. Anderson. *Inorg. Chem.* **2008**, *47*, 274.
[24] G. Mestroni, E. Alessio, G. Sava. **1998**, *WO 98/00431*.
[25] E. Alessio, G. Balducci, M. Calligaris, G. Costa, W. M. Attia, G. Mestroni. *Inorg. Chem.* **1991**, *30*, 609.
[26] E. Urcan, U. Haertel, M. Styllou, R. Hickel, H. Scherthan, F. Reichl. *Dent. Mater.* **2010**, *26*, 51.

Chapter 4

Supporting Information

Fluorescent analogues of NAMI-A:

Synthesis, characterization, fluorescent properties and preliminary biological studies in human lung cancer cells (A549)

Supplementary Material

Sumy Antony,[1,2] Jonathan C. Morris,[3] Toby Bell,[2] Tracey Brown,[4] Leone Spiccia,[2] and Hugh H. Harris.[1]

[1] School of Chemistry and Physics, The University of Adelaide, Adelaide SA 5005, Australia
Corresponding author email: hugh.harris@adelaide.edu.au

[2] School of Chemistry, Monash University, Clayton, Victoria 3800, Australia

[3] School of Chemistry, University of New South Wales, Sydney, NSW 2052, Australia

[4] Department of Biochemistry and Molecular Biology, Monash University, Clayton, Victoria 3800, Australia.

Instrumentation

A Micromass Platform II Quadrupole Mass Spectrometer was used for obtaining low-resolution electrospray mass spectra (ESI-MS). ^{1}H NMR spectra were measured on Bruker DRX 400 spectrometer. The chemical shifts are reported in parts per million (ppm) relative to signals from the residual protons of the deuterated solvent. *UV-Vis* spectra were recorded in quartz cuvettes using a Cary 300 Bio UV-Vis spectrophotometer. Absolute quantum yields and corrected fluorescence spectra were recorded on solutions at low concentration, which gave an absorbance less than 0.1, in quartz cuvettes using a Cary Eclipse fluorescence spectrophotometer. Analytical HPLC was performed on an Agilent 1260 Infinity HPLC using a Supelco Discovery C5 column. Eluent A, 0.1% (v/v) TFA in water; eluent B, 0.1% (v/v) TFA in CH_3CN; gradient elution, 5% to 75% of eluent B in 25 min, 1.5 mL/min. An xCELLigence cell adhesion impedance system (Roche Applied Science and ACEA Biosciences) was used to carry out cytotoxicity measurements.

Mass Spectra

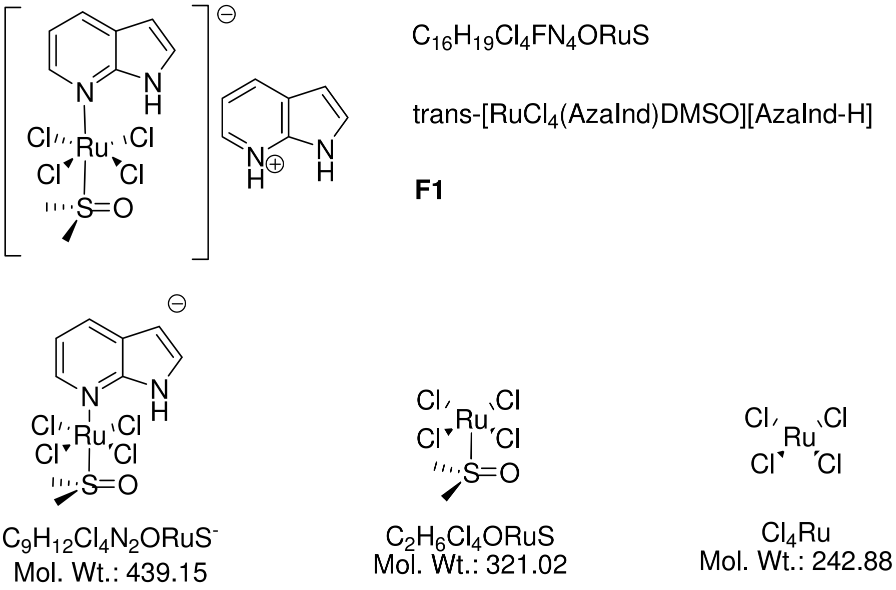

$C_{16}H_{19}Cl_4FN_4ORuS$

trans-[$RuCl_4$(AzaInd)DMSO][AzaInd-H]

F1

$C_9H_{12}Cl_4N_2ORuS^-$
Mol. Wt.: 439.15

$C_2H_6Cl_4ORuS$
Mol. Wt.: 321.02

Cl_4Ru
Mol. Wt.: 242.88

Figure S1: Splitting pattern for **7-azaindolium *trans*-tetrachlorido(7-azaindole)(dimethylsulfoxide)ruthen(III)ate (F1).**

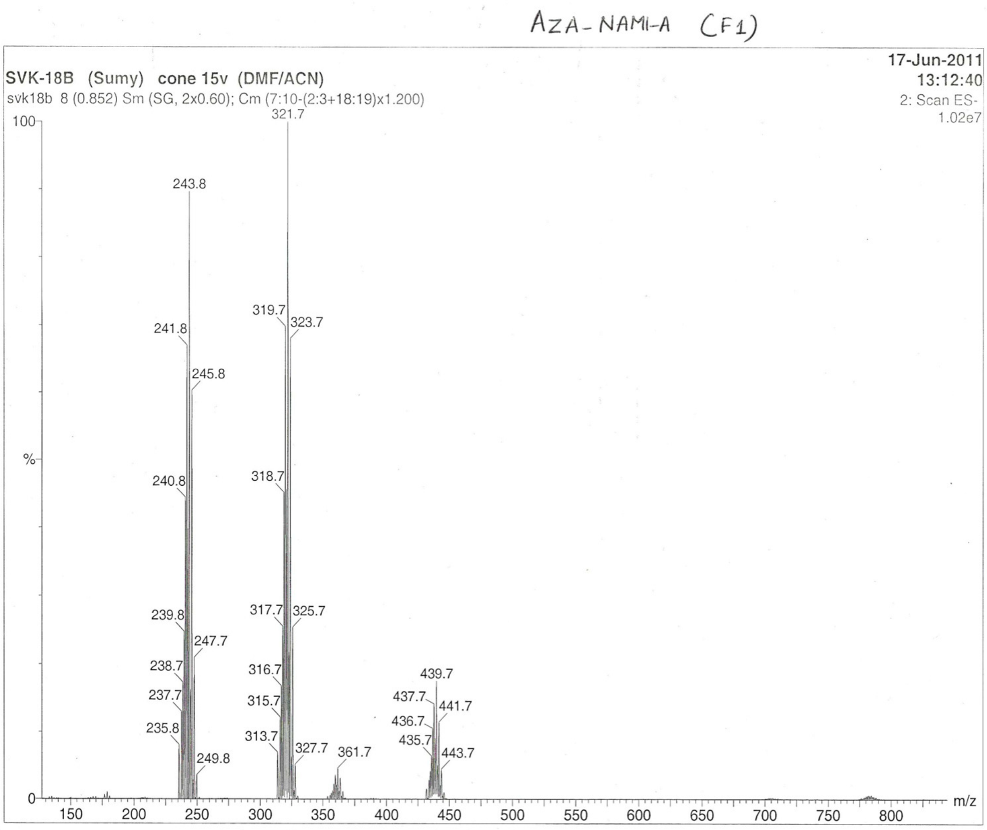

Figure S2: Electrospray mass spectrum (-ve ion) for **F1**; Cone 15V; Solvent – DMF/ACN.

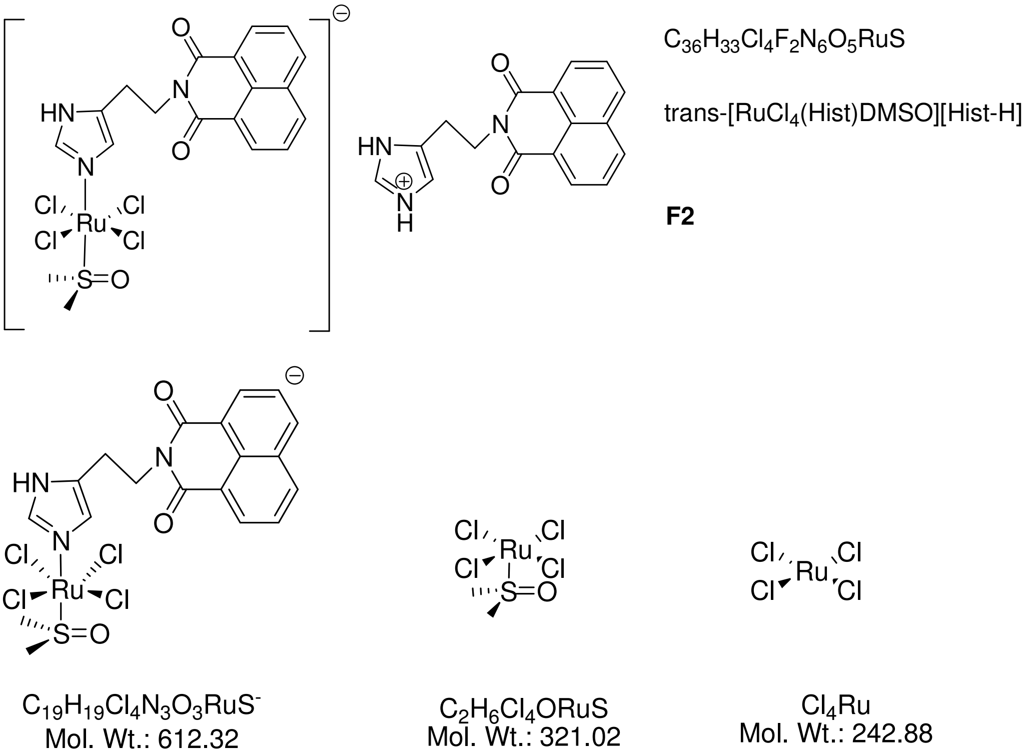

$C_{36}H_{33}Cl_4F_2N_6O_5RuS$

trans-[RuCl$_4$(Hist)DMSO][Hist-H]

F2

$C_{19}H_{19}Cl_4N_3O_3RuS^-$
Mol. Wt.: 612.32

$C_2H_6Cl_4ORuS$
Mol. Wt.: 321.02

Cl_4Ru
Mol. Wt.: 242.88

Figure S3: Splitting pattern for **N-[histaminedihydrolium]-1,8-naphthalenecarboximidic *trans*-tetrachlorido(dimethylsulfoxide)(N-[histaminedihydro]-1,8-naphthalenecarboximide) ruthen(III)ate (F2)**.

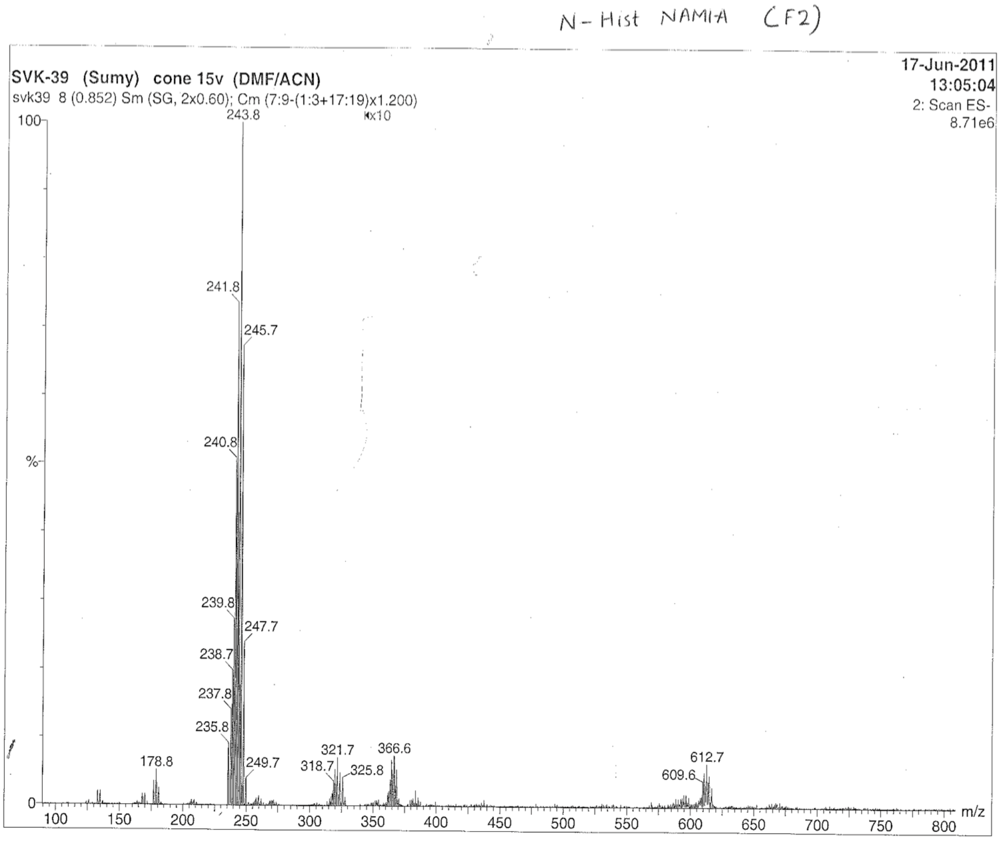
N- Hist NAMIA (CF2)

Figure S4: Electrospray mass spectrum (-ve ion) for **F2**; Cone 15V; Solvent – DMF/ACN.

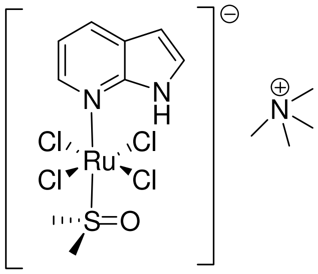

$C_{13}H_{24}Cl_4F_3N_3ORuS$

trans-[$RuCl_4$(AzaInd)DMSO][$(CH_3)_4N$]

F3

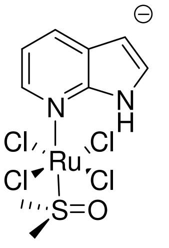

$C_9H_{12}Cl_4N_2ORuS^-$
Mol. Wt.: 439.15

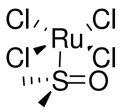

$C_2H_6Cl_4ORuS$
Mol. Wt.: 321.02

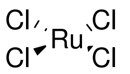

Cl_4Ru
Mol. Wt.: 242.88

Figure S5: Fragmentation pattern for **Tetramethylammonium *trans*-tetrachlorido(7-azaindole)(dimethyl sulfoxide)ruthen(III)ate (F3)**

.

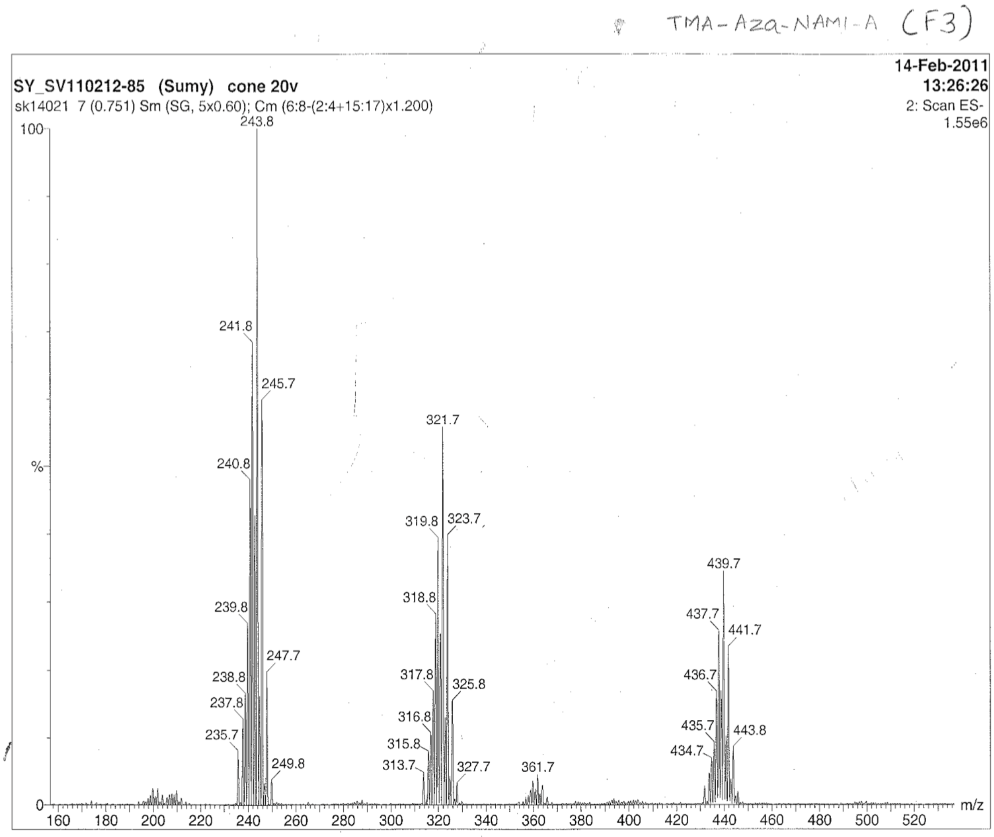

Figure S6: Electrospray mass spectrum (-ve ion) for **F3**; Cone 15V; Solvent – DMF/ACN.

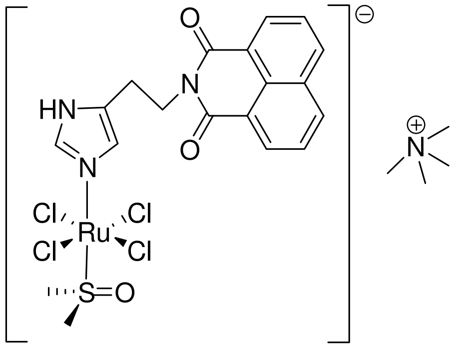

$C_{23}H_{31}Cl_4F_4N_4O_3RuS$

trans-[$RuCl_4$(Hist)DMSO][$(CH_3)_4N$]

F4

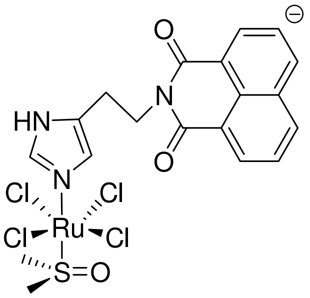

$C_{19}H_{19}Cl_4N_3O_3RuS^-$
Mol. Wt.: 612.32

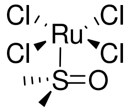

$C_2H_6Cl_4ORuS$
Mol. Wt.: 321.02

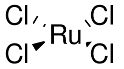

Cl_4Ru
Mol. Wt.: 242.88

Figure S7: Fragmentation pattern for **Tetramethylammonium *trans*-tetrachlorido(dimethylsulfoxide)(N-[histaminedihydro]-1,8-naphthalenecarboximide)ruthen(III)ate (F4)**.

.

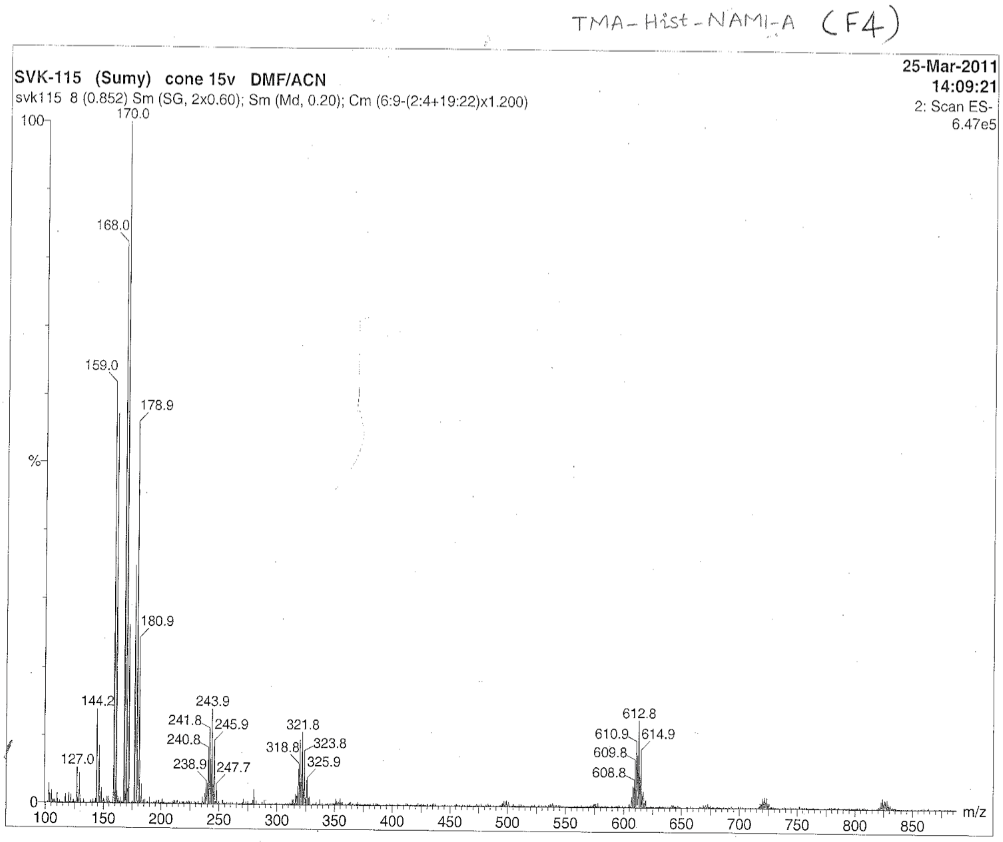

Figure S8: Electrospray mass spectrum (-ve ion) for **F4**; Cone 15V; Solvent – DMF/ACN.

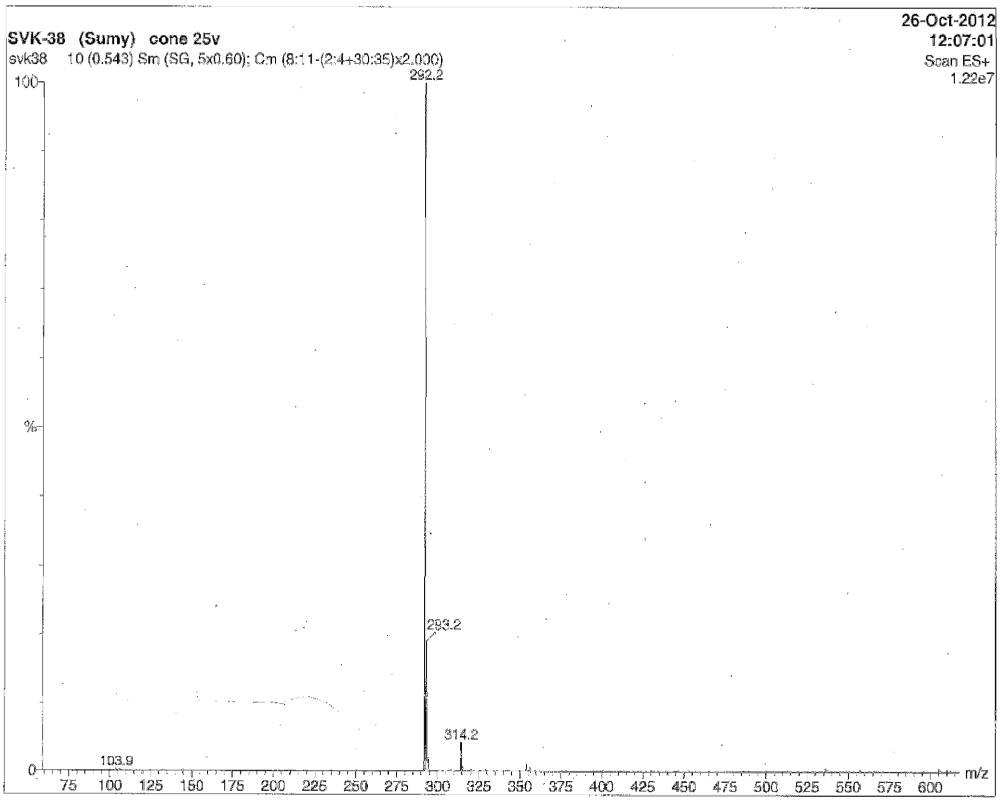

Figure S9: Electrospray mass spectrum for **F6 (N-[histaminedihydro]-1,8-naphthalenecarboximide)**; Cone 15V; Solvent – ACN.

Table SI. Summary of ESI-MS (*m/z* -ve ion) data* with fragmentation pattern

Complex	**Fragment**	**m/z (calcd)**	**m/z (found)**
F1	[RuCl$_4$(DMSO)(7-azaindole)]$^-$	439.8	439.8
	[RuCl$_4$(7-azaindole)]$^-$	361.8	361.8
	[RuCl$_4$(DMSO)]$^-$	321.7	321.8
	[RuCl$_4$]$^-$	243.7	243.8
F2	[RuCl$_4$(DMSO)(**F6**)]$^-$	612.8	612.8
	[RuCl$_4$(DMSO)]$^-$	321.7	321.8
	[RuCl$_4$]$^-$	243.7	243.8

*Measured by Micromass Platform II Quadruple Mass Spectrometer at cone voltage 15 V.

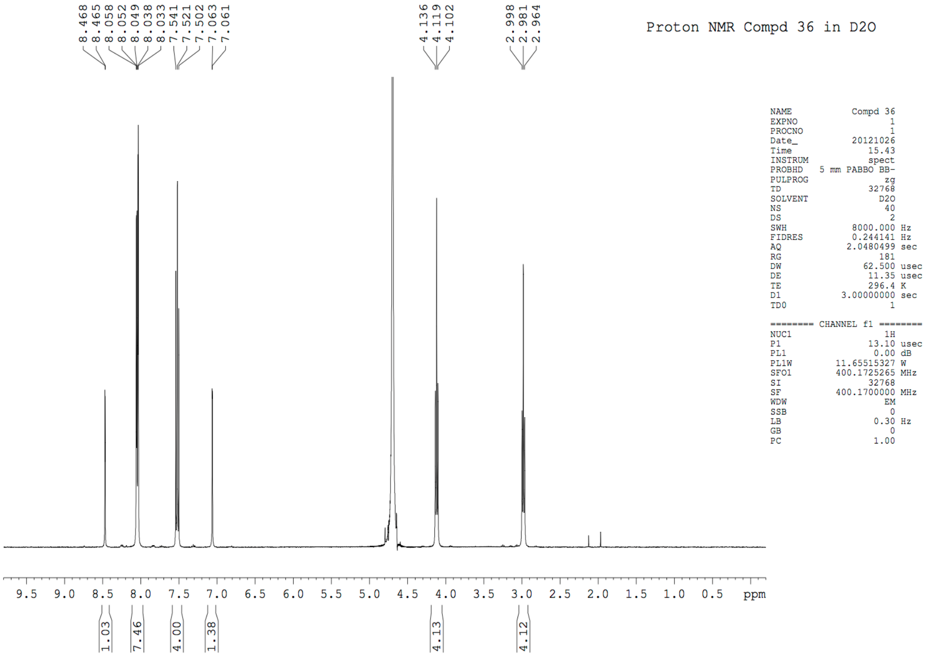

Figure S10: Proton NMR spectrum for **F6** (**N-[histaminedihydro]-1,8-naphthalenecarboximide**) in D_2O.

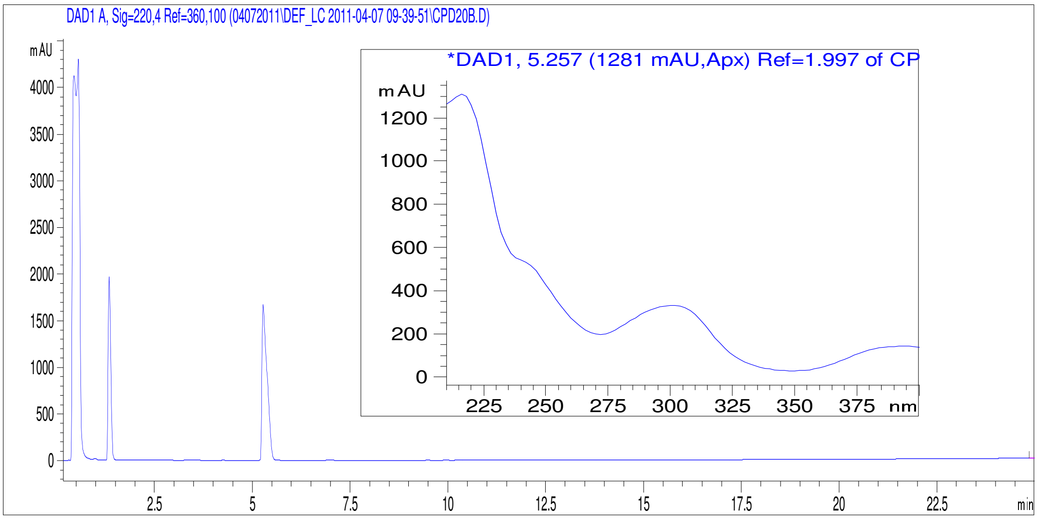

Figure S11: HPLC chromatogram of **F1** (**7-azaindolium *trans*-tetrachlorido(7-azaindole)(dimethylsulfoxide)ruthen(III)ate)** in DMF. Column: Supelco Discovery C5; Flow: 1.5 ml/min; Detection at 220 nm; Mobile phase: Buffer A (0.1% tfa/water), Buffer B (0.1%tfa/CH3CN); Gradient: 5% to 75% B, 25 minutes linear. Retention time = 1.45 and 5.15 min.

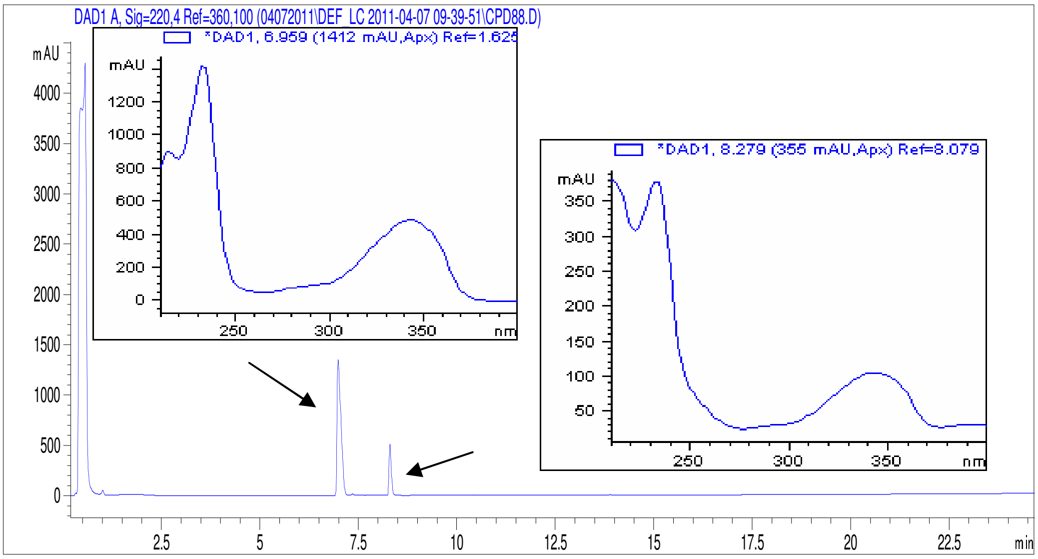

Figure S12: HPLC chromatogram of **F2** (**N-[histaminedihydrolium]-1,8-naphthalenecarboximidic *trans*-tetrachlorido(dimethylsulfoxide)(N-[histaminedihydro]-1,8-naphthalenecarboximide) ruthen(III)ate**) in DMF. Column: Supelco Discovery C5; Flow: 1.5 ml/min; Detection at 220 nm; Mobile phase: Buffer A (0.1% tfa/water), Buffer B (0.1%tfa/CH3CN); Gradient: 5% to 75% B, 25 minutes linear. Retention time = 7 min and 8.25 min.

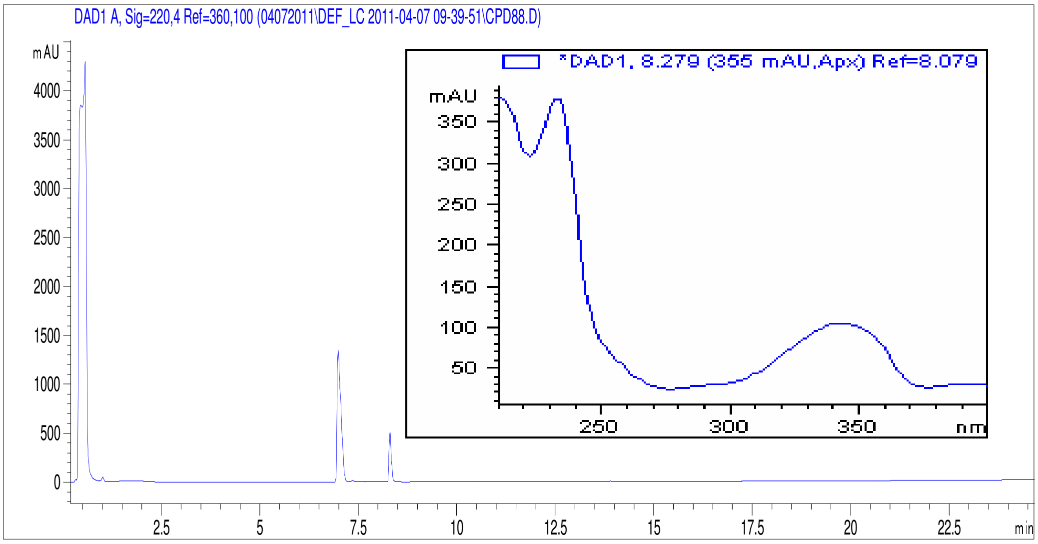

Figure S13: HPLC chromatogram of **F3** (**Tetramethylammonium *trans*-tetrachlorido(7-azaindole)(dimethyl sulfoxide)ruthen(III)ate**) in DMF.

Column: Supelco Discovery C5; Flow: 1.5 ml/min; Detection at 220 nm; Mobile phase: Buffer A (0.1% tfa/water), Buffer B (0.1%tfa/CH3CN); Gradient: 5% to 75% B, 25 minutes linear. Retention time = 5.3 min.

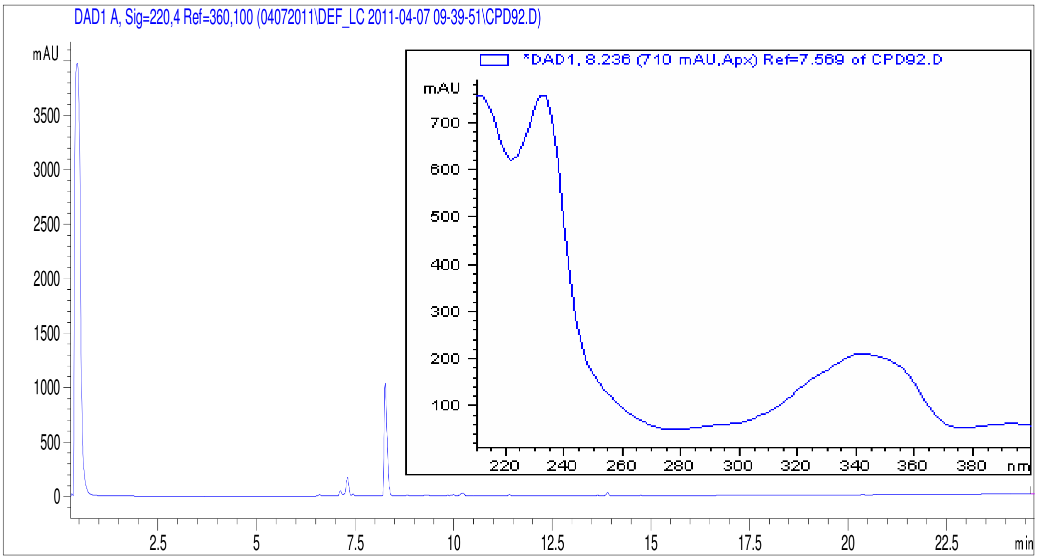

Figure S14: HPLC chromatogram of **F4** (**Tetramethylammonium *trans*-tetrachlorido(dimethylsulfoxide)(N-[histaminedihydro]-1,8-naphthalenecarboximide)ruthen(III)ate**) in DMF. Column: Supelco Discovery C5; Flow: 1.5 ml/min; Detection at 220 nm; Mobile phase: Buffer A (0.1% tfa/water), Buffer B (0.1%tfa/CH3CN); Gradient: 5% to 75% B, 25 minutes linear. Retention time = 8.25 min.

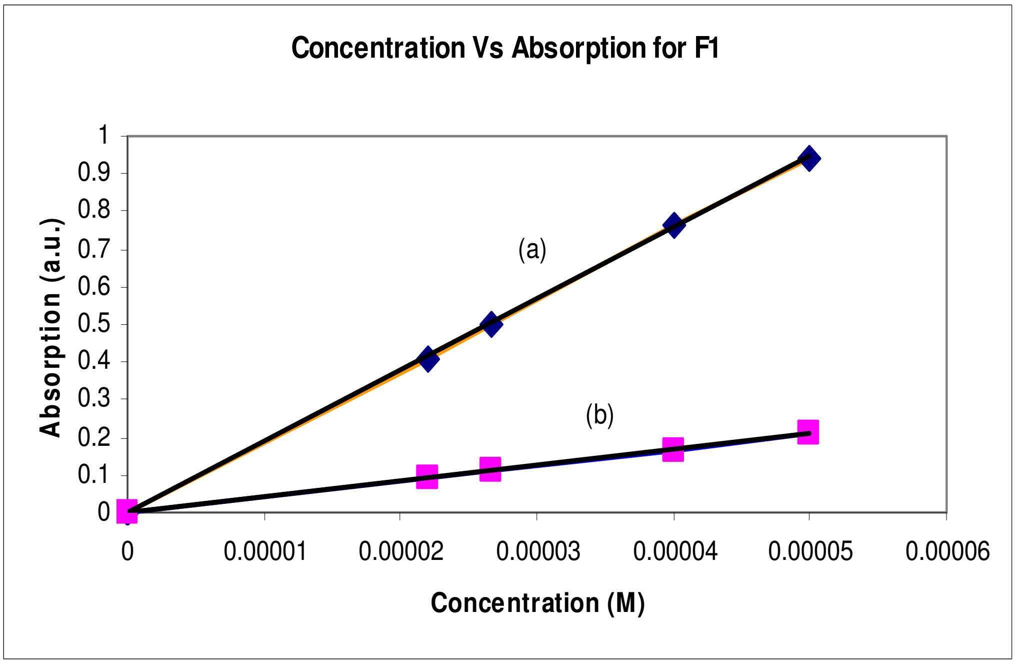

Figure S15: Effect of concentration on absorption for **F1** (7-azaindolium trans-tetrachlorido(7-azaindole)(dimethylsulfoxide)ruthen(III)ate). (a) At 291 nm; molar absorptivity (ε_{max} ; M^{-1} cm^{-1}) = 18,900 and correlation coefficient, r = 0.99. (b) At 400 nm; molar absorptivity (ε_{max} ; M^{-1} cm^{-1}) = 4,200 and correlation coefficient, r = 0.99.

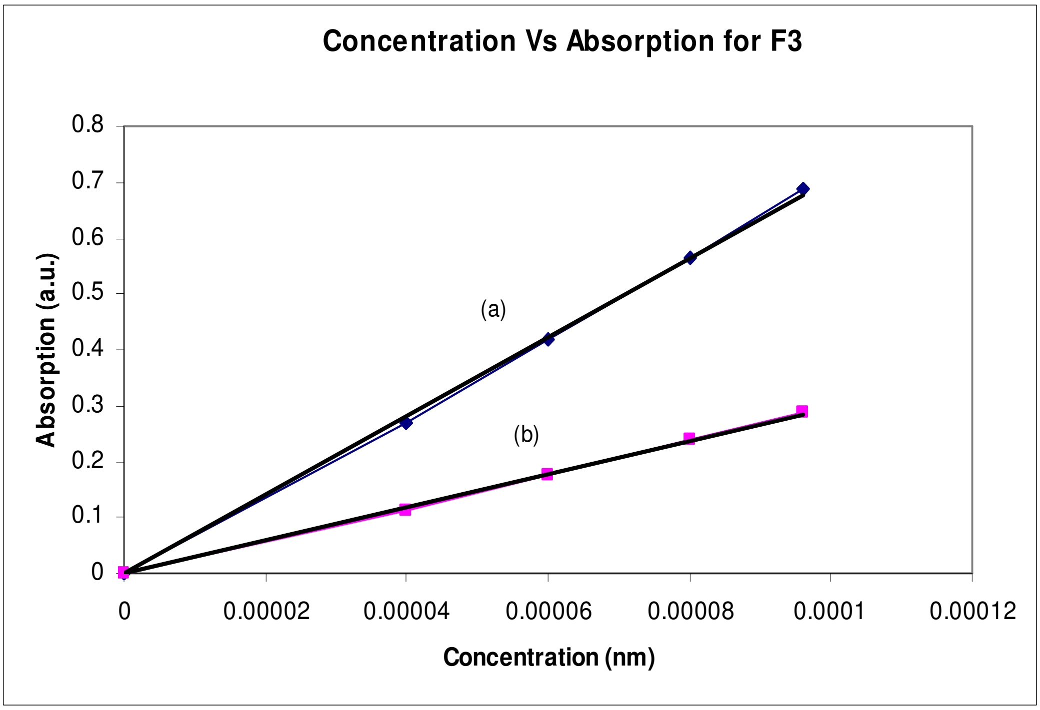

Figure S16: Effect of concentration on absorption for **F3** (Tetramethylammonium trans-tetrachlorido(7-azaindole)(dimethyl sulfoxide)ruthen(III)ate). (a) At 302 nm; molar absorptivity (ε_{max} ; M^{-1} cm^{-1}) = 7,100 and correlation coefficient, r = 0.99. (b) At 402 nm; molar absorptivity (ε_{max} ; M^{-1} cm^{-1}) = 3,000 and correlation coefficient, r = 0.99.

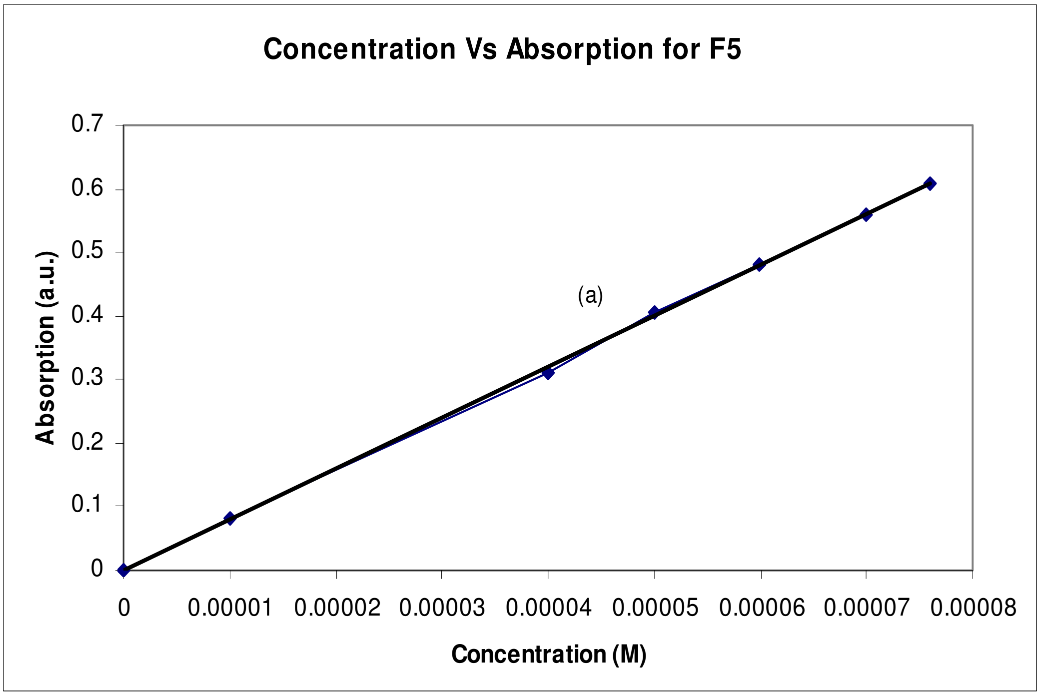

Figure S17: Effect of concentration on absorption for **F5 (7-Azaindole)**. (a) At 290 nm; molar absorptivity (ε_{max} ; M^{-1} cm^{-1}) = 8,000 and correlation coefficient, r = 0.99.

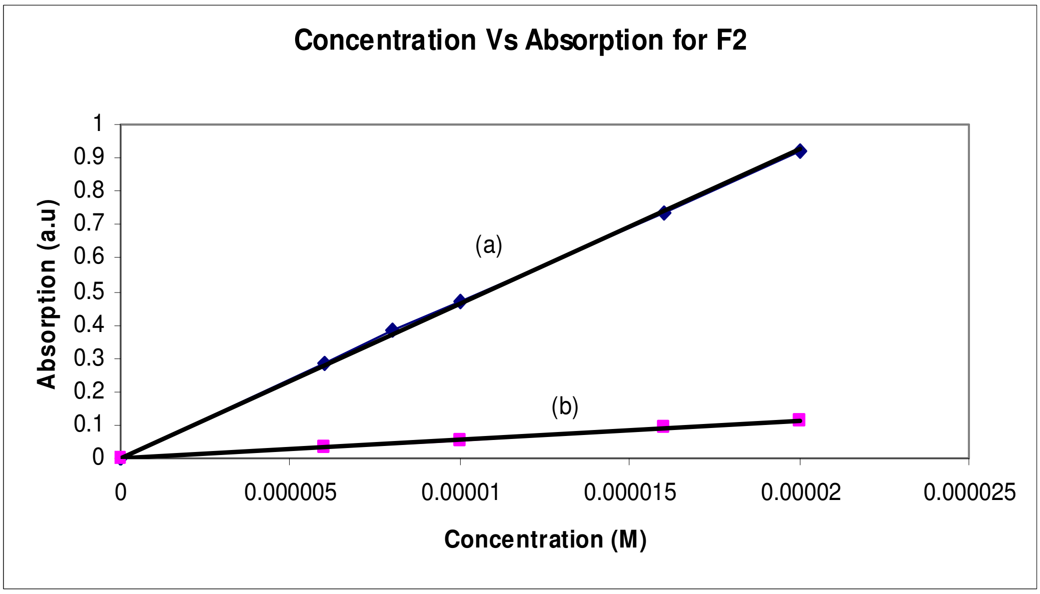

Figure S18: Effect of concentration on absorption for **F2** (N-[histaminedihydrolium]-1,8-naphthalenecarboximidic trans-tetrachlorido(dimethylsulfoxide)(N-[histaminedihydro]-1,8-naphthalenecarboximide) ruthen(III)ate). (a) At 333 nm; molar absorptivity (ε_{max} ; M^{-1} cm^{-1}) = 46,300 and correlation coefficient, r = 0.99. (b) At 390 nm; molar absorptivity (ε_{max} ; M^{-1} cm^{-1}) = 5,600 and correlation coefficient, r = 0.99.

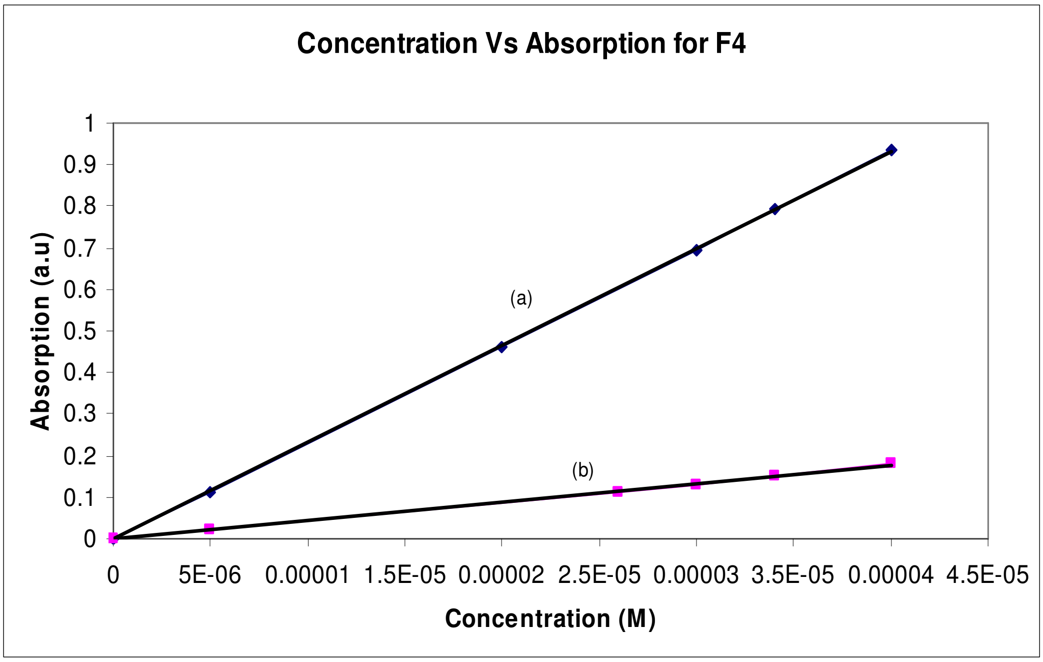

Figure S19: Effect of concentration on absorption for **F4** (Tetramethylammonium trans-tetrachlorido(dimethylsulfoxide)(N-[histaminedihydro]-1,8-naphthalenecarboximide)ruthen(III)ate). (a) At 334 nm; molar absorptivity (ε_{max} ; M^{-1} cm^{-1}) = 23,300 and correlation coefficient, r = 0.99. (b) At 375 nm; molar absorptivity (ε_{max} ; M^{-1} cm^{-1}) = 4,500 and correlation coefficient, r = 0.99.

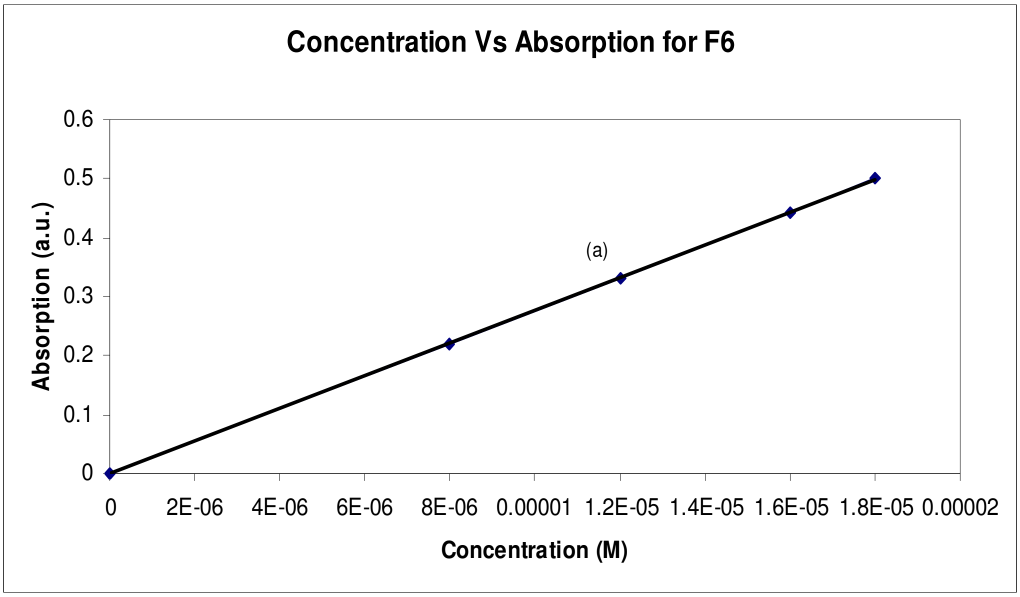

Figure S20: Effect of concentration on absorption for **F6** (N-[histaminedihydro]-1,8-naphthalenecarboximide). (a) At 332 nm; molar absorptivity (ε_{max} ; M^{-1} cm^{-1}) = 27,800 and correlation coefficient, r = 0.99.

X-ray crystal structure analysis

Crystals were grown from DMF/Methanol mixture by solvent layering method. Crystallization of the 7-azaindole derivative (**F1; 7-azaindolium *trans*-tetrachlorido(7-azaindole)(dimethylsulfoxide)ruthen(III)ate)** caused the substitution of one chlorine molecule with one molecule of DMF. Intensity data for violet crystals of **1** (0.20 x 0.20 x 0.13 mm) were collected at 123 K on a Bruker Apex II CCD fitted with graphite monochromated Mo Kα radiation (0.71073 Å). Crystal parameters and details of the data collection are summarized in Table S2.

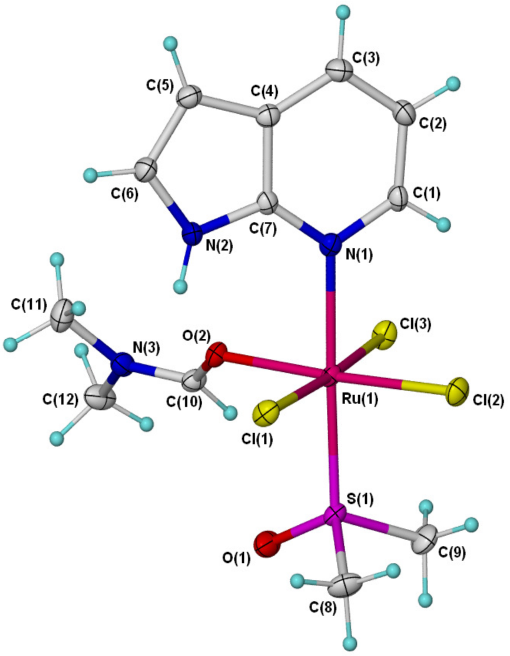

Figure S21: Molecular diagram of [$RuCl_3$(DMSO)(DMF)(7-azaindole)] with non-hydrogen atoms shown as 50% thermal ellipsoids and hydrogen atoms as spheres of arbitrary size.

Table S2: Crystal data and structure refinement for [RuCl3(DMSO)(DMF)(7-azaindole)].

Crystal	**[RuCl3(DMSO)(DMF)(7-azaindole)]**
Empirical formula	C12 H19 Cl3 N3 O2 Ru S
Formula weight	476.78
Temperature	123(2) K
Wavelength	0.71073 Å
Crystal system	Monoclinic
Space group	P21/*n*
Unit cell dimensions	a = 10.9531(6) Å alpha = 90^0
	b = 14.7312(4) Å beta = $93.742(7)^0$
	c = 11.0807(7) Å gamma = 90^0
Volume	1784.08(16) A^3
Z	4
Calculated density	1.775 Mg/m^3
Absorption coefficient (M(Mo Kα)/mm^{-1})	1.453 mm^{-1}
F(000)	956

Crystal size	0.20 x 0.20 x 0.13 mm
Theta range for data collection	2.30 to 32.34^0
Limiting indices	-16<=h<=15, -21<=k<=20, -8<=l<=16
Independent reflections	13501 / 5801 [*R*(int) = 0.0234]
Completeness to theta = 27.50	100.0 %
Absorption correction	Semi-empirical from equivalents
Max. and min. transmission	1.00000 and 0.88914
Refinement method	Full-matrix least-squares on F^2
Data / restraints / parameters	5801 / 1 / 207
Goodness-of-fit on F^2	1.040
Final R indices [I >2 sigma(I)]	$^a R_1$= 0.0295, $^b wR_2$ = 0.0623
R indices (all data)	$^a R_1$ = 0.0391, $^b wR_2$ = 0.0667
Largest diff. peak and hole	1.960 and -0.953 e. Å^{-3}

$^a R = \Sigma(|Fo| - |Fc|)/ \Sigma |Fo|$. $^b R = [\Sigma w(|Fo| - |Fc|)^2/ \Sigma Fo^2]^{1/2}$, where $w = [\sigma^2(Fo)]^{-1}$

Table S3. Atomic coordinates (x 10^4) and equivalent isotropic displacement parameters (A^2 x 10^3) for [RuCl3(DMSO)(DMF)(7-azaindole)]. U(eq) is defined as one third of the trace of the orthogonalized Uij tensor.

	x	y	z	U(eq)
Ru(1)	2933(1)	1952(1)	5412(1)	14(1)
Cl(1)	926(1)	2059(1)	6000(1)	21(1)
Cl(2)	2444(1)	762(1)	4110(1)	22(1)
Cl(3)	4987(1)	1935(1)	4965(1)	21(1)
S(1)	2488(1)	2936(1)	3860(1)	17(1)
O(1)	2732(2)	3902(1)	4122(1)	26(1)
O(2)	3374(1)	2975(1)	6671(1)	18(1)
N(1)	3403(2)	1008(1)	6839(2)	17(1)
N(2)	2488(2)	1791(1)	8474(2)	19(1)
N(3)	4305(2)	4275(1)	7281(2)	20(1)
C(1)	4053(2)	258(1)	6608(2)	19(1)
C(2)	4390(2)	-397(2)	7458(2)	23(1)
C(3)	4060(2)	-315(2)	8638(2)	23(1)
C(4)	3409(2)	458(1)	8926(2)	19(1)

C(5)	2928(2)	812(2)	9995(2)	22(1)
C(6)	2383(2)	1614(2)	9682(2)	22(1)
C(7)	3108(2)	1094(1)	7992(2)	17(1)
C(8)	951(2)	2846(2)	3252(2)	29(1)
C(9)	3266(2)	2659(2)	2555(2)	28(1)
C(10)	4015(2)	3656(1)	6465(2)	19(1)
C(11)	3910(2)	4233(2)	8511(2)	29(1)
C(12)	5043(2)	5061(2)	6978(2)	28(1)

Table S4. Bond lengths [A] and angles [deg] for [RuCl3(DMSO)(DMF)(7-azaindole)].

Ru(1)-O(2)	2.0883(14)
Ru(1)-N(1)	2.1431(17)
Ru(1)-S(1)	2.2772(5)
Ru(1)-Cl(2)	2.3115(5)
Ru(1)-Cl(3)	2.3354(5)
Ru(1)-Cl(1)	2.3387(5)
S(1)-O(1)	1.4726(16)
S(1)-C(9)	1.773(2)
S(1)-C(8)	1.777(2)
O(2)-C(10)	1.255(2)
N(1)-C(7)	1.344(2)
N(1)-C(1)	1.348(3)
N(2)-C(7)	1.360(2)
N(2)-C(6)	1.376(3)
N(3)-C(10)	1.309(3)
N(3)-C(11)	1.457(3)
N(3)-C(12)	1.463(3)
C(1)-C(2)	1.381(3)
C(2)-C(3)	1.385(3)
C(3)-C(4)	1.391(3)
C(4)-C(7)	1.418(3)
C(4)-C(5)	1.426(3)
C(5)-C(6)	1.358(3)
O(2)-Ru(1)-N(1)	86.64(6)

O(2)-Ru(1)-S(1)	94.27(4)
N(1)-Ru(1)-S(1)	177.99(5)
O(2)-Ru(1)-Cl(2)	176.69(4)
N(1)-Ru(1)-Cl(2)	90.15(5)
S(1)-Ru(1)-Cl(2)	88.955(19)
O(2)-Ru(1)-Cl(3)	88.03(4)
N(1)-Ru(1)-Cl(3)	87.77(5)
S(1)-Ru(1)-Cl(3)	90.474(19)
Cl(2)-Ru(1)-Cl(3)	92.667(19)
O(2)-Ru(1)-Cl(1)	86.92(4)
N(1)-Ru(1)-Cl(1)	91.33(5)
S(1)-Ru(1)-Cl(1)	90.505(19)
Cl(2)-Ru(1)-Cl(1)	92.339(19)
Cl(3)-Ru(1)-Cl(1)	174.915(19)
O(1)-S(1)-C(9)	106.95(11)
O(1)-S(1)-C(8)	107.60(11)
C(9)-S(1)-C(8)	99.64(12)
O(1)-S(1)-Ru(1)	116.03(7)
C(9)-S(1)-Ru(1)	112.26(8)
C(8)-S(1)-Ru(1)	112.94(8)
C(10)-O(2)-Ru(1)	124.26(13)
C(7)-N(1)-C(1)	114.82(17)
C(7)-N(1)-Ru(1)	125.39(13)
C(1)-N(1)-Ru(1)	119.79(14)
C(7)-N(2)-C(6)	108.29(17)
C(10)-N(3)-C(11)	122.90(19)
C(10)-N(3)-C(12)	120.33(19)
C(11)-N(3)-C(12)	116.76(18)
N(1)-C(1)-C(2)	124.33(19)
C(1)-C(2)-C(3)	120.6(2)
C(2)-C(3)-C(4)	117.2(2)
C(3)-C(4)-C(7)	118.12(19)
C(3)-C(4)-C(5)	135.4(2)
C(7)-C(4)-C(5)	106.45(18)
C(6)-C(5)-C(4)	106.66(18)
C(5)-C(6)-N(2)	110.49(19)
N(1)-C(7)-N(2)	126.94(18)
N(1)-C(7)-C(4)	124.94(18)
N(2)-C(7)-C(4)	108.11(18)

O(2)-C(10)-N(3)	123.0(2)

Symmetry transformations used to generate equivalent atoms:

Table S5. Anisotropic displacement parameters (A^2 x 10^3) for [RuCl3(DMSO)(DMF)(7-azaindole)].

The anisotropic displacement factor exponent takes the form:
-2 pi^2 [h^2 a*^2 U11 + ... + 2 h k a* b* U12]

	U11	U22	U33	U23	U13	U12
Ru(1)	13(1)	17(1)	12(1)	-1(1)	0(1)	-3(1)
Cl(1)	15(1)	30(1)	18(1)	1(1)	2(1)	-1(1)
Cl(2)	24(1)	22(1)	20(1)	-5(1)	-2(1)	-5(1)
Cl(3)	15(1)	28(1)	21(1)	-3(1)	3(1)	-4(1)
S(1)	18(1)	20(1)	13(1)	0(1)	0(1)	-2(1)
O(1)	35(1)	18(1)	23(1)	1(1)	-3(1)	-3(1)
O(2)	19(1)	20(1)	15(1)	-3(1)	0(1)	-3(1)
N(1)	14(1)	19(1)	17(1)	-1(1)	1(1)	-1(1)
N(2)	21(1)	19(1)	16(1)	-2(1)	1(1)	5(1)
N(3)	20(1)	18(1)	22(1)	-2(1)	-4(1)	0(1)
C(1)	18(1)	21(1)	19(1)	-5(1)	2(1)	2(1)
C(2)	23(1)	21(1)	24(1)	-3(1)	-1(1)	6(1)
C(3)	25(1)	23(1)	22(1)	4(1)	-1(1)	3(1)
C(4)	18(1)	20(1)	18(1)	1(1)	-1(1)	-1(1)
C(5)	22(1)	25(1)	18(1)	1(1)	-1(1)	2(1)
C(6)	23(1)	26(1)	17(1)	-1(1)	1(1)	5(1)
C(7)	14(1)	17(1)	18(1)	-3(1)	-1(1)	-1(1)
C(8)	23(1)	39(1)	24(1)	6(1)	-8(1)	-2(1)
C(9)	34(1)	35(1)	16(1)	1(1)	7(1)	1(1)
C(10)	20(1)	20(1)	17(1)	1(1)	-4(1)	-2(1)
C(11)	29(1)	33(1)	24(1)	-9(1)	2(1)	-1(1)
C(12)	30(1)	19(1)	33(1)	3(1)	-11(1)	-5(1)

Table S6. Hydrogen coordinates (x 10^4) and isotropic displacement parameters (A^2 x 10^3) for [RuCl$_3$(DMSO)(DMF)(7-azaindole)].

	x	y	z	U(eq)
H(1)	4295	173	5808	23
H(2)	4852	-908	7231	28
H(3)	4270	-767	9227	28
H(5)	2980	541	10774	26
H(6)	1984	1998	10221	26
H(8A)	394	3013	3872	43
H(8B)	787	2219	2990	43
H(8C)	825	3255	2558	43
H(9A)	3007	3073	1896	42
H(9B)	3072	2033	2312	42
H(9C)	4150	2718	2737	42
H(10)	4303	3726	5680	23
H(11A)	3273	3769	8556	43
H(11B)	3582	4825	8733	43
H(11C)	4609	4077	9069	43
H(12A)	5321	4986	6161	42
H(12B)	5754	5108	7559	42
H(12C)	4549	5613	7012	42
H(2N)	2160(20)	2221(15)	8040(20)	28(7)

Chapter 5

Development of analogues of NAMI-A aimed at understanding its mode of action: Syntheses, structural characterization, fluorescent properties and preliminary biological studies in human lung cancer cells (A549) †

Sumy Antony, [1,2] Jonathan Morris, [3] Tracey Brown, [4] Leone Spiccia, [2] and Hugh Harris [1]

[1] School of Chemistry and Physics, The University of Adelaide, SA 5005, Australia
[2] School of Chemistry, Monash University, Clayton, Victoria 3800, Australia
[3] School of Chemistry, The University of New South Wales, Sydney, NSW 2052, Australia
[4] School of Biochemistry and Molecular Biology, Monash University, Clayton, VIC 3800, Australia

---

† Antony, S.; Morris, J.; Brown, T.; Spiccia, L.; Harris, H. H., *Aust. J. Chem.* to be submitted

Chapter 5

Antony, S., Morris, J. C., Brown, T., Bell, T., Spiccia, L., & Harris, H. H. (2013), Development of analogues of NAMI-A aimed at understanding its mode of action: Syntheses, structural characterization, fluorescent properties and preliminary biological studies in human lung cancer cells (A549). *Manuscript to be submitted in Aust. J. Chem.*

Antony, S. (Candidate, Principal Author)

Shared responsibility for the design and development of the work. Designed and performed all syntheses and subsequent characterisation, fluorescent imaging and cytotoxicity assays, analysed and interpreted results, conceived the scope of, and wrote the manuscript (with assistance outlined below).

I hereby certify that the statement of contribution is accurate.

Signed: Date: 03/10/2013

Morris, J. C.

Provided guidance in the design and development of synthetic work, and assisted the revision of the manuscript.

I hereby certify that the statement of contribution is accurate and I give permission for the inclusion of the paper in the thesis.

Signed: Date: 3/10/13

Bell, T.

Supervised fluorescent quantum yield experiments and assisted with the revision of the manuscript.

I hereby certify that the statement of contribution is accurate and I give permission for the inclusion of the paper in the thesis.

Signed: Date: 7/10/13

Brown, T.

Supervised cell culture experiments and assisted with the revision of the manuscript.

I hereby certify that the statement of contribution is accurate and I give permission for the inclusion of the paper in the thesis.

Signed: Date: 7/10/2013

Spiccia, L.

Supervised experimental work, assisted with interpretation of results, and in the revision of the manuscript.

I hereby certify that the statement of contribution is accurate and I give permission for the inclusion of the paper in the thesis.

Signed: Date: 3/10/13

Harris, H. H.

Supervised the design and development of the work, assisted with experimental design, interpretation of the data, and the conception and revision of the manuscript and acted as corresponding author.

I hereby certify that the statement of contribution is accurate and I give permission for the inclusion of the paper in the thesis.

Signed: Date: 3/10/13

5.1. Abstract

In an attempt to explore the cellular distribution of NAMI-A and NAMI-A type complexes, a series of new ruthenium complexes were prepared, namely, 4-bromoimidazolium [*trans*-tetrachlorido(4-bromo-1H-imidazole)(S-dimethylsulfoxide)ruthen(III)ate] (**M1**), 2-iodoimidazolium [*trans*-tetrachlorido(2-iodo-1H-imidazole)(S-dimethylsulfoxide)ruthen(III)ate] (**M2**), quinolium [*trans*-tetrachlorido(quinoline)(S-dimethylsulfoxide)ruthen(III)ate] (**M3**), and Hydrogen *trans*-tetrachloridobis(N-[3(methylsulfinyl)propyl]-1,8-napthalenedicarboximide)ruthen(III)ate (**P1**). The compounds were characterised by elemental analysis, mass spectrometry, UV-Vis spectrophotometry and fluorescent spectroscopy. The molar extinction coefficients (ε_{max}) at each absorption maxima, fluorescence emission maxima and fluorescence quantum yield (ϕ_f) were calculated, to compare the electronic properties of the synthesised complexes with those of the model complex NAMI-A. Half-inhibitory concentrations (IC_{50}) of the synthesised complexes were calculated from dose response curves derived from real-time cell adhesion impedance measurements. The IC_{50} values of A549 cells exposed for 24 h were: **M1** (255 ± 13 mean [µM] ± S.E.M.; $n = 3$); **M2** (236 ± 30 µM), and **M3** (182 ± 51 µM). In some cases these IC_{50} values were smaller than that for the model compound NAMI-A (305 ± 18) potentially indicating a greater efficacy. The cellular uptake and distribution of **M3** was investigated by live cell imaging experiments (confocal microscopy), which indicated that it mainly accumulated in the mitochondria or Golgi apparatus of cell line A549, a key target for cancer therapeutics.

5.2. Introduction

The development of ruthenium anti-cancer drugs has accelerated significantly since NAMI-A ((ImH+)[Ru^{III}Cl$_4$(Im)(S-DMSO)], where Im = imidazole and S-DMSO = S-bound dimethylsulfoxide) and KP1019 ((IndH+)[Ru^{III}Cl$_4$(Ind)$_2$], where Ind = indazole) successfully completed phase I clinical trials[1]. Ruthenium compounds are viable alternatives for platinum anti-cancer drugs owing to their lower toxicities and apparently different modes of action[2, 3]. Ruthenium has two accessible oxidation states under physiological conditions; Ru(II) (d^6, diamagnetic) and Ru(III) (d^5, paramagnetic) and the preferred geometry in the solid state is octahedral[1]. The redox potential for the inter-conversion between these oxidation states is small inside the cell when compared to physiological solution; and it has been proposed that Ru(III) compounds are rapidly reduced inside the cell[4]. On reduction, these compounds adhere to bio-molecules within the cell, and remain attached for the rest of that cell lifetime[5].

Ruthenium compounds are considered capable of overcoming the resistance induced by platinum drugs in cancer cells[6]. A recent XAS study[7] on the biotransformation of anti-cancer Ru(III) complexes revealed specific differences between the interactions of the model complexes NAMI-A and KP1019 in treated A549 cancer cells. The outcomes of the study show that KP1019 was taken up by the cells by passive diffusion where as the activity of NAMI-A was induced by cell-surface interactions[7]. On the contrary, the mechanism of anti-cancer activity of platinum drugs has been attributed to the formation of stable adducts with DNA, which prevent the DNA replication leading to tumour cell death[8].

Several distinct ruthenium compounds have been synthesised and examined for their anti-cancer properties, but clarity regarding their mode of anti-neoplastic activity[9, 10] is lacking. The previously investigated ruthenium compounds include; Ru-DMSO compounds[11] (**1** and **2**, Scheme 1), Ru(III) complexes of the type [LH]*trans*-[RuCl$_4$(L)$_2$][12] (**3**, **4** and **5**, Scheme 1), and organometallic

Ru(II)-arene compounds of general formula [(η_6-arene)Ru(en)Cl][PF_6][13] (**6** and **7**, Scheme 1).

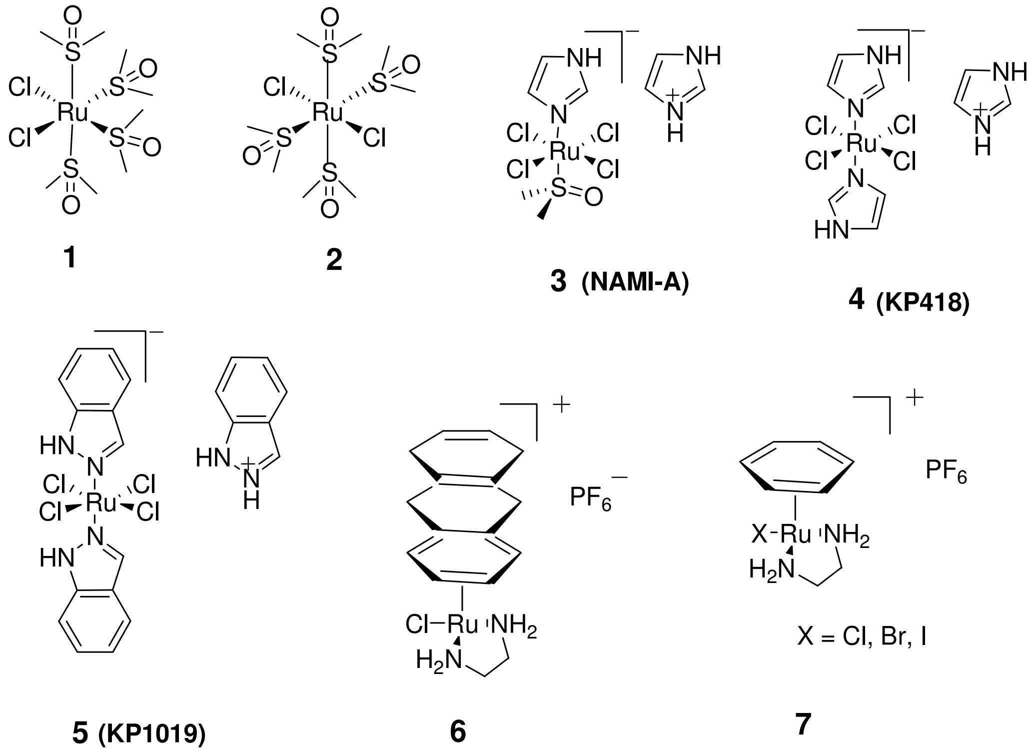

Scheme 1: Structures of some representative Ru(II) and Ru(III) complexes that exhibit anti-cancer activity[6]: **1** (*cis*-[$RuCl_2(DMSO)_4$]); **2** (*trans*-[$RuCl_2(DMSO)_4$]); **3** (NAMI-A) [ImH]*trans*-[$RuCl_4$(Im)(DMSO-S)]; **4** (KP418) [ImH]*trans*-[$RuCl_4(Im)_2$]; **5** (KP1019) [IndH]*trans*-[$RuCl_4(Ind)_2$]; **6** and **7**, organometallic compounds of general formula [(η_6-arene)Ru(en)X][PF_6] where X= Cl, Br or I.

The anti-neoplastic activity of these potential drugs (Scheme 1) is assumed to be different from that of the approved platinum-based anti-cancer agents. The classic ruthenium(III) anti-cancer drugs, NAMI-A and KP1019 (**3** and **5**, Scheme 1), differ in their structure and in their activity against malignant neoplasms. KP1019 is more effective against primary neoplasm[2, 6, 14] (the principle tumour mass which forms first in a patient), while NAMI-A is effective against secondary neoplasm[2] (the metastases formed when cancer cells from the primary neoplasm have displaced to a distant organ). This apparent change in their anti-cancer activity could be related to the fact that

NAMI-A undergoes aquation reactions more rapidly than KP1019[7]. As such, NAMI-A binds more rapidly to plasma proteins and thus inhibits passive uptake into the cells when compared to KP1019[7]. These compounds potentially target bio-molecules (such as DNA) and both intra- and extracellular proteins[7, 15]. KP1019 has been reported to bind to transferrin (an iron transport protein), and then be discharged as a Ru(II) species once reduced by ascorbate or glutathione[16]. Alternatively, the disruption of iron metabolism may be a factor contributing to the anti-tumour activity of Ru(III) complexes as shown by our recent study[10], where we observed that ruthenium from KP1019 was co-localised with iron and that it significantly modified the distribution of iron from that observed in untreated cells. Both the cellular and bio-molecular targets of the drugs are not known at present and hence the precise mechanism of action is not fully understood.

Ruthenium-based drugs, especially NAMI-A type complexes, have been proposed to inhibit different steps in metastases, including: inhibition of tumour cell de-adhesion (separation); motility (directed cell movement); and invasion (entry of foreign particle)[6]. Investigations based on redox transformations (activation by reduction mechanism[17]), aquation (ligand exchange mechanism[2]) and interactions with biologically relevant molecules, such as serum transport proteins[18] and DNA nucleotides[19], revealed that the Ru(III) centre may undergo reduction in the presence of biological reducing agents, e.g., ascorbic acid and glutathione. The correlation between reduction of the drug and its anti-cancer activity was investigated thoroughly[7, 20], but the relationship between them was not fully explained. The partial reduction of the model complexes, NAMI-A and KP1019, was investigated by the XAS analysis of treated cancer cells and the results unambiguously showed that the formation of Ru^{III}-S intermediates is favoured compared to the reduction of Ru(III) to form Ru(II) intermediates[7]. Another investigation[20] characterised the *in vivo* chemistry of KP1019, and its sodium-salt analogue KP1339, by X-ray absorption near edge structure spectroscopy and the oxidation and coordination states were assigned to the drug inside the target tumour tissue. The results demonstrated a strong shift in the edge position of the XANES spectra leading to apparent alterations in the coordination and oxidation environment of the ruthenium metal center[20]. It was concluded that the reduction of Ru(III) to Ru(II) was feasible, but that the majority of ruthenium most likely remained as Ru(III).

Our recent μ-XRF imaging investigation[10] of the cellular distribution of ruthenium in cells treated with NAMI-A and KP1019 demonstrated that KP1019 was internalized into treated cells. The modulated iron distribution suggested that KP1019 might affect iron metabolism and the variation in the fate of the two drugs was clearly understood from the very distinct ruthenium distributions[10]. Meanwhile, μ-XRF investigation[21] of single cultured A549 cells treated with iodine substituted KP1019 or NAMI-A analogues revealed that the addition of an iodine substituent to the ligand contributed to a variation in the distribution of ruthenium throughout the cell. Importantly, the Ru-N bonds remained intact after incubation in culture media and subsequent cellular uptake and processing[21]. In spite of these efforts aimed at revealing the mechanism of action of NAMI-A type complexes, the fundamental reason for the anti-metastatic activities of this class of drugs still remains uncertain.

Herein, we report a series of NAMI-A analogues, **M1**, **M2, M3** and DMSO precursor analogue, **P1** (Scheme 2) as target complexes which were synthesised by replacing the imidazole and DMSO groups with suitable ligands (Scheme 3). **M1** and **M2** were developed with a view to provide a better understanding of the anti-metastatic properties and intracellular distribution of NAMI-A-type complexes by ‘double-tag’ approach similar to our recently reported investigation[21]. **M3** and **P1** were specifically developed to investigate the fluorescent properties and the cellular pathways of the ruthenium species in NAMI-A type complexes labelled with a fluorescent reporter. The cytotoxicity of the synthesised complexes were investigated and reported. Live cell imaging of the cells treated with the complex **M3** and its uncoordinated ligand **L3** were also undertaken.

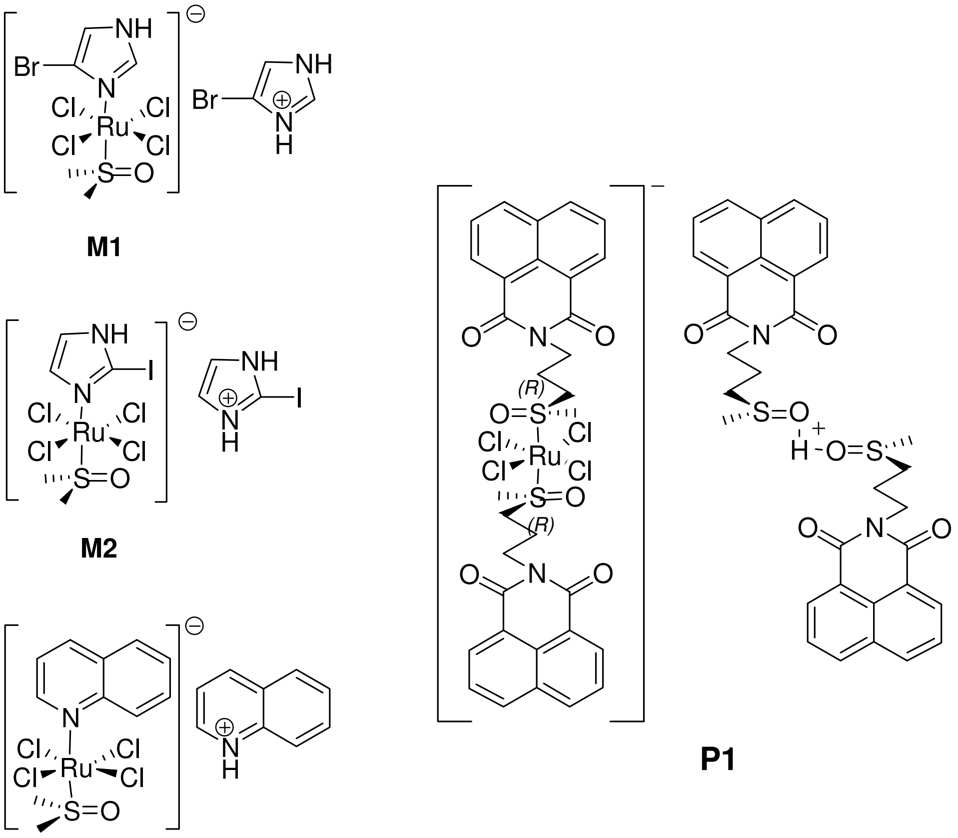

M1

M2

M3

P1

Scheme 2: Structural formulas of the compounds studied; **M1**, **M2**, **M3**, and **P1.**

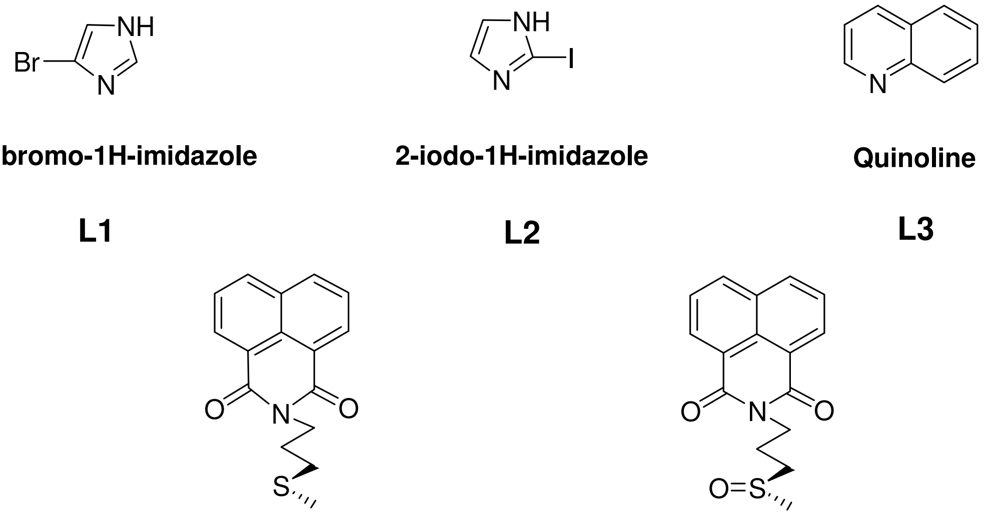

4-bromo-1H-imidazole

L1

2-iodo-1H-imidazole

L2

Quinoline

L3

**N-[3(methylthio)propyl]
1,8-naphthalenedicarboximide**

L4

**N-[3(methylsulfinyl)propyl]
1,8-naphthalenedicarboximide**

L5

Scheme 3: Structural formulas of the ligands used; **L1**, **L2**, **L3**, **L4** and **L5**.

5.3. Results and discussion

The biological activities of a number of derivatives of NAMI-A have been reported in the literature[4, 22, 23]. The fundamental goal of this study was to synthesise analogues of NAMI-A that would provide more information regarding the uptake, distribution and transformation of the compound in treated cancer cells. **M1** and **M2** were synthesised in order to analyse the cellular uptake by cytotoxicity studies and as precursors for ion-exchanged versions similar in design to the compounds shown in chapter 3 that would yield information regarding the stability of the Ru-N bond in cells for NAMI-A type complexes. **M3** was synthesised to investigate cellular uptake, distribution and transformation of the analogues in treated cells by cytotoxicity and fluorescent microscopy investigations.

5.3.1. Syntheses and characterisation

NAMI-A analogues were prepared by modifying the ligands present in the NAMI-A coordination sphere, as shown in Scheme 4.

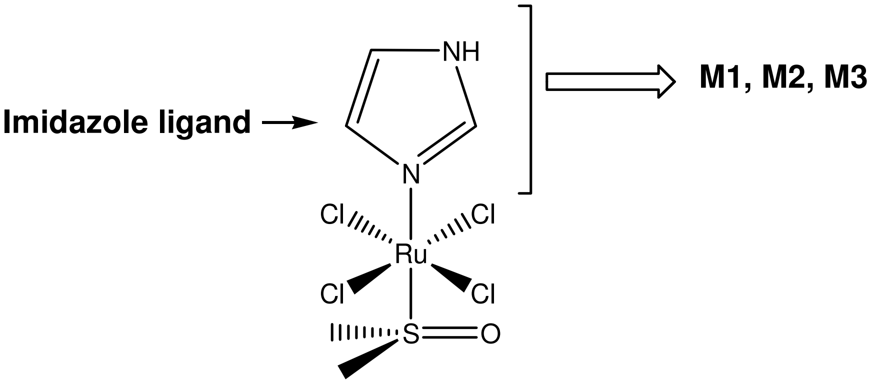

Scheme 4: Structure of the model compound NAMI-A

Complexes **M1**, **M2** and **M3** were synthesised by substituting the imidazole ligand in NAMI-A with **L1**, **L2** and **L3** (Scheme 3), respectively. In general, the synthesis was carried out by mixing a suspension of ruthenium precursor, $[(DMSO)_2H][\textit{trans}\text{-}RuCl_4(DMSO)_2]$, in acetone (for **M2** and **M3**) or ether (for **M1**) and adding an equivalent amount of the appropriate ligand (**L1**, **L2**, **L3**) and stirring overnight (Scheme 5). The complexes **M1**, **M2** and **M3** were characterised by elemental analysis (which correlated with the compounds with the general formula $(LH^+)[RuL(DMSO)Cl_4]^-$ where L = **L1**, **L2** and **L3)**, ESI-MS and UV-Vis spectrophotometry. The ruthenium in complexes **M1**, **M2** and **M3**, is in the +III oxidation state (paramagnetic), and thus the proton NMR spectra were broad and are not reported here).

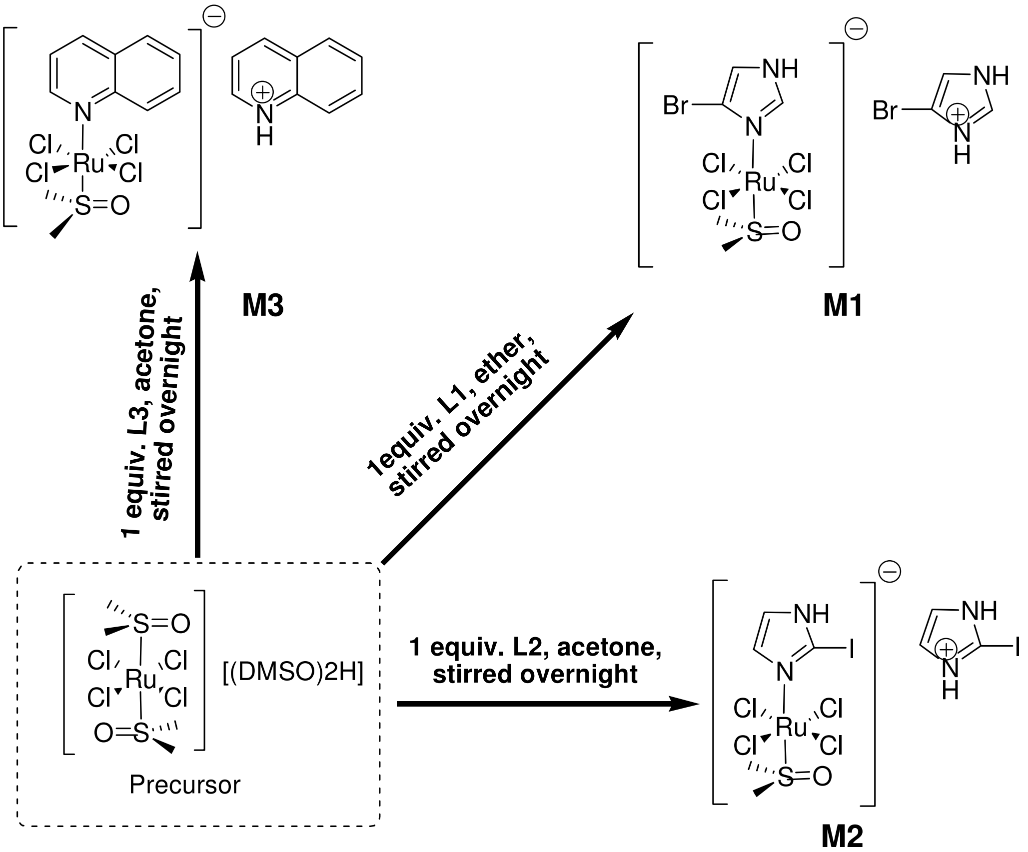

Scheme 5: Schematic representation of the synthetic routes used for the synthesis of complexes; **M1**, **M2** and **M3**.

Table 1. Summary of ESI-MS data with fragmentation pattern*

Complex	Fragment	m/z (negative ion)		m/z (positive ion)	
		calcd	found	calcd	found
M1	$[RuCl_4(DMSO)(4\text{-}Br\text{-}1H\text{-}Im)]^-$	467.1	467.6		
	$(4\text{-}Br\text{-}1H\text{-}Im\text{-}H)^+$			147.1	147.0
	$[RuCl_4(DMSO)]^-$	321.1	321.7		
	$[RuCl_4]^-$	243.7	243.8		
M2	$[RuCl_4(DMSO)(2\text{-}I\text{-}1H\text{-}Im)]^-$	515.1	515.7		
	$(2\text{-}I\text{-}1H\text{-}Im\text{-}H)^+$			195.1	195.1
	$[RuCl_4(CH_3SO)(2\text{-}I\text{-}1H\text{-}Im)]^-$	499.1	499.8		
	$[(RuCl_4)(2\text{-}I\text{-}1H\text{-}Im)]^-$	439.1	439.9		

	$[RuCl_4]^-$	243.7	243.7		
M3	$[RuCl_4(DMSO)(Quin)]^-$	449.8	449.8		
	$(Quin\text{-}H)^+$			129.0	129.5
	$[RuCl_4(DMSO)]^-$	321.7	321.7		
	$[RuCl_4]^-$	243.8	243.8		

* Mass spectra are given in Appendix III.

The sulfide (**L4**) was prepared as described in Scheme 7, by the reaction between **1** and **2** in dry ethanol. The controlled oxidation (to prevent formation of the corresponding sulfone) of **L4** to **L5** was carried out in presence of a catalyst (H_2SO_4/*i*-PrOH) at room temperature (Scheme 8). Both ligands were obtained in good yield (> 90%). The substituted DMSO precursor, **P1** was synthesised from **L5** (Scheme 9) in a yield of more than 75%. For **L4**, the ESI-MS exhibited peaks at m/z = 286.1 and 308.0 can be assigned to $[M+H]^+$ and $[M+Na]^+$, respectively. The ^{1}H-NMR spectrum further confirmed the formation of **L4** by the appearance of a distinct triplet at 4.27 ppm ($-NCH_2CH_2CH_2S-CH_3$), a triplet at 2.62 ppm ($-NCH_2CH_2CH_2S-CH_3$), a multiplet at 2.05 ppm ($-NCH_2CH_2CH_2S-CH_3$) and a singlet at 2.13 ppm ($-S-CH_3$). For **L5**, the ESI-MS exhibited peaks at m/z = 302.0 and 324.1 which can be assigned to $[M+H]^+$ and $[M+Na]^+$, respectively. The absence of any peak at m/z = 318.0 confirmed the exclusive formation of the (mono)sulfoxide. The ^{1}H-NMR spectrum verified the complete oxidation of **L4** to **L5** by the replacement of the signal in the spectrum of **L4** with a distinct singlet at 2.92 ppm ($-SO-CH_3$), a multiplet at 2.62 ppm ($-NCH_2CH_2CH_2S-CH_3$), a triplet at 4.37 ppm ($-NCH_2CH_2CH_2S-CH_3$), and a multiplet at 2.34 ppm ($-NCH_2CH_2CH_2S-CH_3$). For **P1**, ESI-MS exhibited peaks in the positive ion spectrum at m/z = 602.1 and 625.0 can be assigned to $[M+H]^+$ and $[M+Na]^+$, respectively and exhibited peaks in negative ion spectrum at m/z = 845.5 and 810.4 which were assigned to $[(\mathbf{L5})_2RuCl_4]^-$ and $[(\mathbf{L5})_2RuCl_3]^-$, respectively. The ^{1}H-NMR spectrum was found to be complex due to the presence of paramagnetic ruthenium(III) in **P1**.

P1 (Scheme 10) was suspended in acetone and stirred with imidazole at room temperature. A yellow emulsion was formed, with a fragment m/z = 810.4 was observed in the accurate mass spectrum (*see Appendix III – Figure 12*). **P1** may undergo hydrolysis to form **P2**, a neutral complex with ruthenium in +II oxidation state (Scheme 6). Similar reactions have been reported in the literature[24] where the DMSO precursor complex, $[(DMSO)_2H][$*trans*-$RuCl_4(DMSO)_2]$ (Ru(III)), was readily converted to a neutral complex *mer,trans*-$RuCl_3(DMSO\text{-}S)_2(DMSO\text{-}O)$, which is in the +II oxidation state. Similarly, the Ru(III) complex **P1** can be readily converted to more stable Ru(II) complex **P2** due to the strong π-accepting properties of the ligand –CO. In other words, the ligand imidazole can not replace the substituted DMSO ligand (**L5**) as in the model complex NAMI-A where the *trans*-effect of DMSO[25] enhances the formation of the complex.

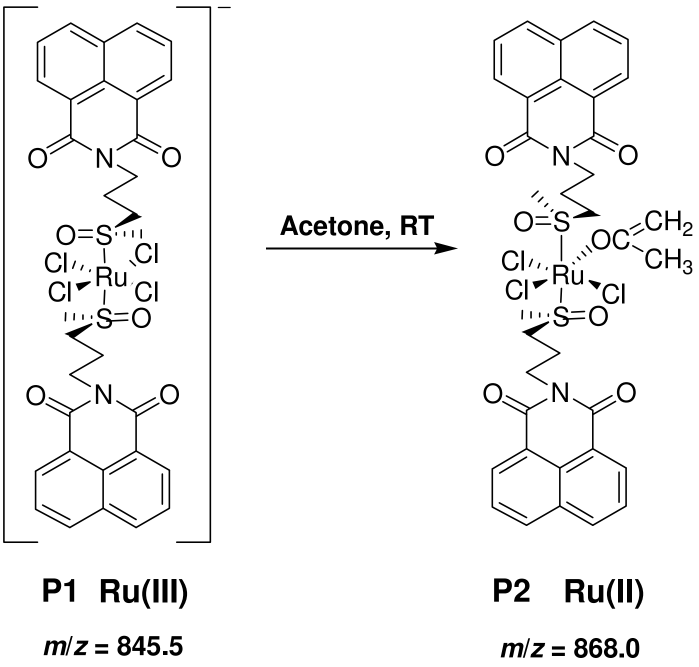

Scheme 6: Possible intermediate complex ions formed when P1 is suspened in acetome with imidazole.

5.3.2. UV-Vis absorption spectra of the complexes

The UV-visible spectra of complexes **M1**, **M2** and **M3** were measured in methanol and reported in comparison with the spectral properties of the model complex NAMI-A. The UV-Vis spectra displayed intense bands for ligand centred (LC; π–π*) and metal-centered (MC; πCl→t_{2g}Ru) transitions as shown in Figure 1. The absorption bands between 250 and 350 nm were assigned to LC transitions. MC transitions between the $\pi-$ orbital of the ligand to a 4d metal orbital (t_{2g}) were evidenced by a broad band centred on 400 nm. These findings were consistent with the literature data reported for NAMI-A type complexes[23, 26].

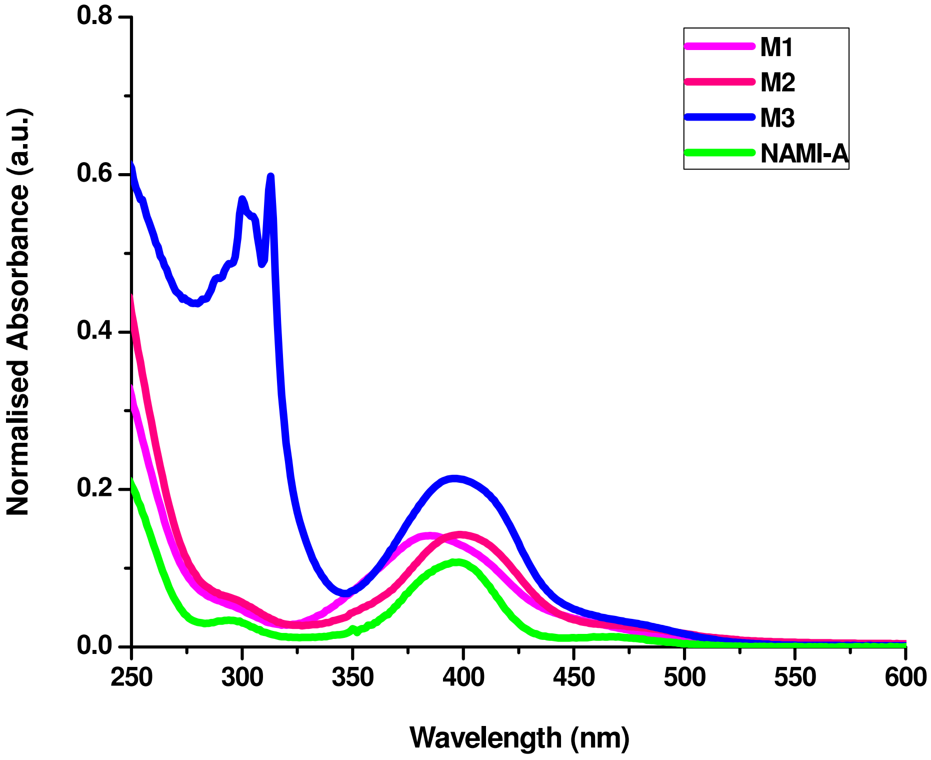

Figure 1: Absorption spectra of studied complexes **M1**, **M2** and **M3**, in comparison with the model complex NAMI-A.

The MC transition for **M3** was found to be more intense than that of either **M2** or **M1**. A summary of UV-Vis data obtained for the complexes and free ligands is shown in Table 2. As expected, modifications made to the NAMI-A coordination sphere have a significant effect on the intensity of the MC transitions. However, apart from **M1,** all complexes exhibit similar increases in absorptivity as the microanalytical data does not match exactly with the calculated value (may be due to the presence of one DMSO moiety from the precursor).

Table 2*. Comparison of the UV-Vis Spectral data for M1, M2 and M3 measured in methanol with their free ligands (L1, L2, and L3 respectively) and model complex NAMI-A.

Complex	λ_{max} (nm) [LC]	Molar extinction coefficient* (M^{-1} cm^{-1}) ; ε_{max}	λ_{max} (nm) [MC]	Molar extinction coefficient* (M^{-1} cm^{-1}) ; ε_{max}
M1	290	1,700	387	4,300
L1	207	4,700	-	-
M2	290	2,900	398	5,800
L2	207	4,700	-	-
M3	299	8,200	398	6,400
	312	7,500	-	-
	277	3,100	-	-
L3	299	2,700	-	-
	312	2,600	-	-
NAMI-A	239	8800	397	3800
	294	1200	-	-

*To measure the molar extinction coefficient standards of known concentration, were prepared and their absorbance were recorded. Graphs were plotted with concentration versus absorbance and the gradient of these graphs (each graph contain minimum 4 curve points) correspond to the molar extinction coefficient of the respective compounds.

The UV-Visible absorption properties of the ligand **L4** and the precursor **P1** were also studied indicating the presence of a light absorbing chromophore.

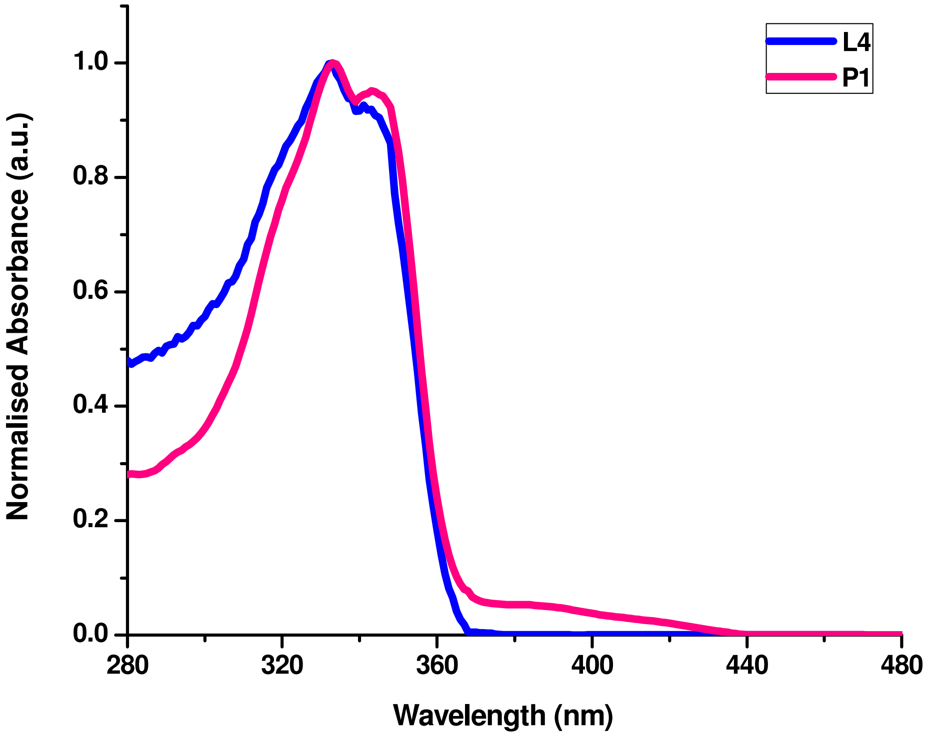

Figure 2: Comparison of UV-Visible spectra of ligand, **L4** and its precursor, **P1**.

A stock solution of **L4** was prepared in methanol and **P1** was prepared in DMF and then diluted with methanol. Both compounds (**L4** and **P1)** display significant absorption bands at λ_{max} = 333 nm and 345 nm. **P1** displayed an additional weak absorption band at 390 nm (MC transition). The value ε_{max} (M^{-1} cm^{-1}) was found to be ε_1 = 55,500 (333 nm) and ε_2 = 51,100 (345 nm) for **L4** and ε_1 = 15,200 (333 nm), ε_2 = 14,100 (345 nm) and ε_3 = 700 (390 nm). The main difference in the spectral properties of **P1** relative to **L4** was attributed to a metal-centered (MC) transition at 390 nm (πLigand → $d\pi$Ru). The results are consistent with the data reported for similar compounds in the literature[11, 23, 26, 27].

5.3.3. Fluorescent spectra

The excitation-emission spectrum obtained for **M3**, in comparison with its free ligand, **L3,** is given in Figure 3. The excitation-emission spectra obtained for **P1** in comparison with its free ligand **L4** is given in Figure 4. Based on the absorption at excitation wavelength, and the area under the emission curve, fluorescent quantum yields for the compounds **M3** and **P1,** and their corresponding ligands **L3** and **L4,** were calculated using equation 1 and values are listed in Table 3. Compound **L3** (ϕ_f = 0.24[28] in methanol at R.T) was used as a reference compound for **M3** and anthracene (ϕ_f = 0.27[29] in ethanol, ref index = 1.361 at 20°C) was used as a reference compound for **L3** and **P1**.

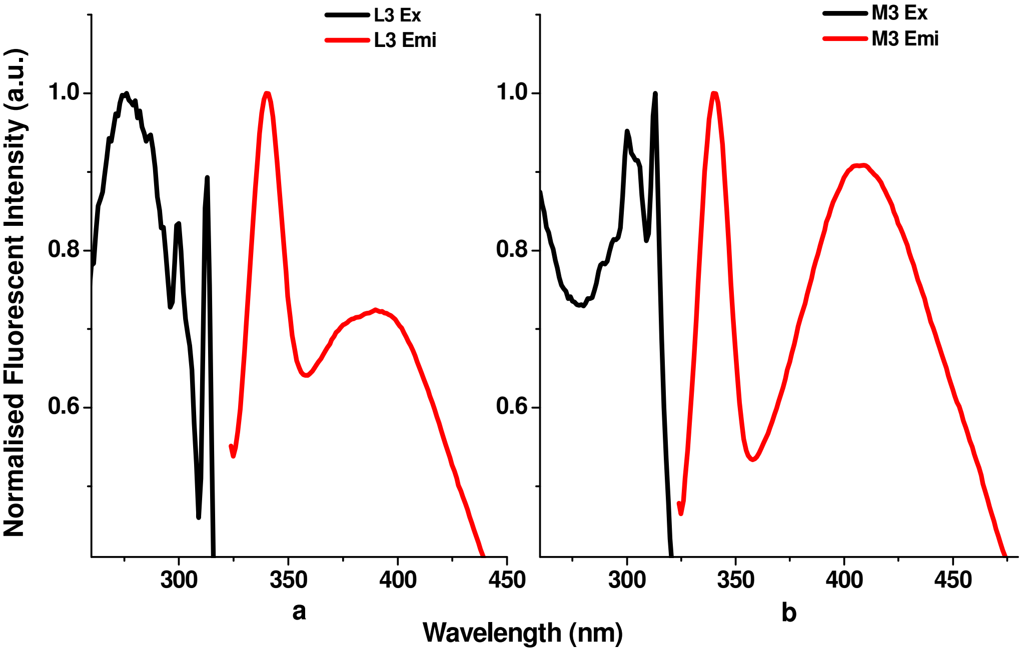

Figure 3: Excitation-emission profiles for **M3** and **L3**; **(a)** black curve represents the excitation spectrum (λ_{ex} = 275 nm) and red curve represents the emission spectrum (λ_{emi} = 340 nm and 390 nm) of **L3**; **(b)** black curve represents the excitation spectrum (λ_{ex} = 312 nm) and red curve represents the emission spectrum (λ_{emi} = 340 nm and 408 m) of **M3**. The summarised data is given in Table 2.

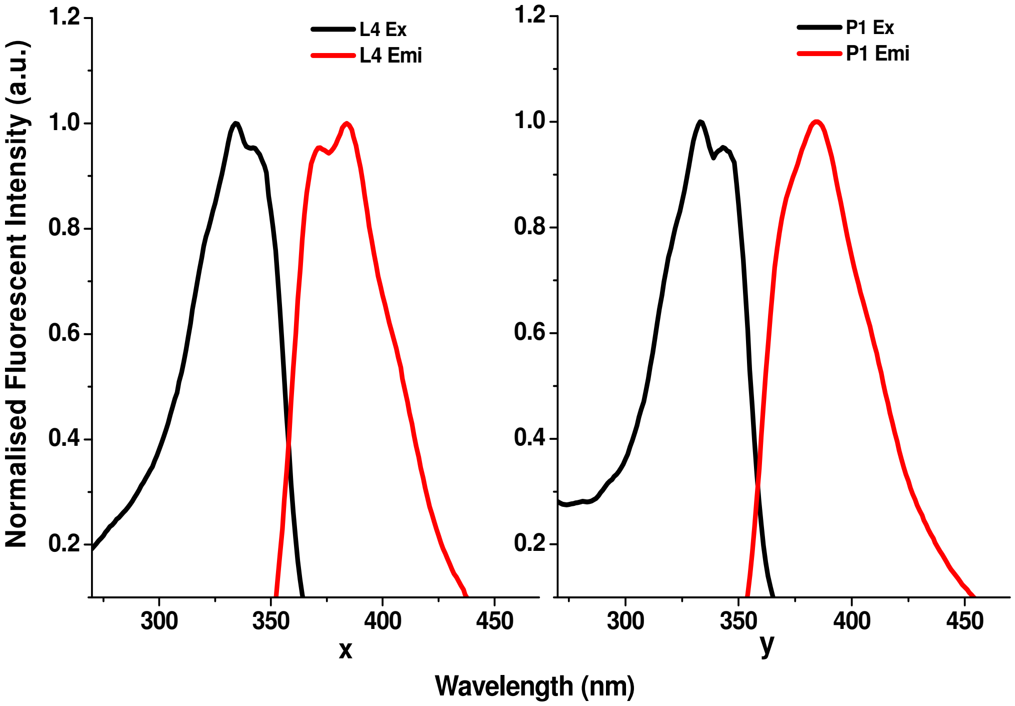

Figure 4: Excitation-emission profiles for **P1** and **L4**; **(x)** black curve represents the excitation spectrum (λ_{ex} = 330 nm) and red curve represents the emission spectrum (λ_{emi} = 370 nm and 380 nm) of **L4**; **(y)** black curve represents the excitation spectrum (λ_{ex} = 330 nm) and red curve represents the emission spectrum (λ_{emi} = 390 nm) of **P1**. The summarised data is given in Table 2.

Table 3*: Summary of spectral data obtained for M3, L3, P1 and L4 with their fluorescent quantum yield:

Complex	λ_{max} (nm) [LC] (from Uv-vis)	Excitation λ (nm);	Emission λ (nm);	Fluorescent quantum yield (ϕ_f)
M3	299 312	312	340 408	0.21[a]
L3	222 299 312	275	340 390	0.24[a]
P1	333 345	330	390	0.011[b]

L4	333 345	330	370 380	0.017[b]

[a] Quantum yield with respect to Quinoline (0.24)[28]; [b] Quantum yield with respect to Anthracene (0.27)[29].

* Dilutions ranging from 0.001 *m*M to 0.01 *m*M (Abs < 0.15) in methanol (Stock solution of compound P1 were prepared in DMF).

The fluorescent emission from complexes **M1** and **M2** was negligible (similar to NAMI-A) and hence not reported here. As expected, significant changes in the fluorescent properties were observed when the imidazole and DMSO ligands in NAMI-A were replaced with ligands with fluorescent character, **L3** and **L4**, as shown in Scheme 4. The emission maxima were at 340 nm and 408 nm for **M3** and 390 nm for **P1** in correlation with their non-coordinated ligand **L3** (340 nm and 390 nm) and **L4** (370 nm and 380 nm) respectively as shown in Figure 3 and 4 and Table 3. The emission maxima were found to be red-shifted for the complex when compared to the free non-coordinated ligand 408 nm for **M3** and 390 nm for its free ligand **L3**; 390 nm for **P1** and 380 nm for its free ligand **L4**. Quantum yields for the emission were estimated using equation 1, to compare the fluorescent properties of the synthesised compounds. Quinoline (ϕ_f = 0.24)[28] and anthracene (ϕ_f = 0.27)[29] were used as reference compounds for **M3** and **P1** respectively. The quantum yields followed the trend; **L3** (0.24) > **M3** (0.21) and **L4** (0.017) > **P1** (0.011). The lower quantum yield of the complexes with respect to its free ligand indicates the influence of the ligand in ^{3}LMCT excited state of the complex.

5.3.4. Cytotoxicity assays (IC_{50})

The cytotoxicities of the complexes **M1**, **M2**, and **M3** against the human lung carcinoma cell line, A549, (10,000 cells/well densities) were determined after 24 hr exposure by measuring cell adhesion. The IC_{50} value for NAMI-A determined by the same method (305 ± 18 µM) was found to be in good agreement with literature results obtained by MTT assay (300 µM)[30]. As expected, structural modifications made to NAMI-A have an effect on the biological properties. The synthesised compounds are more cytotoxic compared to the parent complex NAMI-A. **M3** was found to be most cytotoxic among the complexes (182 ± 51 µM) than **M2** (236 ± 30 µM) and **M1** (255 ± 13 µM). These compounds may be as effective as anti-metastatic agents as NAMI-A, but further biological studies (such as fluorescent imaging) are needed to establish whether the anti-metastatic activity is associated with cytotoxic effect as well as different steps in metastasis other than cytotoxicity[6].

5.3.5. Fluorescent microscopy

Fluorescence microscopy experiments were carried out using **M3** (because of its measurable quantum yield as in Table 3) in human lung carcinoma cells (A549). Samples of A549 cells were treated with **M3** in fluorescence dishes with a density 10,000 cells/dish. Live cell images were taken using LEICA TCS SP5 Inverted Microscope fitted with incubator designed for cell culture experiments at excitation wavelength 405 nm and emission filter range was 439 nm to 477 nm. The results are shown in Figures 5-7.

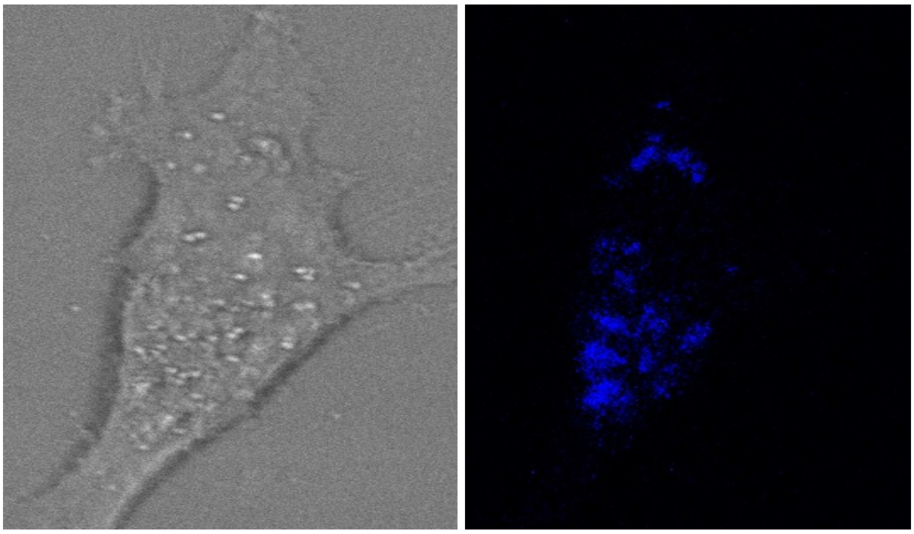

(a) **(b)**

Figure 5: Fluorescent micrographs (63 x magnifications) of A549 cells incubated with **M3** (50 µM) for 3 h at excitation 405 nm and emission profiles were collected from 439 nm to 477 nm. Fluorescence emission is shown in (b). Phase contrast image of treated cells is shown in (a).

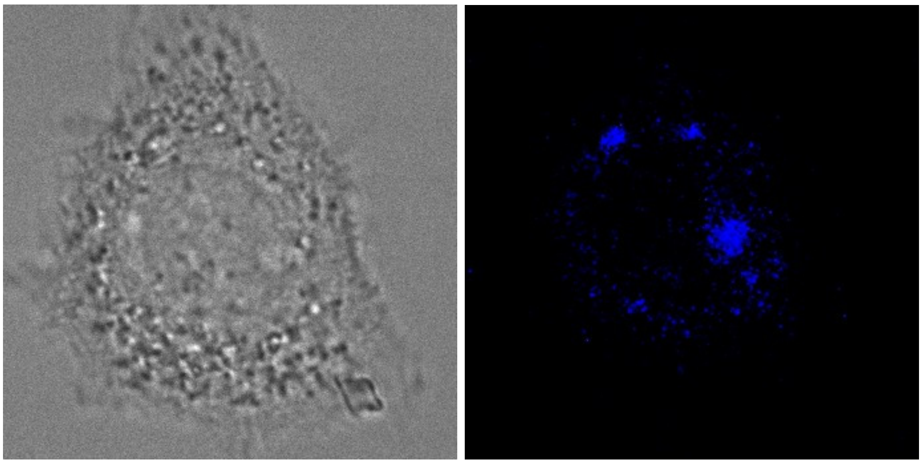

(a) **(b)**

Figure 6: Fluorescent micrographs (63 x magnifications) of A549 cells incubated with **M3** (50 µM) for 3 h at excitation 405 nm and emission profiles were collected from 439 nm to 477 nm. Fluorescence emission is shown in (b). Phase contrast image of treated cells is shown in (a).

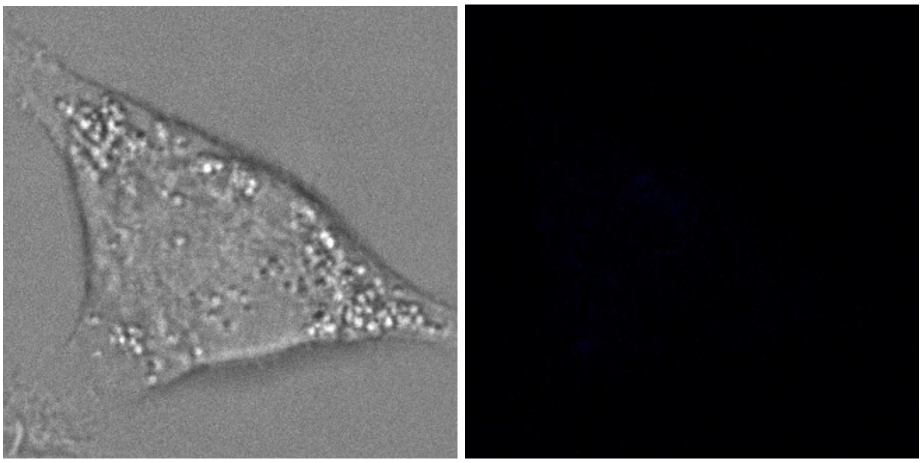

(a) **(b)**

Figure 7: Fluorescent micrographs (63 x magnifications) of control (media only) A549 cells incubated for 3 h at excitation 405 nm and emission profiles were collected from 439 nm to 477 nm. Fluorescence emission is shown in (b). Phase contrast image of treated cells is shown in (a).

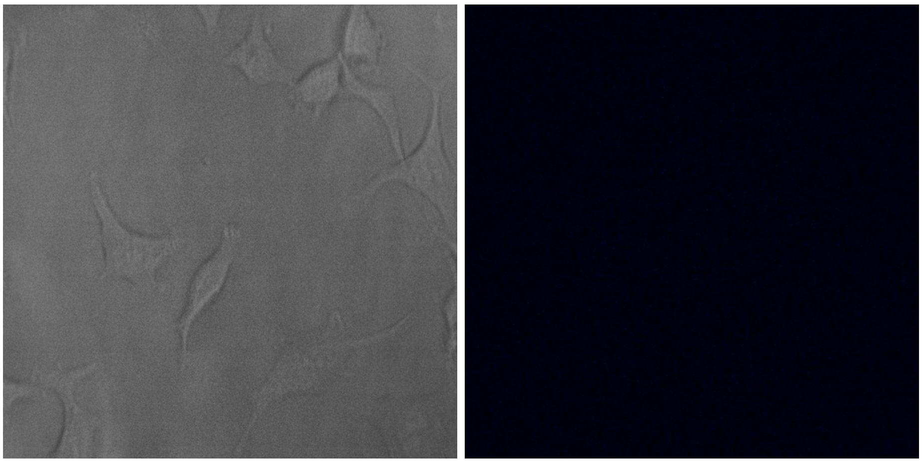

a) **(b)**

Figure 8: Fluorescent micrographs (63 x magnifications) of control (media only) A549 cells incubated for 24 h at excitation 405 nm and emission profiles were collected from 439 nm to 477 nm. Fluorescence emission is shown in (b). Phase contrast image of treated cells is shown in (a).

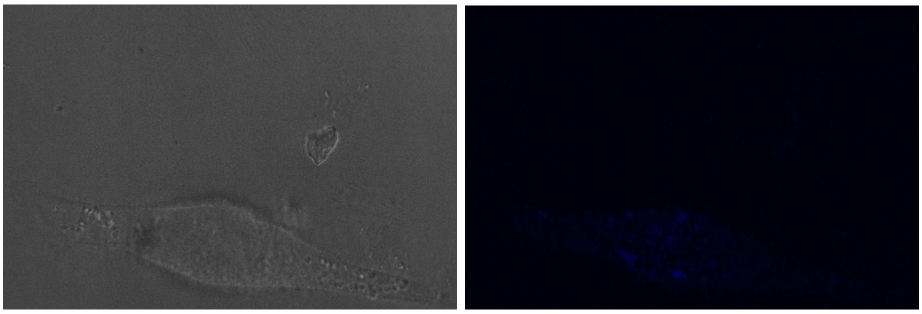

a) **(b)**

Figure 9: Fluorescent micrographs (63 x magnifications) of A549 cells incubated with NAMI-A (400 μM) for 24 h at excitation 405 nm and emission profiles were collected from 439 nm to 477 nm. Fluorescence emission is shown in (b). Phase contrast image of treated cells is shown in (a).

Confocal imaging of A549 cells treated with **M3** for 3 hr showed a punctate distribution of **M3** in the cytoplasm whereas minimal fluorescence was observed in the untreated cells (Figure 7). This was demonstrated by the appearance of small bright vesicles and spots near the nucleus in Figure 5 and 6. This suggested that the compounds were taken up and localised in the mitochondria or Golgi bodies followed by endocytosis[31]; however, other sites of accumulation should be considered and co-staining experiments would be required to confirm the exact location of accumulation. The intensity of fluorescence from the cells were diminished after a few h (~ 7–9 h) of the treatment and the cells became swollen, a common marker of apoptosis.

5.4. Conclusion

The library of NAMI-A analogues has been extended to incorporate three new Ru(III) complexes, 4-bromoimidazolium [*trans*-tetrachlorido(4-bromo-1H-imidazole)(S-dimethylsulfoxide)ruthen(III)ate] (**M1**), 2-iodoimidazolium [*trans*-tetrachlorido(2-iodo-1H-imidazole)(S-dimethylsulfoxide)ruthen(III)ate] (**M2**), and quinolium [*trans*-tetrachlorido(quinoline)(S-dimethylsulfoxide)ruthen(III)ate] (**M3**). The successful synthesis of ligands N-[3(methylthio)propyl]-1,8-napthalenedicarboximide **(L4)**, N-[3(methylsulfinyl)propyl]-1,8-napthalenedicarboximide **(L5)** and complex **P1** (Hydrogen *trans*-bis(N-[3(methylsulfinyl)propyl]-1,8-napthalenedicarboximide)tetrachlororuthenate (III)) is reported. The electronic and cytotoxic properties of the synthesised complexes were investigated. Modification of the NAMI-A coordination sphere caused a increase in the photophysical properties (electronic properties are in order of **M3** > **M2** ~ **M1** > NAMI-A) and cytotoxicities (IC_{50} values found to be increased in order of **M3** > **M2** > **M1** > NAMI-A). Fluorescent live cell imaging studies provided improved understanding of drug targets *in vitro*. Labelling of the NAMI-A skeleton by compounds with greater fluorescent properties might contribute insights of cellular pathways, the role of cellular organelles such as lysosomes, golgi bodies, mitochondria, cytoplasm and nucleus in transport and detoxification of these drugs[32]. In general, we have demonstrated a method of generating NAMI-A analogues with enhanced electronic and cytotoxic properties which can contribute to the development of structure-activity relationships for these types of drug candidates. More detailed investigation is required for expanded comprehension of the anti-metastatic activity of NAMI-A type compounds.

5.5. Experimental

5.5.1. Instrumentation

Samples of the newly synthesised compounds were submitted to Campbell Microanalytical service, Otago, New Zealand for *Microanalytical* (C, H, and N) analyses. A Micromass Platform II quadrupole mass spectrometer fitted with an electrospray source was used to obtain *low-resolution electrospray mass spectra.* The capillary voltage used was 3.5 V, and the cone voltage was 15 V. ^{1}H NMR spectra were collected on a Bruker DRX 400 spectrometer with the signal from the deuterated solvent used as a reference. The residual protons of the deuterated solvent were used as a standard to calculate the chemical shifts in parts per million (ppm). The coupling constants, *J*, are given in Hertz (Hz) and the peak multiplicities are abbreviated as follows: s (singlet), d (doublet), t (triplet), and m (multiplet). *UV−Vis spectra* were recorded on 0.1−2 mM solutions in quartz cuvettes using Cary 300 Bio UV-Vis spectrophotometer. Fluorescent spectra were obtained using Cary Eclipse fluorescence spectrophotometer. The absolute quantum yields and corrected fluorescence spectra were recorded on the same instrument, which was programmed to correct for inner filter effects for solutions with optical densities up to 1.0. For accurate measurements, solutions, whose absorbance was less than 0.1, were used at very low concentration. IR spectra were recorded with Agilent Cary 630 FT-IR spectrometer fitted with a diamond ATR detector and a Bruker Equinox 55 FT-IR spectrometer, fitted with Specac 'Golden Gate' diamond ATR and MCT detectors. Analytical HPLC was performed on an Agilent 1260 Infinity HPLC using Supelco Discovery C5 column. Eluent A, 0.1% (v/v) TFA in water; eluent B, 0.1% (v/v) TFA in CH_3CN; gradient elution, 5% to 75% of eluent B in 25 min, 1.5 mL/min. Cytotoxicity experiments were carried out using an xCELLigence cell adhesion impedance system supplied by Roche Applied Science and ACEA Biosciences. Fluorescence microscopy for live cell imaging was performed using a LEICA TCS SP5 Inverted Microscope fitted with an incubator. The data were then analysed using Metamorph software version 6.2.

5.5.2. Materials and methods

Ruthenium(III) chloride hydrate, 4-bromo-1H-imidazole, 2-iodo-1H-imidazole, quinoline, 1,8-napthalic anhydride, 3-(methylthio)propan-1-amine and the solvents were purchased from Sigma-Aldrich and used without further purification. Dry methanol was obtained by refluxing 2 L of methanol with 5 g of clean dry magnesium turnings and 0.5 g of iodine in a reflux condenser for 6 to 10 h. A vacuum line and Schlenk glassware were used for reactions carried out under nitrogen or dry atmosphere. High purity water was used for cell culture, obtained from a Millipore Synergy 185 UV Ultra pure water system. Dulbecco’s Minimum Essential Medium (DMEM), phosphate-buffered saline (PBS), L-glutamine (2mM), trypsin-EDTA solution (0.25%), pencillin-streptomycin, foetal bovine serum (2% v/v) and non-essential amino acids, used for culturing human lung carcinoma cells (A549), were obtained from Sigma-Aldrich.

5.5.3. Syntheses of complexes

NAMI-A was synthesised according to the previously reported procedure[12].

5.5.3.1. 4-bromoimidazolium [*trans*-tetrachlorido(4-bromo-1H-imidazole)(S-dimethylsulfoxide)ruthen(III)ate] (M1)

The precursor $[(DMSO)_2H][trans\text{-}RuCl_4(DMSO)_2]$ was synthesised according to a previously reported procedure[11] and was stirred for 30 min after suspending (0.12 g, 0.22 mmol) in diethyl ether (5 mL) at room temperature. The ligand, 4-bromo-1H-imidazole, was added (0.12 g, 0.86 mmol) and stirring was maintained overnight at room temperature. A bright yellow precipitate formed which was collected on a sintered filter funnel, washed with acetone (5 mL) followed by diethyl ether (3 mL) and dried under vacuum at room temperature (yield: 0.20 g, 90%).

Microanalysis: *Calc* for $C_8H_{13}Br_2N_4Cl_4ORuS$ (615.97); C 15.60, H 2.13, N 9.10, S 5.21, Br 25.94, Cl 23.02 and *Calc* for $C_8H_{13}Br_2N_4Cl_4ORuS.DMSO$ (694.10); C 17.30, H 2.76, N 8.07, S 9.24, Br 23.02, Cl 20.43 *Found*; C 16.65, H 2.64, N 7.20, S 9.19, Br 23.13, Cl 20.95. ESI-MS (DMF/ACN): –ve ion *m*/*z*, 467.6; +ve ion *m/z*, 147. IR (selected frequencies, cm^{-1}): ν 3111m (NH), 3057s (C-H$_{aromatic}$), 1153s (SO), 1076m, 1011m, 949m, 771m, 682s. UV-Vis (MeOH): λ_{max} (nm) ε_{max} (M^{-1} cm^{-1}): 290 (18,900), 400 (4,200). UV-Vis (MeOH): λ_{max} (nm) ε_{max} (M^{-1} cm^{-1}): 290 (1,700), 387 (4,300). HPLC system: Retention time = 3.13 min.

The original batch sent for elemental analysis was contaminated with excess DMSO as evidenced by the micro analytical results. A subsequent batch was prepared that was not contaminated as evidenced from HPLC (see Figure 17 in Appendix III), ESI-MS (see Figure 2 and 3 in Appendix III) and IR (see Figure 20 in Appendix III), but this was not submitted for elemental analysis.

5.5.3.2. 2-iodoimidazolium [*trans*-tetrachlorido(2-iodo-1H-imidazole)(S-dimethylsulfoxide)ruthen(III)ate] (M2)

[(DMSO)$_2$H][*trans*-RuCl$_4$(DMSO)$_2$][11] (0.12 g, 0.22 mmol) was suspended in acetone (10 mL) and the reaction mixture was stirred for 2 h at room temperature. The ligand, 2-iodo-1H-imidazole (0.18 g, 0.93 mmol) and diethyl ether (5 mL) were added and stirring was continued overnight at room temperature. The brown precipitate that formed was collected on a sintered filter funnel, washed with acetone (7 mL) followed by diethyl ether (10 mL) and dried under vacum at room temperature (yield: 0.15 g, 96%).

Microanalysis: *Calc* for $C_8H_{13}I_2N_4Cl_4ORuS$ (709.97); C 13.53, H 1.85, N 7.89, S 4.52, I 35.75, Cl 19.97 *Found*; C 14.40, H 1.90, N 7.74, S 4.49, I 35.38, Cl 19.60. ESI-MS (DMF/ACN): –ve ion *m/z*, 515.7; +ve ion *m/z*, 195.1. IR (selected frequencies, cm^{-1}): ν 3139m (NH), 3006vs (C-H$_{aromatic}$) 1154s (SO), 1066vs, 976vs, 945s, 754m, 662s. UV-Vis (MeOH): λ_{max} (nm) ε_{max} (M^{-1} cm^{-1}): 290 (18,900), 400 (4,200).UV-Vis (MeOH): λ_{max} (nm) ε_{max} (M^{-1} cm^{-1}): 290 (2,900), 398 (5,800). HPLC system: Retention time = 2.90 min.

5.5.3.3. Quinolium [*trans*-tetrachloro(quinoline)(S-dimethylsulfoxide)ruthen(III)ate] (M3)

$[(DMSO)_2H][trans\text{-}RuCl_4(DMSO)_2]$[11], (0.20 g, 0.36 mmol) was suspended in acetone (10 mL) at room temperature whilst stirring. After 2 h, the quinolone (0.20 mL, 1.69 mmol) was added and the mixture was stirred overnight. A dark yellow precipitate was obtained which was collected on a sintered filter funnel, washed with acetone (10 mL) followed by diethyl ether (10 mL) and dried under vacuum at room temperature (yield: 0.18 g, 86%).

Microanalysis: *Calc* for $C_{20}H_{21}N_2Cl_4ORuS$ (580.34); C 41.39, H 3.65, N 4.83, S 5.53, *Found*; C 41.24, H 3.92, N 4.54, S 5.83. ESI-MS (DMF/ACN): –ve ion *m/z*, 449.8; +ve ion *m/z*, 129.5. ATR-IR (selected frequencies, cm^{-1}): ν 3156m (NH), 3072vs (C-$H_{aromatic}$) 1149s (SO), 1097m, 1049s, 1020s, 785m, 690s. UV-Vis (MeOH): λ_{max} (nm) ε_{max} (M^{-1} cm^{-1}): 290 (18,900), 400 (4,200). UV-Vis (MeOH): λ_{max} (nm) ε_{max} (M^{-1} cm^{-1}): 300 (8,200), 312 (7,500), 398 (2,900). HPLC retention time = 1.50 min and 6.50 min.

5.5.3.4. Hydrogen *trans*-tetrachloridobis(N-[3(methylsulfinyl)propyl]-1,8-napthalenedicarboximide)ruthen(III)ate (P1)

5.5.3.4.1. N-[3(methylthio)propyl]-1,8-napthalenedicarboximide (L4)

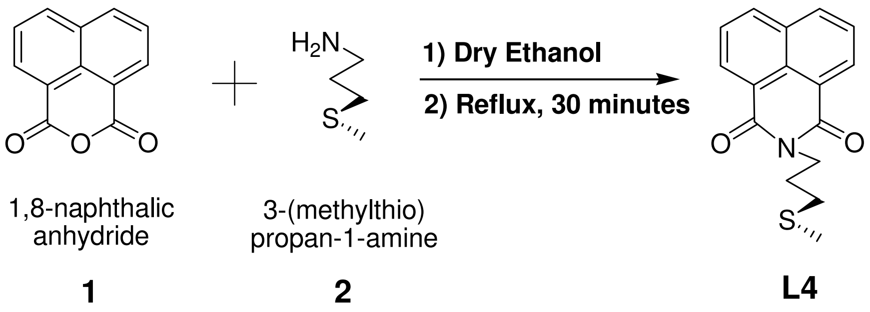

Scheme 7: Synthesis of N-[3(methylthio)propyl]-1,8-napthalenedicarboximide (**L4**)

L4 was synthesised by a modification of a procedure reported in literature[33]. **2** (0.7 mL, 6.25 mmol) was added to a suspension of **1** (0.5 g, 2.5 mmol) in 10 mL dry ethanol whilst stirring under nitrogen. The reaction mixture was refluxed for 30 min under dry experimental conditions (T = 85^0C) and the solvent was removed under reduced pressure. The product **L4**, was recrystallised from ethanol. Yellow crystals were collected by filtration, washed with diethyl ether and dried under vacuum (yield: 0.67 g, 94%).

ESI-MS (MeOH/ACN, +ve ion): *m/z*; 286 [M+H], 308 [M+Na]. ^{1}H NMR (400 MHz, $CDCl_3$, *see Appendix III - Figure 16*): δ 8.59 – 8.61 (m, 1H), 8.2 (d, *J* = 1.04 Hz, 1H), 7.75 – 7.77 (t, *J* = 7.36 Hz, 1H), 4.27 – 4.31 (t, *J* = 8.0 Hz, 2H), 2.61 – 2.64 (t, *J* = 7.32 Hz, 2H), 2.13 (s, 3H), 2.03 – 2.07 (m, 2H). UV-Vis (MeOH): λ_{max} (nm) ε_{max} (M^{-1} cm^{-1}): 333 (55,500), 345 (51,100).

5.5.3.4.2. N-[3(methylsulfinyl)propyl]-1,8-napthalenedicarboximide (L5)

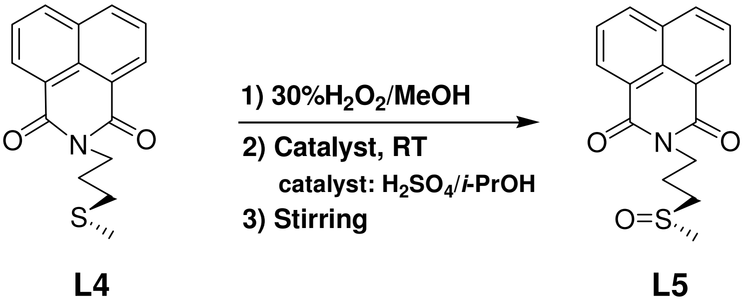

Scheme 8: Synthesis of N-[3(methylsulfinyl)propyl]-1,8-napthalenedicarboximide (**L5**)

The oxidation of sulfide (**L4**) to sulfoxide (**L5**) was carried out by a similar procedure to that reported in the literature[34]. H_2O_2 (30%, 50 µL, 0.50 mmol) was added to a round-bottom flask containing a stirred solution of sulfide **L4** (0.10 g, 0.36 mmol), MeOH (3 mL) and the catalyst (5 µL each of conc.H_2SO_4 and *i*-PrOH (isopropyl alcohol) at room temperature. After 2 h, TLC analysis (silica gel, 10% MeOH in CH_2Cl_2) showed complete oxidation. Water (5 mL) was added to the reaction mixture and it was extracted with $CHCl_3$ (4 x 20 mL). The $CHCl_3$ extracts were dried (over $MgSO_4$) and the volume reduced to give a white precipitate. The precipitate was washed with diethyl ether and dried under vacuum (yield: 0.10 g, 92%).

ESI-MS (MeOH/ACN, +ve ion): *m/z*; 302 [M+H], 324 [M+Na]. ^{1}H NMR (400 MHz, $CDCl_3$, *see Appendix III - Figure 16*): δ 8.60 – 8.62 (m, 1H), 8.23-8.25 (m, 1H), 7.76 – 7.80 (m, 1H), 4.35 – 4.38 (t, J = 6.80 Hz, 2H), 3.15 – 3.19 (m, 2H), 2.92 (s, 3H), 2.30 - 2.37 (m, 2H).

5.5.3.3.4.3. Hydrogen *trans*-tetrachloridobis(N-[3(methylsulfinyl)propyl]-1,8-napthalenedicarboximide)ruthen(III)ate (P1)

A Ru(III) solution was prepared by dissolving 0.12 g (0.60 mmol) of $RuCl_3.3H_2O$ in a mixture of 3 mL of 10N HCl (32%) and 5 mL ethanol as reported previously[35]. A solution of **L5** (0.24 g, 0.80 mmol) in 10N HCl (32%, 4 mL) was stirred under reflux (T = 100^{0}C) for 30 min. The Ru(III) solution was added (0.30 mL, 0.60 mmol) to the reaction mixture and stirred at T < 80^{0}C (not reflux) for 1 to 2 hrs. A bright orange yellow precipitate formed which was collected by filtration, washed with diethyl ether and dried under vacuum (yield: 0.52 g, 75%).

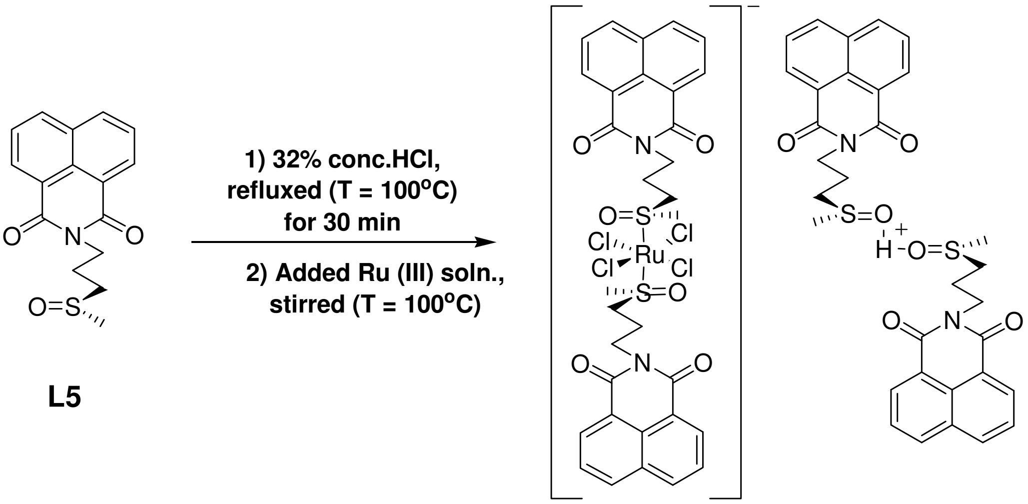

L5

P1

Scheme 9: Synthesis of hydrogen *trans*-tetrachloridobis(N-[3(methylsulfinyl)propyl]-1,8-napthalenedicarboximide) ruthen(III)ate (**P1**).

ESI-MS (DMF/ACN) +ve ion: *m/z*; 324, 625 (M+Na); -ve ion: *m/z*; 243, 813, 845. ^{1}H NMR (400 MHz, $CDCl_3$): δ 8.60 – 8.62 (m, 1H), 8.23-8.26 (m, 1H), 7.75 – 7.80 (m, 1H), 4.35 – 4.38 (t, J = 6.80 Hz, 2H), 3.45 – 3.75 (m, 2H), 2.92

(s, 3H), 2.82 – 2.87 (m, 2H). UV-Vis (MeOH): λ_{max} (nm) ε_{max} (M^{-1} cm^{-1}): 333 (15,200), 345 (14,100), 390 (700).

5.5.4. Fluorescent quantum yield (ϕ_f):

Fluorescent quantum yields were determined as according to the equation 1 given below.

$$\frac{\phi_x}{\phi_{ref}} = \frac{A_x}{A_{ref}} \times \frac{n_x^2}{n_{ref}^2} \times \frac{1-10^{-abs_{ref}}}{1-10^{-abs_x}} \quad \text{.............................Equation } 1^{[36]}$$

Where, ϕ_x and ϕ_{ref} are the fluorescent quantum yields of the unknown and reference standard respectively. A_x and A_{ref} may be related to the integrated emission intensity calculated from the area under the emission spectrum of the sample and reference, respectively, and abs_{ref} and abs_x refer to the absorbance of the reference and unknown from the UV-Vis spectra respectively[37]. The sample solutions of the unknown and the reference were prepared at a concentration for which the absorption is less than 0.1 to avoid, or reduce, any inner filter effects. The solvents used in both absorption and emission measurements were de-aerated (30 minutes of nitrogen bubbling) in a quartz cell (1 cm optical path length) to protect the samples from any fluorescent quenching due to the presence of oxygen.

5.5.5. *In vitro* cytotoxicity studies

Human lung cancer cells (A549) were grown in Dulbecco's modified Eagle's medium (DMEM) as monolayers and were supplemented with foetal bovine serum (2% v/v), antibiotic-antimicotic mixture (100 mg mL^{-1} pencillin and 100 U mL^{-1} streptomycin), L-glutamine (2 mM), and non-essential amino acids (100 U mL^{-1}) at 310 K in a 5% CO_2-humidified incubator and were subcultured in every 4-6 days.

The prepared compounds **M1**, **M2**, and **M3** were tested for *in vitro* cytotoxicity by an electronic cell sensor technology, ACEA (Biosciences, Inc) RT-CES (Real Time – Cell Electronic Sensing) system (xCELLigence; Roche Diagnostics, Germany). The system measures electrical impedance related to the cell attachment to the surface of the sensor plate or E-plate[38]. The treatment stock solutions were made immediately preceding the analysis to limit hydrolysis. A proliferation or growth curve for A549 cells was created by plating cells at the unit densities of 3000 to 60,000 cells for every well of a xCELLigence E-plate or sensor plate[38]. Cell index (CI) impedance measurements were performed in line with the instructions of the supplier. The optimum seeding concentration for the proliferation experiments was determined to be 10,000 cells per well (*see Appendix III - Figure 23*). The impedance was measured every 15 min after seeding a 100 µL of the cell suspensions into the E-plate 96 (10,000 cells per well). After 18 h, the cells were treated with 20 µL of test solutions of complexes **M1**, **M2**, and **M3** in 5% DMF in PBS, corresponding to a final in-media concentration range 30 µM to 3000 µM. Controls were exposed to 5% DMF only in PBS (final DMF concentration was limited to 0.5%). The adhesion of the cells was checked by impedance measurements each 15 min for a period up to 72 h by the xCELLigence system.

The results were analysed using RTCA (Real Time Cell Analyser) -integrated software of the xCELLigence system. The RTCA programming performs a curve fitting of the chosen experimental data points with a sigmoidal dose-response equation and calculates IC_{50} values from the 50% reduction of CI (cell index) value relative to solvent control CI value (100%)[38]. Growth inhibition was expressed as treated/control x 100 (%T/C), a mean of three independent experiments were taken into consideration. The half maximum inhibitory concentrations (IC_{50}) were obtained from the dose-response curves based on curve-fitting plots of cell viability against the log of compound concentration. Data are represented as mean [µM] ± S.E.M. (n = 3).

5.5.6. Fluorescence microscopy and live cell imaging

The A549 cells were cultured directly on a sterilised 2 mm thick fluoro dish at a concentration of 1.0×10^4 cells/dish (volume = 2 mL) in complete DMEM medium for 24 h at 310 K in a 5% CO_2 – humidified incubator prior to the treatment. The media was replaced by fresh DMEM after 24 h and cells were treated with 200 µL of **M3** (50 µM) for 3 h. In order to prevent hydrolysis, the solutions were prepared immediately prior to treatment. Control fluorescence dishes were likewise prepared by treatment with PBS alone under otherwise identical conditions. After treatment, the media was reinstated with fresh DMEM without phenol red (colourless medium) and the live cell images were taken employing a LEICA TCS SP5 inverted microscope equipped with an incubator which is specifically designed for cell culture experiments. The excitation wavelength was 405 nm and emission profiles were collected from 439 nm to 477 nm.

5.6. References:

[1] l. Bratsos, A. Bergamo, G. Sava, t. Gianferrara, E. Zangrando, E. Alessio. *J. Inorg. Biochem.* **2008**, *102*, 606.

[2] I. Kostova. *Curr. Med. Chem.* **2006**, *13*, 1085.

[3] l. Bratsos, S. Jedner, T. Gianferrara, E. Alessio. *Chimia*. **2007**, *61*, 692; G. Sava, A. Bergamo, P. J. Dyson. *Dalton Trans.* **2011**, *40*, 9069.

[4] M. Groessl, E. Reisner, C. G. Hartinger, R. Eichinger, O. Semenova, A. R. Timerbaev, M. A. Jakupec, V. B. Arion, B. K. Keppler. *J. Med. Chem.* **2007**, *50*, 2185.

[5] S. P. Fricker. *Dalton Trans.* **2007**, 4903.

[6] A. Bergamo, G. Sava. *Dalton Trans.* **2007**, 1267.

[7] A. Levina, J. B. Aitken, Y. Y. Gwee, Z. J. Lim, M. Liu, A. M. Singharay, P. F. Wong, P. A. Lay. *Chem. Eur. J.* **2013**, *19*, 3609.

[8] R. A. Alderden, M. D. Hall, T. W. Hambley. *J. Chem. Educ.* **2006**, *83*, 728; I. Kostova. *Recent Pat. Anticancer Drug Discov.* **2006**, *1*, 1.

[9] J. J. Fiol, A. García-Raso, F. M. Albertí, A. Tasada, M. Barceló-Oliver, A. Terrón, M. J. Prieto, V. Moreno, E. Molins. *Polyhedron*. **2008**, *27*, 2851; A. A. Nazarov, M. Baquie, P. Nowak-Sliwinska, O. Zava, J. R. van Beijnum, M. Groessl, D. M. Chisholm, Z. Ahmadi, J. S. McIndoe, A. W. Griffioen, H. van den Bergh, P. J. Dyson. *Sci. Rep.* **2013**, *3*, 1485; R. Fisher, L. Pusztai, C. Swanton. *Br. J. Cancer*. **2013**, *108*, 479; Z. Trávníček, M. Maľarová, R. Novotná, J. Vančo, K. Štěpánková, P. Suchý. *J. Inorg. Biochem.* **2011**, *105*, 937.

[10] J. B. Aitken, S. Antony, C. M. Weekley, B. Lai, L. Spiccia, H. H. Harris. *Metallomics*. **2012**, *4*, 1051.

[11] E. Alessio, G. Balducci, M. Calligaris, G. Costa, W. M. Attia, G. Mestroni. *Inorg. Chem.* **1991**, *30*, 609.

[12] G. Mestroni, E. Alessio, G. Sava. **1998**, *WO 98/00431*.

[13] P. J. Dyson, G. Sava. *Dalton Trans.* **2006**, 1929; L. Ronconi, P. J. Sadler. *Coord. Chem. Rev.* **2007**, *251*, 1633; Y. K. Yan, M. Melchart, A. Habtemariam, P. J. Sadler. *Chem. Commun.* **2005**, 4764.

[14] M. H. Seelig, M. R. Berger, B. K. Keppler. *J. Cancer Res. Clin. Oncol.* **1992**, *118*, 195.

[15] A. Levina, A. Mitra, P. A. Lay. *Metallomics*. **2009**, *1*, 458.

[16] M. Pongratz, P. Schluga, M. A. Jakupec, V. B. Arion, C. G. Hartinger, G. Allmaier, B. K. Keppler. *J. Anal. At. Spectrom.* **2004**, *19*, 46; E. Reisner, V. B. Arion, B. K. Keppler, A. J. L. Pombeiro. *Inorg. Chim. Acta*. **2008**, *361*, 1569.

[17] E. Reisner, V. B. Arion, M. Fatima, C. G. da Silva, R. Lichtenecker, A. Eichinger, B. K. Keppler, V. Y. Kukushkin, A. J. L. Pombeiro. *Inorg. Chem.* **2004**, *43*, 7083.

[18] I. Khalaila, A. Bergamo, F. Bussy, G. Sava, P. J. Dyson. *Int. J. Oncol.* **2006**, *29*, 261.

[19] D. Pluim, R. C. van Waardenburg, J. H. Beijnen, J. H. Schellens. *Cancer Chemother. Pharmacol.* **2004**, *54*, 71.

[20] A. A. Hummer, P. Heffeter, W. Berger, M. Filipits, D. Batchelor, G. E. Buchel, M. A. Jakupec, B. K. Keppler, A. Rompel. *J. Med. Chem.* **2013**, *56*, 1182.

[21] S. Antony, J. B. Aitken, S. Vogt, B. Lai, T. Brown, L. Spiccia, H. H. Harris. *J. Biol. Inorg. Chem.* **2013**, *18*, 845.
[22] F. Zobi, B. B. Mood, P. A. Wood, F. P. A. Fabbiani, S. Parsons, P. J. Sadler. *Eur. J. Inorg. Chem.* **2007**, *18*, 2783; S. Page. *Educ. Chem.* **2012**, *49*, 26; A. Bergamo, G. Sava. *Dalton Trans.* **2011**, *40*, 7817.
[23] M. Delferro, L. Marchio, M. Tegoni, S. Tardito, R. Franchi-Gazzola, M. Lanfranchi. *Dalton Trans.* **2009**, 3766.
[24] E. Alessio, G. Mestroni, A. Bergamo, G. Sava. in *Metal Ions in Biological Systems; Metal Complexes in Tumor Diagnosis and as Anticancer Agents* (Eds. Sigel A, Sigel H) **2004**, pp. 323-351 (Marcel Dekker: New York, NY, USA).
[25] G. Sava, E. Alessio, A. Bergamo, G. Mestroni. in *Topics in Biological Inorganic Chemistry, Volume 1, "Metallo-pharmaceuticals"* (Eds. Clarke MJ, Sadler PJ) **1999**, pp. 143-169 (Springler: Berlin); E. Alessio, G. Balducci, G. Lutman, G. Mestroni, M. Calligaris, W. M. Attia. *Inorg. Chim. Acta*. **1993**, *203*, 205; G. Sava, A. Bergamo, S. Zorzet, B. Gava, C. Casarsa, M. Cocchietto, A. Furlani, V. Scarcia, B. Serli, E. Iengo, E. Alessio, G. Mestroni. *Eur. J. Cancer*. **2002**, *38*, 427; E. Iengo, G. Mestroni, S. Geremia, M. Calligaris, E. Alessio. *J. Chem. Soc. Dalton Trans.* **1999**, 3361.
[26] K. Kalyanasundaram, S. M. Zakeeruddin, M. K. Nazeeruddin. *Coord. Chem. Rev.* **1994**, *132*, 259; F. Kratz, M. Hartmann, B. K. Keppler, L. Messori. *J. Biol. Chem.* **1994**, *269*, 2581; L. Messori, P. Orioli, D. Vullo, E. Alessio, E. Iengo. *Eur. J. Biochem.* **2000**, *267*, 1206; E. M. Nagy, C. Nardon, L. Giovagnini, L. Marchio, A. Trevisan, D. Fregona. *Dalton Trans.* **2011**, *40*, 11885.
[27] I. Grabchev, C. Petkov, V. Bojinov. *Dyes Pigments*. **2001**, *48*, 239; S. Kumar, J. Koh. *Carbohydr. Polym.* **2013**, *94*, 221.
[28] N. A. Masoud. *J. Chem. Soc. Pak.* **2002**, *24*, 171.
[29] W. R. Dawson, M. W. Windsor. *J. Phys. Chem.* **1968**, *72*, 3251.
[30] A. Egger, B. C. Losantos, I. N. Stephaneko, B. K. Keppler. *Chem. Biodivers*. **2008**, *5*, 1588.
[31] G. V. Kalayda, G. Zhang, T. Abraham, H. J. Tanke, J. Reedijk. *J. Med. Chem.* **2005**, *48*, 5191.
[32] G. V. Kalayada, G. Zhang, T. Abraham, H. J. Tanke, J. Reedijk. *J. Med. Chem.* **2005**, *48*, 5191.
[33] K. A. Stevenson, S. F. Yen, N. C. Yang, D. W. Boykin, W. D. Wilson. *J. Med. Chem.* **1984**, *27*, 1677.
[34] A. D. Christopher, A. Shantu, D. Dhimant. *J. Label. Comp. Radiopharma.* **2003**, *46*, 851.
[35] K. Lipponer, E. Vogel, B. K. Keppler. *Met. Based Drugs*. **1996**, *3*, 243.
[36] S. Antony, J. C. Morris, T. Bell, T. Brown, L. Spiccia, H. H. Harris. *Aust. J. Chem.* **2014**, *Accepted.*
[37] M. Zhou, G. P. Robertson, J. Roovers. *Inorg. Chem.* **2005**, *44*, 8317; N. Nickita, G. Gasser, A. M. Bond, L. Spiccia. *Eur. J. Inorg. Chem.* **2009**, *2009*, 2179; N. Nickita, G. Gasser, P. Pearson, M. J. Belousoff, L. Y. Goh, A. M. Bond, G. B. Deacon, L. Spiccia. *Inorg. Chem.* **2008**, *48*, 68.
[38] E. Urcan, U. Haertel, M. Styllou, R. Hickel, H. Scherthan, F. Reichl. *Dent. Mater.* **2010**, *26*, 51.

Chapter 6

Conclusions and Future directions

"Not all cellular poisons are cancer drugs, but all cancer drugs are cellular poisons"

B. Rosenberg, the 'father' of cisplatin[1].

---

1. Rosenberg, B., *Platinum Met. Rev.* 1971, 15, 42-51

Conclusions and future directions

6.1. Conclusions

Research conducted on ruthenium compounds to date demonstrated that these compounds show significant anti-cancer activity in cancer cells, animal models and even in cancer patients [1-7]. More investigations in this field may provide less toxic and more effective ruthenium drugs that could be a substitute for platinum drugs [4, 8, 9]. So far, two ruthenium compounds (NAMI-A and KP1019) were successful in phase I clinical trials[7, 10] and evaluation of anti-neoplastic properties of similar ruthenium analogues is continuing without proper knowledge on their mode of action[5, 6, 11-13].

6.1.1. Summary of the submitted work

The primary objective of the research work described in this thesis has been to develop anti-cancer NAMI-A and KP1019 analogues and to explore their anti-metastatic activity. To focus on understanding the anti-metastatic activity and to investigate the biological activity, a series of NAMI-A and KP1019 analogues were synthesised and structurally characterised. The utility of X-ray fluorescence micro-probe (XRF) imaging of treated single cultured cells, as a method to determine intracellular targets as a function of treatment time and other experimental conditions had already been demonstrated[14-17]. Accordingly, the uptake and distribution of synthesised ruthenium complexes in human lung cancer cells (A549 cell line) was investigated using fluorescence spectroscopy and microscopy. To the best of our knowledge, we describe the first use of XRF imaging to reveal cellular distribution of ruthenium in cells treated with KP1019 and NAMI-A[13].

Chapter 2 illustrated the synchrotron based X-ray fluorescence imaging (μ-XRF) of single human cancer cells treated with KP1019 and the results demonstrated that ruthenium is localised in both cytosol and in the nuclear region[13]. The study also showed that KP1019 was internalized into treated cells and that the modulated iron distribution resembled the ruthenium distribution, without affecting total cellular iron content. Our investigation proved that ruthenium could not be visualised in cells treated with NAMI-A as it was not internalised. The results hence supported the proposition that biological activity of NAMI-A is exerted through a membrane-binding mechanism and that the anti-metastatic effect of NAMI-A is exerted extracellularly[16].

X-ray fluorescence imaging of single cultured A549 cells treated with iodine substituted KP1019 or NAMI-A analogues[18] was described in **Chapter 3**. The results showed that the distribution of ruthenium and iodine was identical and hence that the Ru-N bonds in the anionic complexes remained intact after the incubation in culture media and subsequent cellular uptake and processing. This 'double-tag' approach also revealed that the distribution of ruthenium inside the cells treated with the NAMI analogue was apparently altered from the parent complex, but whether this resulted from the substitution of imidazole for indazole, or from the incorporation of iodine, could not be determined. The result is important because it explains, in part, the variable biology of related analogues and because it provides a permanent "handle" on ruthenium that could be utilised in future to add functionality to this class of drugs.

Fluorescent microscopy investigations have been carried out by labelling the parent complex with a fluorescent reporter[19] (**Chapter 4** and **5)** in order to investigate the cellular targets and uptake mechanism of NAMI-A and its analogues inside living cells. We have developed a synthetic procedure to take advantage of the fact that the N-heterocycle stays attached to ruthenium and thus to create a permanent moiety on ruthenium which could be modified by adding different functional groups to form a new class of drugs. The strategy might contribute to the investigation of mechanism of action of these drugs and could furnish an improved pathway to attain better pharmacological results.

In summary, the research outcomes underlined in this thesis may provide new understanding for the anti-cancer and anti-metastatic activity of NAMI-A and

KP1019 and their analogues. The newly synthesized complexes can readily be modified by ligands with improved fluorophores or tissue/cellular targeting functionalities.

6.1.2. General evaluation

As discussed in detail in **Chapter 1** (**2.2.1 – 2.2.3**), a list of important classes of anti-cancer ruthenium compounds are given below;

(a) Ru(III)-dmso compounds[20],

(b) Ru(III) complexes of the type [LH]trans-[$RuCl_4(L)_2$][21], and

(c) Organometallic (arene)Ru(II) compounds of the general formula - [(η^6-arene)Ru(en)Cl][PF_6][10, 22, 23] which can be divided in to two general types; arene complexes with chelating or PTA ligands[10] and ruthenium polypyridyl complexes[24].

The first two groups include the anionic Ru(III) complexes and the third class contains cationic Ru(II)-organometallic compounds. The organometallic arene compounds are more cytotoxic *in vitro* compared with NAMI-A and the other analogues[10, 13, 25]. The *in vivo* anti-cancer activity of the first two categories are quite different: some are active against primary tumours, whereas others are active against metastases only[23, 25]; some have been demonstrated to interact with DNA[22, 26], whereas others do not (e.g., NAMI-A)[13, 27].

Hence, the fundamental challenge for bio-inorganic chemists involved in this field is to accomplish protocols toward the synthesis of new analogues and manage their pharmacological screening. Research with more selectivity studies (i.e., research on the selectivity of the cancer drug to inhibit the growth of tumour cells while doing minimal damage to the healthy cells)[26-29] of healthy versus cancerous cells similar to platinum therapeutics introduced by Dyson *et al.* (2007)[30] could be advantageous in selecting compounds with most promising activity. Current investigations have focussed more on the hindrance of the processes involved in metastasis, such as adhesion, migration, invasion, and degradation of the extracellular matrix[5, 31]. Since a number of ruthenium compounds exhibit the characteristics expected of an anti-metastatic drug, they appear to hold the greatest promise in preclinical investigations[6]. Additional research focused on increasing the efficiency of these compounds, through some type of targeting method, could increase the likelihood that more analogues will enter clinical trials[6, 27] and ultimately the clinic itself.

6.2. Future Directions

Research and development involved in the investigation of the anti-metastatic activity of ruthenium based therapeutics delivers two main approaches for drug discovery. The first approach is based on thorough examination of the characteristics of selected complexes and their pharmacological targets, to gain insight about their mechanisms of action[6, 32-34]. This includes structural characterisation by examining the chemical and pharmacological properties of the complexes and the investigation of biological distribution through uptake studies[33]. Hence, an interdisciplinary approach is essential for the success of investigations based on this approach[7, 33] and the knowledge about the mechanisms of action can then be used to guide the rational design and synthesis of new and improved drugs.

The second approach can be considered as a trial and error approach in which analogous compounds, whose anti-cancer activity is similar to that of a complex of known activity, have been synthesized and screened for their pharmacological activity[11, 18, 34-37]. These new compounds are then tested for anti-cancer activity, both *in vitro* and *in vivo*. The serendipitous discovery of NAMI-A followed by the synthesis of its analogues, is a well-known example of this approach [21, 38]. It has been proposed that the outcomes of this approach may lead to three promising scenarios for ruthenium-based drug design[29]: (i) development of new drugs by structure-activity relationships, (ii) development of drugs with high affinity for cancer targets, and (iii) the generation of new ruthenium-ODM (organic directing molecule) complexes.

6.2.1. Structure-activity relationships (SARs)

Numerous studies reported in the literature have employed SARs to investigate the effect of change in anti-cancer activity with alteration in the functional groups present in the coordination sphere of NAMI-A. A huge number of compounds have been synthesised and tested to date, to establish systematic structure-activity relationships with NAMI-A[39, 40] by replacing each component of the NAMI-A frame (i.e. replacing sulfoxide and imidazole by other suitable ligands (as illustrated in **Chapter 4** and **5**). Hereafter, more analogues of NAMI-A and KP1019 with promising anti-cancer properties could be synthesised by these tactics and their cellular uptake and other pharmacological properties could be investigated by the different methodologies utilised in this thesis (**Chapter 1**; **8.1 – 8.4**).

6.2.2. High affinity drugs for cancer targets

Chen, Z. G. (2010) has demonstrated that the nanoparticles can be utilised for the discharge of small molecular species in anti-cancer therapy[41]. Suss-Fink *et al.* (2010)[42] have demonstrated the application of ruthenium nanoparticles as anti-cancer agents. They have synthesized a series of arene ruthenium complexes containing a long-chain N-ligands derived from isonicotinic acid, and a series of ruthenium-based nanoparticles coated with the same long-chain ligands. The ruthenium nanoparticles were found to be less cytotoxic than the complexes, and potentially can target tumour tissue selectively via enhanced permeability and retention effect (EPR effect is the tendency of the drugs or nanoparticles to accumulate specifically inside the tumour tissue than in normal tissue)[42].

More *in vivo* and *in vitro* studies are needed to establish whether such systems really can accumulate selectively in tumours. The methodologies illustrated in this thesis, such as synchrotron X-ray fluorescence imaging (XRF; **Chapter 1 - 8.1**, **Chapter 2** and **Chapter 3**), can be employed to determine intracellular elemental distribution and tumour-specific accumulation in nanoparticle treated cells. Fluorescent imaging of ruthenium-based nanoparticles linked with fluorescent reporters could provide more insight on the nature of specific binding target of ruthenium inside the cell (**Chapter 4**, **Chapter 5 and Appendix II**).

6.2.3. Ruthenium-ODM complexes

A ODM complex can be an organic directing molecule in which metal centres are directed to specific enzyme or protein targets by connection of such complexes to an organic ligand (e.g., a drug molecule)[29, 43].

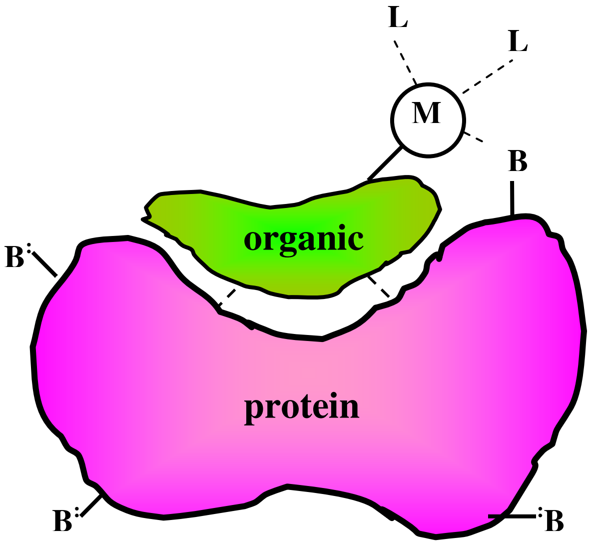

Figure 1: An organic molecule directs a metal (M) to a Lewis Basic Amino Acid (B) near the active site of a target protein[29, 43]. (Adapted from Page, 2012)[29].

It has been proposed that a ruthenium-ODM complex could be used as a powerful tool for effective drug delivery[29, 43]. The organic molecule present in the ruthenium-ODM complex directs the metal towards the tumour where it is attached to the active site of a protein or an enzyme[43]. Consequently, the metal ion (M) is linked to a nearby Lewis amino acid residue (B) of the same protein as shown in the figure 1[29, 43]. The metal then binds to the specific cellular target and enhances the overall cytotoxic effect. The advantage of this concept (compared to the other concepts; **6.2.1 – 6.2.2.**) is that there is a specific cellular target against which examinations such as; DNA binding studies, protein crystallography and enzyme inhibition studies could be performed.

The backbone of the ODM complex can be modified by methodologies mentioned in this thesis (**Chapter 1** to **Chapter 5**), to add more insights to the specific biological target. For instance, the structure of the ruthenium-ODM complex can be modified by replacing ligands attached to the metal atom with more fluorescent ligands. The toxicity and cellular uptake of the drug can be determined by cell culture studies. μ-XRF studies may provide more perception on bio-distribution of the complex and on the specific biological target of the complex inside the cell. These findings could ultimately lead to the introduction of new anti-cancer agents with wide spectrum of anti-metastatic activity.

6.3. Concluding summary

The strategies and methodologies described in this thesis may contribute towards the foundation for the synthesis of further ruthenium anti-cancer complexes with a wider therapeutic window. Experimental approaches, such as synchrotron based XRF and fluorescent microscopy (including live cell imaging studies), may be anticipated to be advantageous in providing better information about the cellular distribution and bio-transformation of the drug inside the tumour and could provide more insight on the specific cellular target/s. The research conducted to date in this field demonstrates various methods for the better understanding of the anti-metastatic activity of the ruthenium-based drugs but the actual mechanism for the metastatic action is still unknown[29]. Advancements in the exploration of ruthenium-based anti-cancer agents may direct towards a future where scientific experts begin to recognise the potency of less investigated areas of the periodic table to produce drugs having wide spectrum of anti-cancer activity[29].

6.4. References

1. Claire, S.; Dyson, P. J., *Platinum Met. Rev.* **2001,** 45, 62-69.
2. Clarke, M. J., *Coord. Chem. Rev.* **2003,** 236, 209-233.
3. Alessio, E.; Mestroni, G.; Bergamo, A.; Sava, G., *Curr. Top. Med. Chem.* **2004,** 4, 1525-1535.
4. Bergamo, A.; Sava, G., *Dalton Trans.* **2011,** 40, 7817-7823.
5. Nazarov, A. A.; Baquie, M.; Nowak-Sliwinska, P.; Zava, O.; van Beijnum, J. R.; Groessl, M.; Chisholm, D. M.; Ahmadi, Z.; McIndoe, J. S.; Griffioen, A. W.; van den Bergh, H.; Dyson, P. J., *Sci. Rep.* **2013,** 3, 1485.
6. Fisher, R.; Pusztai, L.; Swanton, C., *Br. J. Cancer* **2013,** 108, 479-485.
7. Bratsos, l.; Jedner, S.; Gianferrara, T.; Alessio, E., *Chimia* **2007,** 61, 692-697.
8. Kostova, I., *Curr. Med. Chem.* **2006,** 13, 1085-1107.
9. Bergamo, A.; Gaiddon, C.; Schellens, J. H. M.; Beijnen, J. H.; Sava, G., *J. Inorg. Biochem.* **2012,** 106, 90-99.
10. Dyson, P. J.; Sava, G., *Dalton Trans.* **2006**, 1929-1933.
11. Fiol, J. J.; García-Raso, A.; Albertí, F. M.; Tasada, A.; Barceló-Oliver, M.; Terrón, A.; Prieto, M. J.; Moreno, V.; Molins, E., *Polyhedron* **2008,** 27, 2851-2858.
12. Trávníček, Z.; Maľarová, M.; Novotná, R.; Vančo, J.; Štěpánková, K.; Suchý, P., *J. Inorg. Biochem.* **2011,** 105, 937-948.
13. Aitken, J. B.; Antony, S.; Weekley, C. M.; Lai, B.; Spiccia, L.; Harris, H. H., *Metallomics* **2012,** 4, 1051-1056.
14. Harris, H. H.; Levina, A.; Dillon, C. T.; Mulyani, I.; Lai, B.; Cai, Z.; Lay, P. A., *J. Biol. Inorg. Chem.* **2005,** 10, 105-118.
15. Weekley, C. M.; Aitken, J. B.; Vogt, S.; Finney, L. A.; Paterson, D. J.; de Jonge, M. D.; Howard, D. L.; Musgrave, I. F.; Harris, H. H., *Biochem.* **2011,** 50, 1641-1650.
16. Levina, A.; Aitken, J. B.; Gwee, Y. Y.; Lim, Z. J.; Liu, M.; Singharay, A. M.; Wong, P. F.; Lay, P. A., *Chem. Eur. J.* **2013,** 19, 3609-3619.
17. Ortega, R.; Deves, G.; Carmona, A., *J. R. Soc. Interface* **2009,** 6, S649-S658.
18. Antony, S.; Aitken, J. B.; Vogt, S.; Lai, B.; Brown, T.; Spiccia, L.; Harris, H. H., *J. Biol. Inorg. Chem.* **2013,** 18, 845-853.
19. Antony, S.; Morris, J. C.; Bell, T.; Brown, T.; Spiccia, L.; Harris, H. H., *Aust. J. Chem.* **2014,** Accepted.
20. Alessio, E.; Balducci, G.; Calligaris, M.; Costa, G.; Attia, W. M.; Mestroni, G., *Inorg. Chem.* **1991,** 30, 609-618.
21. Mestroni, G.; Alessio, E.; Sava, G., **1998,** WO 98/00431.
22. Ronconi, L.; Sadler, P. J., *Coord. Chem. Rev.* **2007,** 251, 1633-1648.
23. Yan, Y. K.; Melchart, M.; Habtemariam, A.; Sadler, P. J., *Chem. Commun.* **2005**, 4764-4776.
24. Wheate, N. J.; Brodie, C. R.; Collins, J. G.; Kemp, S.; Aldrich-Wright, J. R., *Mini-Rev. Med. Chem.* **2007,** 7, 627-648.
25. Mestroni, G.; Alessio, E.; Sava, G.; Pacor, S.; Coluccia, M.; Boccarelli, A., *Met. Based Drugs* **1994,** 1, 41-63.
26. Levina, A.; Mitra, A.; Lay, P. A., *Metallomics* **2009,** 1, 458-470.

27. Sava, G.; Bergamo, A.; Dyson, P. J., *Dalton Trans.* **2011,** 40, 9069-9075.
28. Nazarov, A. A.; Hartinger, C. G.; Dyson, P. J., *J. Organomet. Chem.* **2014,** 751, 251-260.
29. Page, S., *Educ. Chem.* **2012,** 49, 26-29.
30. Scolaro, C.; Chaplin, A. B.; Hartinger, C. G.; Bergamo, A.; Cocchietto, M.; Keppler, B. K.; Sava, G.; Dyson, P. J., *Dalton Trans.* **2007,** 43, 5065-5072.
31. Gligorojevic, N.; Arandelovic, S.; Filipovic, L.; Jakovljevic, K.; Jankovic, R.; Grguric-Sipka, S.; Ivanovic, I.; Radulovic, S.; Tesic, Z. L., *J. Inorg. Biochem.* **2012,** 108, 53-61.
32. Hait, W. N.; Hambley, T. W., *Cancer Res.* **2009,** 69, 1263-1267.
33. Bergamo, A.; Sava, G., *Dalton Trans.* **2007**, 1267-1272.
34. Vock, C. A.; Ang, W. H.; Scolaro, C.; Phillips, A. D.; Lagopoulos, L.; Juillerat-Jeanneret, L.; Sava, G.; Scopelliti, R.; Dyson, P. J., *J. Med. Chem.* **2007,** 50, 2166-2175.
35. Allardyce, C. S.; Dyson, P. J.; Ellis, D. J.; Heath, S. L., *Chem. Commun.* **2001**, 1396-1397.
36. Rademaker-Lakhai, J. M.; van den Bongard, D.; Pluim, D.; Beijnen, J. H.; Schellens, J. H. M., *Clin. Cancer Res.* **2004,** 10, 3717-3727.
37. Hartinger, C. G.; Zorbas-Seifried, S.; Jakupec, M. A.; Kynast, B.; Zorbas, H.; Keppler, B. K., *J. Inorg. Biochem.* **2006,** 100, 891-904.
38. Delferro, M.; Marchio, L.; Tegoni, M.; Tardito, S.; Franchi-Gazzola, R.; Lanfranchi, M., *Dalton Trans.* **2009**, 3766-3773.
39. Bratsos, l.; Bergamo, A.; Sava, G.; Gianferrara, t.; Zangrando, E.; Alessio, E., *J. Inorg. Biochem.* **2008,** 102, 606-617.
40. Groessl, M.; Reisner, E.; Hartinger, C. G.; Eichinger, R.; Semenova, O.; Timerbaev, A. R.; Jakupec, M. A.; Arion, V. B.; Keppler, B. K., *J. Med. Chem.* **2007,** 50, 2185-2193.
41. Chen, Z. G., *Trends Mol. Med.* **2010,** 16, 594-602.
42. Suss-Fink, G.; Khan, F. A.; Juillerat-Jeanneret, L.; Dyson, P. J.; Renfrew, A. K., *J. Cluster Sci.* **2010,** 21, 313-324.
43. Page, S. M.; Boss, S. R.; Barker, P. D., *Future Med. Chem.* **2009,** 1, 541-559.

Appendix I

Miscellaneous experimental data – Chapter 3

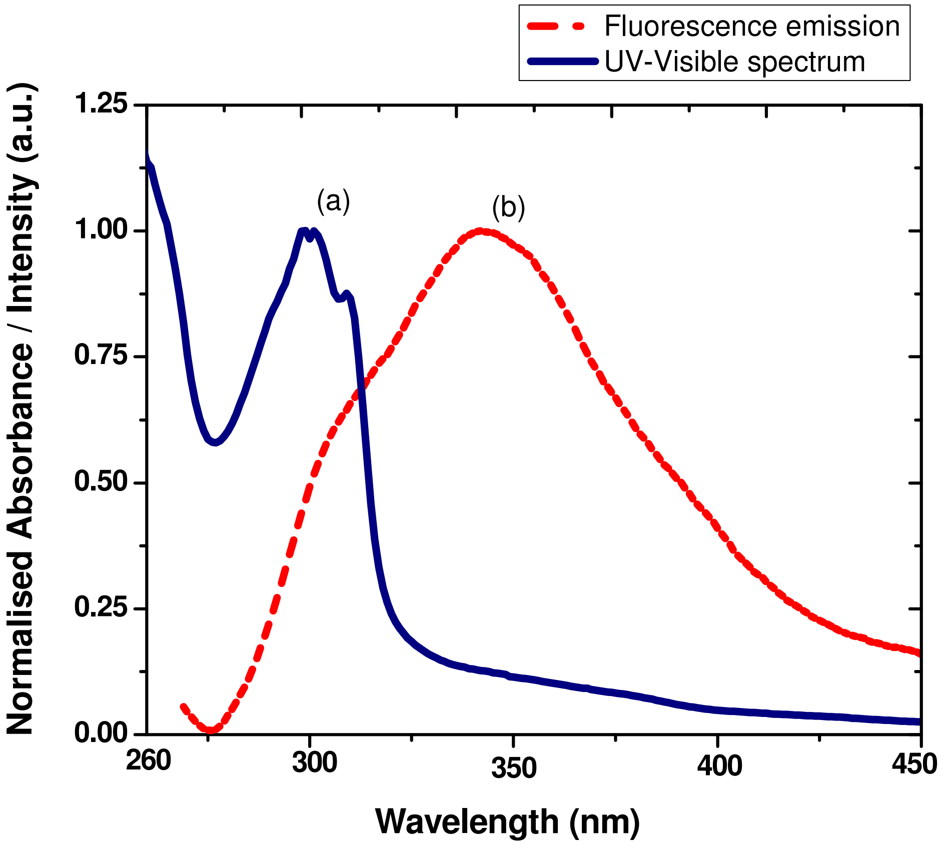

Figure 1: Normalised absorbance and fluorescence intensity (a.u.) vs wavelength (nm) for **1** (**Chapter 3**) in methanol: (a) UV-Vis absorption spectrum (λ_{max} = 300 nm); and (b) Fluorescent emission spectrum ($\lambda_{excitation}$ = 260 nm).

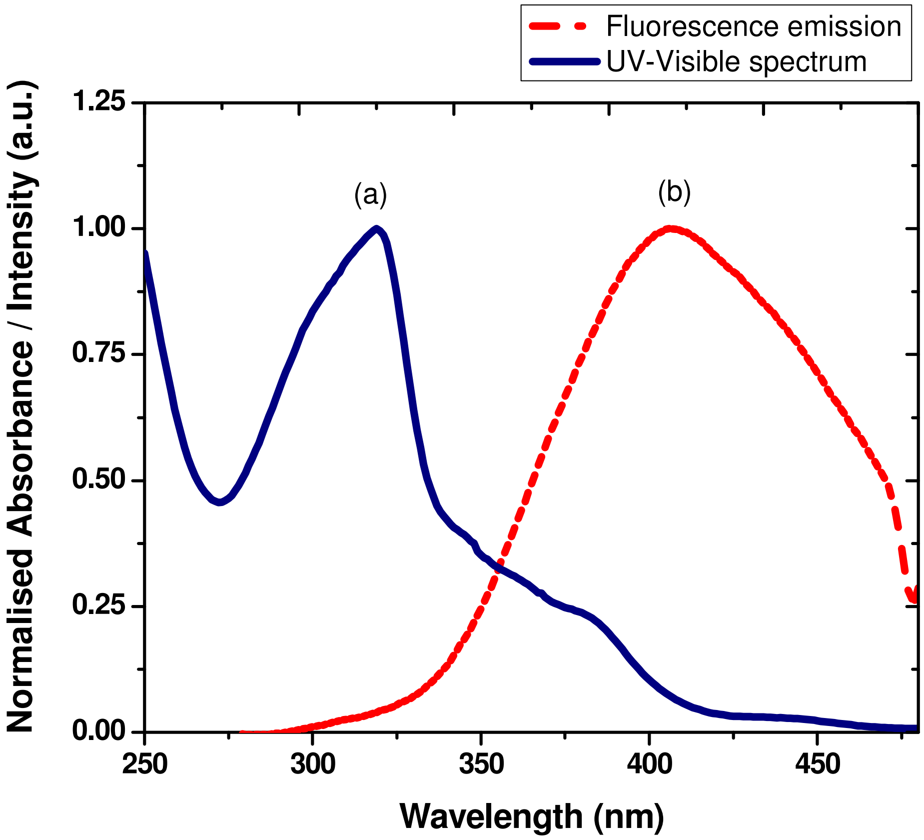

Figure 2: Normalised absorbance and fluorescence intensity (a.u.) vs wavelength (nm) for **2** (**Chapter 3**) in methanol: (a) UV-Vis absorption spectrum (λ_{max} = 319 nm); and (b) Fluorescent emission spectrum ($\lambda_{excitation}$ = 280 nm).

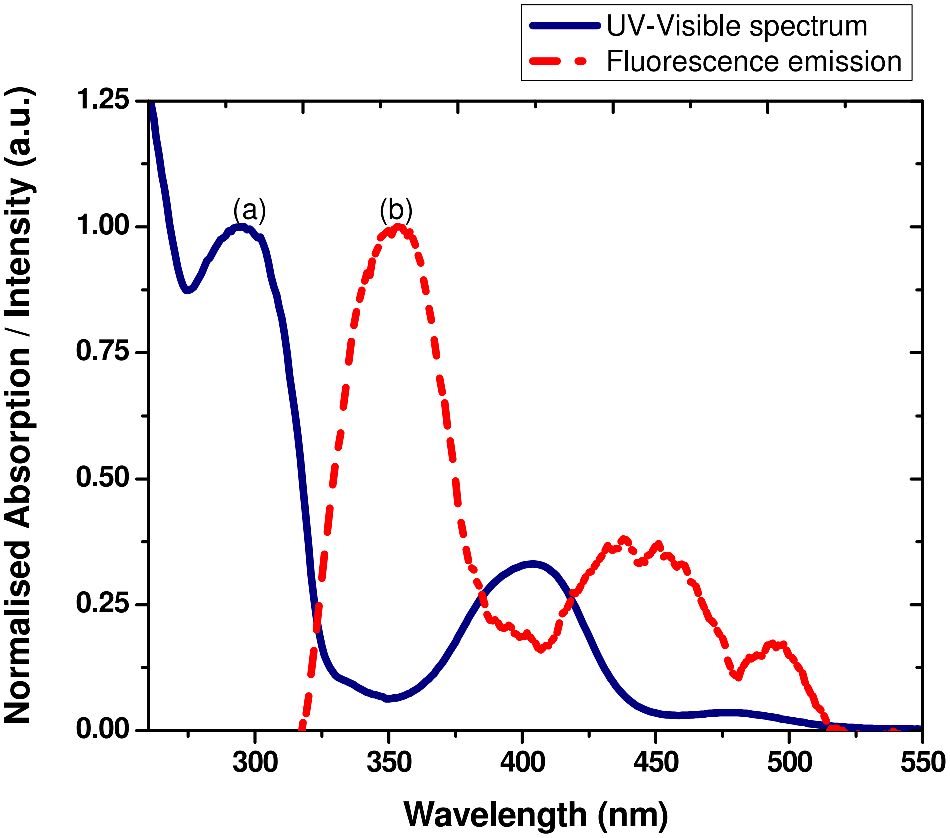

Figure 3: Normalised absorbance and fluorescence intensity (a.u.) vs wavelength (nm) for **3** (**Chapter 3**) in methanol: (a) UV-Vis absorption spectrum (λ_{max} = 295 nm); and (b) Fluorescent emission spectrum ($\lambda_{excitation}$ = 280 nm).

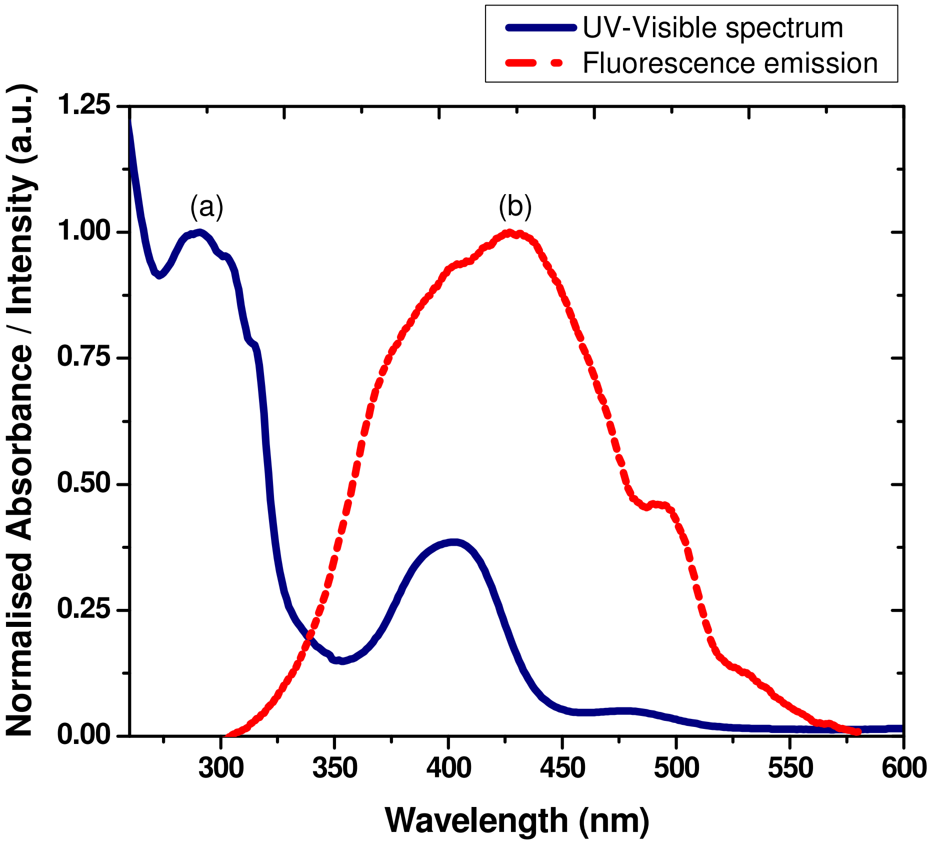

Figure 4: Normalised absorbance and fluorescence intensity (a.u.) vs wavelength (nm) for **4** (**Chapter 3**) in methanol: (a) UV-Vis absorption spectrum (λ_{max} = 291 nm); and (b) Fluorescent emission spectrum ($\lambda_{excitation}$ = 280 nm).

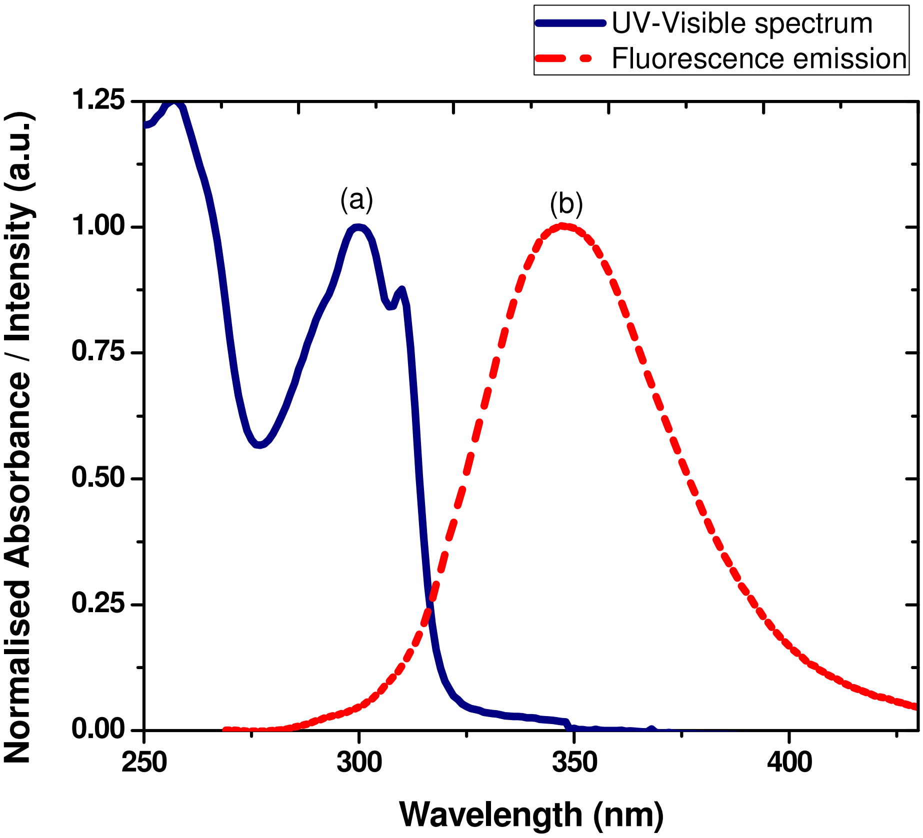

Figure 5: Normalised absorbance and fluorescence intensity (a.u.) vs wavelength (nm) for **5-Iodo-Indazole** (**Chapter 3**) in methanol: (a) UV-Vis absorption spectrum (λ_{max} = 300 nm); and (b) Fluorescent emission spectrum ($\lambda_{excitation}$ = 260 nm).

Fluorescent microscopy studies for TMAS *trans*-[RuCl$_4$(I-Ind)(DMSO)] (4)

Note: We were never able to demonstrate that the fluorescence in the cell images actually arose from the complexes that we treated with as opposed to background fluorescence from the cells themselves and as such the material that appears in this appendix I was removed from the corresponding chapter/manuscript.

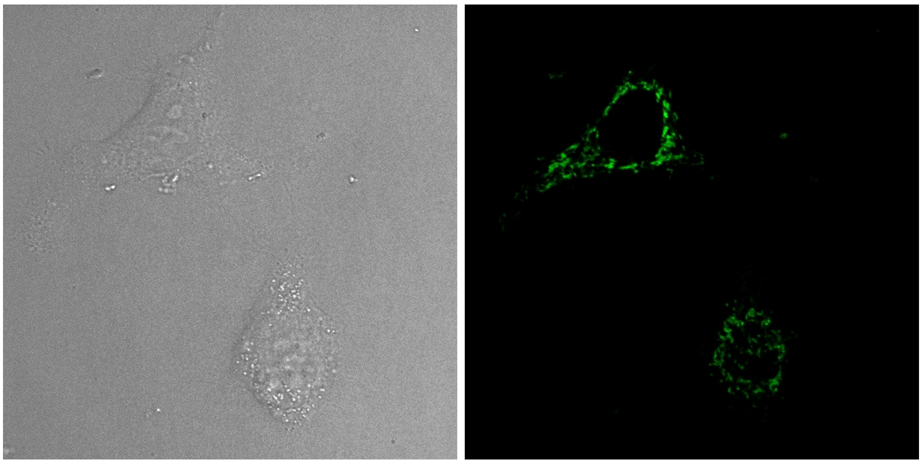

(a) **(b)**

Figure 6: Fluorescent micrographs (63 x magnification) of A-549 cells incubated with **4** (50 μM) for 3 hours to induce apoptosis at excitation 405 nm. Fluorescence emission bandwidth is 498 nm - 639nm. Fluorescence emission is shown in (b). Phase contrast image of treated cells is shown in (a).

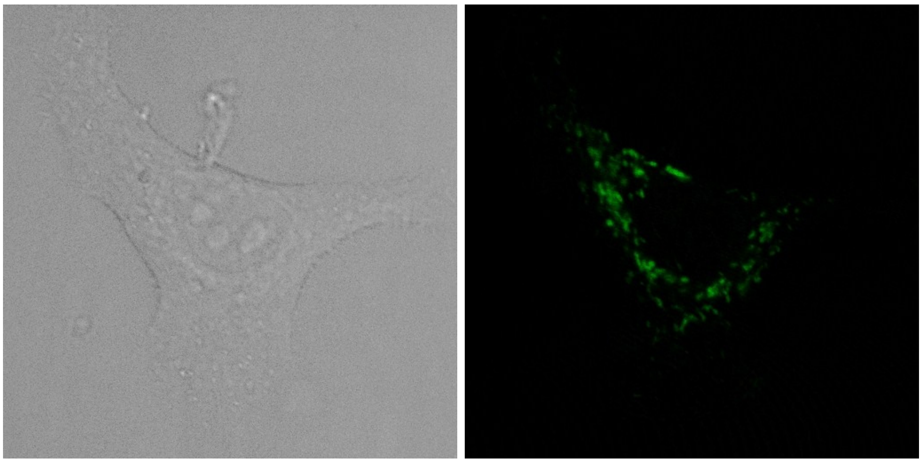

(a) **(b)**

Figure 7: Fluorescent micrographs (63 x magnification) of A-549 cells incubated with **4** (50 μM) for 3 hours to induce apoptosis at excitation 405 nm. Fluorescence emission bandwidth is 498 nm - 639nm. Fluorescence emission is shown in (b). Phase contrast image of treated cells is shown in (a).

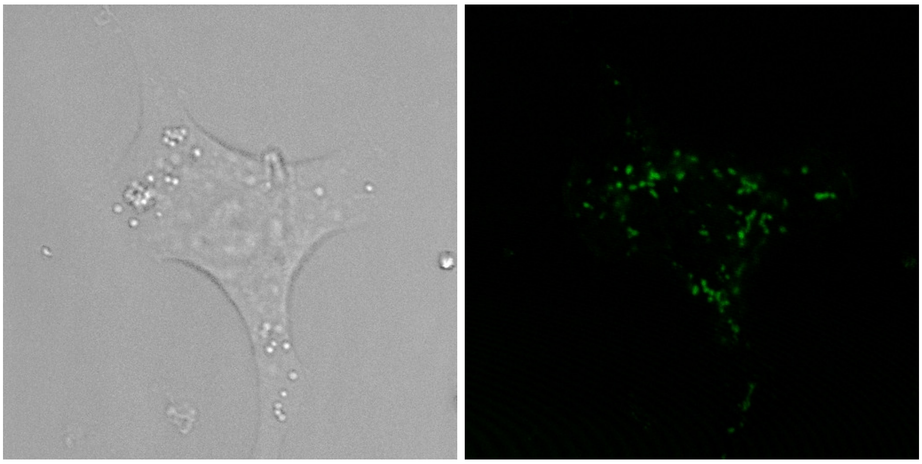

(a) **(b)**

Figure 8: Fluorescent micrographs (63 x magnification) of A-549 cells incubated with **4** (50 μM) for 3 hours to induce apoptosis at excitation 405 nm. Fluorescence emission bandwidth is 498 nm - 639nm. Fluorescence emission is shown in (b). Phase contrast image of treated cells is shown in (a).

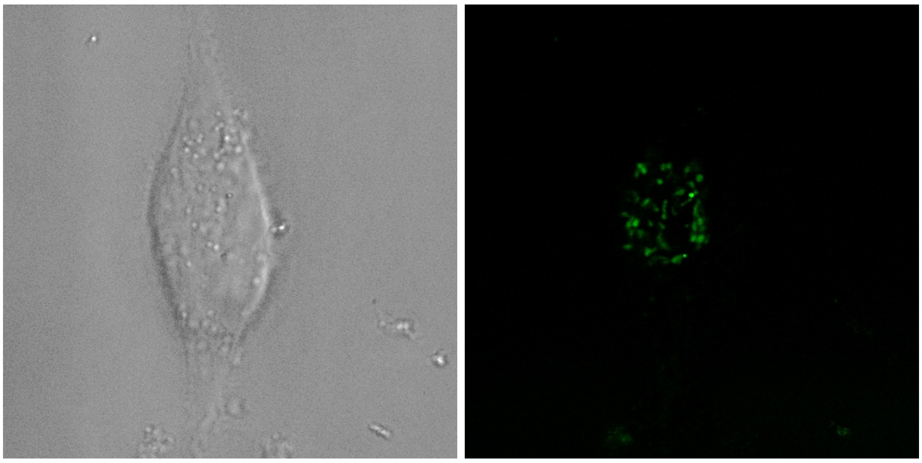
(a) **(b)**

Figure 9: Fluorescent micrographs (63 x magnification) of A-549 cells incubated with **4** (50 μM) for 3 hours to induce apoptosis at excitation 405 nm. Fluorescence emission bandwidth is 498 nm - 639nm. Fluorescence emission is shown in (b). Phase contrast image of treated cells is shown in (a).

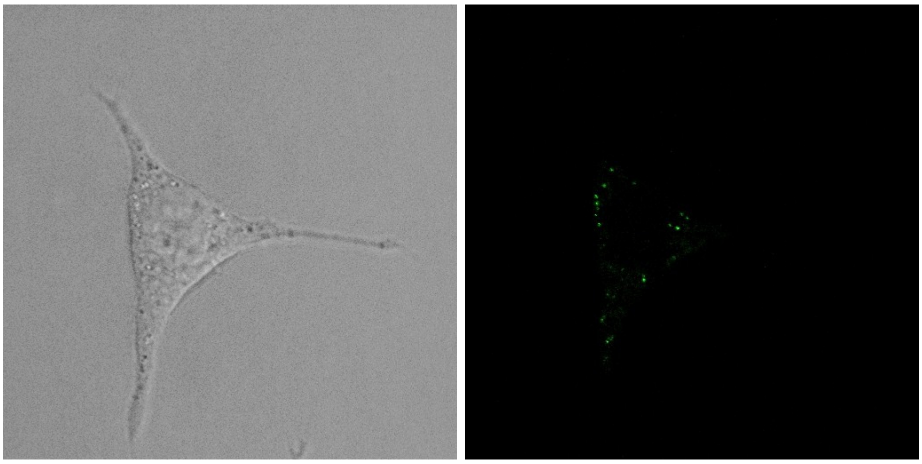
(a) **(b)**

Figure 10: Fluorescent micrographs (63 x magnification) of A-549 cells incubated with **5-Iodo-Indazole** (50 μM) for 3 hours to induce apoptosis at excitation 405 nm. Fluorescence emission bandwidth is 498 nm - 639nm. Fluorescence emission is shown in (b). Phase contrast image of treated cells is shown in (a).

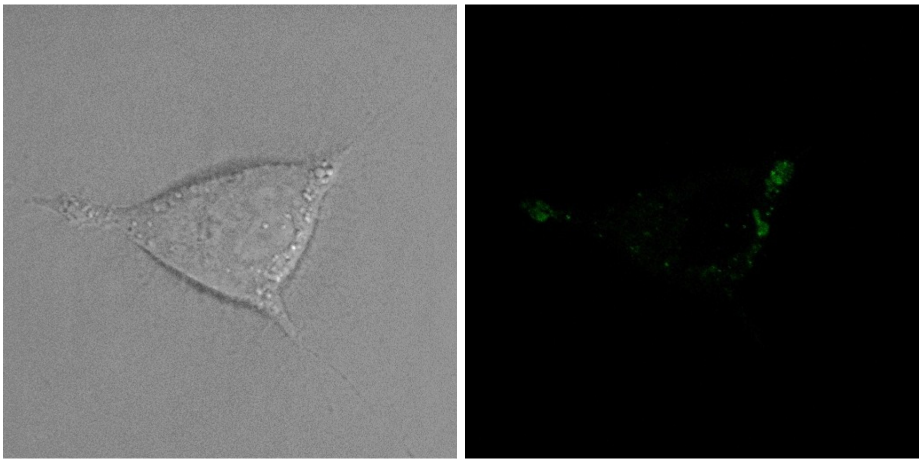

(a) **(b)**

Figure 11: Fluorescent micrographs (63 x magnification) of A-549 cells incubated with **5-Iodo-Indazole** (50 μM) for 3 hours to induce apoptosis at excitation 405 nm. Fluorescence emission bandwidth is 498 nm - 639nm. Fluorescence emission is shown in (b). Phase contrast image of treated cells is shown in (a).

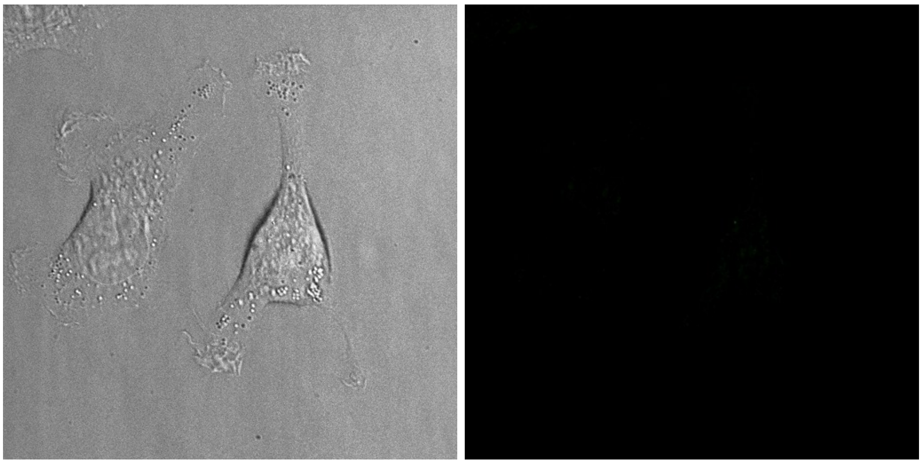

(a) **(b)**

Figure 12: Fluorescent micrographs (63 x magnification) of A-549 control cells incubated for 3 hours to induce apoptosis at excitation 405 nm. Fluorescence emission bandwidth is 498 nm - 639nm. Fluorescence emission is shown in (b). Phase contrast image of treated cells is shown in (a).

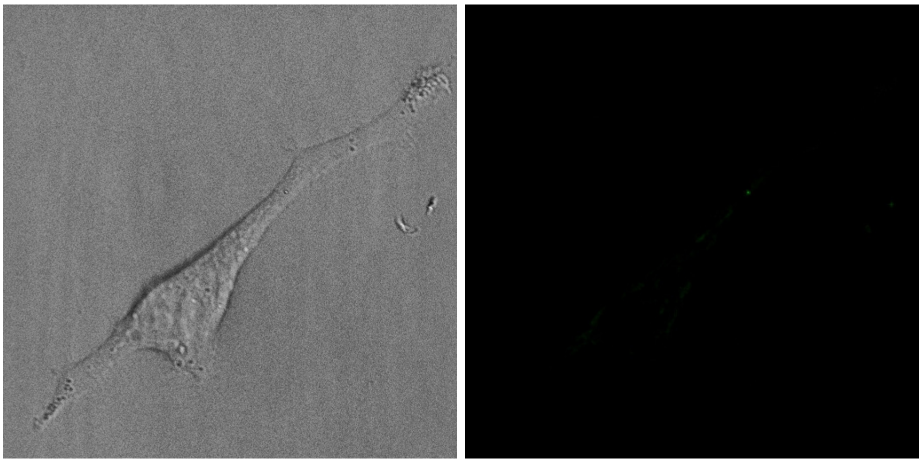

(a) **(b)**

Figure 13: Fluorescent micrographs (63 x magnification) of A-549 control cells incubated for 3 hours to induce apoptosis at excitation 405 nm. Fluorescence emission bandwidth is 498 nm - 639nm. Fluorescence emission is shown in (b). Phase contrast image of treated cells is shown in (a).

Appendix II

Miscellaneous experimental data – Chapter 4

Fluorescence microscopy

Note: We were never able to demonstrate that the fluorescence in the cell images actually arose from the complexes that we treated with as opposed to background fluorescence from the cells themselves and as such the material that appears in this appendix II was removed from the corresponding chapter/manuscript.

Experimental

Fluorescence microscopy was performed using Leica SP5 Spectral Scanning Confocal microscope equipped with filter set DAPI (UV) filter set. A549 cells were grown directly on sterilised 2 mm thick fluoro dishes at a concentration of 5.0 X 10^4 cells/dish (volume = 1 mL) in complete DMEM for 24 h at 310 K in a 5% CO_2–humidified incubator prior to the treatment. After 24 h, the media was replaced with fresh DMEM and 100 μL of 500 μM **F3 - F6** (*see Chapter 4*) was added to 900 μL of media giving a final treatment concentration of 50 μM. In order to avoid premature hydrolysis, the solutions of these compounds were prepared immediately prior to the treatments. Control dishes were prepared under otherwise identical experimental conditions. Following the 3 h treatment, the media was replaced with fresh DMEM without phenol red (colourless medium). Cell images were collected with a Leica SP5 Spectral Scanning Confocal Microscope at an excitation wavelength of 405 nm with an emission profile from 439 nm to 477 nm.

Results and discussion

Fluorescence microscopy experiments were carried out using human lung carcinoma cells (A549 - 50,000 cells/dish) treated with compounds **F3-F6,** along with media-alone controls. Fluorescent images were taken at an excitation wavelength of 405 nm combined with an emission window of 439-477nm, and the results are shown in Figure 3 (A – E).

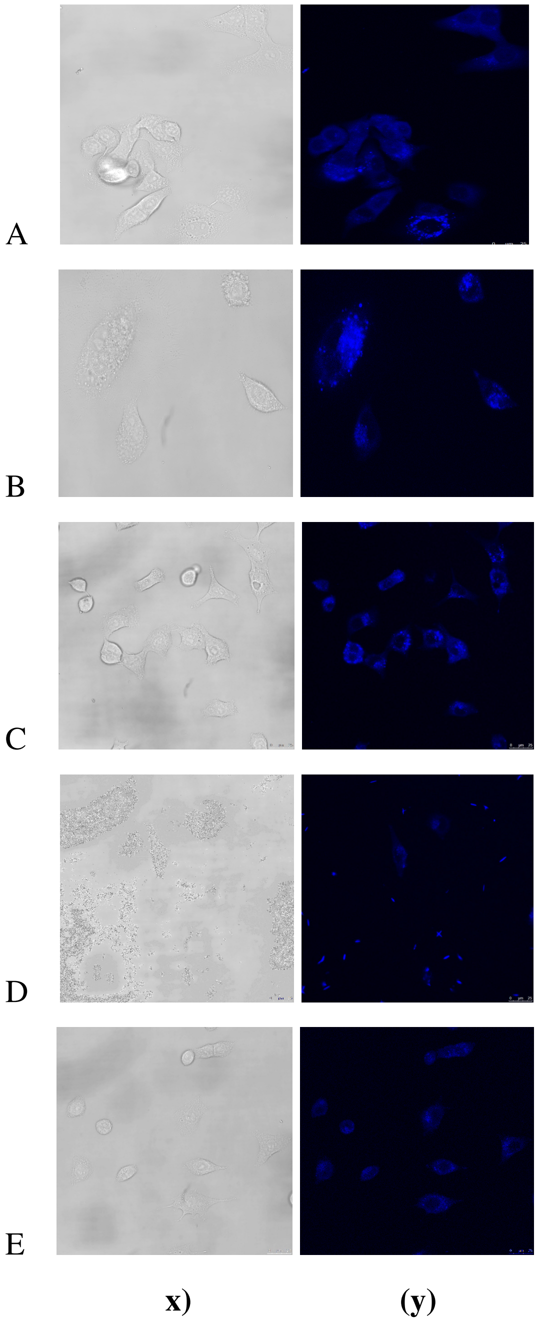

Figure 1: A549 cells incubated with complexes **F3** (A), **F4** (B), **F5** (C), **F6** (D) and control (E) for 3 h (50 μM). A phase contrast image is shown in (x), while a confocal fluorescence emission image is displayed in (y) (excitation at 405 nm and emission collected between 439 nm to 477 nm).

Cells treated with **F3** (50 μM for 3 h) exhibited punctate perinuclear cytoplasmic localisation of fluorescence above a more evenly distributed, lower intensity, fluorescence across most of the cell bodies, including some fluorescence from the nuclear region. The formation of vesicles or vacuoles was apparent from inspection of the optical micrographs of the **F3** treated cells, and these were commonly, although not completely, co-localised with the brightest spots of fluorescence emission observed in some cells. This was most apparent in the cell that appears at the bottom middle of Fig. 1A. A similar distribution of fluorescence intensity was observed for cells treated with **F4** (50 µM for 3 h – see Fig. 1B), with the most intense fluorescence corresponding to vacuoles observed in the optical micrograph. However, unlike cells treated with **F3**, treatment with **F4** resulted in significant modulation of cell morphology that was evident from the optical micrographs. In particular, the cells were rounded and major disturbance of the cell membrane was noted. Unlike **F3** treated cells, no fluorescence was observed in the nuclear region of cells treated with **F4**.

Confocal images were collected under identical experimental conditions from cells treated with the ligands **F5** (50 µM for 3 h) and **F6** (50 µM for 3 h). These experiments were designed as a control to monitor fluorescence that could have arisen from the fluorescent ligands if they had dissociated from **F3** or **F4**, respectively, and then coordinated an endogenous metal ion yielding a similar LMCT band. The observed distribution of fluorescence from the cells treated with **F5** or **F6** was found to be similar to that of cells treated with **F3** or **F4**, however the extent of vacuole formation evident from the optical micrographs was minimal compared to that observed for the cells treated with the ruthenium complexes. No fluorescence arising from the nuclei of cells treated with either **F5** or **F6** was noted.

Compounds **F4** and **F6** were found to be partially insoluble in media and the formation of crystalline solid was noted in the optical micrographs of cells treated with these compounds. The crystals displayed significant fluorescence emission in the emission wavelength window employed for confocal microscopy. The induction of cell toxicity by treatment with these compounds at higher concentrations indicated that they were not completely insoluble.

Confocal images were collected for media-alone treated cells under otherwise identical conditions (see Fig. 1E). Qualitatively, the level of fluorescence observed in these cells was apparently lower than that observed in the treated cells, although again the distribution of intensity was punctate and predominantly cytoplasmic. The observed fluorescence was presumably background autofluorescence arising from endogenous fluorescent species such as NAD(P)H (tryptophan and tyrosine have excitations and emissions at wavelengths that are too short to be observed here).[25]

The overarching goal of our experiments was to create analogues of NAMI-A tagged with fluorescent moieties that would allow tracking of the cellular targeting of this important class of compounds using live cell imaging over the time span of the action of the parent drug. The preparations of compounds **F3** and **F4** were designed as pilot experiments to test the synthetic routes available as neither the quantum yield nor the emission wavelength properties of the fluorophores contained in those molecules were appropriate for the intended final goal. However, the successful synthesis and characterisation of the compounds raised the possibility that the LMCT bands of the complexes (with their longer wavelength excitations and emissions) could be used to image the species in cells using confocal microscopy. This would also have the potential advantage that the fluorescence might be lost if the ligand dissociated from the complex once taken up into cells leading to a reduction in emission, providing some information about the kinetics of the metabolism of the compounds. The imaging experiments described above were then designed to test the feasibility of this concept.

While significant fluorescence was observed in cells treated with **F3** and **F4**, and this was apparently more intense than that observed in untreated cells, we were unable to demonstrate that this was a significant increase in fluorescence arising from the ruthenium compounds over and above the background autofluorescence.

Treatment with the ruthenium complexes, especially **F4**, led to significant changes in the morphology of the cells consistent with the effects of a cytotoxic species, including formation of vesicles or vacuoles. These seemed to be associated with increases in fluorescence possibly arising from the ruthenium complexes or their biotransformation products.

In comparison, such morphological changes were not evident in the images of the cells treated with the ligands **F5** and **F6**, although significant fluorescence emission was observed in the cytoplasm of the cells. Consideration of the excitation-emission spectra for these species indicates that they should not display fluorescence, as they have no notable absorption at the excitation wavelength used for this experiment. Hence, the emission observed in cells could simply be autofluorescence (although the observed intensities are greater than those observed in the media only cells) or it could arise from the formation of complexes with endogenous metal ions once the ligands are taken up into cells, leading to a LMCT band with characteristics similar to those for **F3** and **F4**. If the latter is true, then the possibility also exists that the fluorescence observed in the images of cells treated with **F3** or **F4** arises from complexes formed between endogenous metal ions and **F5** or **F6** which had dissociated from the parent complexes, either before or after cell uptake.

It is impossible to distinguish between these possibilities on the basis of the results presented here, but we note that the likelihood of the last case is diminished by our observation that the N-heterocyclic ligands of iodinated analogues of NAMI-A and KP1019 remain coordinated to ruthenium after cell uptake.[16] The fact that the crystalline solids observed in the images of the **F6** treatments exhibited significant fluorescent emission lends credence to the idea that intracellular fluorescence arises from complexes formed with endogenous metal ions. If the crystals were simply of the treatment compound then they should not display emission at these wavelengths and so the fluorescence must arise from formation of low-solubility complexes with metal ions in the growth media that have excitation and emission characteristics suitable for visualisation.

We believe that there remains potential to develop this approach to allow the implementation of the imaging methodology described above. That is, to use

LMCT (or MLCT) based fluorescence to specifically image intact metal complexes as drug candidates in cultured cells. The intact complexes could then be distinguished from dissociated ligands or metabolised metal ion complexes, especially if this was matched with X-ray fluorescence imaging studies that would delineate the exogenous and endogenous metal ion distributions. For this to become feasible, the strength of the chromophore associated with the LMCT transition would need to be increased dramatically and, in addition, increasing the wavelength of the emission from that fluorophore would potentially avoid some of the issues from background fluorescence that we have identified here.

Fluorescent microscopy images

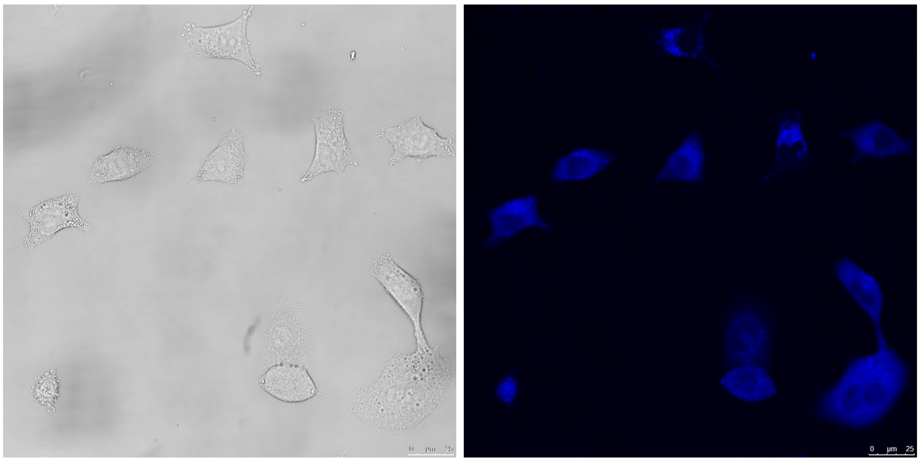

(a) **(b)**

Figure 2: A549 cells incubated with **F3** (50 μM) for 3 h. A phase contrast image is shown in (a), while a confocal fluorescence emission image is displayed in (b) (excitation at 405 nm and emission collected between 439 nm to 477 nm).

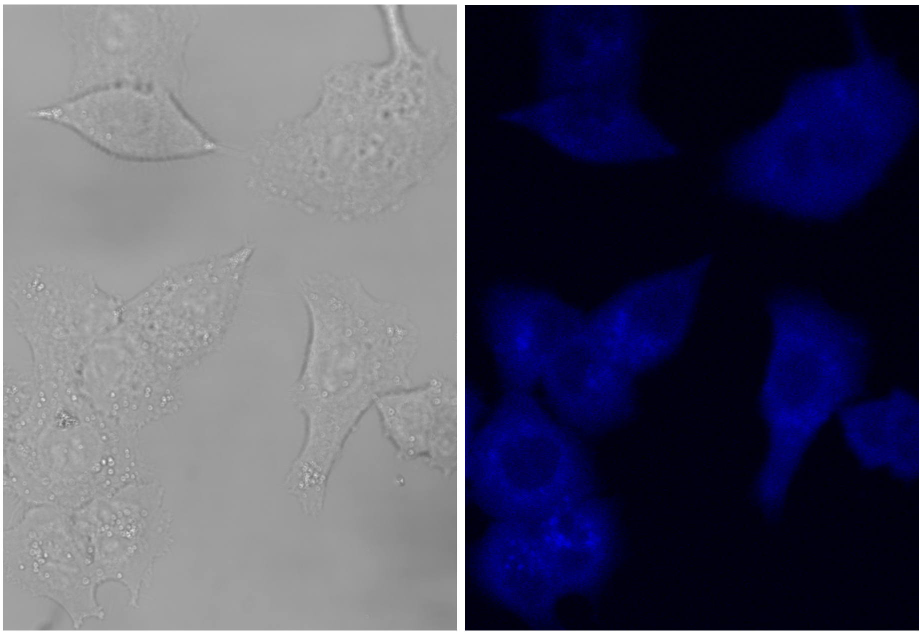

(a) **(b)**

Figure 3: A549 cells incubated with **F3** (50 µM) for 3 h. A phase contrast image is shown in (a), while a confocal fluorescence emission image is displayed in (b) (excitation at 405 nm and emission collected between 439 nm to 477 nm).

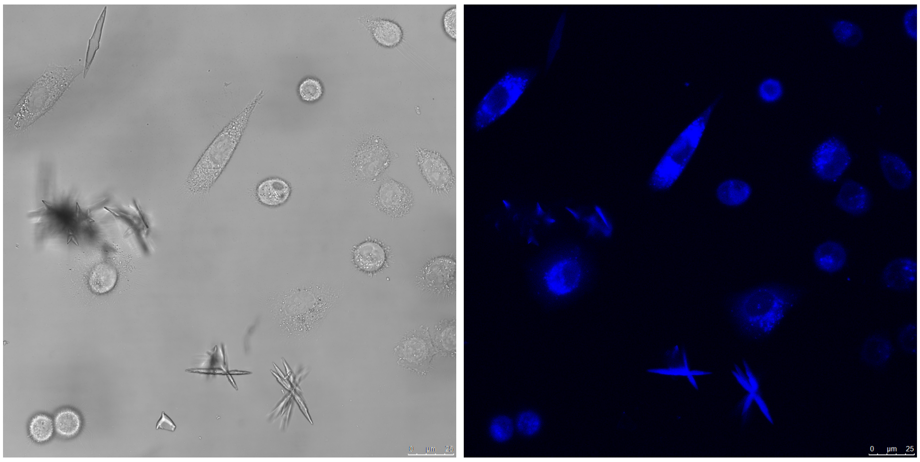

(a) **(b)**

Figure 4: A549 cells incubated with **F4** (50 µM) for 3 h. A phase contrast image is shown in (a), while a confocal fluorescence emission image is displayed in (b) (excitation at 405 nm and emission collected between 439 nm to 477 nm).

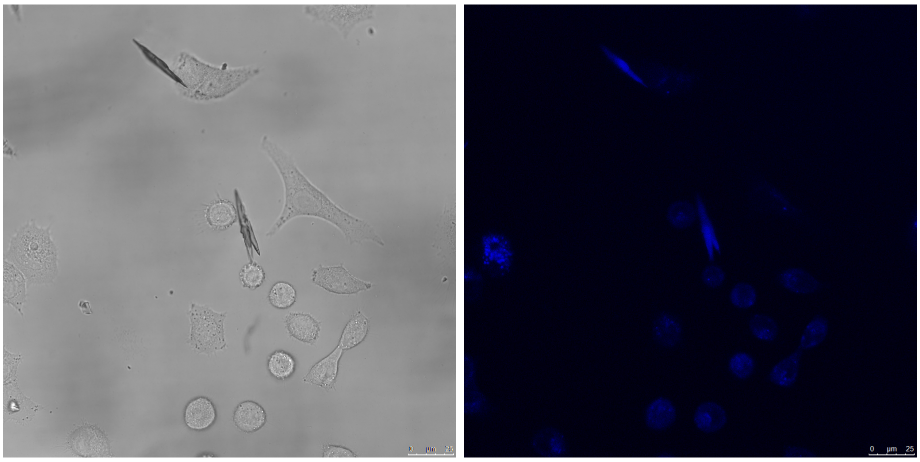

(a) **(b)**

Figure 5: A549 cells incubated with **F4** (50 µM) for 3 h. A phase contrast image is shown in (a), while a confocal fluorescence emission image is displayed in (b) (excitation at 405 nm and emission collected between 439 nm to 477 nm).

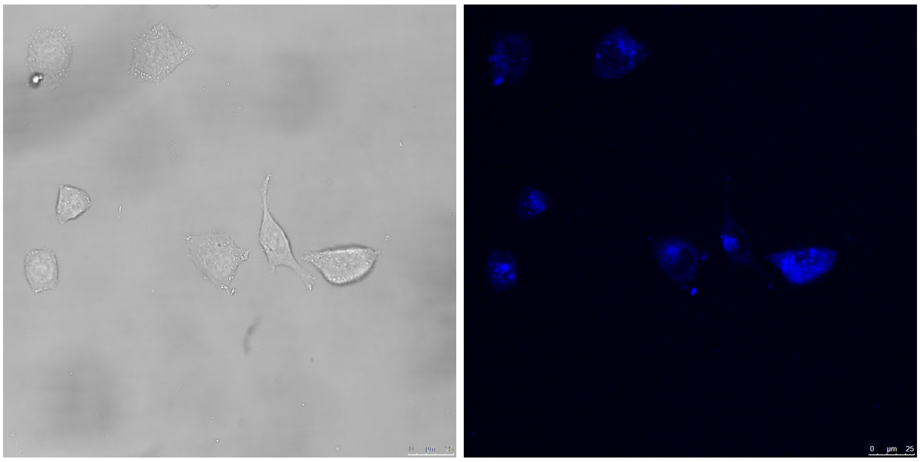

(a) **(b)**

Figure 6: A549 cells incubated with **F5** (50 µM) for 3 h. A phase contrast image is shown in (a), while a confocal fluorescence emission image is displayed in (b) (excitation at 405 nm and emission collected between 439 nm to 477 nm).

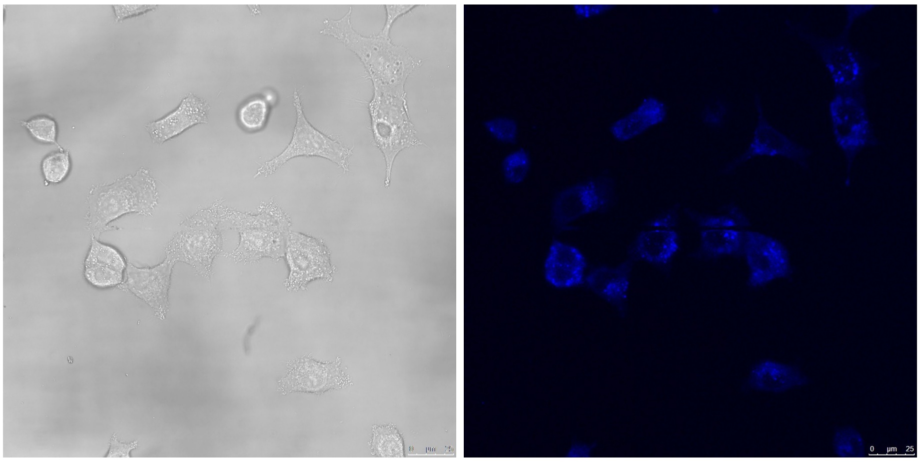

(a) **(b)**

Figure 7: A549 cells incubated with **F5** (50 µM) for 3 h. A phase contrast image is shown in (a), while a confocal fluorescence emission image is displayed in (b) (excitation at 405 nm and emission collected between 439 nm to 477 nm).

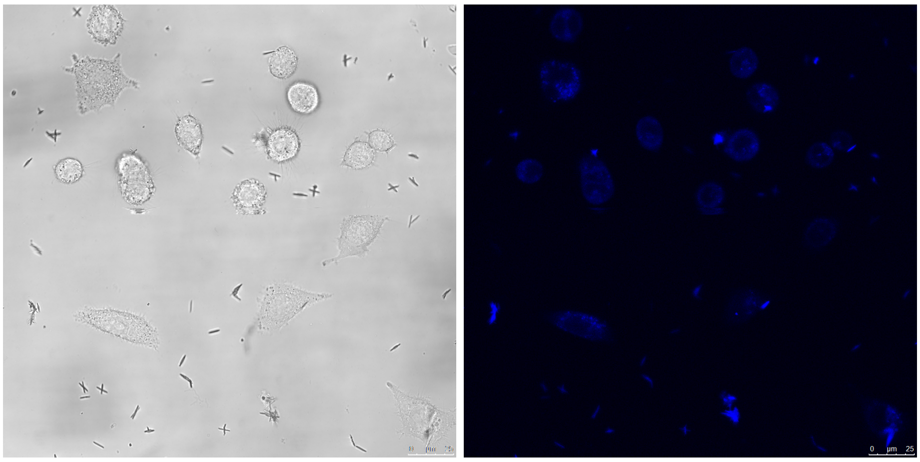

(a) **(b)**

Figure 8: A549 cells incubated with **F6** (50 µM) for 3 h. A phase contrast image is shown in (a), while a confocal fluorescence emission image is displayed in (b) (excitation at 405 nm and emission collected between 439 nm to 477 nm).

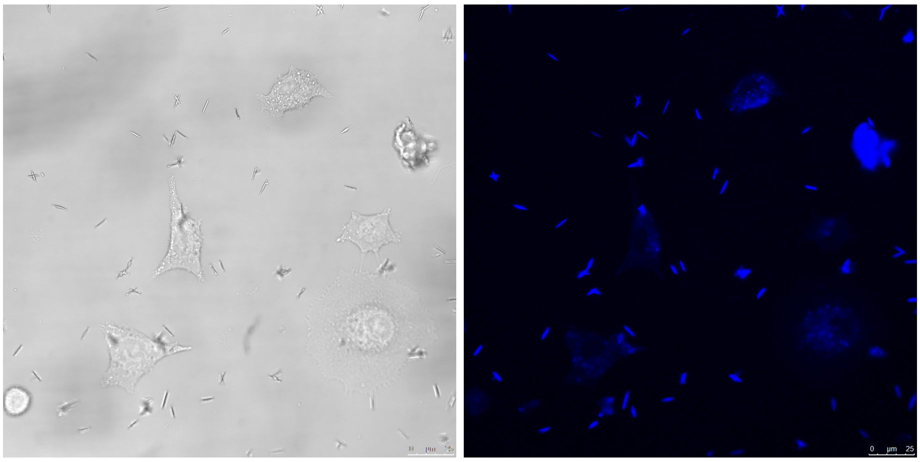

(a) **(b)**

Figure 9: A549 cells incubated with **F6** (50 µM) for 3 h. A phase contrast image is shown in (a), while a confocal fluorescence emission image is displayed in (b) (excitation at 405 nm and emission collected between 439 nm to 477 nm).

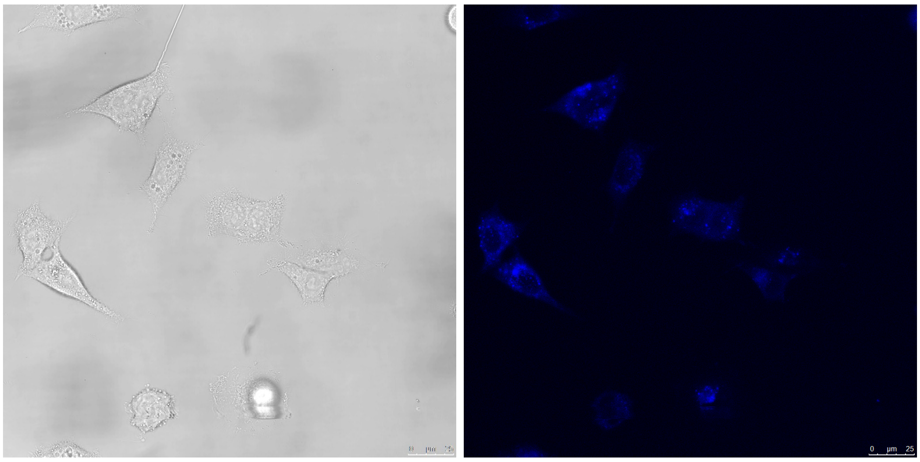

(a) **(b)**

Figure 10: A549 cells incubated with media only for 3 h. A phase contrast image is shown in (a), while a confocal fluorescence emission image is displayed in (b) (excitation at 405 nm and emission collected between 439 nm to 477 nm).

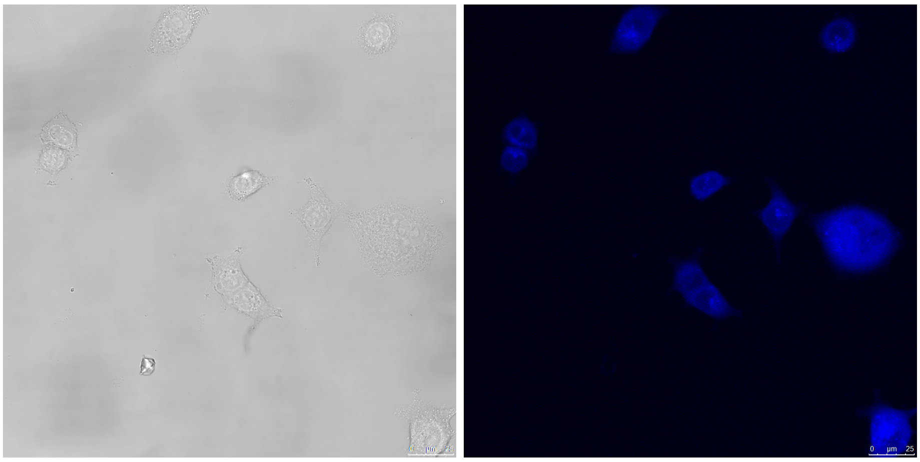

(a) **(b)**

Figure 11: A549 cells incubated with media only for 3 h. A phase contrast image is shown in (a), while a confocal fluorescence emission image is displayed in (b) (excitation at 405 nm and emission collected between 439 nm to 477 nm).

Acknowledgements

We would like to thank Claire M. Weekley, The University of Adelaide, for her help and support in the fluorescent cell imaging studies.

Appendix III

Experimental data - Chapter 5

Mass Spectra

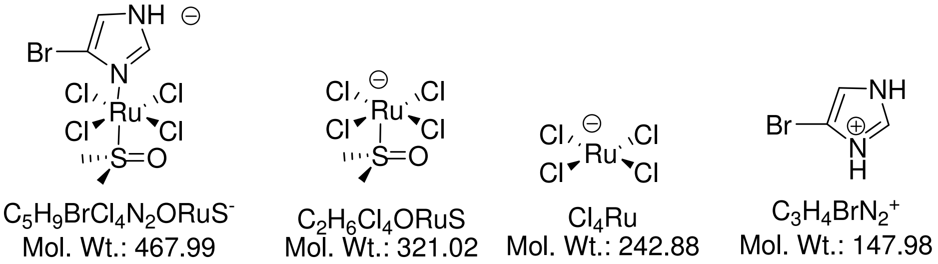

Figure 1: Fragmentation pattern for **M1**.

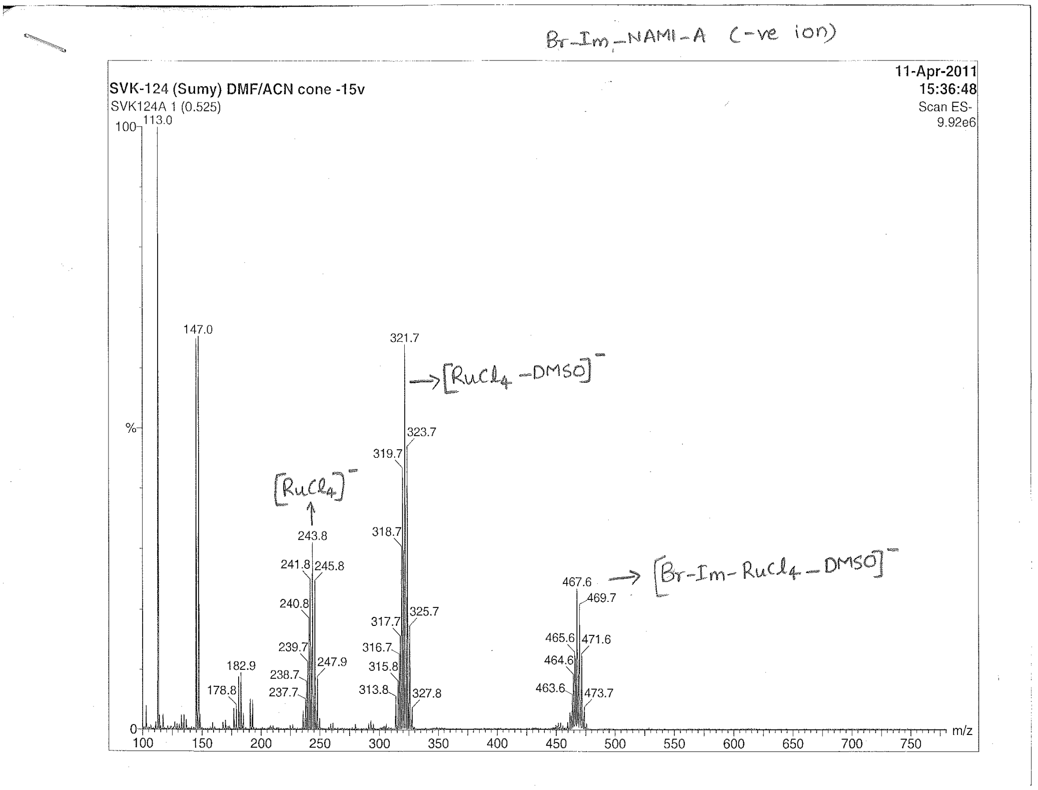

Figure 2: Electrospray mass spectrum (-ve ion) for **M1**; Cone 15V; Solvent – DMF/ACN.

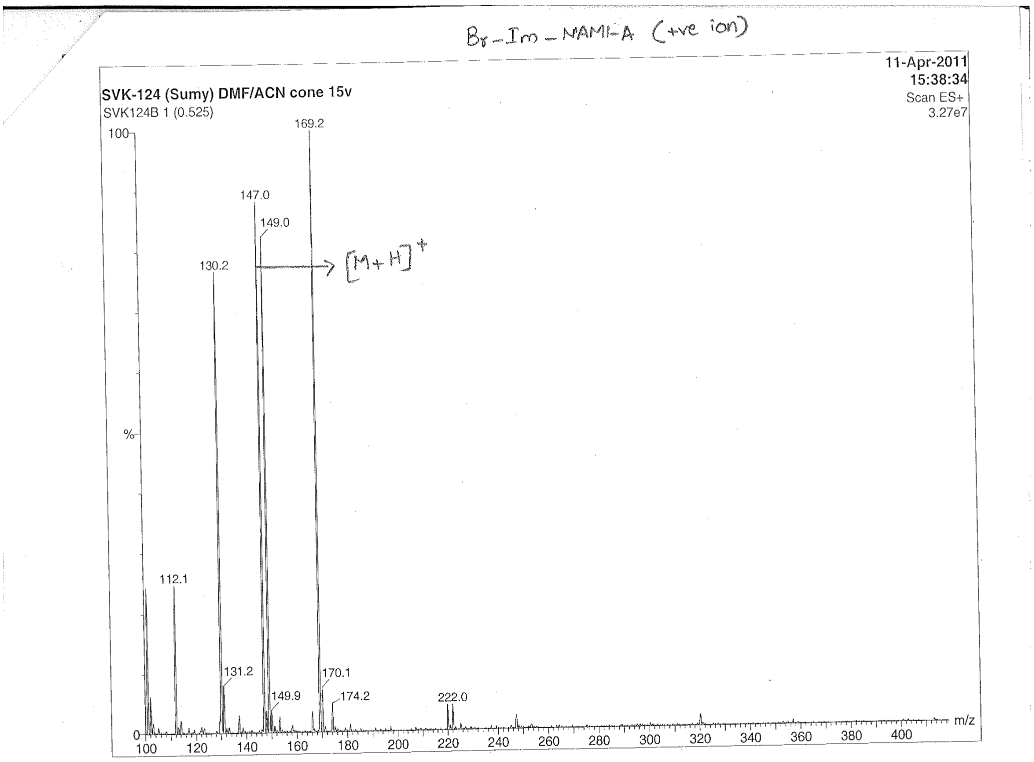

Figure 3: Electrospray mass spectrum (+ve ion) for **M1**; Cone 15V; Solvent – DMF/ACN.

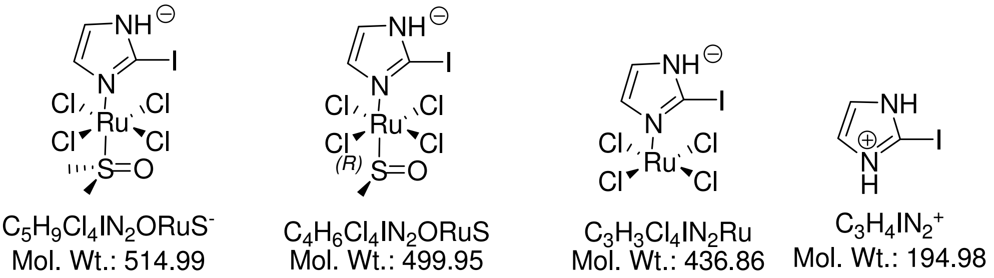

Figure 4: Fragmentation pattern for **M2**.

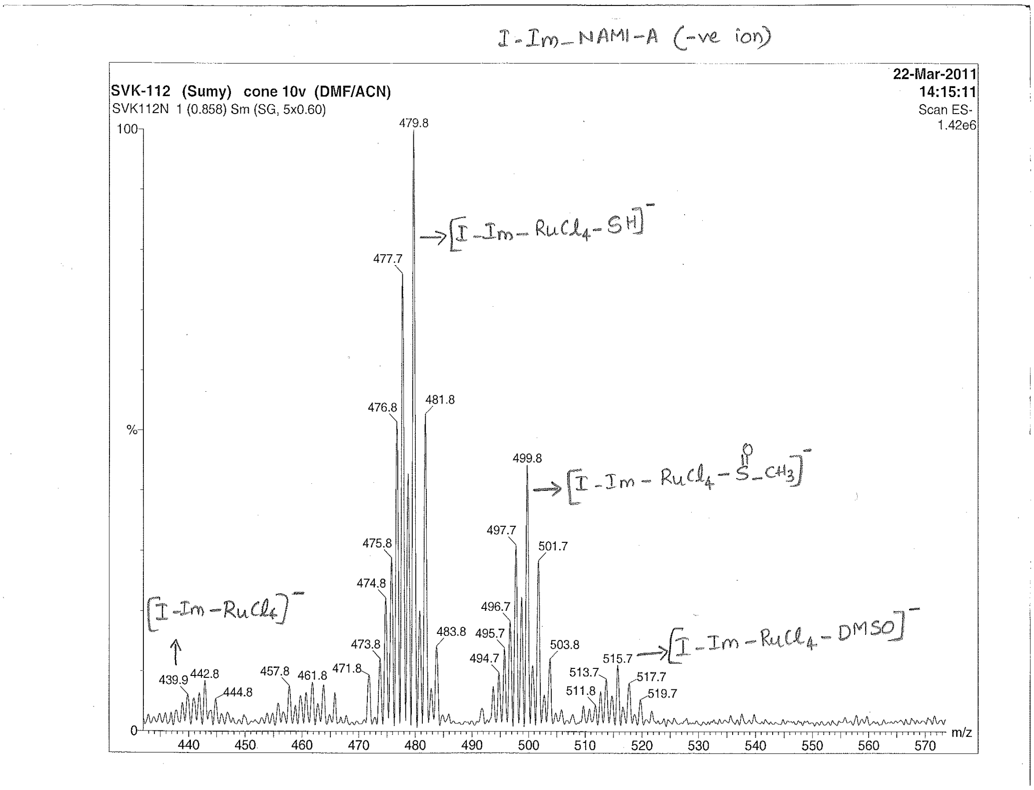

Figure 5: Electrospray mass spectrum (-ve ion) for **M2**; Cone 15V; Solvent – DMF/ACN.

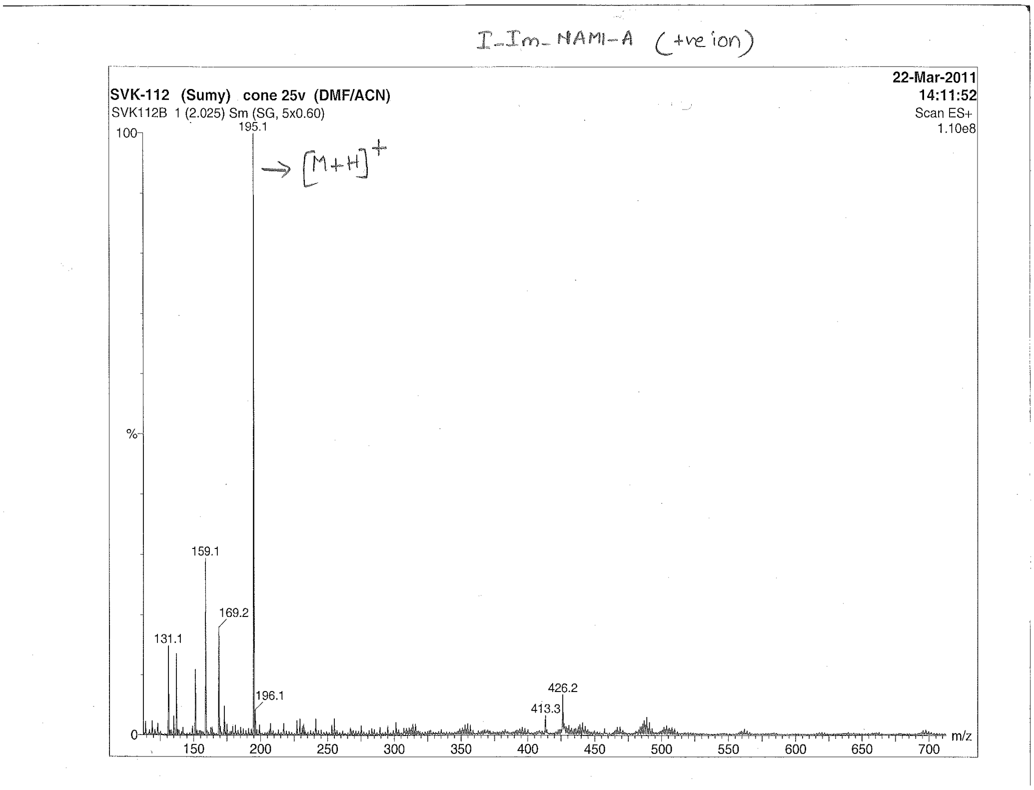

Figure 6: Electrospray mass spectrum (+ve ion) for **M2**; Cone 15V; Solvent – DMF/ACN.

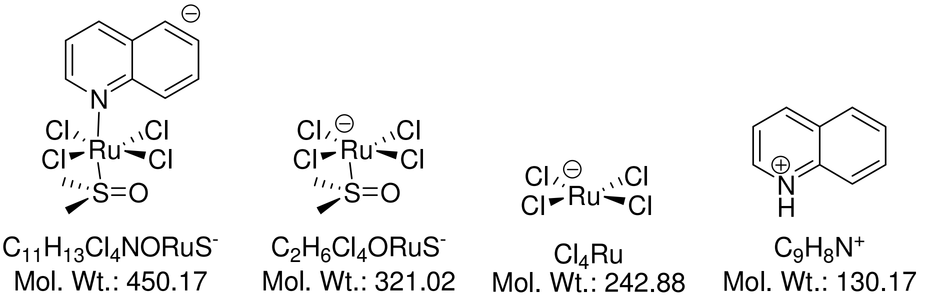

Figure 7: Fragmentation pattern for **M3**.

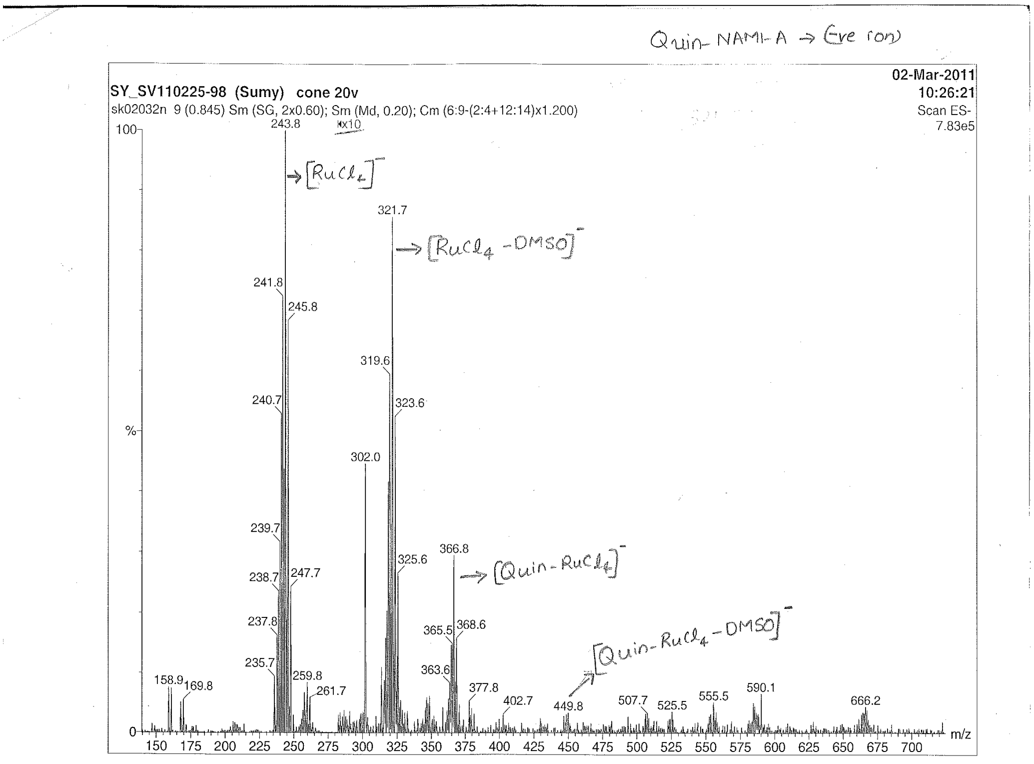

Figure 8: Electrospray mass spectrum (-ve ion) for **M3**; Cone 15V; Solvent – DMF/ACN.

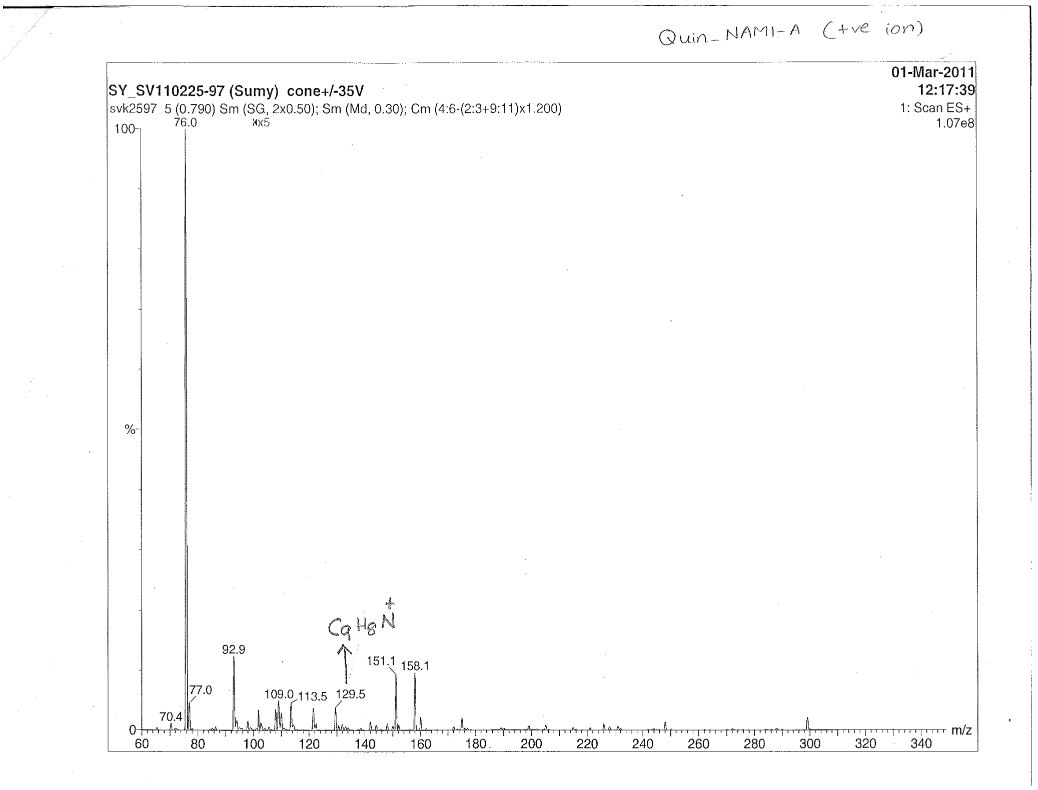

Figure 9: Electrospray mass spectrum (+ve ion) for **M3**; Cone 15V; Solvent – DMF/ACN.

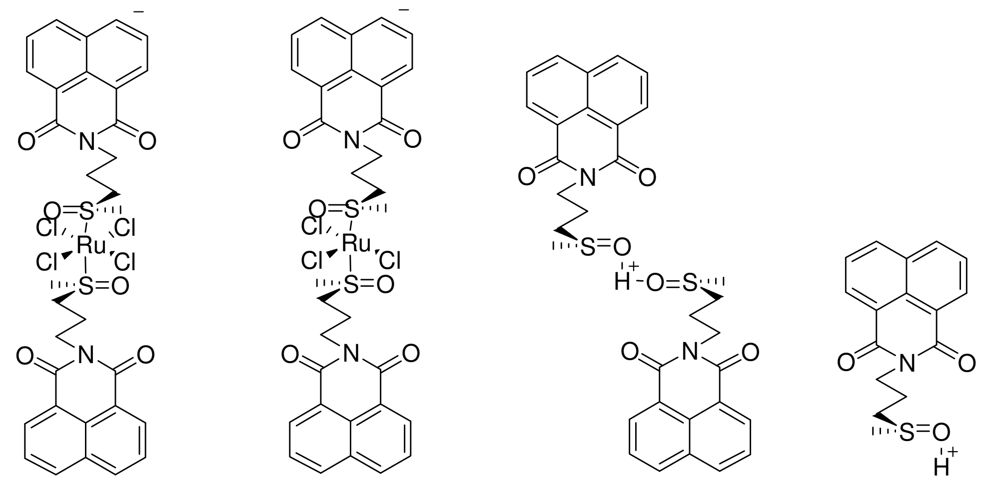

Figure 10: Fragmentation pattern for **P1**.

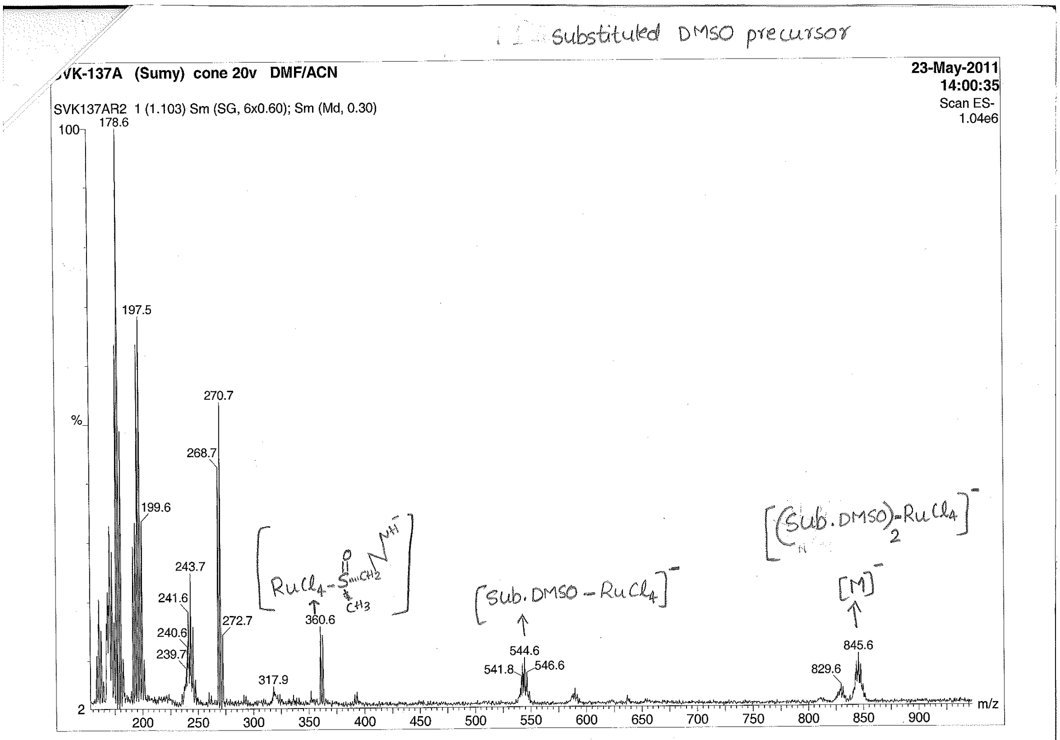

Figure 11: Electrospray mass spectrum (-ve ion) for **P1**; Cone 15V; Solvent – DMF/ACN.

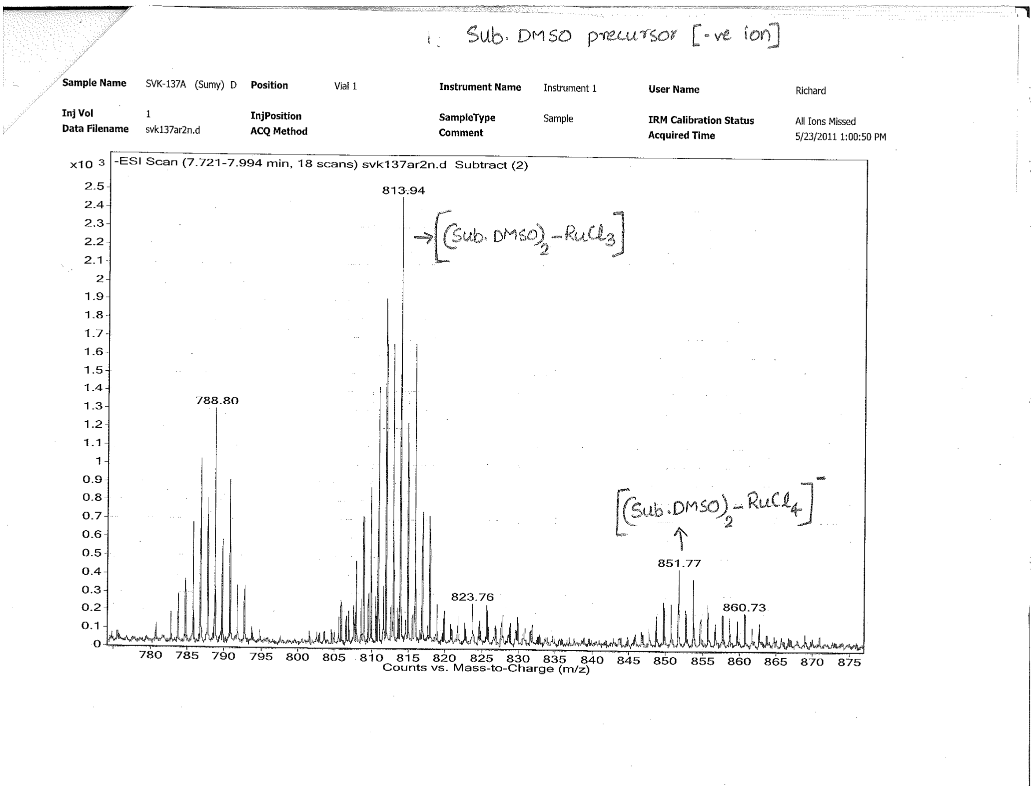

Sample Name SVK-137A (Sumy) D
Position Vial 1
Instrument Name Instrument 1
User Name Richard
Inj Vol 1
Data Filename svk137ar2n.d
InjPosition
ACQ Method
SampleType Sample
Comment
IRM Calibration Status All Ions Missed
Acquired Time 5/23/2011 1:00:50 PM

Figure 12: Accurate mass spectrum (-ve ion) for **P1**; Cone 15V; Solvent – DMF/ACN.

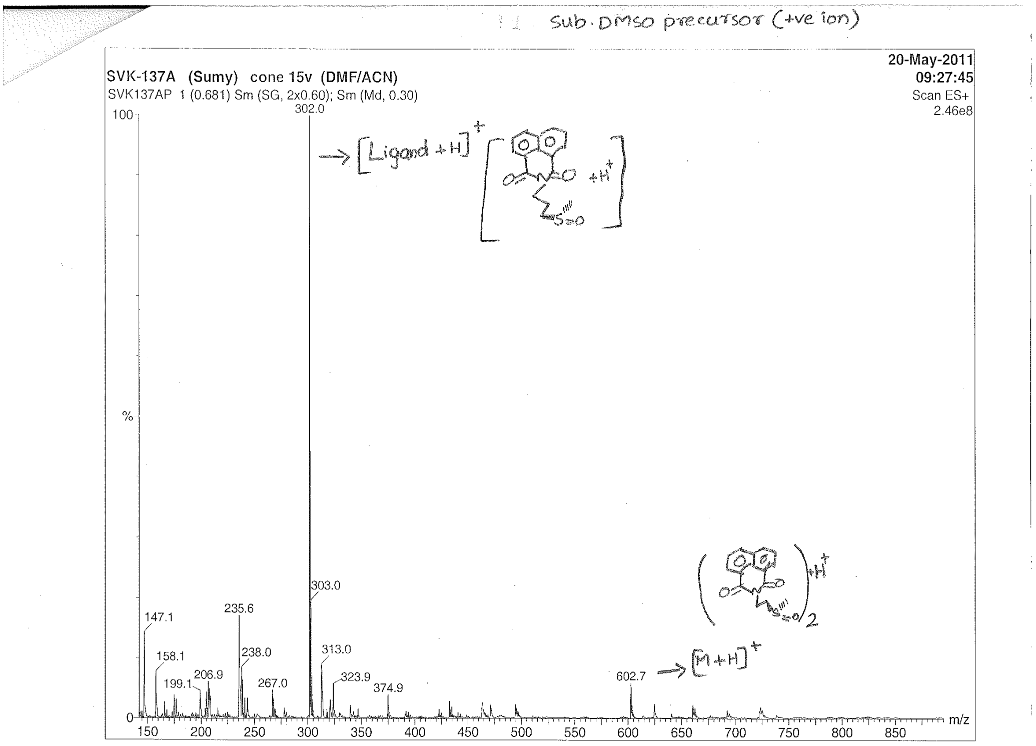

Figure 13: Electrospray mass spectrum (+ve ion) for **P1**; Cone 15V; Solvent – DMF/ACN.

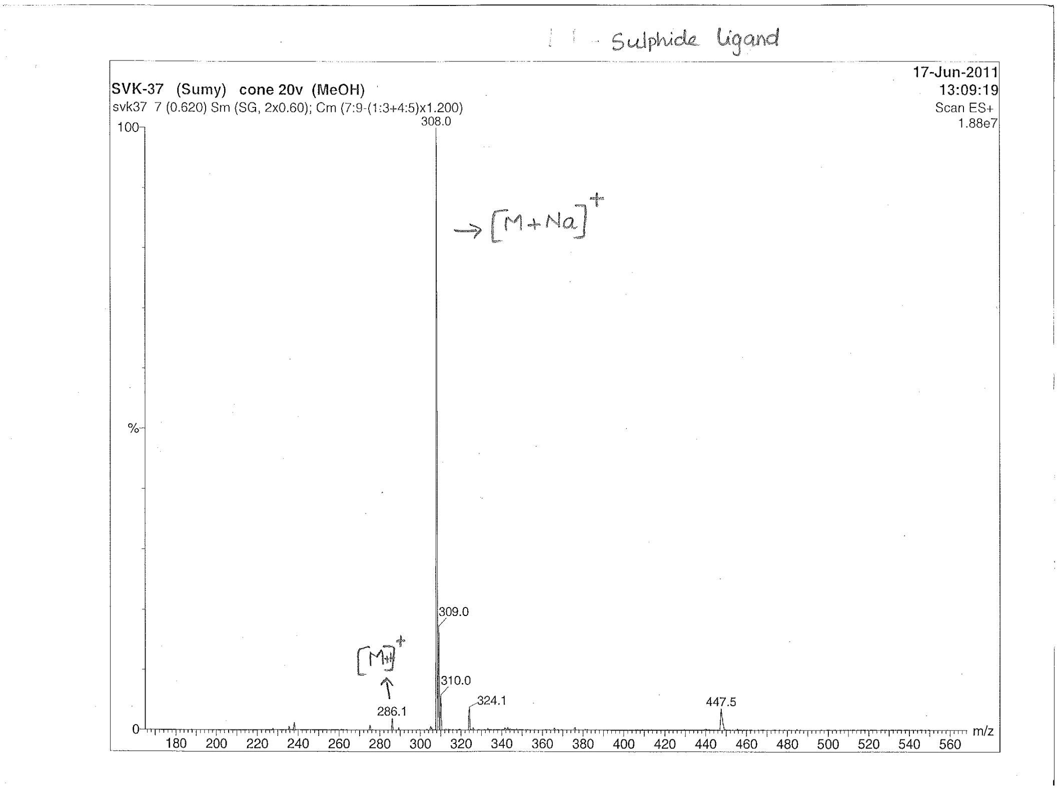

Figure 14: Electrospray mass spectrum (+ve ion) for **L4**; Cone 20V; Solvent – MeOH/ACN.

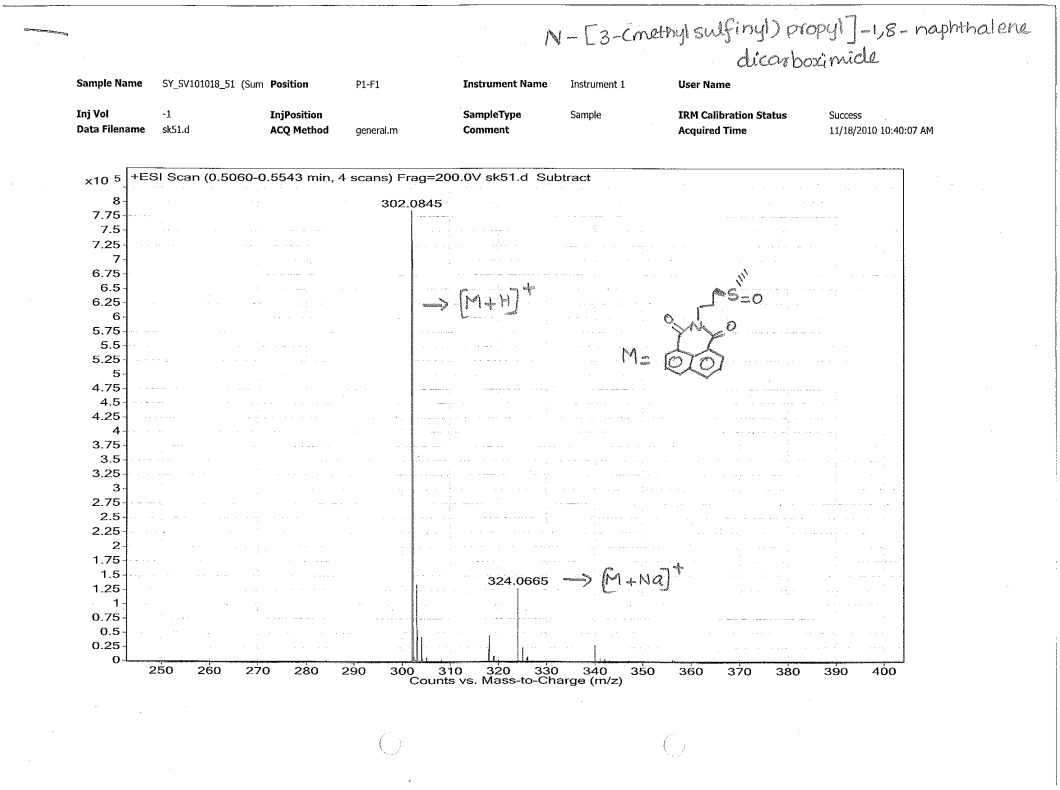

N - [3-(methyl sulfinyl) propyl] -1,8- naphthalene dicarboximide

Sample Name	SY_SV101018_51 (Sum	**Position**	P1-F1	**Instrument Name**	Instrument 1	**User Name**	
Inj Vol	-1	**InjPosition**		**SampleType**	Sample	**IRM Calibration Status**	Success
Data Filename	sk51.d	**ACQ Method**	general.m	**Comment**		**Acquired Time**	11/18/2010 10:40:07 AM

Figure 15: Accurate mass spectrum (+ve ion) for **L5**; Cone 15V; Solvent – MeOH/ACN.

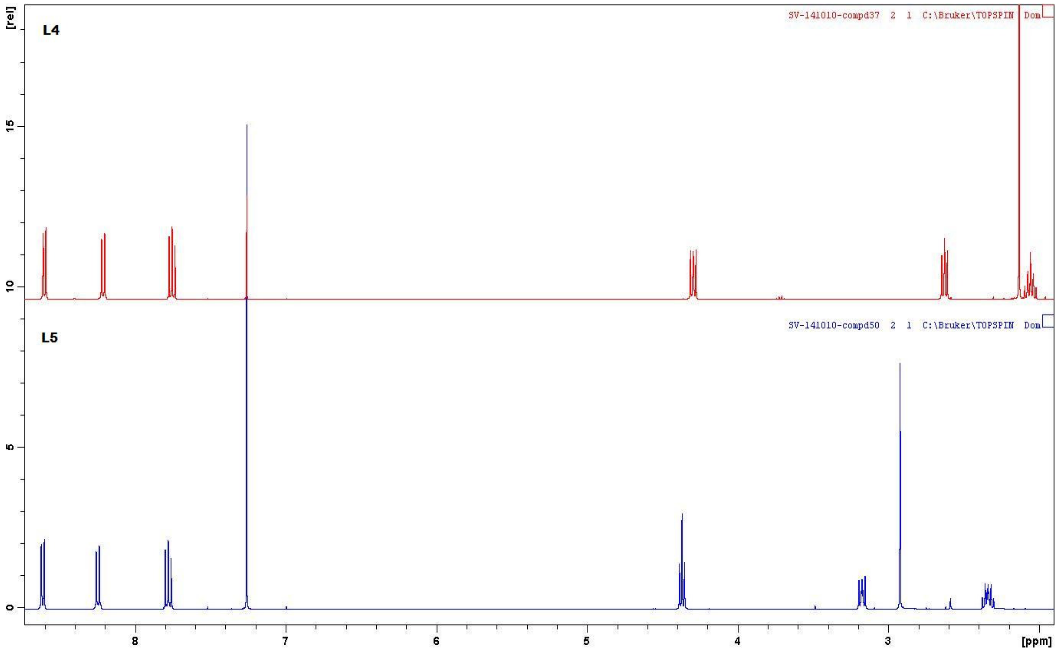

Figure 16: A comparison of ^{1}H NMR (400 MHz) spectrum of **L4** and **L5** in $CDCl_3$

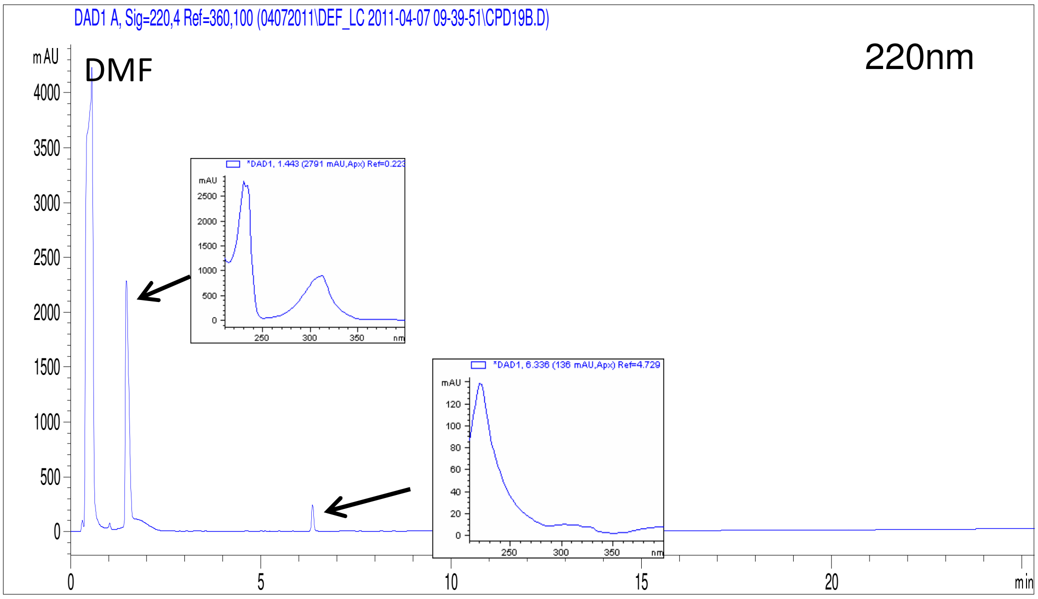

Figure 17: HPLC chromatogram of **M1** in DMF. Column: Supelco Discovery C5; Flow: 1.5 ml/min; Detection at 260 nm; Mobile phase: Buffer A (0.1% tfa/water), Buffer B (0.1%tfa/CH3CN); Gradient: 5% to 75% B, 25 minutes linear. Retention time = 3.13 min.

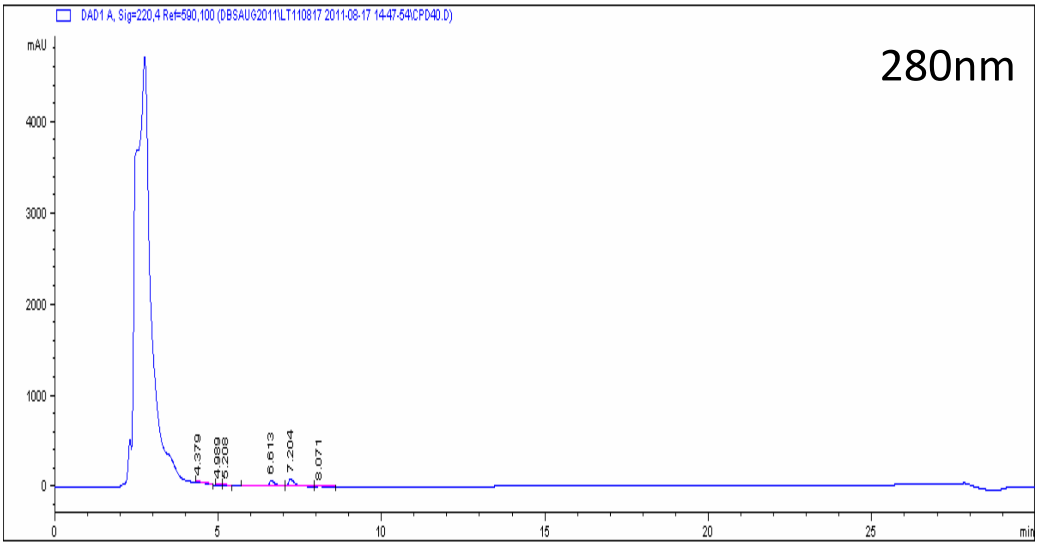

Figure 18: HPLC chromatogram of **M2** in DMF. Column: Supelco Discovery C5; Flow: 1.5 ml/min; Detection at 280 nm; Mobile phase: Buffer A (0.1% tfa/water), Buffer B (0.1%tfa/CH3CN); Gradient: 5% to 75% B, 25 minutes linear. Retention time = 2.90 min.

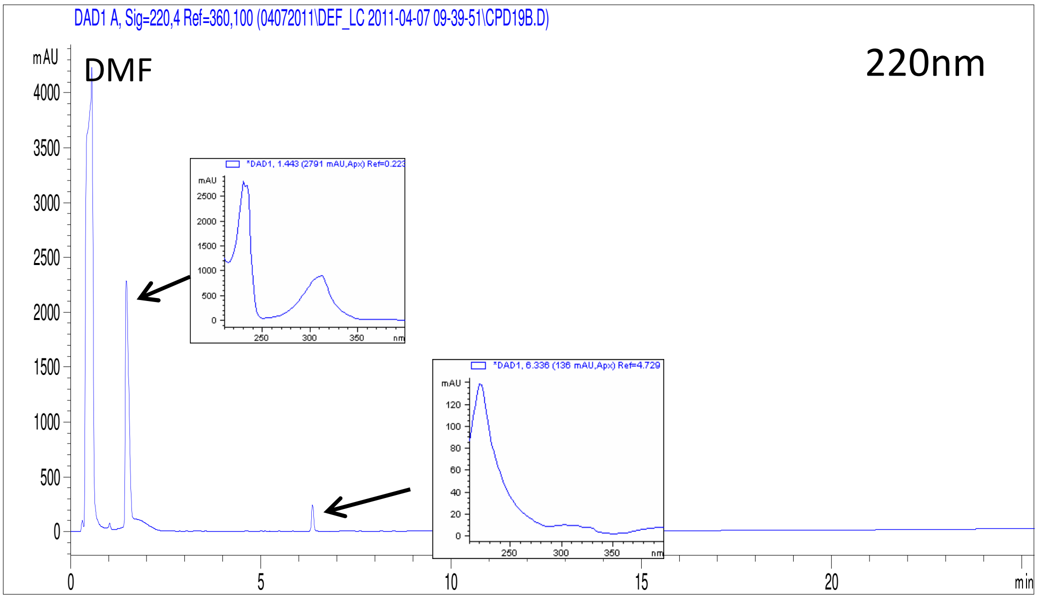

Figure 19: HPLC chromatogram of **M3** in DMF. Column: Supelco Discovery C5; Flow: 1.5 ml/min; Detection at 220 nm; Mobile phase: Buffer A (0.1% tfa/water), Buffer B (0.1%tfa/CH3CN); Gradient: 5% to 75% B, 25 minutes linear. Retention time = 1.50 min and 6.50 min.

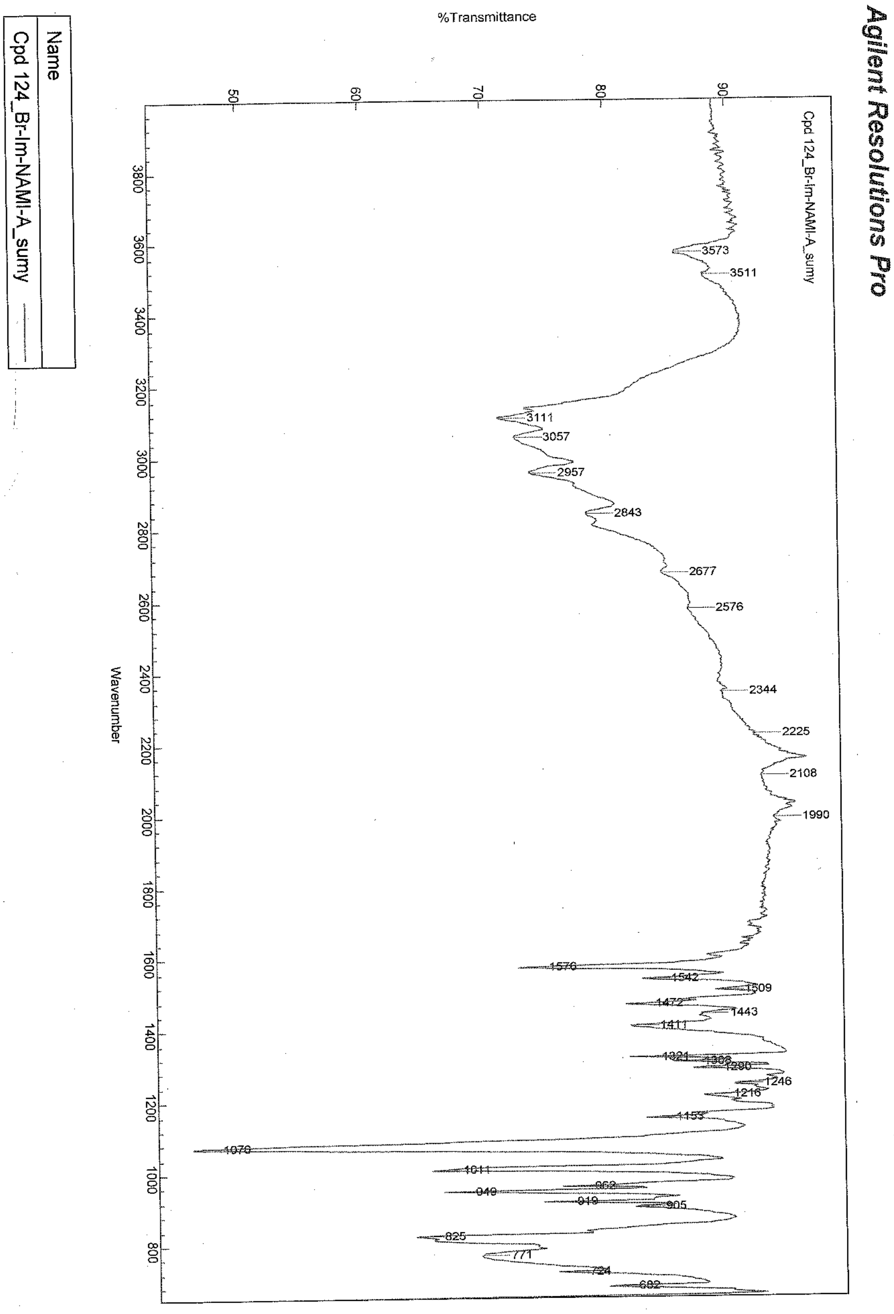

Figure 20: Solid state ATR-IR spectrum for **M1**

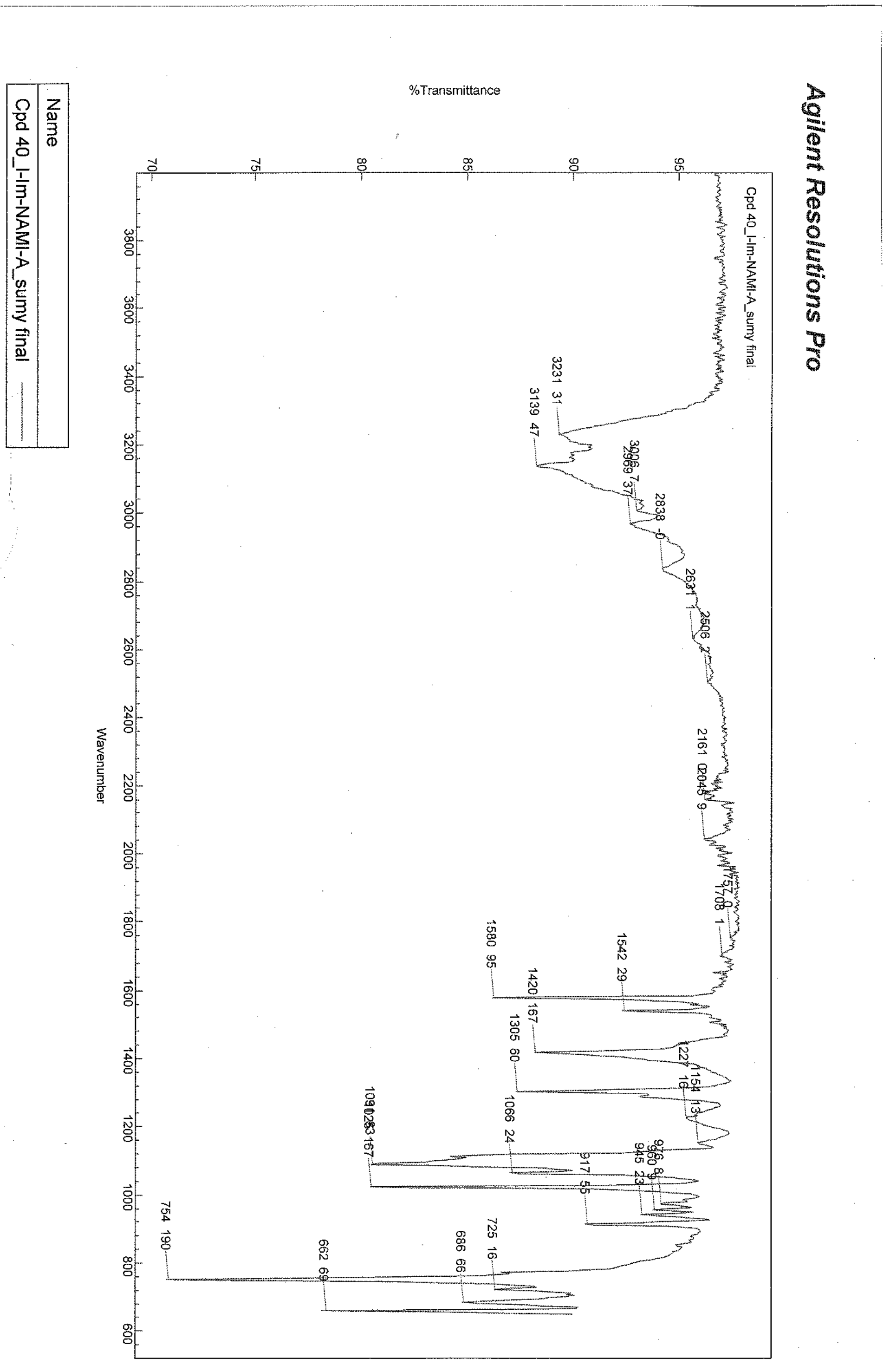

Figure 21: Solid state ATR-IR spectrum for **M2**

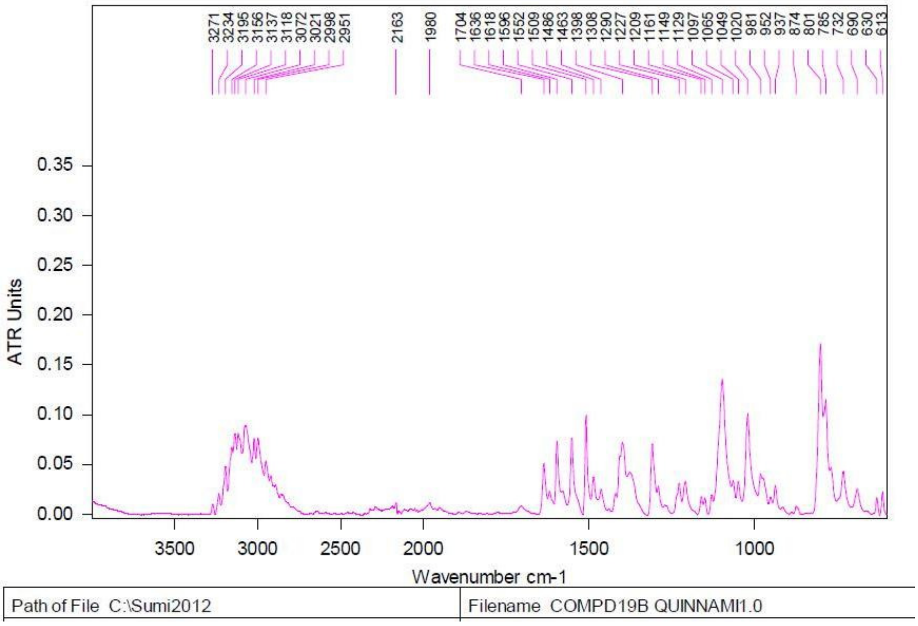

Figure 22: Solid state ATR-IR spectrum for **M3**

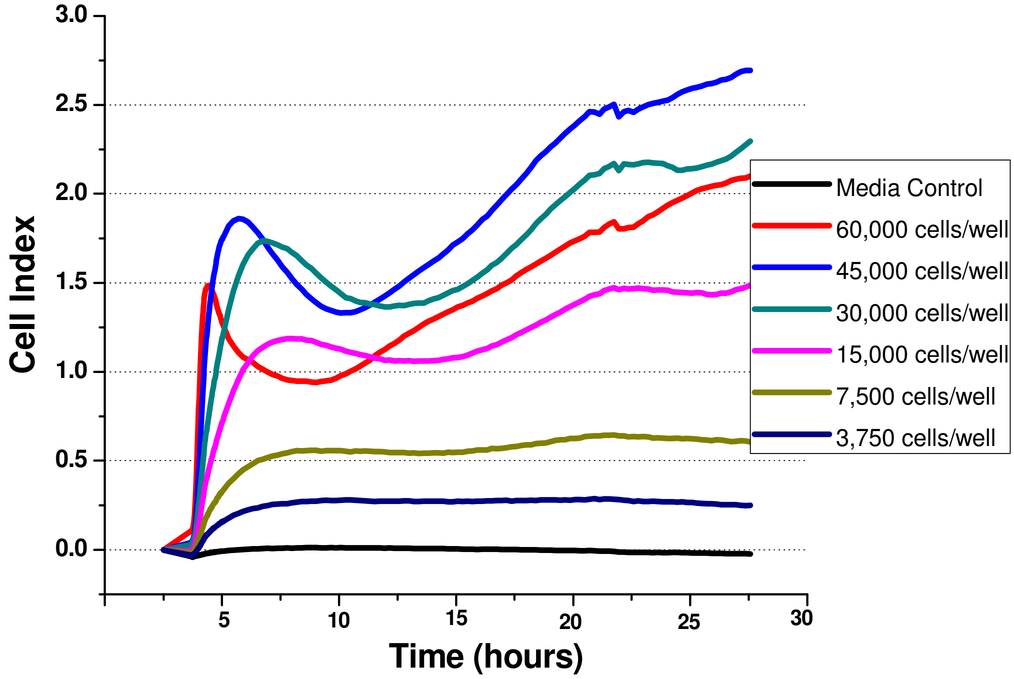

Figure 23: Dynamic monitoring of cell adhesion and proliferation using the xCELLigence system. A-549 cells at a density of 60,000, 45,000, 30,000, 15,000, 7,500, 3,750 cells per well with media control in E-plates 96 were observed during 30 hours.

Thank You